ISSN 2686-7575 (Online)

ТОНКИЕ ХИМИЧЕСКИЕ ТЕХНОЛОГИИ

Fine Chemical Technologies

- Theoretical Basis of Chemical Technology
- Chemistry and Technology of Organic Substances
- Chemistry and Technology of Medicinal Compounds and Biologically Active Substances
- Biochemistry and Biotechnology
- Synthesis and Processing of Polymers and Polymeric Composites
- Chemistry and Technology of Inorganic Materials
- Analytical Methods in Chemistry and Chemical Technology
- Mathematical Methods and Information Systems in Chemical Technology

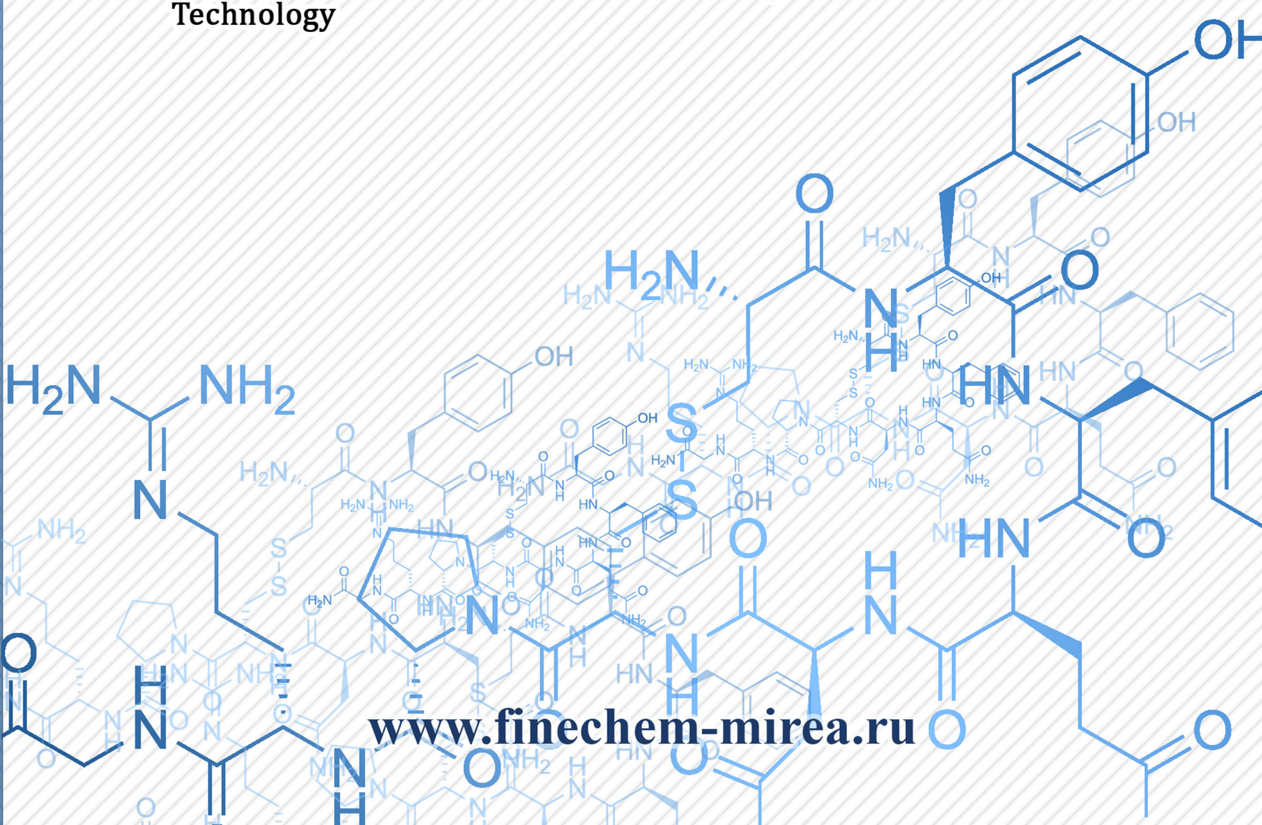

20(1)
2025

www.finechem-mirea.ru

ISSN 2686-7575 (Online)

ТОНКИЕ ХИМИЧЕСКИЕ ТЕХНОЛОГИИ

Fine Chemical Technologies

- Theoretical Basis of Chemical Technology
- Chemistry and Technology of Organic Substances
- Chemistry and Technology of Medicinal Compounds and Biologically Active Substances
- Biochemistry and Biotechnology
- Synthesis and Processing of Polymers and Polymeric Composites
- Chemistry and Technology of Inorganic Materials
- Analytical Methods in Chemistry and Chemical Technology
- Mathematical Methods and Information Systems in Chemical Technology

Tonkie Khimicheskie Tekhnologii =
Fine Chemical Technologies.
Vol. 20, No. 1, 2025

Тонкие химические технологии =
Fine Chemical Technologies.
Том 20, № 1, 2025

https://doi.org/10.32362/2410-6593-2025-20-1
www.finechem-mirea.ru

https://doi.org/10.32362/2410-6593-2025-20-1
www.finechem-mirea.ru
ISSN 2686-7575 (Online)

Tonkie Khimicheskie Tekhnologii =
Fine Chemical Technologies
2025, Vol. 20, No. 1

The peer-reviewed scientific and technical journal Fine Chemical Technologies highlights the modern achievements of fundamental and applied research in the field of fine chemical technologies, including the theoretical basis of chemical technology, chemistry and technology of medicinal compounds and biologically active substances, organic substances and inorganic materials, biochemistry and biotechnology, synthesis and processing of polymers and polymeric composites, analytical and mathematical methods and information systems in chemistry and chemical technology.

Founder and Publisher

Federal State Budget
Educational Institution of Higher Education
“MIREA – Russian Technological University”
78, Vernadskogo pr., Moscow, 119454, Russian Federation.
Publication frequency: bimonthly.
The journal was founded in 2006. The name was Vestnik MITHT until 2015 (ISSN 1819-1487).

The journal is included into the List of peer-reviewed science press of the State Commission for Academic Degrees and Titles of the Russian Federation.

The journal is indexed: SCOPUS, DOAJ, Chemical Abstracts, Science Index, RSCI, Ulrich’s International Periodicals Directory

86, Vernadskogo pr., Moscow, 119571, Russian Federation.
Phone: +7 (499) 600-80-80 (#31288)
E-mail: *seredina@mirea.ru*

The registration number ПИ № ФС 77-74580 was issued in December 14, 2018 by the Federal Service for Supervision of Communications, Information Technology, and Mass Media of Russia

The subscription index of *Pressa Rossii*: **36924**

Тонкие химические технологии =
Fine Chemical Technologies
2025, том 20, № 1

Научно-технический рецензируемый журнал «Тонкие химические технологии» освещает современные достижения фундаментальных и прикладных исследований в области тонких химических технологий, включая теоретические основы химической технологии, химию и технологию лекарственных препаратов и биологически активных соединений, органических веществ и неорганических материалов, биохимию и биотехнологию, синтез и переработку полимеров и композитов на их основе, аналитические и математические методы и информационные системы в химии и химической технологии.

Учредитель и издатель

федеральное государственное бюджетное
образовательное учреждение высшего образования
«МИРЭА – Российский технологический университет»
119454, РФ, Москва, пр-т Вернадского, д. 78.
Периодичность: один раз в два месяца.
Журнал основан в 2006 году. До 2015 года издавался
под названием «Вестник МИТХТ» (ISSN 1819-1487).

Журнал входит в Перечень ведущих рецензируемых научных журналов ВАК РФ.

Индексируется: SCOPUS, DOAJ, Chemical Abstracts, РИНЦ (Science Index), RSCI, Ulrich’s International Periodicals Directory

РФ, 119571, Москва, пр. Вернадского, 86, оф. Р-108.
Тел.: +7 (499) 600-80-80 (#31288)
E-mail: *seredina@mirea.ru*

Регистрационный номер и дата принятия решения о регистрации СМИ: ПИ № ФС 77-74580 от 14.12.2018 г. СМИ зарегистрировано Федеральной службой по надзору в сфере связи, информационных технологий и массовых коммуникаций (Роскомнадзор)

Индекс по Объединенному каталогу «Пресса России»: **36924**

EDITORIAL BOARD

Andrey V. Blokhin – Dr. Sci. (Chem.), Professor, Belarusian State University, Minsk, Belarus. Scopus Author ID 7101971167, ResearcherID AAF-8122-2019, https://orcid.org/0000-0003-4778-5872, *blokhin@bsu.by.*

Sergey P. Verevkin – Dr. Sci. (Eng.), Professor, University of Rostock, Rostock, Germany. Scopus Author ID 7006607848, ResearcherID G-3243-2011, https://orcid.org/0000-0002-0957-5594, *Sergey.verevkin@uni-rostock.de.*

Konstantin Yu. Zhizhin – Corresponding Member of the Russian Academy of Sciences (RAS), Dr. Sci. (Chem.), Professor, N.S. Kurnakov Institute of General and Inorganic Chemistry of the RAS, Moscow, Russian Federation. Scopus Author ID 6701495620, ResearcherID C-5681-2013, http://orcid.org/0000-0002-4475-124X, *kyuzhizhin@igic.ras.ru.*

Igor V. Ivanov – Dr. Sci. (Chem.), Professor, MIREA – Russian Technological University, Moscow, Russian Federation. Scopus Author ID 34770109800, ResearcherID I-5606-2016, http://orcid.org/0000-0003-0543-2067, *ivanov_i@mirea.ru.*

Carlos A. Cardona – PhD (Eng.), Professor, National University of Columbia, Manizales, Colombia. Scopus Author ID 7004278560, http://orcid.org/0000-0002-0237-2313, *ccardonaal@unal.edu.co.*

Elvira T. Krut'ko – Dr. Sci. (Eng.), Professor, Belarusian State Technological University, Minsk, Belarus. Scopus Author ID 6602297257, *ela_krutko@mail.ru.*

Anatolii I. Miroshnikov – Academician at the RAS, Dr. Sci. (Chem.), Professor, M.M. Shemyakin and Yu.A. Ovchinnikov Institute of Bioorganic Chemistry of the RAS, Member of the Presidium of the RAS, Chairman of the Presidium of the RAS Pushchino Research Center, Moscow, Russian Federation. Scopus Author ID 7006592304, ResearcherID G-5017-2017, *aiv@ibch.ru.*

Aziz M. Muzafarov – Academician at the RAS, Dr. Sci. (Chem.), Professor, A.N. Nesmeyanov Institute of Organoelement Compounds of the RAS, Moscow, Russian Federation. Scopus Author ID 7004472780, ResearcherID G-1644-2011, https://orcid.org/0000-0002-3050-3253, *aziz@ineos.ac.ru.*

РЕДАКЦИОННАЯ КОЛЛЕГИЯ

Блохин Андрей Викторович – д.х.н., профессор Белорусского государственного университета, Минск, Беларусь. Scopus Author ID 7101971167, ResearcherID AAF-8122-2019, https://orcid.org/0000-0003-4778-5872, *blokhin@bsu.by.*

Верёвкин Сергей Петрович – д.т.н., профессор Университета г. Росток, Росток, Германия. Scopus Author ID 7006607848, ResearcherID G-3243-2011, https://orcid.org/0000-0002-0957-5594, *Sergey.verevkin@uni-rostock.de.*

Жижин Константин Юрьевич – член-корр. Российской академии наук (РАН), д.х.н., профессор, Институт общей и неорганической химии им. Н.С. Курнакова РАН, Москва, Российская Федерация. Scopus Author ID 6701495620, ResearcherID C-5681-2013, http://orcid.org/0000-0002-4475-124X, *kyuzhizhin@igic.ras.ru.*

Иванов Игорь Владимирович – д.х.н., профессор, МИРЭА – Российский технологический университет, Москва, Российская Федерация. Scopus Author ID 34770109800, ResearcherID I-5606-2016, http://orcid.org/0000-0003-0543-2067, *ivanov_i@mirea.ru.*

Кардона Карлос Ариэль – PhD, профессор Национального университета Колумбии, Манизалес, Колумбия. Scopus Author ID 7004278560, http://orcid.org/0000-0002-0237-2313, *ccardonaal@unal.edu.co.*

Крутько Эльвира Тихоновна – д.т.н., профессор Белорусского государственного технологического университета, Минск, Беларусь. Scopus Author ID 6602297257, *ela_krutko@mail.ru.*

Мирошников Анатолий Иванович – академик РАН, д.х.н., профессор, Институт биоорганической химии им. академиков М.М. Шемякина и Ю.А. Овчинникова РАН, член Президиума РАН, председатель Президиума Пущинского научного центра РАН, Москва, Российская Федерация. Scopus Author ID 7006592304, ResearcherID G-5017-2017, *aiv@ibch.ru.*

Музафаров Азиз Мансурович – академик РАН, д.х.н., профессор, Институт элементоорганических соединений им. А.Н. Несмеянова РАН, Москва, Российская Федерация. Scopus Author ID 7004472780, ResearcherID G-1644-2011, https://orcid.org/0000-0002-3050-3253, *aziz@ineos.ac.ru.*

Ivan A. Novakov – Academician at the RAS, Dr. Sci. (Chem.), Professor, President of the Volgograd State Technical University, Volgograd, Russian Federation.
Scopus Author ID 7003436556, ResearcherID I-4668-2015, http://orcid.org/0000-0002-0980-6591, *president@vstu.ru.*

Alexander N. Ozerin – Corresponding Member of the RAS, Dr. Sci. (Chem.), Professor, Enikolopov Institute of Synthetic Polymeric Materials of the RAS, Moscow, Russian Federation.
Scopus Author ID 7006188944, ResearcherID J-1866-2018, https://orcid.org/0000-0001-7505-6090, *ozerin@ispm.ru.*

Tapani A. Pakkanen – PhD, Professor, Department of Chemistry, University of Eastern Finland, Joensuu, Finland.
Scopus Author ID 7102310323, *tapani.pakkanen@uef.fi.*

Armando J.L. Pombeiro – Academician at the Academy of Sciences of Lisbon, PhD, Professor, President of the Center for Structural Chemistry of the Higher Technical Institute of the University of Lisbon, Lisbon, Portugal.
Scopus Author ID 7006067269, ResearcherID I-5945-2012, https://orcid.org/0000-0001-8323-888X, *pombeiro@ist.utl.pt.*

Dmitrii V. Pyshnyi – Corresponding Member of the RAS, Dr. Sci. (Chem.), Professor, Institute of Chemical Biologyand Fundamental Medicine, Siberian Branch of the RAS, Novosibirsk, Russian Federation.
Scopus Author ID 7006677629, ResearcherID F-4729-2013, https://orcid.org/0000-0002-2587-3719, *pyshnyi@niboch.nsc.ru.*

Alexander S. Sigov – Academician at the RAS, Dr. Sci. (Phys. and Math.), Professor, President of MIREA – Russian Technological University, Moscow, Russian Federation.
Scopus Author ID 35557510600, ResearcherID L-4103-2017, *sigov@mirea.ru.*

Alexander M. Toikka – Dr. Sci. (Chem.), Professor, Institute of Chemistry, Saint Petersburg State University, St. Petersburg, Russian Federation.
Scopus Author ID 6603464176, ResearcherI D A-5698-2010, http://orcid.org/0000-0002-1863-5528, *a.toikka@spbu.ru.*

Andrzej W. Trochimczuk – Dr. Sci. (Chem.), Professor, Faculty of Chemistry, Wrocław University of Science and Technology, Wrocław, Poland.
Scopus Author ID 7003604847, *andrzej.trochimczuk@pwr.edu.pl.*

Aslan Yu. Tsivadze – Academician at the RAS, Dr. Sci. (Chem.), Professor, A.N. Frumkin Institute of Physical Chemistry and Electrochemistry of the RAS, Moscow, Russian Federation.
Scopus Author ID 7004245066, ResearcherID G-7422-2014, *tsiv@phyche.ac.ru.*

Новаков Иван Александрович – академик РАН, д.х.н., профессор, президент Волгоградского государственного технического университета, Волгоград, Российская Федерация.
Scopus Author ID 7003436556, ResearcherID I-4668-2015, http://orcid.org/0000-0002-0980-6591, *president@vstu.ru.*

Озерин Александр Никифорович – член-корр. РАН, д.х.н., профессор, Институт синтетических полимерных материалов им. Н.С. Ениколопова РАН, Москва, Российская Федерация.
Scopus Author ID 7006188944, ResearcherID J-1866-2018, https://orcid.org/0000-0001-7505-6090, *ozerin@ispm.ru.*

Пакканен Тапани – PhD, профессор, Департамент химии, Университет Восточной Финляндии, Йоенсуу, Финляндия.
Scopus Author ID 7102310323, *tapani.pakkanen@uef.fi.*

Помбейро Армандо – академик Академии наук Лиссабона, PhD, профессор, президент Центра структурной химии Высшего технического института Университета Лиссабона, Португалия.
Scopus Author ID 7006067269, ResearcherID I-5945-2012, https://orcid.org/0000-0001-8323-888X, *pombeiro@ist.utl.pt.*

Пышный Дмитрий Владимирович – член-корр. РАН, д.х.н., профессор, Институт химической биологии и фундаментальной медицины Сибирского отделения РАН, Новосибирск, Российская Федерация.
Scopus Author ID 7006677629, ResearcherID F-4729-2013, https://orcid.org/0000-0002-2587-3719, *pyshnyi@niboch.nsc.ru.*

Сигов Александр Сергеевич – академик РАН, д.ф.-м.н., профессор, президент МИРЭА – Российского технологического университета, Москва, Российская Федерация.
Scopus Author ID 35557510600, ResearcherID L-4103-2017, *sigov@mirea.ru.*

Тойкка Александр Матвеевич – д.х.н., профессор, Институт химии, Санкт-Петербургский государственный университет, Санкт-Петербург, Российская Федерация.
Scopus Author ID 6603464176, Researcher ID A-5698-2010, http://orcid.org/0000-0002-1863-5528, *a.toikka@spbu.ru.*

Трохимчук Анджей – д.х.н., профессор, Химический факультет Вроцлавского политехнического университета, Вроцлав, Польша.
Scopus Author ID 7003604847, *andrzej.trochimczuk@pwr.edu.pl.*

Цивадзе Аслан Юсупович – академик РАН, д.х.н., профессор, Институт физической химии и электрохимии им. А.Н. Фрумкина РАН, Москва, Российская Федерация.
Scopus Author ID 7004245066, ResearcherID G-7422-2014, *tsiv@phyche.ac.ru.*

20(1) | Tonkie Khimicheskie Tekhnologii
2025 | Fine Chemical Technologies

Contents

CHEMISTRY AND TECHNOLOGY OF ORGANIC SUBSTANCES

SYNTHESIS AND PROCESSING OF POLYMERS AND POLYMERIC COMPOSITES

CHEMISTRY AND TECHNOLOGY OF INORGANIC MATERIALS

MATHEMATICAL METHODS AND INFORMATION SYSTEMS IN CHEMICAL TECHNOLOGY

СОДЕРЖАНИЕ

ХИМИЯ И ТЕХНОЛОГИЯ ОРГАНИЧЕСКИХ ВЕЩЕСТВ

СИНТЕЗ И ПЕРЕРАБОТКА ПОЛИМЕРОВ И КОМПОЗИТОВ НА ИХ ОСНОВЕ

ХИМИЯ И ТЕХНОЛОГИЯ НЕОРГАНИЧЕСКИХ МАТЕРИАЛОВ

МАТЕМАТИЧЕСКИЕ МЕТОДЫ И ИНФОРМАЦИОННЫЕ СИСТЕМЫ В ХИМИЧЕСКОЙ ТЕХНОЛОГИИ

Tonkie Khimicheskie Tekhnologii = Fine Chemical Technologies.
2025;20(1):7–17 ISSN 2686-7575 (Online)

Chemistry and technology of organic substances

Химия и технология органических веществ

UDC 661.727.6+547.562.1
https://doi.org/10.32362/2410-6593-2025-20-1-7-17
EDN HWFSVA

RESEARCH ARTICLE

Hydroperoxide method for the co-production of methyl ethyl ketone and phenol

Viktoriya S. Kabanova✉, Ekaterina A. Kurganova, Aleksandr S. Frolov, Georgiy N. Koshel, Alina A. Smurova, Egor I. Bayov
Yaroslavl State Technical University, Yaroslavl, 150023 Russia
✉ *Corresponding author, e-mail: kabanovavs@ystu.ru*

Abstract

Objectives. Applying the hydroperoxide method for the co-production of methyl ethyl ketone and phenol, the work studies the kinetic and other characteristics of the individual stages of the developed process to select the optimal conditions for producing the maximum yield of intermediate and target products.

Methods. The research relied on the main theoretical and methodological provisions for the synthesis of intermediate and target products of the cumene technology for the co-production of phenol and acetone. The obtained intermediate and target products were qualitatively and quantitatively analyzed according to modern physicochemical approaches. Gas–liquid chromatography was performed with a Chromatec-Crystal 5000.2 hardware and software complex. The infrared (IR) spectra of the synthesized compounds were recorded with a Spectrum RX-1 IR Fourier spectrometer. ^{1}H nuclear magnetic resonance (NMR) spectroscopy of substances was conducted using a Bruker DRX 400 NMR spectrometer. A quantitative determination of the content of *sec*-butylbenzene hydroperoxide was carried out using iodometric titration.

Results. The main stages of the developed method for the co-production of methyl ethyl ketone and phenol based on the hydroperoxide oxidation of *sec*-butylbenzene were investigated. *sec*-Butylbenzene was synthesized by alkylation of benzene with 1-butanol in the presence of concentrated sulfuric acid at a yield of about 82%. The hydrocarbon compound was subjected to aerobic liquid-phase oxidation catalyzed by *N*-hydroxyphthalimide to the corresponding hydroperoxide with a main substance content of 30–35 wt %, feedstock conversion of 34–37%, and selectivity of hydroperoxide formation above 95%. The kinetic and other characteristics were studied for the final stage of the developed method, comprising the acid decomposition of hydroperoxide to methyl ethyl ketone and phenol. Suitable conditions for obtaining target products with high yields were identified.

Conclusions. Methyl ethyl ketone and phenol of high purity with yields of 72 and 74%, respectively, were obtained by the hydroperoxide method. The structures of the synthesized substances were confirmed by IR and ^{1}H NMR spectroscopy.

Keywords

methyl ethyl ketone, phenol, *sec*-butylbenzene, hydroperoxide, alkylation, aerobic liquid-phase oxidation, *N*-hydroxyphthalimide, acid decomposition

Submitted: 05.09.2024
Revised: 27.09.2024
Accepted: 19.12.2024

For citation

Kabanova V.S., Kurganova E.A., Frolov A.S., Koshel G.N., Smurova A.A., Bayov E.I. Hydroperoxide method for the co-production of methyl ethyl ketone and phenol. *Tonk. Khim. Tekhnol. = Fine Chem. Technol.* 2025;20(1):7–17. https://doi.org/10.32362/2410-6593-2025-20-1-7-17

НАУЧНАЯ СТАТЬЯ

Гидропероксидный способ совместного получения метилэтилкетона и фенола

В.С. Кабанова✉, Е.А. Курганова, А.С. Фролов, Г.Н. Кошель, А.А. Смурова, Е.И. Баёв

Ярославский государственный технический университет, Ярославль, 150023 Россия

✉*Автор для переписки, e-mail: kabanovavs@ystu.ru*

Аннотация

Цели. Разработка научных и прикладных основ химии и технологии гидропероксидного способа совместного получения метилэтилкетона и фенола. Исследование закономерностей протекания отдельных стадий разрабатываемого процесса и подбор условий, обеспечивающих максимальный выход промежуточных и целевых продуктов.

Методы. Методологию исследования составили основные положения о способах синтеза промежуточных и целевых продуктов кумольной технологии получения фенола совместно с ацетоном. Качественный и количественный анализ полученных промежуточных и целевых продуктов осуществлялся с применением современных физико-химических методов анализа. Газожидкостная хроматография проводилась на аппаратно-программном комплексе Хроматэк-Кристалл 5000.2. Инфракрасные (ИК) спектры синтезируемых соединений были записаны на приборе ИК Фурье Spectrum RX-1, анализ веществ методом спектроскопии ядерного магнитного резонанса (ЯМР) ^{1}H был проведен с помощью ЯМР-спектрометра Bruker DRX 400. Количественное определение содержания гидропероксида *втор*-бутилбензола проводилось с использованием йодометрического титрования.

Результаты. Исследованы основные стадии разрабатываемого способа совместного получения метилэтилкетона и фенола на основе гидропероксидного окисления *втор*-бутилбензола. Алкилированием бензола бутанолом-1 в присутствии концентрированной серной кислоты синтезирован *втор*-бутилбензол с выходом около 82%. Данный углеводород подвергнут аэробному жидкофазному окислению, катализируемому *N*-гидроксифталимидом, до соответствующего гидропероксида с содержанием основного вещества 30–35 мас. % при конверсии исходного сырья 34–37% и селективности образования гидропероксида выше 95%. Исследованы закономерности протекания заключительной стадии разрабатываемого метода — кислотного разложения гидропероксида до метилэтилкетона и фенола. Определены условия, позволяющие получать целевые продукты с высокими выходами.

Выводы. Гидропероксидным способом получены метилэтилкетон и фенол высокой степени чистоты с выходами 72 и 74% соответственно. Структуры синтезированных веществ подтверждены методами ИК- и ^{1}H ЯМР-спектроскопии.

Ключевые слова

метилэтилкетон, фенол, *втор*-бутилбензол, гидропероксид, алкилирование, аэробное жидкофазное окисление, *N*-гидроксифталимид, кислотное разложение

Поступила: 05.09.2024
Доработана: 27.09.2024
Принята в печать: 19.12.2024

Для цитирования

Кабанова В.С., Курганова Е.А., Фролов А.С., Кошель Г.Н., Смурова А.А., Баёв Е.И. Гидропероксидный способ совместного получения метилэтилкетона и фенола. *Тонкие химические технологии*. 2025;20(1):7–17. https://doi.org/10.32362/2410-6593-2025-20-1-7-17

INTRODUCTION

Methyl ethyl ketone (MEK) is a basic large-tonnage organic synthesis product widely used in the production of polymers and paints and varnishes [1]. In industry, MEK is widely known as an effective solvent for many substances and materials, such as printing inks and epoxy resins [2]. MEK is also used in the production of glue, magnetic tapes, artificial leather, smokeless powders, and rubber antioxidants [3–5]. In fine organic synthesis, MEK is used as a feedstock for the production of a number of monomers for acrylic glass [4].

In industry, MEK is obtained by several methods, including catalytic oxidation of 2-butanol by silver on a zeolite support [6, 7] and dehydrogenation of butyl alcohol in the presence of zinc copper catalysts [8, 9]. These MEK production processes are characterized by temperatures of about 500°C and the presence of expensive and low-stable catalysts. There are also methods for producing MEK from butylene fractions, e.g., involving the direct oxidation of *n*-butylenes [4, 10], where the catalyst is an aqueous solution of a complex of palladium(II) and Mo-V-phosphoric heteropoly acid (HPA) of the general composition $H_{3+x}PV_xMo_{12-x}O_{40}$ (HPA–x, $2 \leq x \leq 6$).

In the present work, an alternative hydroperoxide method is proposed for the co-production of MEK and phenol, an important petrochemical monomer used

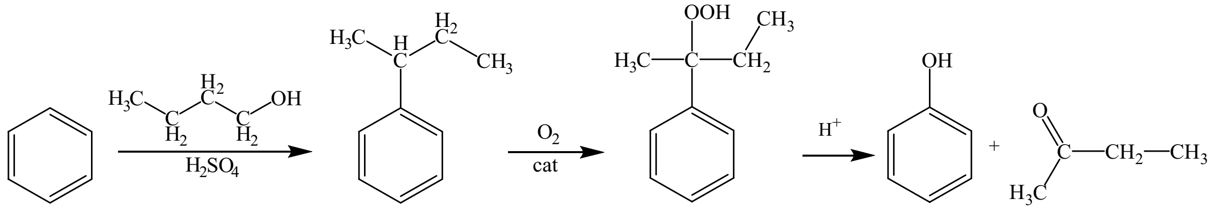

Scheme. Hydroperoxide method for the synthesis of methyl ethyl ketone and phenol

in the production of plastics, fibers, dyes, cosmetics, and medicines [11, 12]. The proposed method is based on the cumene technology for the production of phenol and acetone. Although highly efficient, this technology has the main disadvantage that it produces excess amounts of acetone, which is not a highly demanded product in the chemical market [13].

The developed method includes the stages of synthesis of the initial *sec*-butylbenzene (*sec*-BB) by alkylation of benzene with 1-butanol in the presence of concentrated sulfuric acid, aerobic liquid-phase oxidation of this hydrocarbon to its hydroperoxide (HP) using an effective organic catalyst—*N*-hydroxyphthalimide (*N*-HPI), and acidic decomposition of *sec*-BB HP into target products according to the following scheme:

In this paper, the kinetic and other characteristics of these stages were studied.

MATERIALS AND METHODS

The following reagents were used in the study: benzene (chemical purity grade, GOST 5955-75[1], *EKOS-1*, Russia), 1-butanol (chemical purity grade, GOST 6006-78[2], *EKOS-1*, Russia), sulfuric acid (chemical purity grade, GOST 4204-771[3], *Sigma-Tek*, Russia), sodium hydroxide (analytical purity grade, GOST 4328-77[4], *Komponent-Reaktiv*, Russia), calcium chloride (analytical purity grade, GOST 450-77[5], *Mosreaktiv*, Russia), compressed oxygen (chemical purity grade, GOST 5583-78[6]), *N*-hydroxyphthalimide (*Sisco Research Laboratories*, India), acetic acid (chemical purity grade, GOST 61-75[7], *Spektr Khim*, Russia), potassium iodide (chemical purity grade, GOST 4232-74[8], *Spektr Khim*, Russia), and sodium thiosulfate (analytical purity grade, GOST 27068-86[9], *Uralkhiminvest*, Russia).

Qualitative and quantitative analysis of the synthesized intermediate and target products was carried out using contemporary physicochemical analysis methods. The contents of the synthesized compounds were determined by gas–liquid chromatography with a Chromatec-Crystall 5000.2 hardware and software complex (*Chromatec*, Russia). The obtained compounds were identified by infrared (IR) spectroscopy and ^{1}H nuclear magnetic resonance (NMR) spectroscopy. IR spectra were recorded with a Spectrum RX-1 Fourier-transform IR spectrometer (*PerkinElmer*, USA, 4000–400 cm^{-1}, KBr glass). The IR spectra were mathematically processed using the Spektrum v.5.0.1 software. ^{1}H NMR spectroscopy was performed using a Bruker DRX 400 NMR spectrometer (400.4 MHz). The solvent was a dimethyl sulfoxide d_6–CCl_4 mixture, while the internal standard was tetramethylsilane.

The content of *sec*-BB HP in the oxidation products of *sec*-BB, as well as during the process of acid decomposition of HP, was determined by iodometric titration [14].

EXPERIMENTAL

Sulfuric acid alkylation of benzene with 1-butanol was carried out in a round-bottomed three-necked flask equipped with a thermometer and immersed in a water

---

[1] GOST 5955-75. State Standard of the USSR. Reagents. Benzene. Specifications. Moscow: Izdatelstvo standartov; 1994 (in Russ.).

[2] GOST 6006-78. State Standard of the USSR. Reagents. 1-Butanol. Specifications. Moscow: IPK Izdatelstvo standartov; 1998 (in Russ.).

[3] GOST 4204-77. State Standard of the USSR. Reagents. Sulphuric acid. Specifications. Moscow: Standartinform; 2006 (in Russ.).

[4] GOST 4328-77. Interstate Standard. Reagents. Sodium hydroxide. Specifications. Moscow: IPK Izdatelstvo standartov; 1978 (in Russ.).

[5] GOST 450-77. State Standard of the USSR. Reagents. Calcium chloride. Specifications. Moscow: IPK Izdatelstvo standartov; 1997 (in Russ.).

[6] GOST 5583-78. Interstate Standard. Technical and medical oxygen gas Specifications. Moscow: Standartinform; 2005 (in Russ.).

[7] GOST 61-75. Interstate Standard. Reagents. Acetic acid. Specifications. Moscow: Standartinform; 2006 (in Russ.).

[8] GOST 4232-74. Interstate Standard.Reagents. Potassium iodide. Specifications. Moscow: Standartinform; 2006 (in Russ.).

[9] GOST 27068-86. Interstate Standard. Reagents. Sodium thiosulphate, 5-aqueous. Specifications. Moscow: IPK Izdatelstvo standartov; 1998 (in Russ.).

bath at a given molar ratio of reagents, temperature, and reaction time with continuous stirring of the reaction mass according to the procedure described in [15]. The target product was isolated from the reaction mass by vacuum distillation at a temperature of 85–87°C and a residual pressure of 15–30 mm Hg.

Aerobic liquid-phase oxidation of *sec*-BB was performed in a glass continuous stirred tank reactor at atmospheric pressure with continuous oxygen supply according to a published procedure [16]. Upon completion of the reaction, the oxidized reaction mixture was cooled to room temperature, separated by filtration from the precipitated catalyst (*N*-HPI), and analyzed for *sec*-BB HP content by iodometric titration.

The obtained *sec*-BB HP was concentrated by extraction with a 75% ethyl alcohol solution in a flask with a reflux condenser with continuous vigorous stirring at a temperature of 20–23°C for 1 h until complete phase separation of the reaction mass. Water and alcohol were separated from the extract by vacuum distillation at a temperature of 20–23°C and a residual pressure of 15–30 mm Hg, thereby obtaining the concentrated HP.

Acid decomposition of *sec*-BB HP was performed in a thermostated glass reactor according to a published procedure [17]. The process was conducted at a given temperature with continuous stirring. The progress of the reaction was monitored by the consumption of *sec*-BB HP by taking samples for analysis every 10 min from the start of the reaction. MEK was isolated from the reaction mass by vacuum distillation at a temperature of 36–40°C and residual pressure of 15–20 mm Hg; phenol was isolated by extraction with a 10% aqueous solution of ethanol, followed by evaporation of water and alcohol from the so-called alcohol–phenol layer formed during separation of the mixture.

The characteristics of the synthesized intermediate and target products are presented below.

***sec*-BB.** Yield on the basis of loaded alcohol is 82%. Content of the main substance is 99.3%. IR spectrum, cm^{-1}: 3083, 3063, 3028 (ν C–H$_{arom}$); 2961, 2875 (ν CH$_3$); 2929, 2859 (ν CH$_2$); 1603, 1493 (ν C=C$_{arom}$); 1451 (δ CH$_2$); 1378 (δ CH$_3$); 758, 697 (monosubstitution in aromatic ring). ^{1}H NMR spectrum (400 MHz), δ, ppm: 0.75 t (3H, CH$_3$), 1.17 d (3H, CH$_3$), 1.57 m (2H, CH$_2$), 2.55 m (1H, CH), 7.16 m (3H, CH$_{arom}$), 7.27 m (2H, CH$_{arom}$).

***sec*-BB HP.** The content of the main substance is 95%. IR spectrum, cm^{-1}: 3401 (ν O–OH); 2973 (ν CH$_3$); 2939 (ν CH$_2$); 1601, 1496 (aromatic ring); 1447 (δ CH$_2$), 1372 (δ CH$_3$), 758 and 698 (monosubstitution in the benzene ring).

MEK. Yield on the basis of loaded *sec*-BB HP is 72%. IR spectrum, cm^{-1}: 2980 (ν CH$_2$); 2941 (ν CH$_3$); 1709 (ν C=O); 1365 (δ CH$_2$). ^{1}H NMR (400 MHz), δ, ppm: 2.43 (q, 2H), 2.06 (s, 3H), 0.90 (t, 3H).

Phenol. Yield on the basis of loaded *sec*-BB HP is 74%. IR spectrum, cm^{-1}: 3221 (ν O–H); 3050–3020 (ν C–H$_{arom}$); 1594, 1473 (ν C–C$_{arom}$). ^{1}H NMR (400 MHz), δ, ppm: 9.33 (s, 1H), 7.15 (t, 2H), 6.80–6.72 (m, 3H).

RESULTS AND DISCUSSION

Several methods for obtaining *sec*-BB using unsaturated hydrocarbons are described in the scientific and technical literature [18, 19]. However, their main disadvantage is a relatively low yield of the target product (40–60%). An alternative method for synthesizing *sec*-BB is alkylation of benzene with 1-butanol. This method is attractive due to the possibility of performing it under laboratory conditions. Since we found almost no information on this reaction in the literature, we conducted a series of studies aimed at exploring the effect of some parameters on the formation of *sec*-BB by alkylation of benzene with 1-butanol. In terms of the initial conditions, a molar reagent ratio of benzene : 1-butanol : sulfuric acid = 3 : 1 : 3 was selected. The process temperature

Table 1. Effect of temperature and reaction duration on the formation of *sec*-butylbenzene (*sec*-BB) by alkylation of benzene with 1-butanol. The benzene : 1-butanol : sulfuric acid molar ratio is 3 : 1 : 3

Temperature, °C	Reaction duration, h	Yield of *sec*-BB on the basis of loaded alcohol, %	Conversion of benzene, %
50	2	21.6	7.4
	4	30.7	11.1
60	2	48.9	16.5
	4	54.7	18.4
70	2	75.1	25.2
	4	81.7	28.8

Table 2. Material balance of alkylation of benzene with 1-butanol. The molar ratio of benzene : 1-butanol : sulfuric acid is 3 : 1 : 3. The temperature is 70°C. The reaction duration is 4 h

Substance	Molar mass, g/mol	Loaded		Obtained	
		g	wt %	g	wt %
Benzene	78.1	175.8	38.9	125.1	27.7
1-Butanol	74.1	55.6	12.3	5.0	1.1
H_2SO_4*	98.1	220.7	48.8	230.8	51.1
sec-BB	134.2	0.0	0.0	82.3	18.2
Byproducts	–	0.0	0.0	6.4	1.4
Losses	–	0.0	0.0	2.5	0.5
Total	–	452.1	100.0	452.1	100.0

* Mass of the acid layer containing the water formed during the reaction.

was varied from 50 to 70°C, and the reaction duration was 2–4 h. Table 1 presents the results of studying the effect of these parameters on the formation of *sec*-BB.

Table 1 shows that an increase in temperature and reaction duration promotes an increase in the conversion of benzene and the yield of the target *sec*-BB. It was found that the benzene alkylation with butyl alcohol at 50°C gives an extremely low yield of the target product (no more than 30% on the basis of loaded alcohol). A higher yield of *sec*-BB can be achieved by performing the reaction at 70°C for 4 h. These optimal conditions provide a high yield of *sec*-BB of about 82%. Carrying out the reaction at higher temperatures or for a longer time leads to the formation of an increased content of disubstituted *sec*-BB in the reaction mass, which is a byproduct in the developed technology.

Based on the results of the scaled-up synthesis of *sec*-BB under the selected conditions, the material balance was calculated (Table 2).

The target product was isolated by vacuum distillation at a yield of around 82% on the basis of loaded 1-butanol at a conversion of benzene of about 29%. The characteristics of the compound are presented in the experimental part of this work.

The key stage of the developed method for the co-production of MEK and phenol is the oxidation of the obtained *sec*-BB to its tertiary HP: it is the efficiency of this stage that determines the economy of the entire process. Initially, aerobic oxidation of *v*-BB was studied in the absence of any additives (the so-called autoxidation process). As the results showed, even at a high temperature of 140°C, only 2 wt % HP can be accumulated in 60 min of the reaction (Fig. 2, curve *1*), making this method unacceptable for further studies.

A method for the joint aerobic oxidation of *sec*-BB and isopropylbenzene was proposed [20], where the resulting isopropylbenzene hydroperoxide acts as an oxidation initiator. It was found that the rate of *sec*-BB oxidation in such a process is about 1.7 wt %/h with a conversion of *sec*-BB of about 15% and a selectivity for the formation of *sec*-BB HP of no more than 70%. In technological terms, such results are considered inefficient.

Therefore, an attempt was made to intensify the process under study. To achieve this goal, *N*-HPI was used as a catalyst. The advantages of using this compound include its nontoxicity, a relatively simple synthesis method based on available phthalic anhydride, and a high efficiency of *N*-HPI for various types of substrates [21, 22]. In addition, it was found that the use of *N*-HPI can significantly increase the conversion of the hydrocarbon being oxidized, as well as achieve high selectivity for the formation of the corresponding HP (over 90%) [21].

The work studied the effect of temperature and catalyst content on the oxidation of *sec*-BB to its HP. The process was carried out according to the method described in the experimental section at temperatures of 120–150°C and a catalyst content of 1–4 wt % of loaded *sec*-BB. The HP content in the oxidation products was determined by iodometric titration. The results obtained are presented in Figs. 1 and 2.

According to the obtained results, an increase in temperature favors the accumulation of HP in the reaction products. For example, in 40 min at a temperature

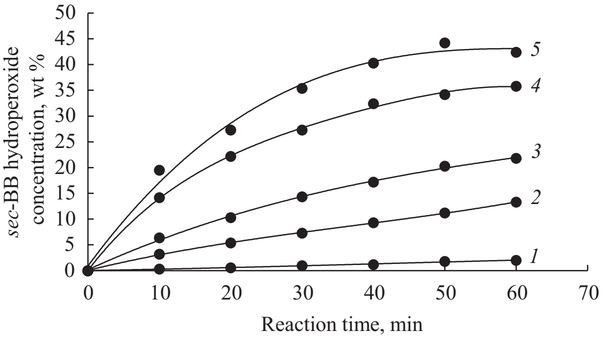

Fig. 1. Kinetics of aerobic liquid-phase oxidation of *sec*-BB to hydroperoxide at *N*-HPI concentrations of (*1*) 0.0 and (*2*)–(*5*) 2.0 wt % and temperatures of (*1*) 140, (*2*) 120, (*3*) 130, (*4*) 140, and (*5*) 150°C

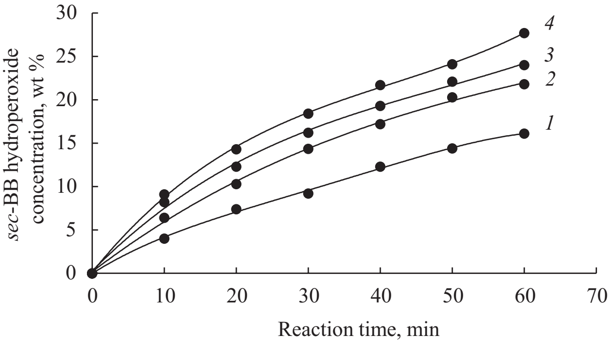

Fig. 2. Effect of the catalyst concentration on aerobic liquid-phase oxidation of *sec*-BB to hydroperoxide at a temperature of 130°C and catalyst concentrations of (*1*) 1.0, (*2*) 2.0, (*3*) 3.0, and (*4*) 4.0 wt %

of 130°C, it is possible to obtain *sec*-BB HP with a main substance content of about 17 wt %, a conversion of *sec*-BB of 18%, and a selectivity for the formation of HP of 97.2%. With an increase in temperature by only 10°C for the same 40 min, the content of *sec*-BB HP is increased to 32 wt % while maintaining the selectivity for its formation at a sufficiently high level (95.5%). A further increase in temperature leads to a sharp decrease in the selectivity for the formation of *sec*-BB HP, which can also reach 90%. This is caused by the predominance of the thermal decomposition of HP formed during the reaction, which leads to the formation of oxidation byproducts.

A study of the effect of the catalyst content on the oxidation of *sec*-BB showed that an increase in the catalyst concentration leads to an increase in the content of *sec*-BB HP. This can be clearly seen when increasing the concentration of *N*-HPI from 1.0 to 2.0 wt % (Fig. 2). Thus, at 130°C in 40 min of reaction in the presence of 1.0% *N*-HPI, it is possible to accumulate HP up to 17 wt %. Increasing the catalyst content by one percent leads to an increase in the oxidation rate of *v*-BB by a factor of 1.3. The use of the *N*-HPI catalyst in an amount of 3 wt % or more is not economically feasible, since an insignificant increase in the HP content is observed in the reaction products.

Thus, oxidation of *sec*-BB at a temperature of 130–140°C and a concentration of *N*-HPI catalyst of 2 wt % in 1 h of reaction can yield *sec*-BB HP with a content of 22 to 35 wt % and a selectivity of about 94–97%.

To ensure that it is the tertiary HP that is actually formed in the course of oxidative transformations of *sec*-BB, the obtained oxidized reaction mixture with a *sec*-BB HP content of 24 wt % was subjected to five-stage extraction. The 75% ethanol solution chosen as an extractant has a proven efficiency when used in processes of extraction and concentration of HP [12]. Table 3 presents the material balance of this process.

Vacuum distillation of the combined extract yielded 95% *sec*-BB *tert*-HP, whose structure was confirmed by IR spectroscopy. The main advantage of this process is the possibility to use isolated concentrated HP as an initiator of polymerization and aerobic oxidation.

The final stage of our work consisted in studying the characteristics of the acid decomposition of *sec*-BB HP to MEK and phenol. A series of experiments were carried out at temperatures of 40–70°C, an initial concentration

Table 3. Material balance of five-stage extraction of *sec*-BB HP from *sec*-BB oxidation products with 75% ethanol solution

Component	Molar mass, g/mol	Loaded		Obtained			
		g	wt %	Raffinate		Combined extract	
				g	wt %	g	wt %
sec-BB	134.1	78.9	18.7	78.0	99.7	0.0	0.0
sec-BB HP	166.1	13.9	3.3	0.2	0.3	13.5	4.0
Ethanol	46.1	260.0	61.5	0.0	0.0	259.0	75.8
Water	18.0	70.0	16.5	0.0	0.0	69.2	20.2
Losses	–	0.0	0.0	2.9			
Total	–	422.8	100.0	78.2	100.0	341.7	100.0

Table 4. Effect of temperature and concentrations of HP and catalyst on the acid-catalytic decomposition of *sec*-BB HP

Initial concentration of *sec*-BB HP, wt %	Concentration of H_2SO_4 catalyst, wt %	Temperature, °C	Initial reaction rate, mol/(L·min)	Conversion of HP, %	Yield on basis of reacted HP, %	
					Phenol	MEK
20	0.8	40	0.024	98.0	73	71
		50	0.054	98.5	74	72
		60	0.133	98.3	75	68
		70	0.239	99.5	73	66
10	0.8	50	0.034	99.0	36	29
15			0.038	98.7	70	69
20	1.0	50	0.067	99.5	78	70
	1.2		0.080	98.5	76	68
	1.4		0.110	97.5	75	64

of *sec*-BB HP of 10–20 wt %, and a content of sulfuric acid used as a catalyst of 0.8–1.4 wt % of the amount of loaded HP. The reaction progress was monitored by the consumption of *sec*-BB HP using iodometric titration. The initial reaction rates were determined from the slope of the kinetic curve at the initial point of time [17], since it is at this point of time that the low concentrations of the reaction products have little effect on the process. Table 4 presents the studied characteristics of the process.

The initial reaction rate was shown to increase significantly with increasing temperature. Moreover, with a change in temperature from 40 to 70°C, the content of byproducts in the reaction mass increases. This fact also explains the sharp decrease in the yield of the target MEK down to 66%. For this reason, it was decided to conduct further studies at a temperature of 50°C. Along with increased temperature, an increase in the initial concentration of HP also leads to a more rapid process rate. For example, with a change in the concentration of *sec*-BB HP from 10 to 20 wt %, the reaction rate increases by a factor of 1.6. Meanwhile, it is the decomposition of 20% HP that is characterized by the highest yield of target products. Increasing the initial concentration of HP above 20 wt % is impractical due to the release of a large amount of heat during the decomposition of HP, which can be hazardous. As for increasing the concentration of the catalyst, even a small change in it (from 0.8 to 1.4 wt %) significantly reduces the selectivity of the formation of target products.

The data obtained in the series of experiments on the effect of various parameters on the process under discussion made it possible to determine the conditions for conducting it with a high yield of products. At a temperature of 50°C, a concentration of HP of 20 wt %, and a catalyst content in the reaction mass of 0.8 wt %, a scaled-up process of acid decomposition of *sec*-BB HP was carried out, the results of which are presented in Table 5.

The yields of MEK and phenol were 72 and 74%, respectively, with a conversion of HP of 99.5%.

Table 5. Material balance of sulfuric acid catalytic decomposition of *sec*-BB HP at a temperature of 50°C, an initial concentration of HP of 20 wt %, and a catalyst concentration of 0.8 wt %

Substance	Molar mass, g/mol	Loaded		Obtained	
		g	wt %	g	wt %
sec-BB	134.2	66.4	79.9	66.4	79.9
sec-BB HP	166.1	16.6	20.0	0.1	0.1
H_2SO_4	98.1	0.1	0.1	0.1	0.1
Phenol	94.1	0.0	0.0	7.0	8.4
MEK	72.1	0.0	0.0	5.2	6.3
Byproducts	–	0.0	0.0	1.2	1.4
Losses	–	0.0	0.0	3.1	3.8
Total	–	83.1	100.0	83.1	100.0

CONCLUSIONS

In the present work, the scientific and applied chemical and technological fundamentals of the hydroperoxide method used for the co-production of MEK and phenol are described and developed. The effects of some parameters on the main stages of the developed method was studied. Alkylation of benzene with 1-butanol at a benzene : 1-butanol : H_2SO_4 molar ratio of 3 : 1 : 3, a temperature of 70°C, and a reaction duration of 4 h, produced *sec*-BB at a yield of about 82% and a conversion of the initial hydrocarbon of about 30%.

The effect of such parameters as temperature, reaction duration, and catalyst concentration on the liquid-phase oxidation of *sec*-BB to its tertiary HP was investigated. Aerobic oxidation of *sec*-BB in the presence of *N*-HPI gave *sec*-BB HP with a selectivity of about 95% at a conversion of *sec*-BB of 35–40%.

Extraction of *sec*-BB HP from the *sec*-BB oxidation products by extraction with a 75% ethanol solution was tested. The obtained concentrated (up to 95%) HP can further be used in polymerization or initiated oxidation of alkyl aromatic hydrocarbons.

Sulfuric acid catalytic decomposition of *sec*-BB HP with a content of the main substance of 20 wt % at 50°C and a catalyst concentration of 0.8 wt % gave MEK and phenol with yields of 72 and 74%, respectively.

The results of the studies confirmed the technological efficiency of this method in comparison with the separate production of MEK and phenol, demonstrating its potential as an alternative to existing technologies for producing these compounds. The proposed hydroperoxide method for the synthesis of MEK and phenol can be used as part of an adapted cumene technology to obtain a wide range of alkylphenols and ketones.

Acknowledgments

The reported study was funded by the Government of the Yaroslavl oblast according to the research project No. 4NP/2024.

Authors’ contributions

V.S. Kabanova—research concept, conducting experiments, data processing, analysis of the results, writing the text of the manuscript.

E.A. Kurganova—research concept, design of the experiments, analysis of the results, writing the text of the manuscript.

A.S. Frolov—research concept, data processing, writing the text of the manuscript.

G.N. Koshel—research concept, analysis of the results, writing the text of the manuscript.

A.A. Smurova—conducting the experiments.

E.I. Bayov—conducting the experiments.

The authors declare no conflicts of interest.

REFERENCES

1. Egizaryan A.M., Golovachev V.A., Kleimenov A.V., Miroshkina V.D., Noskov A.S., Piryutko L.V., Russkikh A.V., Chernyavskii V.S., Kharitonov A.S. *Method of Obtaining Methyl Ethyl Ketone*: RF Pat. RU 2623435. Publ. 26.06.2017 (in Russ.).
2. Matveev K.I., Zhizhina E.G., Odyakov V.F. *Catalyst and Methyl Ethyl Ketone Production Process*: RF Pat. RU 2230612. Publ. 20.06.2004 (in Russ.).
3. Matveev K.I., Zhizhina E.G., Odyakov V.F., *et al.* Homogeneous redox catalysts based on heteropoly acid solutions: I. Pilot testing of a catalyst and methyl ethyl ketone synthesis. *Cat. Ind.* 2014;6(3):202–211. https://doi.org/10.1134/S207005041403009X
   [Original Russian Text: Matveev K.I., Zhizhina E.G., Odyakov V.F., Parmon V.N. Homogeneous catalysts of redox processes based on solutions of heteropoly acids. I. Results of pilot tests of the catalyst and the synthesis process of methyl ethyl ketone. *Kataliz v promyshlennosti.* 2014;3:32–42 (in Russ.).]
4. Zhizhina E.G., Odyakov V.F., Balashov A.L., Matveev K.I. Development of new technology of catalytic synthesis of methyl ethyl ketone by oxidation of *n*-butylenes. *Kataliz v promyshlennosti*. 2005;5:28–35 (in Russ.).
5. Agaguseynova M.M., Amanullayeva G.I., Bayramova Z.E. Catalysts of oxidation reaction of butene-1 to methyl ethyl ketone. *Izv. Vyssh. Uchebn. Zaved. Khim. Khim. Tekhnol. = ChemChemTech*. 2018;61(2):53–57 (in Russ.). https://doi.org/10.6060/tcct.20186102.5693

СПИСОК ЛИТЕРАТУРЫ

1. Егизарьян А.М., Головачев В.А., Клейменов А.В., Мирошкина В.Д., Носков А.С., Пирютко Л.В., Русских А.В., Чернявский В.С., Харитонов А.С. *Способ получения метилэтилкетона:* пат. РФ 2623435. Заявка № 2016130246; заявл. 22.07.2016; опубл. 26.06.2017.
2. Матвеев К.И., Жижина Е.Г., Одяков В.Ф. Катализатор и способ получения метилэтилкетона: пат. РФ 2230612. Заявка № 2003109070/04; заявл. 31.03.2003; опубл. 20.06.2004.
3. Матвеев К.И., Жижина Е.Г., Одяков В.Ф., Пармон В.Н. Гомогенные катализаторы окислительно-восстановительных процессов на основе растворов гетерополикислот. I. Результаты пилотных испытаний катализатора и процесса синтеза метилэтилкетона. *Катализ в промышленности.* 2014;3:32–42.
4. Жижина Е.Г., Одяков В.Ф., Балашов А.Л., Матвеев К.И. Разработка новой технологии каталитического синтеза метилэтилкетона окислением *н*-бутиленов. *Катализ в промышленности*. 2005;5:28–35.
5. Агагусейнова М.М., Амануллаева Г.И., Байрамова З.Э. Катализаторы окисления бутена-1 в метилэтилкетон. *Известия вузов: Химия и хим. технология.* 2018;61(2):53–57. https://doi.org/10.6060/tcct.20186102.5693
6. Torres-Vinces L., Contreras-Zarazua G., Huerta-Rosas B., Saŕnchez-Ramıŕrez E., Segovia-Hernaŕndez J.G. Methyl Ethyl Ketone Production through an Intensified Process. *Chem. Eng. Technol*. 2020;43(7):1433–1441. https://doi.org/10.1002/ceat.201900664

6. Torres-Vinces L., Contreras-Zarazua G., Huerta-Rosas B., Sarnchez-Ramırrez E., Segovia-Hernarndez J.G. Methyl Ethyl Ketone Production through an Intensified Process. *Chem. Eng. Technol*. 2020;43(7):1433–1441. https://doi.org/10.1002/ceat.201900664
7. Azizov M.A., Karimov R.H. Transformation of alcohols into carbonyl compounds on the D-53 catalyst. *Khimicheskaya promyshlennost’ = Chemical Industry*. 1982;10:7–12 (in Russ.).
8. Zak T.S. *Preparation of Methyl Ethyl Ketone*: USA Pat. 4075128. Publ. 21.02.1978.
9. Halawy S.A., Osman A.I., Abdelkader A., Yang H. Boosting NiO Catalytic Activity by x wt % F-ions and K_2O for the Production of Methyl Ethyl Ketone (MEK) via Catalytic Dehydrogenation of 2-Butanol. *ChemCatChem*. 2021;13(9):2200–2214. https://doi.org/10.1002/cctc.202001954
10. Galanov S.I., Golovachev V.A., Dubkov K.A., Zuber V.I., Miroshkina V.D., Mutas I.N., Reshetnikov D.M., Fedotov K.V., Kharitonov A.S. *Method of Producing Methyl Ethyl Ketone*: RF Pat. RU 2731903. Publ. 09.09.2020 (in Russ.).
11. Torlova A.S., Vitkalova I.A., Pikalov E.S. Production technology, properties and applications of compositions based on phenol-formaldehyde resins. *Nauchnoe obozrenie. Tekhnicheskie nauki = Scientific Review. Technical Sciences*. 2017;2:96–114 (in Russ.).
12. Kharlampovich G.D., Churkin Yu.V. *Fenoly* (*Phenols).* Moscow: Khimiya; 1974. 376 p. (in Russ.).
13. Kruzhalov B.D., Golovanenko B.I. *Sovmestnoe poluchenie fenola i atsetona* (*Joint Production of Phenol and Acetone*). Moscow: Goskhimizdat; 1963. 200 p. (in Russ.).
14. Antonovskii V.L., Buzlanova M.M. *Analiticheskaya khimiya organicheskikh peroksidnykh soedinenii* (*Analytical Chemistry of Organic Peroxide Compounds*). Moscow: Khimiya; 1978. 309 p. (in Russ.).
15. Yarkina E.M., Kurganova E.A., Frolov A.S., Koshel G.N., Nesterova T.N., Shakun V.A., Spiridonov S.A. *Para-tert*-butylcumyl synthesis. *Tonk. Khim. Tekhnol. = Fine Chem. Technol*. 2020;16(1):26–35. https://doi.org/10.32362/2410-6593-2020-16-1-26-35
16. Sapunov V.N., Kurganova E.A., Koshel G.N. Kinetics and Mechanism of Cumene Oxidation Initiated by *N*-Hydroxyphthalimide. *Int. J. Chem. Kinet*. 2018;50(1):3–14. https://doi.org/10.1002/kin.21135
17. Kabanova V.S., Kurganova E.A., Frolov A.S., Koshel G.N., Smurova A.A., Baev E.I., Danilova A.S. Acid-catalyzed decomposition of *sec*-butylbenzene hydroperoxide to phenol and methyl ethyl ketone. *Khimicheskaya promyshlennost’ segodnya = Chemical Industry Developments*. 2024;4:77–84 (in Russ.).
18. Minachev Kh.M., Kononov N.F., Mortikov E.S., Lent’ev A.S., Papko T.S., Zhomov A.K., Khlopochkin B.P., Masloboev-Shvedov A.A. *Method of Obtaining Second-Butylbenzene*: USSR Pat. 265349. Publ. 05.10.1976 (in Russ.).
19. Isakov Ya.I., Minachev Kh.M., Eidus Ya.T., Lapidus A.L., Kalinin V.P. *Method of Co-Production of Ethylbenzene and Secondary Benzene*: USSR Pat. 417405. Publ. 28.02.1974 (in Russ.).
20. Zakoshanskii V.M. *Fenol i atseton. Analiz tekhnologii, kinetiki i mekhanizma osnovnykh reaktsii* (*Phenol and Acetone. Analysis of Technologies, Kinetics and Mechanisms of Main Reactions*). St. Petersburg: Khimizdat; 2009. 590 p. (in Russ.).
21. Koshel G.N., Smirnova E.V., Kurganova E.A., Ekimova I.D., Lebedeva N.V., Koshel S.G., Plakhtinskii V.V. Intensification of the isopropylbenzene oxidation process. *Kataliz v Promyshlennosti.* 2010;3:26–29 (in Russ.).

7. Азизов М.А., Каримов Р.Х. Превращение спиртов в карбонильные соединения на катализаторе Д-53. *Химическая промышленность*. 1982;10:7–12.
8. Zak T.S. *Preparation of Methyl Ethyl Ketone*: USA Pat. 4075128. Publ. 21.02.1978.
9. Halawy S.A., Osman A.I., Abdelkader A., Yang H. Boosting NiO Catalytic Activity by x wt % F-ions and K_2O for the Production of Methyl Ethyl Ketone (MEK) via Catalytic Dehydrogenation of 2-Butanol. *ChemCatChem*. 2021;13(9):2200–2214. https://doi.org/10.1002/cctc.202001954
10. Галанов С.И., Головачев В.А., Дубков К.А., Зубер В.И., Мирошкина В.Д., Мутас И.Н., Решетников Д.М., Федотов К.В., Харитонов А.С. *Способ получения метилэтилкетона*: пат. РФ 2731903. Заявка № 2020112471; заявл. 27.03.2020; опубл. 09.09.2020.
11. Торлова А.С., Виткалова И.А., Пикалов Е.С. Технологии производства, свойства и области применения композиций на основе фенолформальдегидных смол. *Научное обозрение. Технические науки.* 2017;2:96–114.
12. Харлампович Г.Д., Чуркин Ю.В. *Фенолы*. М.: Химия; 1974. 376 с.
13. Кружалов Б.Д., Голованенко Б.И. *Совместное получение фенола и ацетона*. М.: Госхимиздат; 1963. 200 с.
14. Антоновский В.Л., Бузланова М.М. *Аналитическая химия органических пероксидных соединений.* М: Химия; 1978. 309 с.
15. Яркина Е.М., Курганова Е.А., Фролов А.С., Кошель Г.Н., Нестерова Т.Н., Шакун В.А., Спиридонов С.А. Синтез *пара-трет*-бутилкумола. *Тонкие химические технологии*. 2020;16(1):26–35. https://doi.org/10.32362/2410-6593-2020-16-1-26-35
16. Sapunov V.N., Kurganova E.A., Koshel G.N. Kinetics and Mechanism of Cumene Oxidation Initiated by *N*-Hydroxyphthalimide. *Int. J. Chem. Kinet*. 2018;50(1):3–14. https://doi.org/10.1002/kin.21135
17. Кабанова В.С., Курганова Е.А., Фролов А.С., Кошель Г.Н., Смурова А.А., Баёв Е.И., Данилова А.С. Кислотно-каталитическое разложение гидропероксида *втор*-бутилбензола до фенола и метилэтилкетона. *Химическая промышленность сегодня*. 2024;4:77–84.
18. Миначев Х.М., Кононов Н.Ф., Мортиков Е.С., Лентьев А.С., Папко Т.С., Жомов А.К., Хлопочкин Б.П., Маслобоев-Шведов А.А. *Способ получения втор-бутилбензола:* А.с. СССР 265349. Заявка № 1262711/23-4; заявл. 03.08.1968; опубл. 05.10.1976.
19. Исаков Я.И., Миначев Х.М., Эйдус Я.Т., Лапидус А.Л., Калинин В.П. *Способ совместного получения этилбензола и вторичного бензола:* А.с. СССР 417405. Заявка № 1789169/23-4; заявл. 26.05.1972; опубл. 28.02.1974.
20. Закошанский В.М. *Фенол и ацетон. Анализ технологий, кинетики и механизма основных реакций*. СПб.: Химиздат; 2009. 590 с.
21. Кошель Г.Н., Смирнова Е.В., Курганова Е.А., Екимова И.Д., Лебедева Н.В., Кошель С.Г., Плахтинский В.В. Интенсификация процесса окисления изопропилбензола. *Катализ в промышленности.* 2010;(3):26–29.
22. Курганова Е.А., Кабанова В.С., Фролов А.С., Кошель Г.Н., Смурова А.А., Баёв Е.И. Гидропероксидный способ синтеза фенола и его алкильных производных совместно с кетонами алифатического и алициклического ряда. *Neftegaz.RU*. 2023;137(5):34–40.

22. Kurganova E.A., Kabanova V.S., Frolov A.S., Koshel G.N., Smurova A.A., Baev E.I. Hydroperoxide method of synthesis of phenol and its alkyl derivatives together with ketones of the aliphatic and alicyclic series. *Neftegaz.RU*. 2023;137(5): 34–40 (in Russ.).

About the authors

Viktoriya S. Kabanova, Postgraduate Student, Department of General and Physical Chemistry, Yaroslavl State Technical University (88, Moskovskii pr., Yaroslavl, 150023, Russia). E-mail: kabanovavs@ystu.ru. Scopus Author ID 57749250400, RSCI SPIN-code 1221-0200, https://orcid.org/0000-0001-6635-6315

Ekaterina A. Kurganova, Dr. Sci. (Chem.), Professor, Department of General and Physical Chemistry, Yaroslavl State Technical University (88, Moskovskii pr., Yaroslavl, 150023, Russia). E-mail: kurganovaea@ystu.ru. Scopus Author ID 24338325800, ResearcherID B-4021-2018, RSCI SPIN-code 2617-8020, https://orcid.org/0000-0002-0087-1784

Aleksandr S. Frolov, Cand. Sci. (Chem.), Associate Professor, Department of General and Physical Chemistry, Yaroslavl State Technical University (88, Moskovskii pr., Yaroslavl, 150023, Russia). E-mail: frolovas@ystu.ru. Scopus Author ID 56412435400, ResearcherID I-8533-2018, RSCI SPIN-code 4081-9087, https://orcid.org/0000-0002-0491-7452

Georgiy N. Koshel, Dr. Sci. (Chem.), Professor, Department of General and Physical Chemistry, Yaroslavl State Technical University (88, Moskovskii pr., Yaroslavl, 150023, Russia). E-mail: koshelgn@ystu.ru. Scopus Author ID 6602886373, ResearcherID I-7782-2017, RSCI SPIN-code 1119-6642, https://orcid.org/0000-0002-1020-4643

Alina A. Smurova, Postgraduate Student, Department of General and Physical Chemistry, Yaroslavl State Technical University (88, Moskovskii pr., Yaroslavl, 150023, Russia). E-mail: smurovaaa@mail.ru. Scopus Author ID 58870183900, RSCI SPIN-code 2706-8704, https://orcid.org/0000-0002-5280-7573

Egor I. Bayov, Postgraduate Student, Department of General and Physical Chemistry, Yaroslavl State Technical University (88, Moskovskii pr., Yaroslavl, 150023, Russia). E-mail: baevei@mail.ru. ResearcherID JOK-1491-2023, RSCI SPIN-code 4586-8520, https://orcid.org/0009-0009-3997-1641

Об авторах

Кабанова Виктория Сергеевна, аспирант, кафедра «Общая и физическая химия», ФГБОУ ВО «Ярославский государственный технический университет» (150023, Россия, Ярославль, Московский пр-т, д 88). E-mail: kabanovavs@ystu.ru. Scopus Author ID 57749250400, SPIN-код РИНЦ 1221-0200, https://orcid.org/0000-0001-6635-6315

Курганова Екатерина Анатольевна, д.х.н., доцент, профессор кафедры «Общая и физическая химия», ФГБОУ ВО «Ярославский государственный технический университет» (150023, Россия, Ярославль, Московский пр-т, д. 88). E-mail: kurganovaea@ystu.ru. Scopus Author ID 24338325800, ResearcherID B-4021-2018, SPIN-код РИНЦ 2617-8020, https://orcid.org/0000-0002-0087-1784

Фролов Александр Сергеевич, к.х.н., доцент кафедры «Общая и физическая химия», ФГБОУ ВО «Ярославский государственный технический университет» (150023, Россия, Ярославль, Московский пр-т, д. 88). E-mail: frolovas@ystu.ru. Scopus Author ID 56412435400, ResearcherID I-8533-2018, SPIN-код РИНЦ 4081-9087, https://orcid.org/0000-0002-0491-7452

Кошель Георгий Николаевич, д.х.н., профессор, профессор кафедры «Общая и физическая химия», ФГБОУ ВО «Ярославский государственный технический университет» (150023, Россия, Ярославль, Московский пр-т, д. 88). E-mail: koshelgn@ystu.ru. Scopus Author ID 6602886373, ResearcherID I-7782-2017, SPIN-код РИНЦ 1119-6642, https://orcid.org/0000-0002-1020-4643

Смурова Алина Александровна, аспирант, кафедра «Общая и физическая химия», ФГБОУ ВО «Ярославский государственный технический университет» (150023, Россия, Ярославль, Московский пр-т, д. 88). E-mail: smurovaaa@mail.ru. Scopus Author ID 58870183900, SPIN-код РИНЦ 2706-8704, https://orcid.org/0000-0002-5280-7573

Баёв Егор Игоревич, аспирант, кафедра «Общая и физическая химия», ФГБОУ ВО «Ярославский государственный технический университет» (150023, Россия, Ярославль, Московский пр-т, д 88). E-mail: baevei@mail.ru. ResearcherID JOK-1491-2023, SPIN-код РИНЦ 4586-8520, https://orcid.org/0009-0009-3997-1641

Translated from Russian into English by V. Glyanchenko
Edited for English language and spelling by Thomas A. Beavitt

Tonkie Khimicheskie Tekhnologii = Fine Chemical Technologies.
2025;20(1):18–26
ISSN 2686-7575 (Online)

UDC 547.333+544.47
https://doi.org/10.32362/2410-6593-2025-20-1-18-26
EDN ILGHIV

RESEARCH ARTICLE

Development of new supported catalysts for the continuous alkylation of amines with alcohols

Vladimir M. Mokhov✉, Denis N. Nebykov, Aleksandr O. Panov, Anastasiya V. Razvalyaeva, Snezhana E. Latyshova, Marat A. Vaniev
Volgograd State Technical University, Volgograd, 400005 Russia
✉ *Corresponding author, e-mail: tons@vstu.ru*

Abstract

Objectives. The work set out to develop catalysts based on nickel and copper obtained by active phase chemical reduction and investigate their activity including the influence of the type of supports on the course of alkylation of amines with primary or secondary alcohols in a plug-flow reactor with a fixed catalyst bed.

Methods. The reactions were carried out in a continuous mode on a fixed bed of an appropriate catalyst in a plug flow microcatalytic apparatus at 160–240°C. NaX zeolite, magnesium oxide, and γ-Al_2O_3 were used as supports. After preparing the catalysts by impregnation from an excess solution of metal salts, the active metal phase was reduced with a sodium tetrahydridoborate aqueous solution. The composition of the resulting products was analyzed by gas–liquid chromatography, while their structure was confirmed by gas chromatography-mass spectrometry. The alkylating agents were ethanol, 2-propanol, 1-butanol, 1-pentanol, benzyl alcohol, and 1-octanol; alkylated amines were 1-butylamine, 1-hexylamine, 1-octylamine, aniline, morpholine, piperidine, and hexamethyleneimine.

Results. The alkylation of amines with alcohols catalyzed by metal (nickel and copper) nanoparticles supported on NaX zeolite, magnesium oxide MgO, and γ-Al_2O_3 in a plug-flow reactor with a fixed catalyst bed at atmospheric hydrogen pressure and 160–240°C leads to the formation of predominantly mono-*N*-alkylated products with yields up to 99%.

Conclusions. Nickel (or nickel and copper) nanoparticles supported on various supports are effective catalysts for the synthesis of secondary or tertiary amines in the plug-flow reactor.

Keywords

catalysis, nanoparticles, nickel, alkylation, alkanols

Submitted: 03.04.2024
Revised: 17.10.2024
Accepted: 23.12.2024

For citation

Mokhov V.M., Nebykov D.N., Panov A.O., Razvalyaeva A.V., Latyshova S.E., Vaniev M.A. Development of new supported catalysts for the continuous alkylation of amines with alcohols. *Tonk. Khim. Tekhnol. = Fine Chem. Technol.* 2025;20(1):18–26. https://doi.org/10.32362/2410-6593-2025-20-1-18-26

НАУЧНАЯ СТАТЬЯ

Разработка новых нанесенных катализаторов непрерывного алкилирования аминов спиртами

В.М. Мохов✉, Д.Н. Небыков, А.О. Панов, А.В. Разваляева, С.Е. Латышова, М.А. Ваниев

Волгоградский государственный технический университет, Волгоград, 400005 Россия

✉*Автор для переписки, e-mail: tons@vstu.ru*

Аннотация

Цели. Расширение исследований по разработке катализаторов на основе никеля и меди, получаемых химическим восстановлением активной фазы, и по изучению влияния типа носителей на их активность в процессах алкилирования аминов первичными и вторичными спиртами в проточном реакторе с неподвижным слоем катализатора.

Методы. Процесс осуществлялся на неподвижном слое исследуемых катализаторов в проточной микрокаталитической установке при 160–240°С. В качестве носителей были использованы цеолит γ-Al_2O_3, NaX, оксид магния. Катализаторы готовились методом пропитки адсорбцией из избытка раствора солей металлов. Восстановление активной металлической фазы проводилось водным раствором тетрагидридобората натрия. Субстратами выступали первичные или вторичные амины: 1-бутиламин, 1-гексиламин, 1-октиламин, анилин, морфолин, пиперидин, гексаметиленимин. Алкилирующими агентами являлись этанол, пропанол-2, бутанол-1, пентанол-1, бензиловый спирт, октанол-1. Состав полученных продуктов анализировался газожидкостной хроматографией, их строение подтверждалось методом хромато-масс спектрометрии.

Результаты. Алкилирование спиртами аминов при катализе частицами металлов (никеля и меди), нанесенными на цеолит NaX, оксид магния MgO и γ-Al_2O_3, в проточном реакторе с неподвижным слоем катализатора при 160–240°С и атмосферном давлении водорода приводит к образованию преимущественно моно-*N*-алкилированных продуктов с выходами до 99%.

Выводы. Наночастицы никеля (или никеля и меди), нанесенные на различные носители, являются эффективными катализаторами синтеза вторичных или третичных аминов в проточном реакторе с неподвижным слоем катализатора.

Ключевые слова

катализ, наночастицы, никель, алкилирование, амины, алканолы

Поступила: 03.04.2024
Доработана: 17.10.2024
Принята в печать: 23.12.2024

Для цитирования

Мохов В.М., Небыков Д.Н., Панов А.О., Разваляева А.В., Латышова С.Е., Ваниев М.А. Разработка новых нанесенных катализаторов непрерывного алкилирования аминов спиртами. *Тонкие химические технологии*. 2025;20(1):18–26. https://doi.org/10.32362/2410-6593-2025-20-1-18-26

INTRODUCTION

Di- and trialkylamines are of high practical importance as vulcanization accelerators and intermediate products in the production of surfactants, antioxidants, pesticides, corrosion inhibitors, absorbents, solvents, extractants, etc. The products of alkylation at the nitrogen atom are additionally used as catalysts in the synthesis of polycondensation polymers. The most applicable industrial-scale method for the synthesis of these chemicals is catalytic *N*-alkylation of ammonia or primary amines with alcohols. The advantages of this method including the wide availability of reagents and the formation of water as the only byproduct [1, 2].

Currently, the main direction of research is the development of effective catalysts for this process. For the purposes of *N*-alkylation, oxides [3–5], salts, complexes [6, 7], and nanoparticles of metals of variable valence [8–10] are used as catalysts. However, supported metal catalysts that combine the implementation of the alkylation process at moderate temperatures and ease of separation from the reaction mass are of greatest practical interest.

The authors of [11] studied aniline *N*-alkylation with benzyl alcohol in the presence of Ru/CeO_2. The reaction was carried out at 160°C using *p*-xylene as a solvent under an N_2 atmosphere for 24 h. The yield of the product was found to strongly depend on the support morphology. Ru/CeO_2–R with a rod morphology exhibits both higher activity and selectivity for the formation of *N*-benzylaniline (yield 88%) than cubic Ru/CeO_2–C (52%) and octahedral Ru/CeO_2–O (32%).

A copper catalyst on a porous *N,P*-doped carbon support obtained from wheat straw showed efficiency in the *N*-monoalkylation of aromatic amines with aromatic alcohols. The reaction was carried out in cyclohexane as a solvent at 140°C under an argon atmosphere for 12 h. Anilines containing electron-donating groups were converted into the corresponding secondary amines in yields of 66–91% [12].

A catalyst based on palladium and carbon nitride C_3N_4 showed high activity in the synthesis of *N*-substituted aminopyridine with good regenerability indices. When carrying out the synthesis at 110°C in toluene for 12 h, the yield of the target product was 95% [13].

The authors of [14] studied the use of a catalyst based on encapsulated platinum nanoparticles and beta-zeolite in the *N*-alkylation of amines with aromatic alcohols. When carrying out aniline alkylation with benzyl alcohol at 160°C for 2.5 h under an N_2 atmosphere (1 atm), the yield of the product was 93%.

The typically long time taken for the alkylation of amines with alkanols is due to the mechanism of this complex three-stage reaction. First, the alkanol undergoes reversible dehydrogenation into an aldehyde (ketone), which then condenses with the amine; the final product is formed from the intermediate aldimine (ketimine) following its hydrogenation. As a result, a periodic method for implementing this type of process is more common. In [15], the use of nickel or copper nanoparticles deposited on γ-Al_2O_3 by a modified coprecipitation method as catalysts for the alkylation of amines with alkanols was investigated. Using this approach, it was possible to obtain target products in a continuous mode with high yields and selectivity up to 100% at 180–220°C and atmospheric hydrogen pressure.

The purpose of the present work is to accumulate the research of a group of authors on the study of the activity of catalysts based on nickel and copper nanoparticles deposited on various substrates in the continuous process of alkylation of amines with alkanols in a flow reactor with a fixed catalyst bed.

MATERIALS AND METHODS

Zeolite NaX, MgO, γ-Al_2O_3 (*EKROS*, Russia) were used as supports. The catalysts were prepared by adsorption impregnation without coprecipitants; the active metal phase was reduced with an aqueous solution of sodium tetrahydridoborate (*EKROS*, Russia). The metal content in the resulting catalysts was (wt %): Ni/MgO: 23.8; Ni/Al_2O_3: 5.0; Ni/NaX: 5.6; NiCu/Al_2O_3: Ni, 2.4, Cu, 2.3; NiCu/NaX: Ni, 5, Cu, 5.

The following primary or secondary amines served as substrates: 1-butylamine, 1-hexylamine, 1-octylamine, aniline, morpholine, piperidine, and hexamethyleneimine (*EKROS*, Russia). The alkylating agents were ethanol, 2-propanol, 1-butanol, 1-pentanol, benzyl alcohol, and 1-octanol (*EKROS*, Russia). The process was carried out using a flow-through microcatalytic unit (*Meta-Khrom*, Russia) in continuous mode on a fixed catalyst bed at 160–240°C. A small amount of hydrogen was supplied using a GV-7 hydrogen generator (*Meta-Khrom*, Russia) as a diluent and for exhaustive hydrogenation of intermediate imines or enamines (Figure).

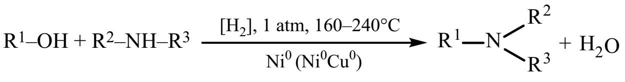

1a–f **2a–g** **3a–m**

R^1 = Et (**1a**), *i*-Pr (**1b**), Bu (**1c**), C_5H_{11} (**1d**), $C_6H_5CH_2$ (**1e**), C_8H_{17} (**1f**).
R^2 = H; R^3 = Bu (**2a**), C_6H_{13} (**2b**), C_8H_{17} (**2c**), C_6H_5 (**2d**);
R^2–R^3 = $(CH_2CH_2)_2O$ (**2e**), $(CH_2)_5$ (**2f**), $(CH_2)_6$ (**2g**).
R^1 = *i*-Pr, R^2 = H, R^3 = C_6H_{13} (**3a**), C_8H_{17} (**3b**);
R^1 = Bu, R^2–R^3 = $(CH_2)_5$ (**3c**); R^2 = H, R^3 = C_6H_5 (**3g**);
R^1 = C_5H_{11}, R^2–R^3 = $(CH_2)_5$ (**3d**); $(CH_2CH_2)_2O$ (**3e**);
R^2 = H, R^3 = C_6H_5 (**3h**); R^1 = Et, R^2 = H, R^3 = C_6H_5 (**3f**);
R^1 = $C_6H_5CH_2$, R^2 = H, R^3 = C_6H_{13} (**3i**); R^3 = C_8H_{17} (**3j**);
R^1 = C_8H_{17}, R^2 = H, R^3 = C_6H_{13} (**3k**); R^2–R^3 = $(CH_2)_5$ (**3l**);
R^2–R^3 = $(CH_2)_6$ (**3m**)

Fig. Reaction scheme

The composition of the catalyzate was established by gas–liquid chromatography. The structure of the target products **3a**–**m** was confirmed by chromatography-mass spectrometry. Chromatographic mass spectrometry was performed on a Saturn 2100 T/GC3900 instrument (*Varian*, USA) using electron impact (EI) ionization with an ionization energy of 70 eV. Chromatographic analysis was performed on a Crystallux 4000M chromatograph (*Meta-Khrom*, Russia) with an HP-5 column (*Agilent Technologies*, USA) at a column temperature of 100°C and evaporator temperature of 250°C. Scanning electron microscopy was performed using a FEI Versa 3D DualBeam instrument (*FEI*, USA). Elemental analysis was carried out by energy-dispersive X-ray spectroscopy (EDS) using FEI Versa 3D DualBeam (*FEI*, USA).

RESULTS AND DISCUSSION

At a temperature range of 180–220°C and atmospheric hydrogen pressure with a liquid reagent load of 1.8–3.6 L/(kg_{cat}·h), the conversion of the initial amines **2a**–**g** reached 99%. Nickel nanoparticles supported on MgO or Al_2O_3 were shown to selectively catalyze the monoalkylation of primary amines. In this case, the use of reagent ratios close to equimolar is accompanied by a side process of disproportionation of the initial primary amines, which was described earlier for the studied type of catalysts [16]. As the alkanol excess increases twofold, the selectivity for the target products increases to 98%. When using zeolite NaX as a substrate, the selectivity of the monoalkylation reaction of primary amines decreases, while forming up to 40% of tertiary amines [17].

Thus, the chemically reduced nickel phase on different supports demonstrated strong catalytic activity with high selectivity for the formation of monoalkylated products observed on MgO and γ-Al_2O_3. In addition to the excess of the initial alkanols, no traces of the corresponding carbonyl compounds were found in the catalyzate. This indicates that alkylation is limited by the alkanol dehydrogenation stage. Since copper is a known catalyst for alcohol dehydrogenation, it becomes interesting to study its promoting effect on the alkylation of amines with alkanols.

Further studies showed that the catalyst obtained by reducing nickel and copper ions coprecipitated in a 1 : 1 ratio on NaX zeolite (Ni^0Cu^0/NaX) or on pressed magnesium oxide (Ni^0Cu^0/NaX) was more effective as compared to the nickel ones described above. In particular, the target *N*-alkylanilines were obtained in 66–85% yields with a process selectivity of 83–89% by the alkylation of aniline with ethanol, 1-butanol or 1-pentanol at a temperature of 240°C on the Cu^0Ni^0/NaX catalyst. In addition to *N*-ethylaniline (**3f**) (71.1%), *N,N*-diethylaniline (13.5%) was formed. For alkanols with a higher molecular weight, an increase in selectivity was observed. For example, when obtaining *N*-1-butylaniline (**3g**), the conversion of aniline (**2g**) and the reaction selectivity took on maximum values (95.1% and 89.5%, respectively) [18].

Alkylation of morpholine (**2e**) with 1-pentanol (**1d**) on the Ni^0Cu^0/MgO catalyst occurs in the temperature range of 100–200°C at an increased morpholine conversion from 8 to 100% and 1-pentylmorpholine (**3e**) yield ranging from 4 to 92.5%. However, a similar nickel-free catalyst obtained by reducing copper chloride on magnesium oxide (Cu^0/MgO) showed low activity (the morpholine conversion at 200–220°C was 10–15%, while the yield of 1-pentylmorpholine was 4–14%). The conversion of morpholine during its alkylation with 1-pentanol on Ni^0/MgO or Ni^0/Al_2O_3 catalysts at 180°C did not exceed 50%, while the product yield was 36% (on Ni^0/Al_2O_3) and 18% (on Ni^0/MgO). In the latter case, 15% of the corresponding enamine is also formed. Thus, the activity of metals in the catalysis of this reaction is in the series Cu < Ni < Cu–Ni.

EXPERIMENTAL

The catalysts were prepared according to the methods described in [16–18].

Conducting reactions

Isopropyl-1-hexylamine (3a). Hydrogen was fed to the Cu^0Ni^0/Al_2O_3 catalyst at a flow rate of 1 L/h and a mixture of 2-propanol (**1b**) and 1-hexylamine (**2b**) with a molar ratio of **1b** : **2b** = 10 : 1 at a flow rate of 1.8 L/(kg_{cat}·h) at 220°C. Conversion of 1-hexylamine was 100%. Selectivity was 98%. The yield of isopropyl-1-hexylamine was 98%. Mass spectrum (EI, 70 eV), *m*/*z* (I_{rel}, %): 144.0 (17) [M^{+1}], 143.1 (23) [M], 72.0 (100), 44.2 (35), 30.3 (60).

Isopropyl-1-octylamine (3b). Hydrogen at a flow rate of 1 L/h and a mixture of 2-propanol (**1b**) and 1-octylamine (**2c**) with a molar ratio of **1b** : **2c** = 10 : 1 at a flow rate of 1.8 L/(kg_{cat}·h) at 180°C were fed to the Ni^0/Al_2O_3 catalyst. Conversion of 1-octylamine was 99%. Selectivity was 97%. The yield of isopropyl-1-octylamine was 96%. Mass spectrum (EI, 70 eV), *m*/*z* (I_{rel}, %): 172.2 (5) [M^{+1}], 171.1 (16) [M], 113.2 (100), 55.2 (6), 44.1 (26).

1-Butylpiperidine (3c). a) Hydrogen at a flow rate of 1 L/h and a mixture of 1-butanol (**1c**) and piperidine (**2f**) with a molar ratio of **1c** : **2f** = 2.5 : 1 at a flow rate of 1.8 L/(kg_{cat}·h) at 200°C were fed to the Cu^0Ni^0/Al_2O_3 catalyst. Piperidine conversion was 99%. Selectivity was 98%. The yield of 1-butylpiperidine was 97%. Mass spectrum (EI, 70 eV), *m*/*z* (I_{rel}, %): 141.9 (6) [M^{+1}], 140.7 (2) [M], 139.9 (5), 98.9 (6), 98 (100), 70 (10), 42.1 (7).

b) Hydrogen at a flow rate of 1 L/h and a mixture of 1-butanol (**1c**) and piperidine (**2f**) with a molar ratio of **1c** : **2f** = 2.5 : 1 at a flow rate of 1.8 L/(kg_{cat}·h) at 200°C were fed to the Ni^0/Al_2O_3 catalyst. Piperidine conversion was 99%. Selectivity was 92.4%. The yield of 1-butylpiperidine was 91.5%.

c) Hydrogen at a flow rate of 3 L/h and a mixture of 1-butanol (**1c**) and piperidine (**2f**) with a molar ratio of **1c** : **2f** = 4 : 1 at a flow rate of 1.8 L/(kg_{cat}·h) at 240°C were fed to the Ni^0/Al_2O_3 catalyst. Piperidine conversion was 45.5%. Selectivity was 100%. The yield of 1-butylpiperidine was 45.5%.

1-Pentylpiperidine (3d). Hydrogen at a flow rate of 3 L/h and a mixture of 1-pentanol (**1d**) and piperidine (**2f**) with a molar ratio of **1d** : **2f** = 3 : 1 at a flow rate of 1.8 L/(kg_{cat}·h) at 200°C were fed to the Cu^0Ni^0/Al_2O_3 catalyst. Piperidine conversion was 98.5%. Selectivity was 100%. The yield of 1-pentylpiperidine was 98.5%. Mass spectrum (EI, 70 eV), *m*/*z* (I_{rel}, %): 159.1 (2) [M^{+2}], 158.0 (32) [M^{+1}], 156.1 (6) [M], 126.0 (5), 100.0 (100), 98.3 (5), 70.1 (12), 56.1 (2).

1-Pentylmorpholine (3e). a) Hydrogen at a flow rate of 1 L/h and a mixture of 1-pentanol (**1d**) and morpholine (**2f**) with a molar ratio of **1d** : **2f** = 1 : 1 with a flow rate of 3.6 L/(kg_{cat}·h) at 240°C were fed to the Cu^0Ni^0/NaX catalyst.

Morpholine conversion was 85%. Selectivity was 97%. The yield of 1-pentylmorpholine was 82.5%. Mass spectrum (EI, 70 eV), *m*/*z* (I_{rel}, %): 158.1 (28) [M^{+1}], 100.1 (100), 99.2 (7), 70.1 (12).

b) Hydrogen at a flow rate of 1 L/h and a mixture of 1-pentanol (**1d**) and morpholine (**2f**) with a molar ratio of **1d** : **2f** = 3 : 1 with a flow rate of 1.8 L/(kg_{cat}·h) at 160°C were fed to the Cu^0Ni^0/MgO (1 : 1) catalyst. Morpholine conversion was 99.5%. Selectivity was 93%. The yield of 1-pentylmorpholine was 92.5%.

c) Hydrogen at a flow rate of 1 L/h and a mixture of 1-pentanol (**1d**) and morpholine (**2f**) with a molar ratio of **1d** : **2f** = 5 : 1 at a flow rate of 1.8 L/(kg_{cat}·h) at 180°C were fed to the Ni^0/Al_2O_3 catalyst. Morpholine conversion was 50.3%. Selectivity was 98%. The yield of 1-pentylmorpholine was 49.3%.

d) Hydrogen at a flow rate of 1 L/h and a mixture of 1-pentanol (**1d**) and morpholine (**2f**) with a molar ratio of **1d** : **2f** = 5 : 1 at a flow rate of 1.8 L/(kg_{cat}·h) at 220 °C were fed to the Cu^0/MgO catalyst. Morpholine conversion was 25%. Selectivity was 98%. The yield of 1-pentylmorpholine was 24.5%.

The compounds *N*-ethylaniline (**3f**), *N*-1-butylaniline (**3g**), *N*-1-pentylaniline (**3h**) were prepared in a manner similar to that described in [18].

***N*-Benzyl-1-hexylamine (3i).** Hydrogen at a flow rate of 0.3 L/h and a mixture of benzyl alcohol (**1e**) and 1-hexylamine (**2b**) with a molar ratio of **1e** : **2b** = 1 : 1 at a flow rate of 3.6 L/(kg_{cat}·h) at 240°C were fed to the Ni^0/NaX catalyst. The conversion of 1-hexylamine was 98%. Selectivity was 70%. The yield of *N*-benzyl-1-hexylamine was 68.6%, mass spectrum (EI, 70 eV), *m*/*z* (I_{rel}, %): 193.0 (4) [M^{+2}], 192.0 (32) [M^{+1}], 190.1 (4), 119.8 (65), 106.0 (15), 92.0 (8), 91.1 (100), 65.0 (9), 41.0 (5). The yield of di-1-hexylamine (byproduct) was 24.2%, mass spectrum (EI, 70 eV), *m*/*z* (I_{rel}, %): 187.0 (12) [M^{+2}], 186.1 (100) [M^{+1}], 184.3 (2), 114.2 (34), 44.0 (84), 41.0 (7). The yield of *N*-hexyl-1-benzylimine (byproduct) was 5.3%, mass spectrum (EI, 70 eV), *m*/*z* (I_{rel}, %): 191.0 (5) [M^{+2}], 190.1 (31) [M^{+1}], 189.0 (2) [M^{+}], 174.0 (7), 160.0 (100), 146.1 (10), 131.9 (34), 118.0 (54), 104.0 (23), 91.1 (78), 77.1 (11), 65.0 (11), 41.0 (13.5).

***N*-Benzyl-1-octylamine (3j)**. Hydrogen at a flow rate of 0.3 L/h and a mixture of benzyl alcohol (**1e**) and 1-octylamine (**2c**) with a molar ratio of **1e** : **2c** = 1.1 : 1 were fed to the Ni^0/NaX catalyst at a flow rate of 1.8 L/(kg_{cat}·h) at 220°C. The conversion of 1-octylamine was 98.5%. Selectivity was 53.3%. *N*-Benzyl-1-octylamine, yield 52.5%, mass spectrum (EI, 70 eV), *m*/*z* (I_{rel}, %): 220.1 (51) [M^{+2}], 218.2 (5) [M], 128.0 (8), 121.0 (7), 119.9 (80), 106.0 (13.6), 92.0 (7.4), 91.1 (100), 65.0 (8), 41.0 (7). Benzyl-1-octylimine (byproduct), yield 6.3%, mass spectrum (EI, 70 eV), *m*/*z* (I_{rel}, %): 218.1 (97) [M^{+2}], 216.2 (7) [M], 174.1 (19), 160.0 (100), 132.1 (26), 118.2 (41), 91.1 (45), 77.2 (5), 65 (7), 51.0 (6), 41.0 (14). Di-1-octylamine (byproduct), yield 40.2%, mass spectrum (EI, 70 eV), *m*/*z* (I_{rel}, %): 243.3 (16) [M^{+2}], 242.3 (100) [M^{+1}], 142.2 (9.4), 44.0 (44).

***N*-1-Hexyl-1-octylamine (3k)**. Hydrogen at a flow rate of 3 L/h and a mixture of 1-octanol (**1f**) and 1-hexylamine (**2b**) with a molar ratio of **1f** : **2b** = 2 : 1 at a flow rate of 1.8 L/(kg_{cat}·h) at 220°C were fed to the Ni^0/MgO catalyst. The conversion of 1-hexylamine was 99%. Selectivity was 98%. The yield of *N*-1-hexyl-1-octylamine was 97%. Mass spectrum (EI, 70 eV), *m*/*z* (I_{rel}, %): 215.1 (14.5) [M^{+2}], 214.2 (83) [M^{+1}], 212.3 (4), 142.0 (21), 114.0 (31), 44.0 (100).

1-Octylpiperidine (3l). Hydrogen at a flow rate of 4 L/h and a mixture of 1-octanol (**1f**) and piperidine (**2f**) with a molar ratio of **1f** : **2f** = 3 : 1 at a flow rate of 1.8 L/(kg_{cat}·h) at 180°C were fed to the Cu^0Ni^0/NaX catalyst. Piperidine conversion was 93.7%. Selectivity was 100%. The yield of 1-oct-1-yl-piperidine was 93.7%. Mass spectrum (EI, 70 eV), *m*/*z* (I_{rel}, %): 199.1 (4) [M^{+2}], 198.2 (25) [M^{+1}], 196.2 (8), 98.2 (100), 70.2 (8).

1-Octyl-1-azacycloheptane (3m). Hydrogen at a flow rate of 2 L/h and a mixture of 1-octanol (**1f**) and hexamethyleneimine (**2g**) with a molar ratio of **1f** : **2g** = 3 : 1 with a flow rate of 1.8 L/(kg_{cat}·h) at 240°C were fed to the Ni^0/Al_2O_3 catalyst. Hexamethyleneimine conversion was 97%. Selectivity was 100%. The yield of 1-octyl-1-azacycloheptane was 97%. Mass spectrum (EI, 70 eV), *m*/*z* (I_{rel}, %): 211.0 (10) [M], 99 (7), 98.1 (100).

CONCLUSIONS

The reported studies confirm that heterogeneous catalysts containing nickel (or nickel and copper) nanoparticles obtained by chemical reduction and deposited on various carriers (zeolite NaX, magnesium oxide MgO, γ-Al_2O_3) in amine alkylation reactions with alcohols in the temperature range of 160–240°C and at atmospheric pressure exhibit high catalytic activity to obtain target products with yields of up to 99% and selectivity of 53–100% in a continuous process mode.

Acknowledgments

The study was financially supported by the Ministry of Science and Higher Education of the Russian Federation (project No. FZUS-2023-0007 based on Agreement No. 075-03-2024-126, January 17, 2024, with amendments).

Authors' contributions

V.M. Mokhov—developing the experiment, conducting experimental studies, writing the text of the article.

D.N. Nebykov—developing the research concept, analyzing the results, writing the text of the article.

A.O. Panov—conducting experimental studies, writing the text of the article.

A.V. Razvalyaeva—conducting experimental studies, writing the text of the article.

S.E. Latyshova—analyzing the results, writing the text of the article.

M.A. Vaniev—scientific consulting, writing the text of the article.

The authors declare no conflicts of interest.

REFERENCES

1. Hayes K.S. Industrial processes for manufacturing amines. *Appl. Catal. A: Gen.* 2001;221(1):187–195. https://doi.org/10.1016/S0926-860X(01)00813-4
2. Bayguzina A.R., Khusnutdinov R.I. Catalytic *N*-Alkylation of Anilines. *Russ. J. Gen. Chem*. 2021;91(3):305–347. https://doi.org/10.1134/S1070363221030014
   [Original Russian Text: Bayguzina A.R., Khusnutdinov R.I. Catalytic *N*-Alkylation of Anilines. *Zhurnal Obshchei Khimii*. 2021;91(3):331–375 (in Russ.). https://doi.org/10.31857/S0044460X2103001X]
3. Brown A.B., Reid E.E. Catalytic alkylation of aniline *J. Am. Chem. Soc.* 1924;46(8):1836–1839. https://doi.org/10.1021/ja01673a011
4. Chen A., Wang H., Liu R., Bo Y., Hu J. *N*-Alkylation of Alkylolamines with Alcohols Over Mesoporous Solid Acid–Base Cs–B–Zr Catalyst. *Catal. Lett.* 2016;146(7):1182–1193. https://doi.org/10.1007/s10562-016-1737-2
5. Niu F., Wang Q., Yan Z., Kusema B.T., Khodakov A.Y., Ordomsky V.V. Highly Efficient and Selective *N*-Alkylation of Amines with Alcohols Catalyzed by *in Situ* Rehydrated Titanium Hydroxide. *ACS Catal*. 2020;10(5):3404−3414. https://doi.org/10.1021/acscatal.9b05525
6. Bayguzina A.R., Khusnutdinov R.I., Musina C.F. *N*-Alkylation of Aniline and Its Derivatives by Alcohols in the Presence of Copper Compounds. *Russ. J. Org. Chem*. 2018;54(11):1652–1659. https://doi.org/10.1134/S1070428018110052
   [Original Russian Text: Bayguzina A.R., Musina C.F., Khusnutdinov R.I. *N*-Alkylation of Aniline and Its Derivatives by Alcohols in the Presence of Copper Compounds. *Zhurnal Organicheskoi Khimii.* 2018;54(11):1642–1648 (in Russ.). https://doi.org/10.1134/S0514749218110055]
7. Yan T., Feringa B.L., Barta K. Iron catalysed direct alkylation of amines with alcohols. *Nat. Commun*. 2014;5:5602. https://doi.org/10.1038/ncomms6602
8. Ma Z., Zhou B., Li X., Kadam R.G., Gawande M.B., Petr M., Zboril R., Beller M., Jagadeesh R.V. Reusable Co-nanoparticles for general and selective *N*-alkylation of amines and ammonia with alcohols. *Chem. Sci*. 2022;13(1):111–117. https://doi.org/10.1039/d1sc05913k
9. Wang G., Sun L., Liu W., Zhan H., Bi S. Iron-nickel alloy particles with *N*-doped carbon “armor” as a highly selective and long-lasting catalyst for the synthesis of *N*-benzylaniline molecules. *Nano Res*. 2024;17(4):2308–2319. https://doi.org/10.1007/s12274-023-6041-z

СПИСОК ЛИТЕРАТУРЫ

1. Hayes K.S. Industrial processes for manufacturing amines. *Appl. Catal. A: Gen.* 2001;221(1):187–195. https://doi.org/10.1016/S0926-860X(01)00813-4
2. Байгузина А.Р., Хуснутдинов Р.И. Каталитическое *N*-алкилирование анилинов. *Журн. общей химии.* 2021;91(3):331–375. https://doi.org/10.31857/S0044460X2103001X
3. Brown A.B., Reid E.E. Catalytic alkylation of aniline *J. Am. Chem. Soc.* 1924;46(8):1836–1839. https://doi.org/10.1021/ja01673a011
4. Chen A., Wang H., Liu R., Bo Y., Hu J. *N*-Alkylation of Alkylolamines with Alcohols Over Mesoporous Solid Acid–Base Cs–B–Zr Catalyst. *Catal. Lett.* 2016;146(7):1182–1193. https://doi.org/10.1007/s10562-016-1737-2
5. Niu F., Wang Q., Yan Z., Kusema B.T., Khodakov A.Y., Ordomsky V.V. Highly Efficient and Selective *N*-Alkylation of Amines with Alcohols Catalyzed by *in Situ* Rehydrated Titanium Hydroxide. *ACS Catal*. 2020;10(5):3404−3414. https://doi.org/10.1021/acscatal.9b05525
6. Байгузина А.Р., Мусина Ч.Ф., Хуснутдинов Р.И. *N*-Алкилирование анилина и его производных спиртами в присутствии соединений меди. *Журн. орг. химии*. 2018;54(11):1642–1648. https://doi.org/10.1134/S0514749218110055
7. Yan T., Feringa B.L., Barta K. Iron catalysed direct alkylation of amines with alcohols. *Nat. Commun*. 2014;5:5602. https://doi.org/10.1038/ncomms6602
8. Ma Z., Zhou B., Li X., Kadam R.G., Gawande M.B., Petr M., Zboril R., Beller M., Jagadeesh R.V. Reusable Co-nanoparticles for general and selective *N*-alkylation of amines and ammonia with alcohols. *Chem. Sci*. 2022;13(1):111–117. https://doi.org/10.1039/d1sc05913k
9. Wang G., Sun L., Liu W., Zhan H., Bi S. Iron-nickel alloy particles with *N*-doped carbon “armor” as a highly selective and long-lasting catalyst for the synthesis of *N*-benzylaniline molecules. *Nano Res*. 2024;17(4):2308–2319. https://doi.org/10.1007/s12274-023-6041-z
10. Попов Ю.В., Мохов В.М., Танкабекян Н.А. Коллоидные и наноразмерные катализаторы в органическом синтезе. III. Алкилирование аминов первичными спиртами при катализе коллоидными частицами никеля и кобальта. *Журн. общей химии.* 2014;84(5):733–737.
11. Zou Y., Dong L., Yan S., Liu J., Mu L., Li L., Hu Y., Qi H., Mao S., Chen Z. Activity enhancement of Ru/CeO_2 for *N*-alkylation of amines with alcohols through tailoring metal-support interaction. *J. Catalysis.* 2024;429:115241. https://doi.org/10.1016/j.jcat.2023.115241

10. Popov Yu.V., Mokhov V.M., Tankabekyan N.A. Colloid and nanodimensional catalysts in organic synthesis: III. Alkylation of amines with primary alcohols catalyzed by colloidal nickel and cobalt. *Russ. J. Gen. Chem*. 2014;84(5):826–830. https://doi.org/10.1134/S1070363214050065
[Original Russian Text: Popov Yu.V., Mokhov V.M., Tankabekyan N.A. Colloid and nanodimensional catalysts in organic synthesis: III. Alkylation of amines with primary alcohols catalyzed by colloidal nickel and cobalt. *Zhurnal Obshchei Khimii*. 2014;84(5):733–737 (in Russ.).]
11. Zou Y., Dong L., Yan S., Liu J., Mu L., Li L., Hu Y., Qi H., Mao S., Chen Z. Activity enhancement of Ru/CeO_2 for *N*-alkylation of amines with alcohols through tailoring metal-support interaction. *J. Catalysis.* 2024;429:115241. https://doi.org/10.1016/j.jcat.2023.115241
12. Zhang D., Tian J.., Yan Y., Zhang L., Hu H. Cu-decorating on N, P-Codoped porous carbon derived from wheat straw as advanced catalysts for *N*-alkylation of amines with alcohols. *Arabian J. Chem*. 2023;16(10):105124. https://doi.org/10.1016/j.arabjc.2023.105124
13. Pan J., Li J., Xia X.-F, Zeng W., Wang D. High Active Palladium Composite and Catalytic Applications on the Synthesis of Substituted Aminopyridine Derivatives Through Borrowing Hydrogen Strategy. *Catal. Lett.* 2023;153:2378–2387. https://doi.org/10.1007/s10562-022-04024-0
14. Wu Y., Xi S., Chen C., Hu Q., Xiong Z., Wang J., Dai Y., Han Y., Jiang S., Wang J., Zhou Y. Synergistic roles of platinum nanoparticles and sodium ions within beta zeolites in *N*-alkylation of amines with aromatic alcohols. *Sci. China Chem.* 2023;66(9):2690–2699. https://doi.org/10.1007/s11426-023-1719-y
15. Nebykov D.N., Panov A.O., Razvalyaeva A.V., Latyshova S.E., Mokhov V.M. Colloidal and Nanosized Catalysts in Organic Synthesis: XXVI. Amines Alkylation with Alcohols Catalyzed by γ-Al_2O_3-Supported Nickel and Copper Nanoparticles. *Russ. J. Gen. Chem*. 2023;93(8):1931–1940. https://doi.org/10.1134/S1070363223080017
[Original Russian Text: Nebykov D.N., Panov A.O., Razvalyaeva A.V., Latyshova S.E., Mokhov V.M. Colloidal and Nanosized Catalysts in Organic Synthesis: XXVI. Amines Alkylation with Alcohols Catalyzed by γ-Al_2O_3-Supported Nickel and Copper Nanoparticles. *Zhurnal Obshchei Khimii*. 2023;93(8):1151–1161 (in Russ.). https://doi.org/10.31857/S0044460X23080012]
16. Popov Yu.V., Mokhov V.M., Latyshova S.E., Nebykov D.N., Panov A.O., Davydova T.M. Colloid and Nanosized Catalysts in Organic Synthesis: XVIII. Disproportionation and Cross-Coupling of Amines During Catalysis with Immobilized Nickel Nanoparticles. *Russ. J. Gen. Chem*. 2017;87(12):2757–2761. https://doi.org/10.1134/S1070363217120015
[Original Russian Text: Popov Yu.V., Mokhov V.M., Latyshova S.E., Nebykov D.N., Panov A.O., Davydova T.M. Colloid and Nanosized Catalysts in Organic Synthesis: XVIII. Disproportionation and Cross-Coupling of Amines During Catalysis with Immobilized Nickel Nanoparticles. *Zhurnal Obshchei Khimii*. 2017;87(12):1937–1941 (in Russ.).]
17. Paputina A.N., Popov Yu.V., Mokhov V.M. Alkylation of amines by alkanols during catalysis by alloused nickel and copper nanoparticles. In: *New Materials and Advanced Technologies: collection of materials of the Fifth Interdisciplinary Scientific Forum with International Participation*. V. I. Moscow: Intellektual'nye sistemy; 2019. P. 218–219 (in Russ.).

12. Zhang D., Tian J.., Yan Y., Zhang L., Hu H. Cu-decorating on N, P-Codoped porous carbon derived from wheat straw as advanced catalysts for *N*-alkylation of amines with alcohols. *Arabian J. Chem*. 2023;16(10):105124. https://doi.org/10.1016/j.arabjc.2023.105124
13. Pan J., Li J., Xia X.-F, Zeng W., Wang D. High Active Palladium Composite and Catalytic Applications on the Synthesis of Substituted Aminopyridine Derivatives Through Borrowing Hydrogen Strategy. *Catal. Lett.* 2023;153:2378–2387. https://doi.org/10.1007/s10562-022-04024-0
14. Wu Y., Xi S., Chen C., Hu Q., Xiong Z., Wang J., Dai Y., Han Y., Jiang S., Wang J., Zhou Y. Synergistic roles of platinum nanoparticles and sodium ions within beta zeolites in *N*-alkylation of amines with aromatic alcohols. *Sci. China Chem.* 2023;66(9):2690–2699. https://doi.org/10.1007/s11426-023-1719-y
15. Небыков Д.Н., Панов А.О., Разваляева А.В., Латышова С.Е., Мохов В.М. Коллоидные и наноразмерные катализаторы в органическом синтезе: XXVI. Алкилирование аминов спиртами при катализе нанесенными на γ-Al_2O_3 наночастицами никеля и меди. *Журн. общей химии.* 2023;93(8):1151–1161. https://doi.org/10.31857/S0044460X23080012
16. Попов Ю.В., Мохов В.М., Латышова С.Е., Небыков Д.Н., Панов А.О., Давыдова Т.М. Коллоидные и наноразмерные катализаторы в органическом синтезе. XVIII. Диспропорционирование и кросс-сочетание аминов при катализе иммобилизованными наночастицами никеля. *Журн. общей химии.* 2017;87(12):1937–1941.
17. Папутина А.Н., Попов Ю.В., Мохов В.М. Алкилирование аминов алканолами при катализе нанесенными наночастицами никеля и меди. *Новые материалы и перспективные технологии: сб. материалов Пятого междисциплинарного научного форума с международным участием*. Т. I. М.: Интеллектуальные системы; 2019. С. 218–219.
18. Попов Ю.В., Мохов В.М., Небыков Д.Н., Папутина А.Н., Немцева Н.В. Получение вторичных аминов алкилированием анилина спиртами при катализе наночастичами никеля и меди, иммобилизованными на цеолите NaX. *Известия Волгоградского государственного технического университета*. 2019;12(235):60–63. (in Russ.)

18. Popov Yu.V., Mokhov V.M., Nebykov D.N., Paputina A.N., Nemtseva N.V. The secondary amines synthesis by alkylation of aniline with alcohols catalized by zeolite NaX supported nickel and copper nanoparticles. *Izvestiya Volgogradskogo gosudarstvennogo tekhnicheskogo universiteta = Izvestia VSTU*. 2019;12(235):60–63 (in Russ.).

About the authors

Vladimir M. Mokhov, Dr. Sci. (Chem.), Professor, Technology of Organic and Petrochemical Synthesis Department, Volgograd State Technical University (28, pr. Imeni Lenina, Volgograd, 400005, Russia). E-mail: tons@vstu.ru. Scopus Author ID 7003930850, RSCI SPIN-code 1337-1106, https://orcid.org/0000-0003-2984-1877

Denis N. Nebykov, Cand. Sci. (Chem.), Associate Professor, Technology of Organic and Petrochemical Synthesis Department, Volgograd State Technical University (28, pr. imeni Lenina, Volgograd, 400005, Russia). E-mail: nervwho@gmail.com. Scopus Author ID 56146258500, RSCI SPIN-code 3061-6359, https://orcid.org/0000-0002-5338-8569

Alexandr O. Panov, Senior Lecturer, Technology of Organic and Petrochemical Synthesis Department, Volgograd State Technical University (28, pr. Imeni Lenina, Volgograd, 400005, Russia). E-mail: alexandropanov@gmail.com. Scopus Author ID 57193649148, RSCI SPIN-code 6669-2840, https://orcid.org/0000-0001-7392-849X

Anastasia V. Razvalyaeva, Assistant, Technology of Organic and Petrochemical Synthesis Department, Volgograd State Technical University (28, pr. imeni Lenina, Volgograd, 400005, Russia). E-mail: anastasia.razvalieva@yandex.ru. Scopus Author ID 58205069200, RSCI SPIN-code 3163-1403, https://orcid.org/0009-0004-6305-3051

Snezhana E. Latyshova, Cand. Sci. (Chem.), Associate Professor, Technology of Organic and Petrochemical Synthesis Department, Volgograd State Technical University (28, pr. Imeni Lenina, Volgograd, 400005, Russia). E-mail: snezhana5@rambler.ru. Scopus Author ID 57193645336, RSCI SPIN-code 2860-9142, https://orcid.org/0000-0003-2496-3242

Marat A. Vaniev, Dr. Sci. (Eng.), Heard of the Department of Chemistry and Technology of Elastomer Processing, Volgograd State Technical University (28, pr. imeni Lenina, Volgograd, 400005, Russia). E-mail: vaniev@vstu.ru. Scopus Author ID 14063995400, RSCI SPIN-code 9260-2745, https://orcid.org/0000-0001-6511-5835

Об авторах

Мохов Владимир Михайлович, д.х.н., профессор, кафедра «Технология органического и нефтехимического синтеза», ФГБОУ ВО «Волгоградский государственный технический университет» (400005, Россия, Волгоград, пр-т им. В.И. Ленина, д. 28) E-mail: tons@vstu.ru. Scopus Author ID 7003930850, SPIN-код РИНЦ 1337-1106, https://orcid.org/0000-0003-2984-1877

Небыков Денис Николаевич, к.х.н., доцент, кафедра «Технология органического и нефтехимического синтеза», ФГБОУ ВО «Волгоградский государственный технический университет» (400005, Россия, Волгоград, пр-т им. В.И. Ленина, д. 28). E-mail: nervwho@gmail.com. Scopus Author ID 56146258500, SPIN-код РИНЦ 3061-6359, https://orcid.org/0000-0002-5338-8569

Панов Александр Олегович, старший преподаватель, кафедра «Технология органического и нефтехимического синтеза», ФГБОУ ВО «Волгоградский государственный технический университет» (400005, Россия, Волгоград, пр-т им. В.И. Ленина, д. 28). E-mail: alexandropanov@gmail.com. Scopus Author ID 57193649148, SPIN-код РИНЦ 6669-2840, https://orcid.org/0000-0001-7392-849X

Разваляева Анастасия Владимировна, ассистент, кафедра «Технология органического и нефтехимического синтеза», ФГБОУ ВО «Волгоградский государственный технический университет» (400005, Россия, Волгоград, пр-т им. В.И. Ленина, д. 28). E-mail: anastasia.razvalieva@yandex.ru. Scopus Author ID 58205069200, SPIN-код РИНЦ 3163-1403, https://orcid.org/0009-0004-6305-3051

Латышова Снежана Евгеньевна, к.х.н., доцент, кафедра «Технология органического и нефтехимического синтеза», ФГБОУ ВО «Волгоградский государственный технический университет» (400005, Россия, Волгоград, пр-т им. В.И. Ленина, д. 28). E-mail: snezhana5@rambler.ru. Scopus Author ID 57193645336, SPIN-код РИНЦ 2860-9142, https://orcid.org/0000-0003-2496-3242

Ваниев Марат Абдурахманович, д.т.н., доцент, заведующий кафедрой «Химия и технология переработки эластомеров», ФГБОУ ВО «Волгоградский государственный технический университет» (400005, Россия, Волгоград, пр-т им. В.И. Ленина, д. 28). E-mail: vaniev@vstu.ru. Scopus Author ID 14063995400, SPIN-код РИНЦ 9260-2745, https://orcid.org/0000-0001-6511-5835

Translated from Russian into English by M. Povorin
Edited for English language and spelling by Thomas A. Beavitt

Tonkie Khimicheskie Tekhnologii = Fine Chemical Technologies.
2025;20(1):27–36 ISSN 2686-7575 (Online)

Chemistry and technology of organic substances

Химия и технология органических веществ

UDC 541.128:13:542.91:547.211.547.214
https://doi.org/10.32362/2410-6593-2025-20-1-27-36
EDN LXJSOV

RESEARCH ARTICLE

Study into optimizing the temperature regime for the reduction of Fischer–Tropsch synthesis catalysts

Igor G. Solomonik[1,2,✉], Vladimir Z. Mordkovich[1,2], Andrei S. Gorshkov[2]
[1] *NRC "Kurchatov Institute" – TISNCM, Troitsk, Moscow, 108840 Russia*
[2] *INFRA, Moscow, 125009 Russia*
✉ *Corresponding author, e-mail: solomonik@tisnum.ru*

Abstract

Objectives. The work set out to investigate the potential for developing an efficient cobalt catalyst for Fischer–Tropsch synthesis through low-temperature activation by reduction in hydrogen directly in the synthesis reactor. Such an approach could be used to enhance the overall economic viability of the process.

Methods. The reduction of a zeolite-containing catalyst with a heat-conducting system based on thermally expanded graphite in an aluminum oxide binder carrier was investigated within the temperature range of 300–400°C. The degree of reduction of the powdered catalyst (to remove diffusion restrictions) was determined by conducting temperature-programmed reduction subsequent to the reduction at the studied temperature. Autosorb-1C and STA 449 F1 (*Netzsch*, Germany) devices were used in this work. The identified activation mode was evaluated at a Fischer–Tropsch synthesis pilot plant at *INFRA* (Moscow, Russia).

Results. Activity and selectivity values of the catalyst reduced at 325°C are determined from chromatographic analysis of the products. Low-temperature (325°C) reduction is shown to provide better catalytic parameters due to the implementation of a larger number of highly dispersed cobalt-oxide structures fixed on the hydrated surface of the support, resulting in the appearance of $Co^{\delta+}$ centers with increased activity and selectivity for the formation of C_{5+} hydrocarbons.

Conclusions. The described catalytic system demonstrates the potential advantages in carrying out reductive activation in hydrogen at 325°C as opposed to the conventional 400°C. This approach markedly enhances the economic viability of the entire process, particularly for small-scale installations, due to the reduced thermal stability of the steel material reactor.

Keywords

Fischer–Tropsch synthesis, cobalt catalyst, low-temperature reduction, thermally expanded graphite

Submitted: 24.09.2024
Revised: 15.10.2024
Accepted: 23.12.2024

For citation

Solomonik I.G., Mordkovich V.Z., Gorshkov A.S. Study into optimizing the temperature regime for the reduction of Fischer–Tropsch synthesis catalysts. *Tonk. Khim. Tekhnol. = Fine Chem. Technol.* 2025;20(1):27–36. https://doi.org/10.32362/2410-6593-2025-20-1-27-36

НАУЧНАЯ СТАТЬЯ

Исследование возможности оптимизации температурного режима восстановления катализаторов синтеза Фишера–Тропша

И.Г. Соломоник[1,2,✉], **В.З. Мордкович**[1,2], **А.С. Горшков**[2]

[1] *НИЦ «Курчатовский институт» – ТИСНУМ, г. Троицк, Москва, 108840 Россия*

[2] *ООО ИНФРА, Москва, 125009 Россия*

✉ *Автор для переписки, e-mail: solomonik@tisnum.ru*

Аннотация

Цели. Изучить возможность получения высокоэффективного кобальтового катализатора для синтеза Фишера–Тропша при низкотемпературной активации восстановлением в водороде непосредственно в реакторе синтеза с целью повышения общей экономической привлекательности процесса.

Методы. Восстановление цеолитсодержащего катализатора с теплопроводящей системой на базе терморасширенного графита в составе носителя с алюмооксидным связующим изучено для диапазона температур 300–400°C. Методом термопрограммированного восстановления, проводимого после восстановления при изучаемой температуре, определялась степень восстановления порошкообразного (для снятия диффузионных ограничений) катализатора. В работе использованы приборы Autosorb-1C и STA 449 F1 (*Netzsch*, Германия). Найденный режим активации испытан на опытной установке синтеза Фишера–Тропша в *ООО «ИНФРА»* (Москва, Россия).

Результаты. Представлены определенные из хроматографического анализа продуктов значения активности и селективности в синтезе Фишера–Тропша восстановленного при 325°C катализатора. Показано, что низкотемпературное (325°C) восстановление обеспечивает лучшие каталитические параметры за счет реализации большего количества закрепленных на гидратированной поверхности носителя высокодисперсных кобальт-оксидных структур, обуславливающих возникновение центров $Co^{\delta+}$ с повышенной активностью и селективностью образования углеводородов C_{5+}.

Выводы. Для исследованной каталитической системы показана возможность и желательность восстановительной активации в водороде при 325°C вместо стандартных 400°C. Это существенно повышает экономическую привлекательность процесса в целом, особенно для малотоннажных установок и в связи со снижением требований к термоустойчивости материала стального реактора.

Ключевые слова

синтез Фишера–Тропша, кобальтовый катализатор, низкотемпературное восстановление, терморасширенный графит

Поступила: 24.09.2024
Доработана: 15.10.2024
Принята в печать: 23.12.2024

Для цитирования

Соломоник И.Г., Мордкович В.З., Горшков А.С. Исследование возможности оптимизации температурного режима восстановления катализаторов синтеза Фишера–Тропша. *Тонкие химические технологии.* 2025;20(1):27–36. https://doi.org/10.32362/2410-6593-2025-20-1-18-26

INTRODUCTION

A substantial body of research and industrial experience with catalysts for Fischer–Tropsch synthesis (FTS) has demonstrated that their properties are contingent upon a number of factors, including the chemical and phase composition of the systems (including the realized porous structure), as well the conditions of formation, activation, and operation in the process.

The reduction procedure, which has historically been conducted on disparate equipment with subsequent loading of the operational system into the synthesis reactor or directly in the FTS reactor with selective conditioning, is of paramount importance for the efficient and economically viable production of hydrocarbons for a multitude of applications.

Depending on the nature and concentration of the active metal and the type of carrier, as well as the temperature (250–500°C) and reduction time, the volume and linear velocity of the gas and its composition vary from pure hydrogen to its mixtures with inert gas and CO_2, including direct activation in synthesis gas [1–11]. It is obvious that activation in synthesis gas can potentially reduce (in the case of sufficiently high catalytic activity) the costs of the FTS process. As noted in [12], synthesis gas reduction contributes to the formation of cobalt carbides (Co_xC, $x = 2, 3$), which improve activity by converting from carbides to metallic cobalt with a hexagonal close-packed (hcp) crystal phase. In other cases, inactive Co_xC blocks the active centers of the metal, leading to deactivation of the catalyst. The observed improvement in activity is largely due to an increase in the number of working cobalt centers due to the high dispersion of the metal; however, CO conversion and selectivity for the formation of C_{5+} remain significantly lower than in the presence of a catalyst reduced in pure hydrogen. As found for the model Co/SiO_2 catalyst offering a relatively weak metal-carrier interaction [13], the structural parameters of cobalt previously reduced in hydrogen do not significantly change due to aggregation up to 500°C. At the same time, the presence of CO in the reducing gas leads to the formation of carbonaceous compaction products on the metal surface (at 300–500°C), which reduce the availability of reactants for catalysis.

High-performance catalysts for FTS with thermally conductive additives in the form of flaked aluminum [14], carbon fiber or thermally expanded graphite [15–17] may differ significantly from each other in terms of activation conditions that should be developed for specific systems.

The interaction of a catalytically active metal and its precursors with carriers of various natures is a complex phenomenon that gives rise to a number of effects. The crucial presence in this process of an aluminum oxide binder (boehmite and pseudoboehmite) plays a role in the formation of granules with distinctive properties. These differences are attributed to the varying chemical structures and the manner in which substances are produced by different manufacturers. As shown by the example of the reduction of catalysts with a thermally conductive network of metallic aluminum [18], the reduction of cobalt oxides with hydrogen occurs simultaneously with the appearance of metallic cobalt and disordered defective nonstoichiometric cobalt oxides, removal of reaction water from a porous system, oxidation with water of different genesis of already reduced cobalt, and the formation of boehmite from aluminum. Temperature-dependence additionally conditions its subsequent transformations with the production of protospinel and spinel cobalt-containing structures in various ratios.

It is important to note that the temperature of reduction and heat treatment can result in the formation of different dispersion of excess cobalt crystallites relative to the interaction with the corresponding carrier. Such conditions can also lead to the development of distinct crystallographic modifications in the metal cobalt itself. The hcp phase prevails in massive cobalt crystallites at low temperatures (up to 298 K). Up to a temperature of 500°C, it coexists with the face-centered cubic (fcc) phase, which stabilizes at average temperatures of about 200°C, while above 500°C, the hcp phase again becomes dominant [19]. Nevertheless, the structure and crystallographic structure of intermediate CoO oxides are also influenced by deformation stresses in crystallites when cobalt nanoparticles are realized in catalysts. This is dependent on the location of particles on different carriers and production conditions, specifically on their dispersion and surface chemistry [20, 21].

The reduction of catalysts in hydrogen on a number of carriers (on silicon, aluminum, and titanium oxides at 250, 300, and 350°C) [22] showed a significant difference in the realized states of cobalt for different carriers. For example, on silica gel, the CoO phase is observed at temperatures above 190°C. Up to 380°C, 29% of CO remains in the oxide form, while the mixed phase of Co^0 (fcc/hcp) occurs after 310°C: the size of the crystallites of Co^0 (hcp) making up about 15% of the total is about 5 nm; the content of the phase of Co^0 (fcc) is twice as large, and it is dominant. Up to the reduction temperature of 430°C, the sizes of the crystallites do not change and there is no sintering. Moreover, when activated at 250°C, this system has the necessary catalytic properties, allowing a significant reduction in both capital and operating costs, which is especially important for small installations.

From a technological standpoint, achieving the minimum requisite reactor heating temperature is conducive to the reduction process, which also informs the specifications for the material used in its construction. The restoration of the catalytic system represents a critical procedure for the entire FTS, necessitating a comprehensive understanding of the fundamental issues and conditions that are essential for normal operation. From both applied and theoretical standpoints, investigating this problem for a modern industrial FTS catalyst, such as the impregnating catalyst INFRA S2 on a granular carrier with high thermal conductivity containing thermally expanded graphite (TEG) or, synonymously, penografite [23], is a worthwhile endeavor.

The purpose of this study was to determine under laboratory conditions the temperature dependence of the degree of reduction of the FTS catalyst with a highly efficient heat-conducting network due to the percolation effect and to test a catalytic system having a low reduction temperature at a pilot plant.

EXPERIMENTAL

The paper investigates a carrier and a 20% cobalt catalyst (of one batch) S2 based thereupon, which were prepared at *INFRA* (Russia). The starting materials for extrusion and for catalyst preparation were boehmite DISPERAL P2 (produced by *SaSol*, Germany); zeolite Hβ Zeolyst™ CP 814C *(Zeolyst*, USA); thermally expanded graphite TEG-50/4 (*R&D UNIKHIMTEK*, Russia); $Co(NO_3)_26H_2O$ (GOST 4228-78[1], analytical or reagent grades without nickel, *SPC 'Baltiyskaya Manufaktura'*, Russia). The corresponding solutions are obtained on the basis of distilled water.

Cylindrical granules of the carrier of the initial mass composition (50% DisperalP2 + 30% zeolite Hß with a modulus of 38 + 20% TEG) and a size of 1.5 × (2–4) mm were obtained by extrusion, then impregnated with a solution of cobalt nitrate and calcined in accordance with the existing regulations at the *INFRA* catalytic factory. In order to ascertain the correct data for determining the degree of reduction (without the confounding effect of diffusion factors), the granules were subjected to mechanical grinding in an agate mortar. The resulting powder fraction was 0.2–0.4 mm. A single sample of the powder subsequently used in all subsequent experiments was thermally vacuumed (350°C, 3 h, 10^{-3} mmHg) in a cuvette on an Autosorb-1C device (*Quantachrome Instruments*, USA). The initial powdered catalyst S2 lost 9.67% of its mass, which corresponds to a cobalt content of ~17 wt % in the studied sample. This value converges with the spectrophotometrically determined concentration of 20% cobalt in a freshly calcined carrier, with a calculated cobalt content of 18 wt %. The aforementioned figures are elucidated as follows: 100 g of the calculated catalyst, containing 20% cobalt (by preparation), comprises 80 g of dry carrier and 20 g of Co metal. Following decomposition of nitrate to Co_3O_4, these dry calculated 100 g should actually weigh 107.24 g (considering the weight of cobalt oxide 27.24 g instead of 20 g of Co^0). The actual wet catalyst has lost 9.67% of its mass, i.e., every 100 g of the studied sample contains 90.33 g of an idealized dry catalyst with cobalt in the oxide form of Co_3O_4. A total of 16.85 g of metallic cobalt is present in the 90.33 g of the substance under examination. This figure is based on the proportion of 20 g of cobalt per 107.24 g of the dry catalyst used for preparation. However, the weight of the sample with 16.85 g of cobalt was initially 100 g; therefore, the concentration of metallic cobalt in the initial catalyst under study was 16.85%. Thus, the actual concentration of cobalt in the granules loaded into the reactor is 17–18 wt %.

The catalyst powder was activated directly in the U-shaped flow cell of the device under the conditions of the catalytic experiment (i.e., 300–400°C and appropriate time). The restoration was carried out with hydrogen grade B 6.0 (analytical grade, TU 2118-06-18136415-06, *Moscow Gas Processing Plant*, Russia) followed by partial blow-off in helium grade "A" (TU 0271-135-31323949-2005, *Moscow Gas Processing Plant*, Russia) from sorbed reaction water and residual hydrogen. After initial reduction, the sample in the cuvette was cooled to 40°C during vacuuming. In the same cell, without contact with air, the catalyst was restored at a volume flow rate of dry hydrogen $(30–60) \cdot 10^3$ h^{-1} to a temperature of 980°C on Autosorb-1C with fixation of thermoprogrammed reduction curves after preliminary reduction (TPR-PR) at a given activation temperature.

It should be noted that, in contrast to a granular catalyst in a reactor, the maximum possible reduction level is achievable under these conditions, which are not complicated by diffusion.

In order to accurately quantify the consumption of hydrogen, the katharometer signal was recorded for the drained gas stream that passed through a low-temperature (−95 to −80°C) regenerated zeolite trap following the reaction. The weight of the samples was recorded before and after the experiment. The experimental TPR-PR data were processed in the Origin Pro8 program[2] with baseline subtraction. The degree of reduction was quantified by measuring the ratio of the total effect areas in the range of 50–980°C from the S2 catalyst (which exhibited complete reduction) and that following preliminary reduction in the specified modes.

An STA 449 F1 complex thermal analysis device (*Netzsch*, Germany) was also used to study the systems.

The catalyst activated at a temperature of 325°C for 6 h with a volumetric flow rate of 3000 h^{-1} of hydrogen in a 0.5-inch reactor (12 cm^3 of granular catalyst S2, bulk density 0.658 g/cm^3) was tested in an experimental installation according to the previously described method [24]. The data obtained during testing were compared with the results in the standard activation mode (400°C, 3000 h^{-1} H_2, 1 h). The composition of synthesis gas and gaseous, as well that of liquid products, was analyzed on a Crystal-Lux 4000M chromatograph (*Meta-Chrome*, Russia).

---

[1] GOST 4228-78. Interstate Standard. Reagents. Sodium hydroxide. Specifications. Moscow: IPK Izdatelstvo standartov; 1978 (in Russ.).

[2] https://www.originlab.com/. Accessed December 23, 2024.

RESULTS AND DISCUSSION

Figure 1 presents a summary of the data pertaining to the degrees of reduction of catalysts at varying temperatures and pretreatment times.

The control of reproducibility of the results for a number of experimental points with different sample weights (the initial sample of the S2 catalyst with a zero degree of reduction and restored for 1 h at 350 and 400°C), as well as when processing TPR-PR curves with a change in the zero-line parameters, showed that the discrepancy from the average was no more than 5%.

For the described method, the potential for minor discrepancies in the measured values of the degree of reduction as a result of the consumption of hydrogen when interacting with the free surface of thermally expanded graphite in the catalyst composition is not a significant concern due to the comparison of identical samples following duplicate processing. While the diffusion of metal over the surface with different treatments may result in slight alterations to the absolute figures, it does not impact the reduction dynamics, which are contingent upon the experimental conditions. The diffusion of metal over the surface with different treatments may result in slight alterations to the absolute figures, but does not impact the dynamics of the degree of reduction, which is contingent upon the experimental conditions. At the same time, the intensity of the TPR signal of the initial S2 carrier after 10 h of thermal vacuum treatment at 300°C is significantly less than after 3 h. This suggests the presence of a substantial number of recoverable surface centers, which necessitates the comparison of samples with strictly identical characteristics to offset the impact of the catalyst surface.

As follows from the thermogravimetric data, catalysts in the helium flow for the range 700–900°C have sharp mass losses that are not typical for carrier components (including TEG). In the case of catalyst granules having a diameter of 1.5 mm in the temperature range of 723–862°C, these losses are about 9.2 wt %, and for granules with a diameter of 2.5 mm in the temperature range of 800–885°C—about 8.1 wt %. If we assume that all of losses are due to the formation of CO or CO_2 during thermolysis due to the autothermal reduction of cobalt oxides with carbon [25], then, counting on the transformations of Co_3O_4 (also for Co_2O_3), this gives a complete conversion of metal oxides to Co^0 when CO_2 occurs. Thus, almost all of the deposited oxidized cobalt is reduced by carbon in this temperature range. This means that in the initial catalyst, the oxidized metal (including in the form of embedding structures and protospinel formations) is located on the surface of the TEG in the form of polylayers fixed to this component of the carrier or in sufficient proximity to it, which allows for the possibility of high-temperature diffusion-thermal interaction with carbon to determine the efficiency of heat removal in the FTS. Accordingly, at low temperatures, due to strong interaction with the carrier, their reduction is difficult. Nevertheless, the quantitative loss of the degree of reduction can be partially compensated for the catalyst in FTS by the increased activity of highly dispersed cobalt located on the oxidized metal. According to the data of [17, 25], cobalt oxide crystallites on the carbon surface (TEG, nanotubes) are characterized by a particle size less than 20 nm that is close to optimal in FTS in terms of selectivity with C_{5+}. At the same time, the amount of cobalt in direct contact with carbon recorded by the mapping method of energy dispersive X-ray spectroscopy and a scanning electron microscope in [17] is small, being (as found for the model catalyst only on TEG) mainly located at the ends of carbon plates.

The degree of reduction varies slightly after 1 h of treatment in the range of 300–350°C and increases only at 380–400°C (Figs. 1 and 2). At the same time, the number of disordered spinel and protospinel cobalt-containing phases fixed on the surface in the temperature range 500–800°C [18] varies slightly. When reduced at temperatures up to 350°C, low-temperature peaks from surface hydrated structures are almost constant; however, when reduced at 380°C, due to better dehydration of the surface, a solid solution of CoO in Co_3O_4 is formed, which is fixed by the maximum TPR-PR characteristic of large particles of cobalt oxides of about 400°C.

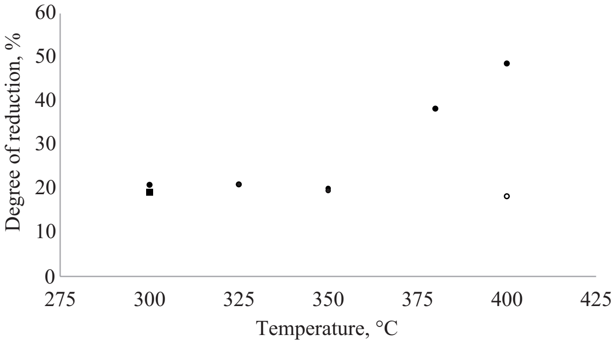

Fig. 1. Degree of reduction of S2 catalyst (fraction of 0.2–0.4 mm) at different temperatures and reduction times. The samples were pre-annealed in vacuum at 350°C for 1 h, then reduced during 1 h (black and white circles) or 4 h (square). A white-circle sample was additionally pre-heated at 400°C in He flow for 5 h

As follows from the analysis of Figs. 1 and 3, an increase in reduction time at low temperature (300°C) does not affect the degree of reduction (black circles and square, Fig. 1); however, pretreatment for 5 h in an inert gas flow at 400°C more than halves (white circle, Fig. 1) the degree of reduction. The latter is attributable to the intensification of interaction with the carrier and the emergence of spinel-type cobalt-containing structures that are irremediable under these conditions (see Figs. 3 and 4).

At the same time, the maximum value of the reduction of residual phases from Co_3O_4 to CoO also decreases (the first maximum) with increasing temperature (Fig. 2). However, as can be seen from Figs. 3 and 4, its relative intensity increases in the case of prolonged reduction or thermolysis. This indicates their active formation due to surface diffusion both during thermolysis and reduction, as well as subsequent oxidation due to functional surface groups of cobalt-containing structures. It is evident that the reduction in the observed degree of reduction resulting from the use of non-dried hydrogen in a humid environment will be relative.

The table compares the results of catalytic testing of the S2 catalyst (synthesis gas $H_2 : CO = 2 : 1$) recovered under selected activation conditions (325°C, 3000 h^{-1} H_2, 6 h) in a single-section tube reactor of *INFRA* of the pipe-in-pipe type with the results for standard conditions (400°C, 3000 h^{-1} H_2, 1 h) having an equal bulk density of the catalyst (0.66 g/cm^3).

The data were obtained under stationary conditions following a gradual increase in temperature and synthesis gas consumption. The necessity for the development of a catalyst to prevent overheating arises from the fact that this phenomenon is associated with deactivation as a result of the agglomeration of cobalt particles and increased interaction with the carrier.

As can be seen from the table, the most significant differences are observed in the selectivity of the formation of C_{5+} hydrocarbons, which is maximal with low-temperature reduction of absolutely identical initial catalysts with the same gas and hydrodynamics in the reactor.

This is in good agreement with the increase found for the S2 catalyst at a low reduction temperature or during prolonged thermolysis of the content of oxidized cobalt states (steinerite phases) due to interaction with surface hydroxyls. The same processes are observed in systems comprising a heat-conducting network of metallic aluminum, as well as in catalysts lacking a heat-conducting component on carriers of diverse natures. It is obvious that during the primary low-temperature reduction, a large number of $Co^{\delta+}$ structures are realized on which C_{5+} hydrocarbons are selectively formed [26].

When considering the dynamics of temperature influence and the magnitude of initial reduction on catalytic parameters, it is important to note that the relevant figures obtained are only determined for these systems following a period of 6–7 days

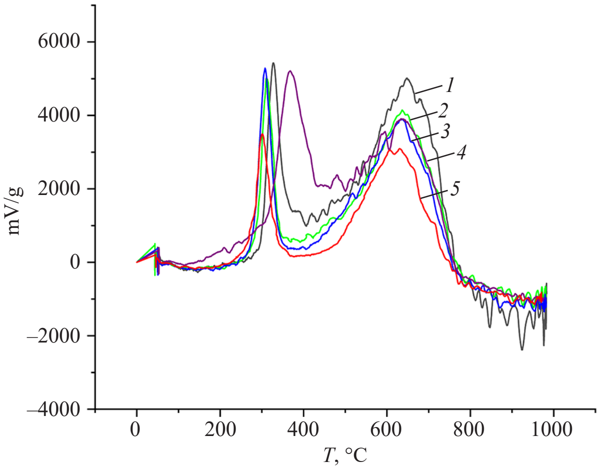

Fig. 2. Curves of thermoprogrammed reduction (TPR) after reduction of S2 catalyst for 1 h at different temperatures, °C: *1* — 300; *2* — 325; *3* — 350; *4* — 380; *5* — 400

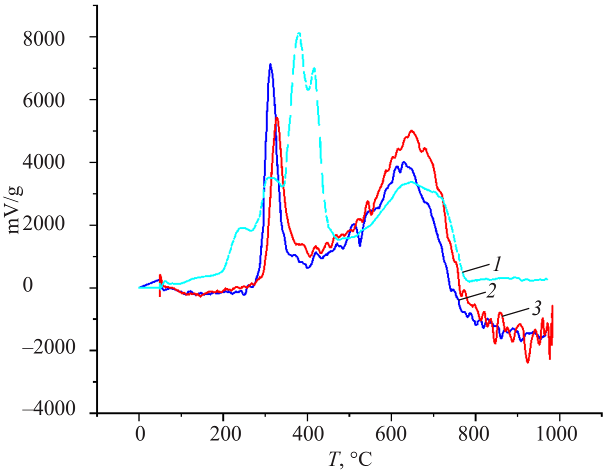

Fig. 3. TPR curves of the initial S2 catalyst (*1*) and after preliminary reduction of the catalyst at 300°C for 4 h (*2*) and 300°C for 1 h (*3*)

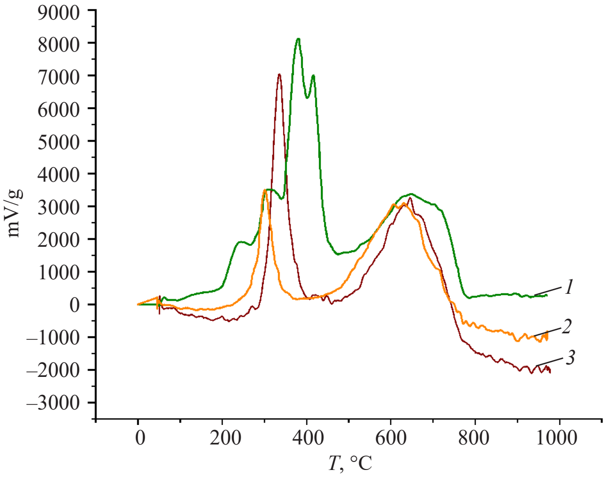

Fig. 4. TPR curves of the initial S2 catalyst (*1*) and after preliminary thermolysis of the catalyst at 400°C for 5 h with reduction at 400°C for 1 h (*2*) or without thermolysis (*3*)

Table. Comparison of catalytic performance of catalysts reduced at different temperatures

Activation conditions	*T*, °C	Gas hourly space velocity, h^{-1}	CO conversion, %	Selectivity of C_{5+} formation, %	Productivity, C_{5+}, g/(L·h)
325°C, 3000 h^{-1} H_2, 6 h	242	3000	56.4	63.7	207.4
400°C, 3000 h^{-1} H_2, 2 h	243		53.9	54.9	173.3

of catalyst development. This can be accompanied by additional activation of the systems (when restored in synthesis gas, an acceptable conversion is achieved after a week of development [8]), as well as their deactivation.

Thus, a catalyst with a higher initial degree of reduction and sufficiently large cobalt agglomerates is partially deactivated during the FTS due to the deposition of synthesized high-molecular hydrocarbons and metal coalescence with the formation of even larger aggregates with lower activity. For small crystallites formed in the S2 catalyst at a low reduction temperature, there is less mobility due to the bond with the surface and better activity both due to the realized structure and due to their large number (Figs. 3 and 4). At the same time, for unambiguous conclusions, it is necessary to determine the actual degrees of reduction of systems following prolonged operation and the extraction of catalysts from the reactor.

CONCLUSIONS

Zeolite-containing cobalt catalysts for FTS with a highly efficient heat-conducting network based on graphite of the TRG brand were studied by the TPR method after preliminary reduction with hydrogen at 300–400°C. It is shown that the catalysts reduced at low temperatures (325°C), despite the low degree of reduction, have the best catalytic parameters. This was demonstrated during the operation of the *INFRA* experimental installation of FTS.

The improvement of the catalytic parameters of the systems is caused by the more efficient implementation of highly dispersed cobalt-oxide structures fixed on the hydrated surface, which cause the appearance of $Co^{\delta+}$ centers with increased activity and selectivity of the formation of C_{5+} hydrocarbons during the reaction.

The obtained data open up the possibility for optimizing technology for reducing FTS catalysts using lower temperatures and with reduced requirements for the thermal stability of the materials used.

Acknowledgments

The work was performed using the Shared Research Facilities “Research of Nanostructured, Carbon and Superhard Materials” at the NRC “Kurchatov Institute” – TISNCM.

Authors’ contribution

All authors equally contributed to the research work.

The authors declare no conflict of interest warranting disclosure in this article.

REFERENCES

1. Ngamcharussrivichai C., Liu X., Li X., Vitidsant T., Fujimoto K. An active and selective production of gasoline-range hydrocarbons over bifunctional Co-based catalysts. *Fuel.* 2007;86(1–2):50–59. https://doi.org/10.1016/J.FUEL.2006.06.021
2. Bechara R., Balloy D., Vanhove D. Catalytic properties of Co/Al_2O_3 system for hydrocarbon synthesis. *Appl. Cat. A: Gen*. 2001;207(1–2):343–353. https://doi.org/10.1016/S0926-860X(00)00672-4
3. Xiong H., Zhang Y., Liew K., Li J. Catalytic performance of zirconium-modified Co/Al_2O_3 for Fischer–Tropsch synthesis. *J. Mol. Cat. A: Chem*. 2005;231(1–2):145–151. https://doi.org/10.1016/J.MOLCATA.2004.12.033
4. Pankina G.V., Chernavskii P.A., Lermontov A.S., *et al.* Prediction of the activity and selectivity of supported cobalt Fischer–Tropsch catalysts. *Petroleum Chemistry*. 2001;41(5):319–323.

СПИСОК ЛИТЕРАТУРЫ

1. Ngamcharussrivichai C., Liu X., Li X., Vitidsant T., Fujimoto K. An active and selective production of gasoline-range hydrocarbons over bifunctional Co-based catalysts. *Fuel.* 2007;86(1–2):50–59. https://doi.org/10.1016/J.FUEL.2006.06.021
2. Bechara R., Balloy D., Vanhove D. Catalytic properties of Co/Al_2O_3 system for hydrocarbon synthesis. *Appl. Cat. A: Gen*. 2001;207(1–2):343–353. https://doi.org/10.1016/S0926-860X(00)00672-4
3. Xiong H., Zhang Y., Liew K., Li J. Catalytic performance of zirconium-modified Co/Al_2O_3 for Fischer–Tropsch synthesis. *J. Mol. Cat. A: Chem*. 2005;231(1–2):145–151. https://doi.org/10.1016/J.MOLCATA.2004.12.033
4. Панкина Г.В., Чернавский П.А., Лермонтов А.С., Лунин В.В. Прогнозирование активности и селективности Co-нанесенных катализаторов синтеза Фишера–Тропша, *Нефтехимия*. 2001;41(5):348–353.

[Original Russian Text: Pankina G.V., Chernavskii P.A., Lermontov A.S., Lunin V.V. Prediction of the activity and selectivity of supported cobalt Fischer–Tropsch catalysts. *Neftekhimiya*. 2001;41(5):348–353 (in Russ.).]

5. Das T.K., Jacobs G., Patterson P.M., Conner W.A., Li J., Davis B.H. Fischer–Tropsch synthesis: characterization and catalytic properties of rhenium promoted cobalt alumina catalysts. *Fuel.* 2003;82(7):805–815. https://doi.org/10.1016/S0016-2361(02)00361-7
6. Clarkson J.S., Colley S.W. *Cobalt Catalyst Activation Process*: Pat. WO2002083717. Publ. 24.10.2002
7. Moen A., Nicholson D.G., Rønning M., Emerich H. *In situ* X-ray absorption spectroscopic studies at the cobalt K-edge on an Al_2O_3-supported rhenium-promoted cobalt Fischer–Tropsch catalyst. Comparing reductions in high and low concentration hydrogen. *J. Mater. Chem*. 1998;8(11):2533–2539. https://doi.org/10.1039/A804261F
8. Loginova A.N., Mikhailov M.N., Grigor'ev D.A., Sviderskii S.A. *Method of Activation of Cobalt Catalyst of Fischer–Tropsch Synthesis*: RF Pat. RU 2445161 C1. Publ. 20.03.2012 (in Russ.).
9. Lok K.M., West J. *High Cobalt Content, High Cobalt Surface Area Catalysts, Preparation and Use Thereof*: Pat. WO-A-2006/021754. Publ. 02.03.2006.
10. Khangale P.R., Meijboom R., Jalama K. Reduction Behaviour for Co/Al_2O_3 Fischer–Tropsch Catalyst in Presence of H_2 or CO. In: *Proceedings of the World Congress on Engineering 2014.* 2014. V. II. URL: http://www.iaeng.org/publication/WCE2014/WCE2014_pp1048-1051.pdf
11. Khangale P.R., Meijboom R., Jalama K. Fischer–Tropsch synthesis over unpromoted Co/ɣ-Al_2O_3 catalyst: Effect of activation with CO compared to H_2 on catalyst performance. *Bull. Chem. React. Eng. Catal*. 2019;14(1):35–41. https://doi.org/10.9767/bcrec.14.1.2519.35-41
12. Shiba N.C., Liu X., Hildebrandt D., Yao Y. Effect of pre-treatment conditions on the activity and selectivity of cobalt-based catalysts for CO hydrogenation. *Reactions*. 2021;2(3):258–274. https://doi.org/10.3390/reactions2030016
13. Solomonik I.G., Gogol' O.V. The influence of the gas environment and temperature on the structural characteristics and the possibility of cobalt agglomeration in Fischer–Tropsch catalysts. In: *Proceedings of the 6th Russian Conference with the participation of CIS countries "Scientific Foundations of the Preparation and Technology of Catalysts" and 3rd Russian Conference "Problems of Deactivation of Catalysts."* 2008. V. 2. P. 210–211 (in Russ.).
14. Mordkovich V.Z., Ermolaev V.S., Mitberg E.B., Sineva L.V., Solomonik I.G., Ermolaev I.S., Asalieva E.Yu. Composite pelletized catalyst for higher one-pass conversion and productivity in Fischer–Tropsch process. *Res. Chem. Intermed.* 2015;41(12):9539–9550. https://doi.org/10.1007/s11164-015-1978-5
15. Ghogia A.C., Nzihou A., Serp P., Soulantica K., Pham Minh D. Cobalt catalysts on carbon-based materials for Fischer–Tropsch synthesis: a review. *Appl. Cat. A: Gen.* 2021;609:117906. https://doi.org/10.1016/j.apcata.2020.117906
16. Mikhailova Ya.V., Sineva L.V., Mordkovich V.Z., Sviderskii S.A., Solomonik I.G., Ermolaev V.C. *Catalyst for Fischer–Tropsch Synthesis and the Method of its Preparation*: RF Pat. RU 2325226 C1. Publ. 20.06.2008 (in Russ.).
17. Asalieva E., Sineva L., Sinichkina S., Solomonik I., Gryaznov K., Pushina E., Kulchakovskaya E., Gorshkov A., Kulnitskiy B., Ovsyannikov D., Zholudev S., Mordkovich V. Exfoliated graphite as a heat-conductive frame for a new pelletized Fischer–Tropsch synthesis catalyst. *Appl. Cat. A: Gen*. 2020;601:117639. https://doi.org/10.1016/j.apcata.2020.117639

5. Das T.K., Jacobs G., Patterson P.M., Conner W.A., Li J., Davis B.H. Fischer–Tropsch synthesis: characterization and catalytic properties of rhenium promoted cobalt alumina catalysts. *Fuel.* 2003;82(7):805–815. https://doi.org/10.1016/S0016-2361(02)00361-7
6. Clarkson J.S., Colley S.W. *Cobalt catalyst activation process*: Pat. WO2002083717. Publ. 24.10.2002.
7. Moen A., Nicholson D.G., Rønning M., Emerich H. *In situ* X-ray absorption spectroscopic studies at the cobalt K-edge on an Al_2O_3-supported rhenium-promoted cobalt Fischer–Tropsch catalyst. Comparing reductions in high and low concentration hydrogen. *J. Mater. Chem*. 1998;8(11):2533–2539. https://doi.org/10.1039/A804261F
8. Логинова А.Н., Михайлов М.Н., Григорьев Д.А., Свидерский С.А. *Способ активации кобальтового катализатора синтеза Фишера–Тропша*: пат. RU 2445161 C1. Заявка № 2010134601/04; заявл. 19.08.2010; опубл. 20.03.2012.
9. Lok K.M., West J. *High cobalt content, high cobalt surface area catalysts, preparation and use thereof*: Pat. WO-A-2006/021754. Publ. 02.03.2006.
10. Khangale P.R., Meijboom R., Jalama K. Reduction Behaviour for Co/Al_2O_3 Fischer–Tropsch Catalyst in Presence of H_2 or CO. In: *Proceedings of the World Congress on Engineering 2014.* 2014. V. II. URL: http://www.iaeng.org/publication/WCE2014/WCE2014_pp1048-1051.pdf
11. Khangale P.R., Meijboom R., Jalama K. Fischer–Tropsch synthesis over unpromoted Co/ɣ-Al_2O_3 catalyst: Effect of activation with CO compared to H_2 on catalyst performance. *Bull. Chem. React. Eng. Catal*. 2019;14(1):35–41. https://doi.org/10.9767/bcrec.14.1.2519.35-41
12. Shiba N.C., Liu X., Hildebrandt D., Yao Y. Effect of pre-treatment conditions on the activity and selectivity of cobalt-based catalysts for CO hydrogenation. *Reactions*. 2021;2(3):258–274. https://doi.org/10.3390/reactions2030016
13. Соломоник И.Г., Гоголь О.В. Влияние газовой среды и температуры на структурные характеристики и возможность агломерации кобальта в катализаторах Фишера–Тропша. *Тезисы докладов: VI Российская конференция «Научные основы приготовления и технологии катализаторов» и III Российская конференция «Проблемы дезактивации катализаторов»* (*с участием стран СНГ*). 2008. Т. 2. С. 210–211.
14. Mordkovich V.Z., Ermolaev V.S., Mitberg E.B., Sineva L.V., Solomonik I.G., Ermolaev I.S., Asalieva E.Yu. Composite pelletized catalyst for higher one-pass conversion and productivity in Fischer–Tropsch process. *Res. Chem. Intermed*. 2015;41(12):9539–9550. https://doi.org/10.1007/s11164-015-1978-5
15. Ghogia A.C., Nzihou A., Serp P., Soulantica K., Pham Minh D. Cobalt catalysts on carbon-based materials for Fischer–Tropsch synthesis: a review. *Appl. Cat. A: Gen.* 2021;609:117906. https://doi.org/10.1016/j.apcata.2020.117906
16. Михайлова Я.В., Синева Л.В., Мордкович В.З., Свидерский С.А., Соломоник И.Г., Ермолаев В.С. *Катализатор для синтеза Фишера–Тропша и способ его получения*: пат. RU 2325226 C1. Заявка № 2006146573/04; заявл. 27.12.2006; опубл. 20.06.2008.
17. Asalieva E., Sineva L., Sinichkina S., Solomonik I., Gryaznov K., Pushina E., Kulchakovskaya E., Gorshkov A., Kulnitskiy B., Ovsyannikov D., Zholudev S., Mordkovich V. Exfoliated graphite as a heat-conductive frame for a new pelletized Fischer–Tropsch synthesis catalyst. *Appl. Cat. A: Gen*. 2020;601:117639. https://doi.org/10.1016/j.apcata.2020.117639

18. Solomonik I.G., Mordkovich V.Z. Determination of the conditions of technologically optimized reduction of high-performance Fischer–Tropsch synthesis catalysts. *Kataliz v promyshlennosti*. 2024;24(3):60–70 (in Russ.). https://doi.org/10.18412/1816-0387-2024-3-60-70
19. Sewak R., Dey C.C., Toprek D. Temperature induced phase transformation in Co. *Sci. Rep.* 2022;12(1):10054. https://doi.org/10.1038/s41598-022-14302-x
20. Santos R.V., Cabrera-Pasca G.A., Costa C.S., Bosch-Santos B., Otubo L., Pereira L.F.D., Correa B.S., Effenberger F.B., Burimova A., Freitas R.S., Carbonari A.W. Crystalline and magnetic properties of CoO nanoparticles locally investigated by using radioactive indium tracer. *Sci. Rep.* 2021;11(1):21028. https://doi.org/10.1038/s41598-021-99810-y
21. Dubos P.A., Fajoui J., Iskounen N., *et al.* Temperature effect on strain-induced phase transformation of cobalt. *Mat. Lett.* 2020;281:128821. https://doi.org/10.1016/j.matlet.2020.128812
22. Shiba N.C., Yao Y., Forbes R.P., Okoye-Chine C.G., Liu X., Hildebrandt D. Role of CoO–Co nanoparticles supported on SiO_2 in Fischer–Tropsch synthesis: Evidence for enhanced CO dissociation and olefin hydrogenation. *Fuel Process. Technol*. 2021;216:106781. https://doi.org/10.1016/j.fuproc.2021.106781
23. Mordkovich V.Z., Sineva L.V., Kulchakovskaya E.V., Asalieva E.Yu., Gryaznov K.O., Sinichkina S.G. *Catalyst for Fischer–Tropsch Synthesis and Method of its Preparation*: RF Pat. RU 2685437 C2. Publ. 18.04.2019 (in Russ.).
24. Ermolaev V.S., Gryaznov K.O., Mitberg E.B., Mordkovich V.Z., Tretyakov V.F. Laboratory and pilot plant fixed-bed reactors for Fischer–Tropsch synthesis: Mathematical modeling and experimental investigation. *Chem. Eng. Sci*. 2015;138:1–8. https://doi.org/10.1016/j.ces.2015.07.036
25. LÜ J., Huang C., Bai S., Jiang Y., Li Z. Thermal decomposition and cobalt species transformation of carbon nanotubes supported cobalt catalyst for Fischer–Tropsch synthesis. *J. Nat. Gas Chem*. 2012;21(1):37–42. https://doi.org/10.1016/S1003-9953(11)60330-7
26. Solomonik I.G., Gryaznov K.O., Mitberg E.B., Mordkovich V.Z. Preparation of Raney Cobalt and Identification of Surface Structures Responsible for Catalytic Activity in Fischer–Tropsch Process. *Appl. Res.* 2023;2:e202200029. https://doi.org/10.1002/appl.202200029

18. Соломоник И.Г., Мордкович В.З. Определение условий технологически оптимизированного восстановления высокопроизводительных катализаторов синтеза Фишера–Тропша. *Катализ в промышленности*. 2024;24(3):60–70. https://doi.org/10.18412/1816-0387-2024-3-60-70
19. Sewak R., Dey C.C., Toprek D. Temperature induced phase transformation in Co. *Sci. Rep.* 2022;12(1):10054. https://doi.org/10.1038/s41598-022-14302-x
20. Santos R.V., Cabrera-Pasca G.A., Costa C.S., Bosch-Santos B., Otubo L., Pereira L.F.D., Correa B.S., Effenberger F.B., Burimova A., Freitas R.S., Carbonari A.W. Crystalline and magnetic properties of CoO nanoparticles locally investigated by using radioactive indium tracer. *Sci. Rep.* 2021;11(1):21028. https://doi.org/10.1038/s41598-021-99810-y
21. Dubos P.A., Fajoui J., Iskounen N., *et al.* Temperature effect on strain-induced phase transformation of cobalt. *Mat. Lett.* 2020;281:128821. https://doi.org/10.1016/j.matlet.2020.128812
22. Shiba N.C., Yao Y., Forbes R.P., Okoye-Chine C.G., Liu X., Hildebrandt D. Role of CoO–Co nanoparticles supported on SiO_2 in Fischer–Tropsch synthesis: Evidence for enhanced CO dissociation and olefin hydrogenation. *Fuel Process. Technol*. 2021;216:106781. https://doi.org/10.1016/j.fuproc.2021.106781
23. Мордкович В.З., Синева Л.В., Кульчаковская Е.В., Асалиева Е.Ю., Грязнов К.О., Синичкина С.Г. *Катализатор для синтеза Фишера–Тропша и способ получения этого катализатора*: пат. RU 2685437 C2. Заявка № 2017118372; заявл. 26.05.2017; опубл. 18.04.2019.
24. Ermolaev V.S., Gryaznov K.O., Mitberg E.B., Mordkovich V.Z., Tretyakov V.F. Laboratory and pilot plant fixed-bed reactors for Fischer–Tropsch synthesis: Mathematical modeling and experimental investigation. *Chem. Eng. Sci*. 2015;138:1–8. https://doi.org/10.1016/j.ces.2015.07.036
25. LÜ J., Huang C., Bai S., Jiang Y., Li Z. Thermal decomposition and cobalt species transformation of carbon nanotubes supported cobalt catalyst for Fischer–Tropsch synthesis. *J. Nat. Gas Chem*. 2012;21(1):37–42. https://doi.org/10.1016/S1003-9953(11)60330-7
26. Solomonik I.G., Gryaznov K.O., Mitberg E.B., Mordkovich V.Z. Preparation of Raney Cobalt and Identification of Surface Structures Responsible for Catalytic Activity in Fischer–Tropsch Process. *Appl. Res.* 2023;2:e202200029. https://doi.org/10.1002/appl.202200029

About the authors

Igor G. Solomonik, Cand. Sci. (Chem.), Leading Researcher, Laboratory of New Chemical Technologies, Department of Carbon Nanostructures, Technological Institute for Superhard and Novel Carbon Materials of National Research Center “Kurchatov Institute” (7a, Tsentralnaya ul., Troitsk, Moscow, 108840, Russia). E-mail: solomonik@tisnum.ru. Scopus Author ID 57191762433, RSCI SPIN-code 1370-1485, https://orcid.org/0000-0003-0628-6073

Vladimir Z. Mordkovich, Dr. Sci. (Chem.), Research Deputy Director, Technological Institute for Superhard and Novel Carbon Materials of National Research Center “Kurchatov Institute” (7a, Tsentralnaya ul., Troitsk, Moscow, 108840, Russia). E-mail: mordkovich@tisnum.ru. Scopus Author ID 7005798833, ResearcherID L-2077-2013, ResearcherID J-7201-2015, RSCI SPIN-code 1626-7370, https://orcid.org/0000-0002-9553-7657

Andrey S. Gorshkov, Leading Engineer, INFRA, (2 B-1/3, Promyshlennaya ul., Troitsk, Moscow, 108841, Russia). E-mail: gorshkov@infratechnology.com. Scopus Author ID 57216969878, https://orcid.org/0000-0001-6521-8682

Об авторах

Соломоник Игорь Григорьевич, к.х.н., ведущий научный сотрудник, лаборатория новых химических технологий, отделение углеродных наноструктур, ФГБУН «Технологический институт сверхтвердых и новых углеродных материалов», НИЦ «Курчатовский институт» (НИЦ «Курчатовский институт» – ТИСНУМ) (108840, Россия, Москва, г. Троицк, ул. Центральная, д. 7а). E-mail: solomonik@tisnum.ru. Scopus Author ID 57191762433, SPIN-код РИНЦ 1370-1485, https://orcid.org/0000-0003-0628-6073

Мордкович Владимир Зальманович, д.х.н, заместитель директора по научной работе, ФГБУН «Технологический институт сверхтвердых и новых углеродных материалов», НИЦ «Курчатовский институт» (НИЦ «Курчатовский институт» – ТИСНУМ) (108840, Россия, Москва, г. Троицк, ул. Центральная, д. 7а). E-mail: mordkovich@tisnum.ru. Scopus Author ID 7005798833, ResearcherID L-2077-2013, ResearcherID J-7201-2015, SPIN-код РИНЦ 1626-7370, https://orcid.org/0000-0002-9553-7657

Горшков Андрей Сергеевич, ведущий инженер, ООО «ИНФРА», (108841, Россия, Москва, г. Троицк, ул. Промышленная, д. 2Б, стр. 1, к. 3). E-mail: gorshkov@infratechnology.com. Scopus Author ID 57216969878, https://orcid.org/0000-0001-6521-8682

Translated from Russian into English by N. Isaeva
Edited for English language and spelling by Thomas A. Beavitt

Tonkie Khimicheskie Tekhnologii = Fine Chemical Technologies.
2025;20(1):37–46

ISSN 2686-7575 (Online)

UDC 544.02
https://doi.org/10.32362/2410-6593-2025-20-1-37-46
EDN NZKCWQ

RESEARCH ARTICLE

The influence of halogen-containing modifier on the thermo-oxidative stability of styrene–butadiene–styrene triblock copolymers

Irina S. Almatova[1], Ksenia V. Sukhareva[1,2,✉], Lyudmila R. Lyusova[3], Svetlana G. Karpova[2], Tatyana V. Monakhova[2], Natalya O. Belyaeva[1]

[1] *Plekhanov Russian University of Economics, Moscow, 117997 Russia*

[2] *N.M. Emanuel Institute of Biochemical Physics, Russian Academy of Sciences, Moscow, 119991 Russia*

[3] *MIREA – Russian Technological University, Moscow, 119454 Russia*

✉ *Автор для переписки, e-mail: Sukhareva.KV@rea.ru*

Abstract

Objectives. Elastomeric materials based on styrene–butadiene–styrene (SBS) triblock copolymers occupy approximately three-quarters of the global thermoplastic elastomer market; in the Russian elastomer market, their share exceeds 80%. Their primary applications include the production of shoe sole materials, anticorrosion coatings, waterproofing, and roofing mastics. The predominant form of degradation of such rubber products, which occurs in the presence of heat and oxygen, is known as thermal-oxidative aging. However, the creation of new functional materials based on modified styrene–butadiene block copolymers will enable the development of materials with enhanced resistance to thermal-oxidative degradation. Chlorinated paraffins, comprising a constituent mixture of polychlorinated *n*-alkanes, can be applied as halogen-containing modifiers for thermoplastic elastomers to enhance their strength and thermal properties. The aim of the present study is to create climate-resistant elastomeric composite materials based on modified SBS triblock copolymers and investigate the influence of a low molecular weight polychlorinated *n*-alkane modifier (chlorinated paraffin) on their thermal-oxidative stability.

Methods. Composite materials based on the SBS triblock copolymers with various amounts of chlorinated paraffin were prepared using the solution blending method. Fourier-transform infrared spectroscopy (FTIR) was used to analyze the impact of the amount of added modifier on the kinetics of thermal-oxidative degradation. The molecular mobility of the elastomers following thermal-oxidation was studied using the paramagnetic probe method to determine the correlation time that characterizes the rotational mobility of the probe in the elastomer matrix. The strength characteristics of the modified elastomer were investigated using a universal testing machine. The kinetics of the thermal-oxidative process were studied using the manometric solid-phase oxidation method.

Results. The results show that oxidation of SBS thermoplastic elastomers occurs mainly in the butadiene blocks. The degradation of unmodified elastomers is caused by chemical bond breakage reactions in the macromolecules. However, due to the sensitivity of double bonds in the polybutadiene segment of SBS, this thermoplastic elastomer is susceptible to light, ozone, and heat.

Conclusions. The multifunctional effect of the halogen-containing modifier on the elastomer leads to increased thermal-oxidative stability of the SBS triblock copolymer thermoplastic elastomer.

Keywords

thermal oxidation, styrene–butadiene–styrene triblock copolymer, modification, polychlorinated *n*-alkanes (chlorinated paraffin), solid-phase oxidation, electron paramagnetic resonance, FTIR spectroscopy

Submitted: 05.06.2024
Revised: 28.10.2024
Accepted: 24.12.2024

For citation

Almatova I.S., Sukhareva K.V., Lyusova L.R., Karpova S.G., Monakhova T.V., Belyaeva N.O. The influence of halogen-containing modifier on the thermo-oxidative stability of styrene–butadiene–styrene triblock copolymers. *Tonk. Khim. Tekhnol. = Fine Chem. Technol.* 2025;20(1):37–46. https://doi.org/10.32362/2410-6593-2025-20-1-37-46

НАУЧНАЯ СТАТЬЯ

Влияние галогеносодержащих модификаторов на термоокислительную стабильность стирол–бутадиен–стирольных триблок-сополимеров

И.С. Алматова[1], К.В. Сухарева[1,2,✉], Л.Р. Люсова[3], С.Г. Карпова[2], Т.В. Монахова[2], Н.О. Беляева[1]

[1] *Российский экономический университет им. Г.В. Плеханова, Москва, 117997 Россия*

[2] *Институт биохимической физики им. Н.М. Эмануэля, Российская академия наук, Москва, 119334 Россия*

[3] *МИРЭА – Российский технологический университет, Москва, 119454 Россия*

✉ *Corresponding author, e-mail: Sukhareva.KV@rea.ru*

Аннотация

Цели. Эластомерные материалы на основе триблок-сополимеров стирола–бутадиена–стирола (СБС) занимают примерно три четверти мирового рынка термопластичных эластомеров, а их доля превышает 80% на российском рынке эластомеров. К сферам их применения относятся производства обувных подошв, антикоррозионных покрытий, гидроизоляционных и кровельных мастик. Резиновые изделия подвержены в разной степени повреждению в результате нагрева и воздействия кислорода. Старение эластомерных изделий в присутствии тепла и кислорода известное как термоокислительное старение, является преобладающим методом старения данных материалов. Создание новых функциональных материалов на основе модифицированных блок-сополимеров стирола и бутадиена позволит разработать материалы с повышенной устойчивостью к термоокислительной деструкции. Хлорированные парафины представляют собой сложную смесь полихлорированных *н*-алканов и могут быть применены в качестве галогенсодержащих модификаторов термопластичных эластомеров для повышения их прочностных и термических свойств. Цель работы — создать климатически стойкие эластомерные композиционные материалы на основе модифицированных триблок-сополимеров СБС и исследовать влияние модификатора низкомолекулярного полихлорированного *н*-алкана (хлорпарафина) на термоокислительную стабильность триблок-сополимера СБС.

Методы. Методом растворного смешения получены композиционные материалы на основе триблок-сополимера СБС с различным количеством хлорпарафина. Инфракрасная спектроскопия с преобразованием Фурье была использована для анализа влияния количества добавленного модификатора на кинетику термоокислительной деструкции. Молекулярную подвижность эластомеров после термоокисления изучали методом парамагнитного зонда, определяя время корреляции, характеризующее вращательную подвижность зонда в матрице эластомера. Прочностные характеристики модифицированного эластомера исследовали на универсальной испытательной машине. Кинетику термоокислительного процесса изучали методом манометрического твердофазного окисления.

Результаты. Результаты показывают, что окисление термопластичных эластомеров СБС происходит преимущественно в бутадиеновых блоках. Деструкция немодифицированных эластомеров вызвана реакциями разрыва химических связей в макромолекулах. Из-за чувствительности двойных связей в полибутадиеновом сегменте СБС данный термопластичный эластомер чувствителен к воздействию света, озона и тепла.

Выводы. Галогенсодержащий модификатор оказывает многофункциональное воздействие на эластомер, повышая термоокислительную стабильность триблок-сополимера термопластичного эластомера СБС.

Ключевые слова

термическое окисление, стирол–бутадиен–стирольный триблок-сополимер, модификация, полихлорированные *н*-алканы (хлорпарафин), твердофазное окисление, электронный парамагнитный резонанс, ИК-Фурье спектроскопия

Поступила: 05.06.2024
Доработана: 28.10.2024
Принята в печать: 24.12.2024

Для цитирования

Almatova I.S., Sukhareva K.V., Lyusova L.R., Karpova S.G., Monakhova T.V., Belyaeva N.O. The influence of halogen-containing modifier on the thermo-oxidative stability of styrene–butadiene–styrene triblock copolymers. *Tonk. Khim. Tekhnol. = Fine Chem. Technol.* 2025;20(1):37–46. https://doi.org/10.32362/2410-6593-2025-20-1-37-46

INTRODUCTION

Significant expanded areas of application for elastomeric composite materials and products based on styrene–butadiene–styrene (SBS) indicates increased attention to this type of material. Thermoplastic elastomers are of great interest due to the possibility of purposeful combination of the physicochemical properties of the original elastomers. SBS triblock copolymer, which shares many characteristics with styrene–butadiene rubber, is the most widely used thermoplastic elastomer worldwide. However, SBS exhibits weak thermal oxidation stability, restricting its processing to temperatures up to 80°C [1, 2]. The unsaturation of the polymer indicates the presence of a double carbon–carbon bond –C=C– in its main chain, making it vulnerable to oxygen in the surrounding environment. The aging of composite elastomeric products as a result of oxidative degradation, leads to a deterioration in their physical and mechanical properties, including fatigue characteristics, which directly affects the lifespan of such products. The production of SBS is continuously expanding and has become an important part of the petrochemical industry. Similar to butadiene rubbers, the double bonds in the polybutadiene segment of SBS are sensitive to light, heat, and oxidation. This susceptibility leads to yellowing, crosslinking, and hardening, which can adversely affect its performance [3]. Elastomers are significantly influenced by environmental factors such as temperature, radiation, oxygen, ozone, ultraviolet radiation, humidity, etc. [4]. Thermal oxidation due to exposure of the material to heat in the presence of air, which has a substantial impact on the lifespan of such products, involves the combined effects of thermal energy and atmospheric oxygen on the elastomer.

While butadiene polymers and copolymers experience both scission and crosslinking during thermal oxidation, scission slightly predominates. Although research on their degradation remains limited, degradation processes in SBS triblock copolymers are known to occur in both the polystyrene and elastomer phases. The elastomer phase is more susceptible to degradation due to its low triglyceride level, which enhances oxygen permeability [5]. Research into the impact of thermo-oxidative aging on SBS structure reveals thermo-oxidative aging to be a critical factor leading to structural damage and performance deterioration in SBS [6–8]. Understanding the type and quantity of oxygen-containing groups in aged SBS under various conditions is essential for reconstructing the SBS molecule. While several studies have qualitatively analyzed the structure and properties of aged SBS, quantitative results are rarely reported. Wang *et al.* used Fourier-transform infrared spectroscopy (FTIR) to study SBS thermal oxidation involving the emergence of polar hydroxyl and carbonyl groups to reveal that the 1,4-polybutadiene portion degrades more easily than the 1,2-polybutadiene portion [9]. Munteanu *et al.* examined the thermo-oxidative behavior of SBS with different structures and detected hydroxyl and carboxyl groups on the molecular chain through FTIR [10]. Singh *et al.*, who used dynamic contact angle, FTIR spectrometry, and scanning electron microscopy to investigate changes in SBS following ultraviolet irradiation, propose a photo-oxidation aging mechanism [11]. Prasad *et al.* analyzed SBS aging after dissolution in various solvents using ^{13}C nuclear magnetic resonance to identify epoxides and alcohols as photoproducts [12]. The effects of aging on rubber materials can manifest as increased hardness [13], reduced surface energy, and decreased surface roughness [14].

Over the past 50 years, significant elaborations have been made to increase the oxidative resistance of elastomers by studying the causes and consequences of their degradation when exposed to oxygen and ozone in the air. Resistance to thermo-oxidative degradation is a critical criterion for rubber products used in outdoor applications. The degradation of rubber is well known to result from its reaction with molecular oxygen. This reaction can be mitigated by reducing the number of double bonds or by introducing functional groups that can deactivate these bonds. A described method for modifying SBS with maleic anhydride (MAH) involves an increase in the induction temperature and oxidation time of SBS-g-MAH compared to pure SBS due to the reduction of double bonds and α–H in the polybutadiene segment. This suggests that the thermo-oxidative stability of SBS-g-MAH is superior to that of SBS in polymer-modified asphalt applications.

Previously, the enhancement of flame resistance in highly flammable SBS was investigated through chemical modification with phosphorus-containing substances [15]. It was found that phosphorus-modified SBS undergoes charring, which correlates with the reduced flammability of the modified elastomer. The resistance of polymer composites to ultraviolet radiation is typically improved by introducing antioxidants [16] and ultraviolet absorber/ultraviolet stabilizers into the polymer matrix [17]. However, due to the tendency of such additives to migrate to the polymer surface, only short-term protection is provided. Currently, chemical modification of elastomers with organic halogen-containing (primarily chlorine-containing) compounds is widely researched and implemented. Chlorinated rubbers are used to produce elastomeric materials offering a wide range of desirable properties, including heat-, flame-, gasoline-, oil-, and ozone resistance, as well as resistance to aggressive environments, nonflammability, high strength, and gas impermeability [18]. The introduction of polar groups can also be used to enhance resistance to oil, ozone, flame, and solvents [19]. In order to increase the physical properties of rubbers to satisfy the growing demand for materials offering specific properties for extreme conditions, chemical modification of polymers becomes a crucial factor [20]. The halogenation of thermoplastic elastomers represents a convenient means to increase their compatibility with polar polymers, providing versatile curing possibilities that enhance adhesion, resistance to aging, and chemical resistance.

MATERIALS AND METHODS

A radial SBS (SBS R 3000A grade) triblock copolymer supplied by *Sibur*, Russia, having a styrene/butadiene ratio of 30 : 70 and melt mass-flow rate <1 g/10 min (200°C, 5 kg), was used as the polymer matrix. SBS R 3000A is widely used for modifying bitumen, plastics, rubber products, and protective coatings.

Industrial chlorinated paraffins (CPs) are constituent mixtures of polychlorinated *n*-alkanes that vary in chain length and degree of chlorination. Technical CP mixtures (CP-66T) obtained from *Kaustik*, Volgograd, Russia, which contain 69.5 ± 0.1 wt % chlorine, appear as a yellow-tinged, partly clotted powder. CPs produced by chlorinating alkane mixtures are used in complex products having thousands of homologs and congeners. CP-66T, which typically has one chlorine that can be changed to almost every carbon atom, is classified as a long-chain chlorinated paraffin. The mean carbon formula of CP ($C_{30}H_{38}Cl_{24}$) reveals the approximate average number of chlorine and hydrogen atoms per carbon atom; accordingly, 1 g of CP contains 0.695 g of chlorine.

SBS/CP composites were prepared by incorporating various amounts (2, 5, 10, 15, and 20 g per 100 g of resin (phr)) of chlorinated paraffin using the solution blending compounding method according to the formulation in the table. After casting the SBS/CP solutions into glass Petri dishes, the solvent was evaporated at room temperature of 22 ± 2°C until a constant weight was obtained.

A sample of 0.5 g dried SBS/CP was dissolved in a beaker including 50 mL of toluene at room temperature 22 ± 2°C over a period of 3 days. The solution concentration was adjusted to contain 1% solution (w/v). The sample for measurement of the Fourier-transform infrared spectroscopy (FTIR) spectroscopy was prepared as follows. A transparent thin film of raw SBS and SBS/CP was made on a transparent KBr window with dimension of 20 × 20 × 3 mm (width × length × thickness) by coating from 1% solution. The solution (0.2 mL) was dropped and coated thinly on a KBr window using a glass capillary. A sample coating on a KBr window was maintained to evaporate toluene in a dark at room temperature for 5 days. Thermal oxidation was performed on transparent thin films of the original SBS and modified SBS samples, applied to a KBr optical window, and then thermostated for 120 h at a temperature of 70°C.

Table. Formulation of chlorinated paraffin and thermoplastic elastomer solutions, mass parts per 100 mass parts of SBS (phr) and wt %

Copolymer	SBS	CP	Toluene	Total
SBS-0, phr	100	0	695	795
wt %	12.58	0	87.42	100
SBS-2, phr	100	2	695	797
wt %	12.55	0.25	87.20	100
SBS-5, phr	100	5	695	800
wt %	12.50	0.62	86.88	100
SBS-10, phr	100	10	695	805
wt %	12.42	1.24	86.34	100
SBS-15, phr	100	15	695	810
wt %	12.35	1.85	85.80	100
SBS-20, phr	100	20	695	815
wt %	12.27	2.45	85.28	100

The chemical composition of the samples was analyzed using FTIR with a Lumos FTIR microscope (*Bruker*, Germany). Spectra were recorded at a temperature of 22 ± 2°C in the wavenumber range of 4600–650 cm^{-1}. The spectra were processed using Bruker OPUS software. Transmission FTIR can be used to study rubber oxidation due to its high sensitivity to carbonyl groups.

Electron paramagnetic resonance (ESR) spectra were obtained using a EMX spectrometer (*Bruker*, Germany) with 100 kHz magnetic field modulation. The experiment was conducted at 22°C at a modulation amplitude of <0.5 G, microwave power of 2.1 mW, sweep width of 100 G, and 1,024 recorded points. 2,2,6,6-Tetramethylpiperidine-1-oxyl (TEMPO) chosen as a spin probe had a radical concentration not exceeding $1 \cdot 10^{-3}$ mol·dm^{-3}. TEMPO introduced into the sample at 30°C was initially in the vapor phase. ESR spectral data were obtained without saturation, verified by the signal intensity dependence on the microwave field power. The probe rotation correlation time τ_c was determined using the equation involving the width of the low-field spectral component (ΔH_{+1}) and intensities of high/low-field components ($I_{\pm 1}$):

$$\tau_c = \Delta H_{+1} \times [(I_{+1}/I_{-1})^{0.5-1}] \times 6.65 \times 10^{-10}\ \text{(s)}.$$

Data were mathematically processed using WINESR and SIMFONIA (*Bruker*, Germany) software.

The influence of the amount of chlorinated paraffin introduced into the SBS thermoplastic elastomer matrix on the kinetics of thermo-oxidation of the samples was studied using the manometric solid-phase oxidation method for determining the resistance of elastomers to the impact of oxygen at elevated temperatures. Since the oxidation reaction is always accompanied by the absorption of oxygen from the surrounding medium of the oxidizing substance, the oxidation process can be recorded by measuring the amount of oxygen absorbed by the elastomer. In this case, the oxidation rate was determined by the amount of captured oxygen using a manometric device. Rubber oxidation was conducted in the temperature range of 120°C ± 2°C and $p(O_2)$ = 500 torr. Solid KOH was used to absorb volatile oxidation products. The experiment was carried out for 400 min. The sample weight was 0.1 ± 0.001 g.

The tests for determining the elastic-strength properties were conducted on a Tinius Olsen universal testing machine (USA) designed for axial tensile testing in accordance with GOST 270-75[1]. Samples were prepared in the form of rectangular blades with dimensions of 100 × 10 mm; the length of the working section was 60 mm. The blade breakage speed was 50 mm/min. Each data point was confirmed by five measurements.

RESULTS AND DISCUSSION

Figure 1 present the FTIR spectra of the received SBS (SBS-0) and SBS/CP blends with different chlorinated paraffin amount (SBS-2, SBS-5, SBS-10, SBS-15, SBS-20).

The FTIR spectra of SBS triblock copolymers with different chlorinated paraffin contents clearly show the following absorption bands: 699 cm^{-1} (styrene block vibrations), 730 cm^{-1} (*cis*-1,4-polybutadiene vibrations), 910 cm^{-1} (vinyl bonds vibrations), and 965 cm^{-1} (*trans*-1,4-polybutadiene vibrations). The absorption intensity at 699 cm^{-1}, which remained constant during sample oxidation, was used as an internal standard for quantitative calculations of the degree of oxidation. The kinetics of carbonyl group accumulation, represented as the ratio of the optical absorption bands at 1731 cm^{-1} and 699 cm^{-1} over the thermostation time, is indicated in Fig. 2.

Transmission FTIR was successfully used to study the oxidation of rubber due to the high sensitivity of the carbonyl groups. The kinetics of oxidation of the original SBS sample and SBS with various amounts of chlorinated paraffin were studied using FTIR spectroscopy (transmission mode) (Fig. 3).

Thermal oxidation of unsaturated elastomers follows an autocatalytic free radical chain reaction. Consequently, the progression of oxidation can be tracked by the enhance in oxygen-containing functional groups, such as carbonyls (C=O). Here, the absorption intensity of the carbonyl stretching vibration at 1731 cm^{-1} is used as an indicator of the degree of oxidation [21].

The ESR spectra of radical probes in SBS-0, SBS-2, and SBS-20 samples before and after 120 h of thermo-oxidation are indicated in Fig. 4, while the correlation time dependencies for the samples over the oxidation period are exposed in Fig. 5.

According to molecular dynamics data, the introduction of more than 10% chlorinated paraffin

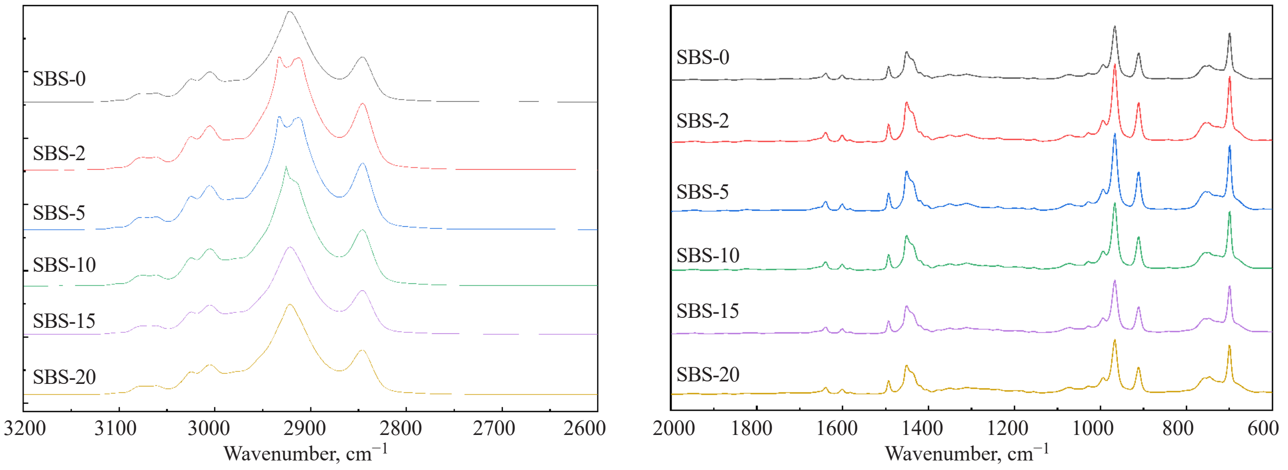

(a)

(b)

Fig. 1. FTIR spectra of SBS-0, SBS-2, SBS-5, SBS-10, SBS-15, and SBS-20: (a) in the wavelength range 3200–2600 cm^{-1}, (b) in the wavelength range 2000–600 cm^{-1}

---

[1] GOST 270-75. Interstate Standard. Rubber. Method of the determination elastic and tensile stress-strain properties. Moscow: IPK Izdatelstvo standartov; 1978 (in Russ.).

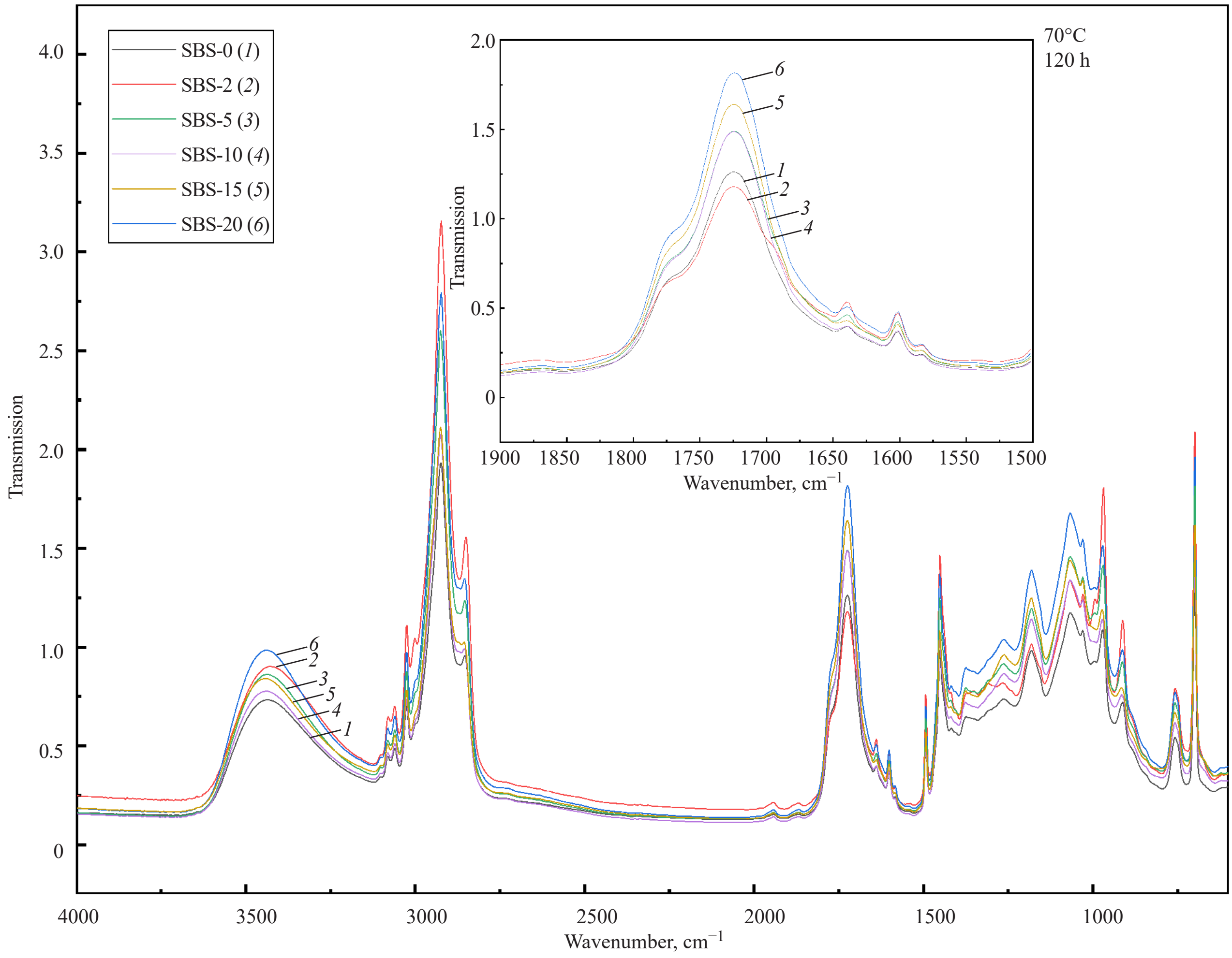

Fig. 2. FTIR spectra of SBS-0, SBS-2, SBS-5, SBS-10, SBS-15, and SBS-20 after 120 h of thermo-oxidation (70°C) in the wavelength range 4000–600 cm^{-1}

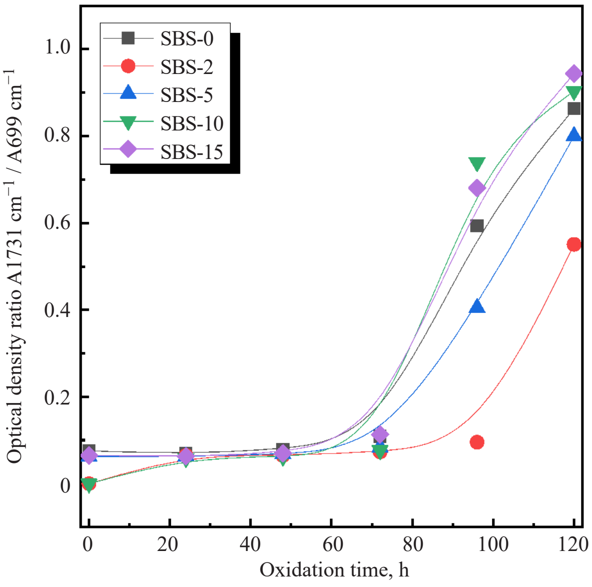

Fig. 3. Dependence of ratio between integrated absorbance values of bands at 1731 cm^{-1} and 699 cm^{-1} on the oxidation time

into the SBS matrix increases the correlation time of the radical probe, thereby reducing the segmental mobility of the elastomer chains. This indicates that chlorinated paraffins do not act as plasticizers in the mixture, since plasticizers typically increase the molecular mobility of elastomers. The unified approach presented in the literature suggests that lower molecular mobility in elastomers due to reduced intermolecular interactions results in higher thermal and thermo-oxidative stability. This approach is valid only for SBS-2 and SBS-5 samples, where the initial correlation time of the radical probe increases compared to the original SBS; according to FTIR spectroscopy, this indicates reduced molecular mobility and enhanced thermo-oxidative stability. The introduction of more than 5% chlorinated paraffin significantly increases the initial correlation time, including an extreme rise after 96 h of oxidation, which indicates further reduced molecular mobility during active oxidation. SBS-0, SBS-2, and SBS-5 samples do not exhibit a sharp increase in correlation

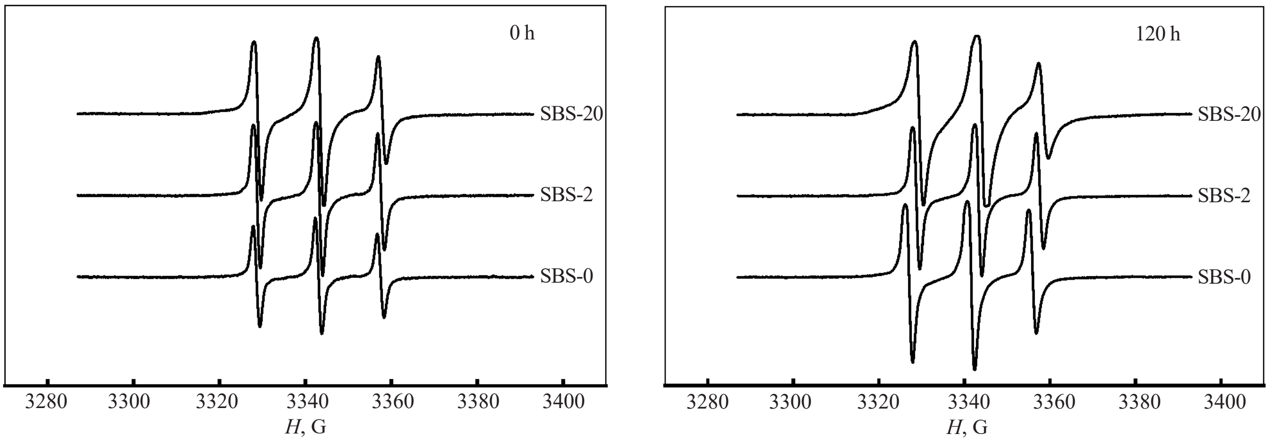

Fig. 4. ESR spectra of the spin probe incorporated in SBS-0, SBS-2, and SBS-20 before and after 120 h of thermal oxidation

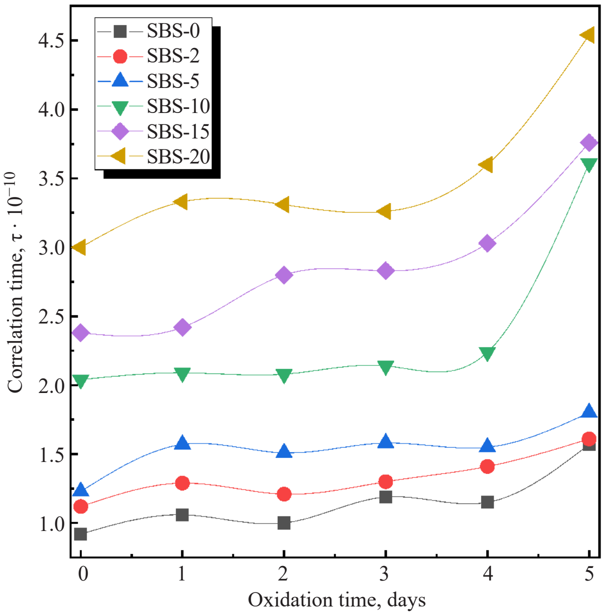

Fig. 5. Dependence of the rotational correlation times of TEMPO spin probe in SBS-0, SBS-2, SBS-5, SBS-10, SBS-15, and SBS-20 on the oxidation time

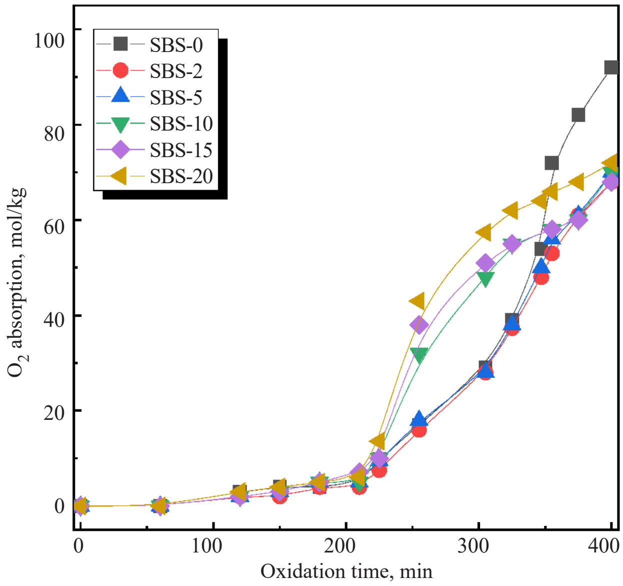

Fig. 6. Oxygen absorption kinetic curves for as-received SBS (SBS-0) and SBS with different chlorinated paraffins amounts (SBS-2, SBS-5, SBS-10, SBS-15, and SBS-20) at temperature 120°C and oxygen pressure 500 torr

time after 96 h of thermo-oxidation. Correlation time is defined as the time required for a molecule to rotate by one radian. The EPR spectrum of the nitroxide radical provides information about the nature of its microenvironment. Introducing nitroxide radicals into the studied systems allows the aggregation parameters and dynamics of these processes to be examined using ESR. Kinetic curves of oxygen absorption by the original SBS thermoplastic elastomer and SBS samples with different chlorinated paraffin contents at 120°C are shown in Fig. 6.

According to analysis of the oxygen absorption time dependence for modified SBS samples with different amounts of the modifier and the received SBS sample, all samples exhibit high hermos-oxidative stability during the initial oxidation stage (up to 200 min) at a low initial oxidation rate. The induction time for oxidation is the same for all samples. A sharp acceleration in the oxidation process observed in samples with 10, 15, and 20 wt % chlorinated paraffin after 200 min is due to a rapid increase in oxygen absorption by the elastomers. During this oxidation stage, the oxygen absorption rate can be reduced by introducing 2 wt % of chlorinated paraffin to enhance hermos-oxidative stability. Various studies suggest that low-molecular-weight additives that transfer free valence during co-oxidation with the elastomer can be used to inhibit oxidation.

In SBS samples with 10, 15, and 20% chlorinated paraffin, a heterogeneous system forms in which modifier molecule aggregates act as inclusion phases to offer a more developed surface than tightly packed polymer chains. Aggregation of modifier molecules at concentrations above 5 wt % is due to the accumulation of unreacted modifier to form clusters. The consequent creation of micropores offering a more developed surface allows higher oxygen diffusion compared to a homogeneous system based on SBS and SBS with low modifier concentrations. The observed reduction in the autocatalytic oxidation stage rate in SBS-2 and SBS-5 samples may result from decreased conformational mobility of thermoplastic elastomer chains in the presence of low-chlorinated paraffin additives and the absence of aggregate formation. The introduction of 2 wt % chlorinated paraffin reduces the initial oxidation and autocatalysis rates, serving to inhibit oxidation and increase the activation energy of autocatalysis in the elastomer mixture.

The dependence of physicomechanical properties on the amount of modifier introduced is shown in Fig. 7.

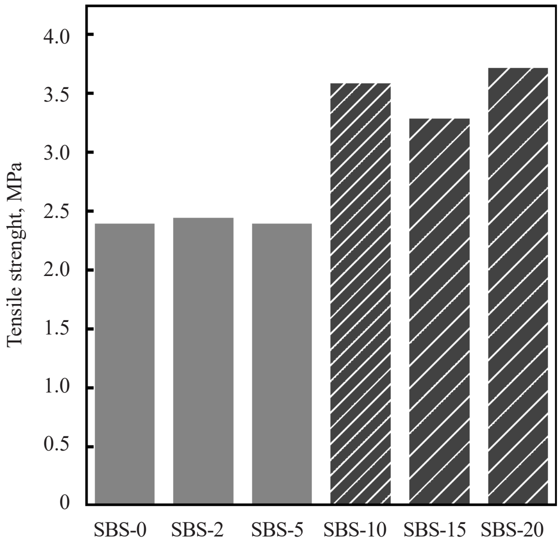

Fig. 7. Mechanical properties of the initial samples SBS-0, SBS-2, SBS-5, SBS-10, SBS-15, and SBS-20

Analysis of the strength characteristics of the original SBS-0 and samples with different modifier amounts revealed the following trend: the introduction of up to 5 wt % chlorinated paraffin into SBS maintains the strength characteristics at the level of the original SBS-0. Small amounts of low-molecular-weight halogen-containing modifiers do not significantly affect the elastomer strength properties. SBS-10, SBS-15, and SBS-20 form a distinct group with higher strength characteristics compared to SBS-0, SBS-2, and SBS-5 samples. This trend aligns with ESR spectroscopy data, indicating that reduced polymer molecule flexibility, or molecular mobility, results in a stiffer polymer with higher modulus of elasticity and strength.

CONCLUSIONS

According to FTIR spectroscopy data, the introduction of 2 and 5 wt % chlorinated paraffin results in uniform distribution of modifier molecules within the elastomer phase, which interact with elastomer macromolecules during swelling. However, higher chlorinated paraffin concentrations hinder uniform distribution due to the aggregation of chlorinated paraffin molecules as reflected in increased radical probe correlation time in samples with over 5% paraffin. The mechanical characteristics are significantly improved in samples with 10 to 20 wt % paraffin. As unreacted chlorinated paraffin accumulates, its particles aggregate due to thermodynamic affinity to form polar-polar interactions within the nonpolar polymer matrix. Consequently, the introduction of more than 5 wt % chlorinated paraffin creates a heterogeneous system with an unstable inclusion phase based on chlorinated paraffin aggregates, which is more diffusively accessible to oxygen during oxidation processes.

Acknowledgments

The work was carried out using the equipment of the Joint Research Center of Plekhanov Russian University of Economics and the Center of Shared Usage "New Materials and Technologies" at the Emanuel Institute of Biochemical Physics.

Authors' contributions

I.S. Almatova—investigating the composition and properties of mechanoactivated SBS triblock copolymers, analyzing the data and writing the manuscript.

K.V. Sukhareva—supervising the project.

L.R. Lyusova— analysis the results, critical feedback and shaping the research.

S.G. Karpova—contributing to the final version of the manuscript.

T.V. Monakhova—performing the experiments/calculations/simulations, analyzing the data.

N.O. Belyaeva—performing the experiments, contributing to the interpretation of the results.

The authors declare no conflict of interest warranting disclosure in this article.

REFERENCES

1. Li H., Wu H., Wang C., Zheng J. Styrene–butadiene–styrene/graphene nanocomposites with improved thermal oxidation stability. *Polym. Int*. 2024;73(6):446–453. https://doi.org/10.1002/pi.6611
2. Adhikari R., Michler G.H. Influence of molecular architecture on morphology and micromechanical behavior of styrene/butadiene block copolymer systems. *Prog. Polym. Sci*. 2004;29(9):949–986. https://doi.org/10.1016/j.progpolymsci.2004.06.002
3. Xu J., Zhang A., Zhou T., Cao X., Xie Z. A study on thermal oxidation mechanism of styrene–butadiene–styrene block copolymer (SBS). *Polym. Degrad. Stab*. 2007;92(9):1682–1691. https://doi.org/10.1016/j.polymdegradstab.2007.06.008
4. Rezig N., Bellahcene T., Aberkane M., Nait A.M. Thermo-oxidative ageing of a SBR rubber: effects on mechanical and chemical properties. *J. Polym. Res*. 2020;27(10):339. https://doi.org/10.1007/s10965-020-02330-y
5. Allen N.S., Barcelona A., Edge M., Wilkinson A., Merchan C.G., Ruiz Santa Quiteria V. Thermal and photooxidation of high styrene–butadiene copolymer (SBC). *Polym. Degrad. Stab*. 2004;86(1):11–23. https://doi.org/10.1016/j.polymdegradstab.2003.10.010
6. Su T-T., Jiang H., Gong H. Thermal Stabilities and Thermal Degradation Kinetics of a Styrene-Butadiene-Styrene Star Block Copolymer. Polym. Plast. Technol. Eng. 2009;48(5):535–541. https://doi.org/10.1080/03602550902824341
7. Chiantore O., Tripodi S., Sarmoria C., Vallés E. Mechanism and molecular weight model for thermal oxidation of linear ethylene–butene copolymer. *Polymer*. 2001;42(9):3981–3987. https://doi.org/10.1016/S0032-3861(00)00736-9
8. Xu X., Yu J., Xue L., Zhang C., Zha Y., Gu Y. Investigation of Molecular Structure and Thermal Properties of Thermo-Oxidative Aged SBS in Blends and Their Relations. *Materials*. 2017;10(7):768. https://doi.org/10.3390/ma10070768
9. Wang S-M., Chang J-R., Tsiang RC-C. Infrared studies of thermal oxidative degradation of polystyrene-*block* polybutadiene-*block*-polystyrene thermoplastic elastomers. *Polym. Degrad. Stab*. 1996;52(1):51–57. https://doi.org/10.1016/0141-3910(95)00226-X
10. Munteanu S.B., Brebu M., Vasile C. Thermal and thermo-oxidative behaviour of butadiene–styrene copolymers with different architectures. *Polym. Degrad. Stab*. 2005;89(3):501–512. https://doi.org/10.1016/j.polymdegradstab.2005.01.037
11. Singh R.P., Desai S.M., Solanky S.S., Thanki P.N. Photodegradation and stabilization of styrene-butadiene-styrene rubber. *J. Appl. Polym. Sci*. 2000;75(9):1103–1114. https://doi.org/10.1002/(SICI)1097-4628(20000228)75:9<1103::AID-APP3>3.0.CO;2-M
12. Prasad A.V., Singh R.P. Photooxidative degradation of styrenic polymers: ^{13}C-NMR and morphological changes upon irradiation. *J. Appl. Polym. Sci*. 1998;70(4):637–645. https://doi.org/10.1002/(SICI)1097-4628(19981024)70:4<637::AID-APP2>3.0.CO;2-R
13. Li X.G., Zhang Y.L., Yang M.Y. Study on Thermal Oxidative Aging of Nitrile Rubber. *Appl. Mech. Mater*. 2013;299:199–202. http://doi.org/10.4028/www.scientific.net/AMM.299.199
14. Garcia-Garcia D., Crespo-Amorós J.E., Parres F., Samper M.D. Influence of Ultraviolet Radiation Exposure Time on Styrene-Ethylene-Butadiene-Styrene (SEBS) Copolymer. *Polymers*. (Basel). 2020;12(4):862. https://doi.org/10.3390/polym12040862
15. Chernyy S., Ullah S., Jomaas G., Leisted R.R., Mindykowski P.A., Ravnsbæk J.B., *et al*. Modification of poly(styrene-*block*-butadiene-*block*-styrene) [SBS] with phosphorus containing fire retardants. *Eur. Polym. J*. 2015;70:136–146. https://doi.org/10.1016/j.eurpolymj.2015.07.015
16. Li Y., Li L., Zhang Y., Zhao S., Xie L., Yao S. Improving the aging resistance of styrene-butadiene-styrene tri-block copolymer and application in polymer-modified asphalt. *J. Appl. Polym. Sci*. 2010;116(2):754–761. https://doi.org/10.1002/app.31458
17. Ching Y.C., Gunathilake T.U., Ching K.Y., Chuah C.H., Sandu V., Singh R., Liou K.Y. Effects of high temperature and ultraviolet radiation on polymer composites. In: *Durability and Life Prediction in Biocomposites, Fibre-Reinforced Composites and Hybrid Composites*. Elsevier; 2019. P. 407–426. https://doi.org/10.1016/B978-0-08-102290-0.00018-0
18. Sukhareva K.V., Mikhailov I.A., Mamin E.A., Monakhova T.V., Kasparov V.V., Kolesnikov E.A., Popov A.A. Modification of nitrile-butadiene rubber surface by immersion into 1,1,2-trifluoro-1,2,2-trichlor-ethane and its physio-chemical properties. *Polym. Eng. Sci*. 2023;63(9):2891–2904. https://doi.org/10.1002/pen.26413
19. Ramesan M.T., Kumar T.A. Preparation and properties of different functional group containing styrene butadiene rubber. *J. Chil. Chem. Soc*. 2009;54(1):23–27. http://doi.org/10.4067/S0717-97072009000100006
20. Sukhareva K.V., Sukharev N.R., Levina I.I., Offor P.O., Popov A.A. Solvent Swelling-Induced Halogenation of Butyl Rubber Using Polychlorinated N-Alkanes: Structure and Properties. *Polymers*. 2023;15(20):4137. https://doi.org/10.3390/polym15204137
21. Li G-Y., Koenig J.L. A Review of Rubber Oxidation. *Rubber Chemistry and Technology*. 2005;78(2):355–390. https://doi.org/10.5254/1.3547888

About the authors

Irina S. Almatova, Postgraduate Student, Basic Department of Chemistry of Innovative Materials and Technologies, Plekhanov Russian University of Economics (36, Stremyannyi per., Moscow, 115054, Russia). E-mail: AlmatovaIS@rea.ru. https://orcid.org/0009-0005-3415-9196

Ksenia V. Sukhareva, Cand. Sci. (Chem.), Senior Researcher, Associate Professor, Higher Engineering School "New Materials and Technologies," Plekhanov Russian University of Economics (36, Stremyannyi per., Moscow, 115054, Russia). E-mail: Sukhareva.KV@rea.ru. Scopus Author ID 57191042974, RSCI SPIN-code 1883-8039, https://orcid.org/0000-0002-0282-7015

Lyudmila R. Lyusova, Dr. Sci. (Eng.), Professor, Head of the F.F. Koshelev Department of Chemistry and Technology of Processing of Elastomers, M.V. Lomonosov Institute of Fine Chemical Technologies, MIREA – Russian Technological University (78, Vernadskogo pr., Moscow, 119454, Russia). E-mail: lyusova@mirea.ru. Scopus Author ID 6508196636, RSCI SPIN-code 6390-2313, https://orcid.org/0000-0001-9515-6347

Svetlana G. Karpova, Cand. Sci. (Chem.), Senior Researcher, N.M. Emanuel Institute of Biochemical Physics, Russian Academy of Sciences (4, Kosygina ul., Moscow, 119334, Russia). E-mail: karpova@sky.chph.ras.ru. Scopus Author ID 16218970000, RSCI SPIN-code 4449-9506, https://orcid.org/0000-0003-3514-5843

Tatyana V. Monakhova, Cand. Sci. (Chem.), Senior Researcher, N.M. Emanuel Institute of Biochemical Physics, Russian Academy of Sciences (4, Kosygina ul., Moscow, 119334, Russia). E-mail: monakhova-81@mail.ru. https://orcid.org/0000-0002-0731-8412

Natalya O. Belyaeva, Research Assistant, Basic Department of Chemistry of Innovative Materials and Technologies; Student, Higher Engineering School "New Materials and Technologies," Plekhanov Russian University of Economics (36, Stremyannyi per., Moscow, 115054, Russia). E-mail: nataly12022004@yandex.ru. Scopus Author ID 59172652500, RSCI SPIN-code 2652-3760, https://orcid.org/0009-0004-1566-2952

Об авторах

Алматова Ирина Сергеевна, аспирант, базовая кафедра химии инновационных материалов и технологий, ФГБОУ ВО «Российский экономический университет им. Г.В. Плеханова» (115054, Россия, Москва, Стремянный пер., д. 36). E-mail: AlmatovaIS@rea.ru. https://orcid.org/0009-0005-3415-9196

Сухарева Ксения Валерьевна, к.х.н., старший научный сотрудник, доцент, Высшая инженерная школа «Новые материалы и технологии», ФГБОУ ВО «Российский экономический университет им. Г.В. Плеханова» (115054, Россия, Москва, Стремянный пер., д. 36). E-mail: Sukhareva.KV@rea.ru. Scopus Author ID 57191042974, SPIN-код РИНЦ 1883-8039, https://orcid.org/0000-0002-0282-7015

Люсова Людмила Ромуальдовна, д.т.н., профессор, заведующая кафедрой химии и технологии переработки эластомеров им. Ф.Ф. Кошелева, Институт тонких химических технологий им. М.В. Ломоносова, ФГБОУ ВО «МИРЭА – Российский технологический университет» (119454, Россия, Москва, пр-т Вернадского, д. 78). E-mail: lyusova@mirea.ru. Scopus Author ID 6508196636, SPIN-код РИНЦ 6390-2313, https://orcid.org/0000-0001-9515-6347

Карпова Светлана Геннадьевна, к.х.н., старший научный сотрудник, ФГБУН Институт биохимической физики им. Н.М. Эмануэля Российской академии наук (199334, Россия, Москва, ул. Косыгина, д. 4). E-mail: karpova@sky.chph.ras.ru. Scopus Author ID 16218970000, SPIN-код РИНЦ 4449-9506, https://orcid.org/0000-0003-3514-5843

Монахова Татьяна Вадимовна, к.х.н., старший научный сотрудник, ФГБУН Институт биохимической физики им. Н.М. Эмануэля Российской академии наук (199334, Россия, Москва, ул. Косыгина, д. 4). E-mail: monakhova-81@mail.ru. https://orcid.org/0000-0002-0731-8412

Беляева Наталья Олеговна, лаборант-исследователь, базовая кафедра химии инновационных материалов и технологий; студент, Высшая инженерная школа «Новые материалы и технологии», ФГБОУ ВО «Российский экономический университет им. Г.В. Плеханова» (115054, Россия, Москва, Стремянный пер., д. 36). E-mail: nataly12022004@yandex.ru. Scopus Author ID 59172652500, SPIN-код РИНЦ 2652-3760, https://orcid.org/0009-0004-1566-2952

The text was submitted by the authors in English
and edited for English language and spelling by Thomas A. Beavitt

Tonkie Khimicheskie Tekhnologii = Fine Chemical Technologies.
2025;20(1):47–54. ISSN 2686-7575 (Online)

Chemistry and technology of inorganic materials
Химия и технология неорганических материалов

UDC 66.01
https://doi.org/10.32362/2410-6593-2025-20-1-47-54
EDN KJJVQA

RESEARCH ARTICLE

Synthesis and characterization of rare earth metal complexes with novel Schiff base

Gulu G. Abbasova@, Ajdar A. Medjidov, Rayyat H. Ismayilov, Aydin M. Pashajanov, Perizad A. Fatullayeva
Ministry of Science and Education of the Republic of Azerbaijan, Academician M. Nagiyev Institute of Catalysis and Inorganic Chemistry, AZ 1143 Baku, Azerbaijan
✉ *Corresponding author, e-mail: veliyeva_g23@yahoo.com*

Abstract

Objectives. The work set out to synthesize Schiff base ligands containing a hydrazone moiety of (*Z*)-2-((*E*)-1-hydroxyethylidene)-hydrazineylidene)-2-phenylacetic acid, as well as their praseodymium, samarium, europium, and gadolinium complexes, and to study their structure.

Methods. The structure of ligands was identified by infrared (IR), ultraviolet (UV), and nuclear magnetic resonance (NMR) spectroscopy. The structure of the complexes was confirmed by elemental analysis, IR and UV spectroscopy, and thermogravimetric analysis.

Results. The Schiff base ligands containing a hydrazone moiety of (*Z*)-2-((*E*)-1-hydroxyethylidene)hydrazineylidene)-2-phenylacetic acid, as well as their praseodymium, samarium, europium, and gadolinium complexes, were synthesized using the authors' procedure.

Conclusions. NMR and IR spectroscopic data confirm that the Schiff base ligand is in the keto form. There are three absorption bands in the wavelength range of 205–306 nm in the UV spectrum of the ligand. A bathochromic shift is observed in the spectrum of all complexes. The molar ratio of ligand and metal in the complexes was 3 : 1.

Keywords

hydrazones, phenylglyoxylic acid, Schiff base, rare earth elements, complexing

Submitted: 30.05.2024
Revised: 14.10.2024
Accepted: 24.12.2024

For citation

Abbasova G.G., Medjidov A.A., Ismayilov R.H., Pashajanov A.M., Fatullayeva P.A. Synthesis and characterization of rare earth metal complexes with novel Schiff base. *Tonk. Khim. Tekhnol. = Fine Chem. Technol.* 2025;20(1):47–54. https://doi.org/10.32362/2410-6593-2025-20-1-47-54

НАУЧНАЯ СТАТЬЯ

Синтез и характеристика комплексов металлов редкоземельных элементов на новом основании Шиффа

Г.Г. Аббасова@, А.А. Меджидов, Р.Х. Исмаилов, А.М. Пашаджанов, П.А. Фатуллаева

Министерство науки и образования Азербайджанской республики, Институт катализа и неорганической химии имени академика М. Нагиева, Баку, AZ 1143 Азербайджан

@Автор для переписки, e-mail: veliyeva_g23@yahoo.com

Аннотация

Цели. Синтезировать лиганды основания Шиффа, содержащие гидразоновую часть (*Z*)-2-((*E*)-1-гидроксиэтилиден)гидразинилиден)-2-фенилуксусной кислоты, и их комплексы празеодима, самария, европия и гадолиния, а также исследовать их структуру.

Методы. Структура лигандов была идентифицирована с помощью инфракрасной (ИК) и ультрафиолетовой (УФ) спектроскопии и спектроскопии ядерного магнитного резонанса (ЯМР). Структура комплексов была подтверждена с помощью элементного анализа, ИК- и УФ-спектроскопии и термогравиметрического анализа.

Результаты. Лиганды основания Шиффа, содержащие гидразоновую часть (*Z*)-2-((*E*)-1-гидроксиэтилиден)гидразинилиден)-2-фенилуксусной кислоты, и их комплексы с празеодимом, самарием, европием и гадолинием были синтезированы по методике авторов.

Выводы. Данные ЯМР- и ИК-спектроскопии подтверждают, что лиганд на основе Шиффа находится в кето-форме. В УФ-спектре лиганда имеются три полосы поглощения в диапазоне длин волн 205–306 нм. В спектре всех комплексов наблюдается батохромный сдвиг. Молярное соотношение лиганда и металла в комплексах составило 3 : 1.

Ключевые слова

гидразоны, фенилглиоксиловая кислота, основание Шиффа, редкоземельные элементы, комплексообразование

Поступила:	30.05.2024
Доработана:	14.10.2024
Принята в печать:	24.12.2024

Для цитирования

Abbasova G.G., Medjidov A.A., Ismayilov R.H., Pashajanov A.M., Fatullayeva P.A. Synthesis and characterization of rare earth metal complexes with novel Schiff base. *Tonk. Khim. Tekhnol. = Fine Chem. Technol.* 2025;20(1):47–54. https://doi.org/10.32362/2410-6593-2025-20-1-47-54

INTRODUCTION

With the existence of an azomethine bond affecting biological activity [1–3], Schiff bases are a special type of ligands with a variety of donor atoms that exhibit remarkable ways of coordinating to transition metals [4–6]. The salen-type Schiff bases obtained by the condensation of salicylaldehyde (sal) and primary ethylenediamine (en) are thought to be workable ligands for coordination chemistry, due to the possibility of arranging their steric and electronic features by the primary amine and aldehyde. Due to the inclusion of donor centers for metal ions in their composition, which allow for the design of different geometries with other ligands, a significant number of metal complexes have been synthesized using salen-type Schiff bases [7]. Schiff bases, containing imine or azomethine groups, and their metal complexes are used in encapsulation and separation processes, in industry, and in supramolecular chemistry as catalysts, corrosion inhibitors, pigments, and dyes [8–14]. Over the past few decades, numerous studies have been carried out on the use of this class of compounds, especially in medicine, due to the presence of diverse biological and pharmacological properties, including antimicrobial, anti-inflammatory, analgesic, antifungal, anti-tuberculosis, antiviral, anticancer, antiplatelet, antimalarial, anticonvulsant, cardioprotective, anthelminthic, antiprotozoal, antitrypanosomal, and antischistosomal [15–30].

Versatile applications of Schiff bases and their metal complexes stimulate interest in developing their synthesis methods. Hence the development of new effective, easy, and selective synthesis methods is still relevant for chemists. The aim of the work is to synthesize

Schiff base ligands, containing a hydrazone moiety of (*Z*)-2-((*E*)-1-hydroxyethylidene)hydrazineylidene)-2-phenylacetic acid, along with their praseodymium, samarium, europium, and gadolinium complexes.

EXPERIMENTAL

Materials and methods

All chemicals and solvents were purchased from commercial suppliers and were reagent grade. Salts were obtained from *Merck*, Germany, while solvents were procured from *Qualikems*, India. Phenyl glyoxylic acid and acetyl chloride purchased from *Sigma-Aldrich* (USA) were used without further purification.

Electronic absorption spectra were recorded on an Evolution 60S ultraviolet-visible (UV-VIS) spectrophotometer (*Thermo Fisher Scientific*, USA) in ethanol. Infrared (IR) spectra (KBr pellets) were recorded on a spectrophotometer Nicolet IS10 (*Thermo Fisher Scientific*, USA) in the range 500–4000 cm^{-1}.

^{1}H and ^{13}C nuclear magnetic resonance (NMR) spectra were recorded on a Bruker (300 MHz) spectrometer (*Bruker*, Germany) in CD_4O at room temperature (19–20°C). Thermogravimetric analysis was performed using a NETZSCH STA 449F3 derivatograph (*NETZSCH*, Germany). The elemental analyses were performed at the Tubitak analytical laboratory, in Ankara, Turkey, using a CHNS-932 analyzer (*Leco*, Germany).

Synthesis of (*Z*)-2-(2-acetylhydrazineylidene)-2-phenylacetic acid (LH_2)

The starting hydrazide was synthesized according to the following procedure.

The mixture of 4 mL of triethylamine and 10 mL of anhydrous hydrazine was stirred with a magnetic stirrer. To this mixture, 14.4 mL of acetyl chloride was added with the rate of 1 drop in every 5 s. The reaction mixture was cooled with ice to avoid overheating. The resulting white slurry was separated and recrystallized from ethanol to give pure needle acetylhydrazine, having a melting temperature $T_{\text{m.p.}} = 70 \pm 3$°C.

To obtain the target (*Z*)-2-(2-acetylhydrazineylidene)-2-phenylacetic acid (LH_2), phenylglyoxylic acid and acetylhydrazine was taken in a molar ratio of 1 : 1. After dissolving 450 mg (5 mmol) of phenylglyoxylic acid in 5 mL of ethanol, 222 mg (5 mmol) of the acetylhydrazine solution in 5 mL water was added with stirring and heating to 70°C. From the resulting yellowish homogenous solution, bright yellow thin needle-like crystals precipitated within one day. The obtained crystals were filtered, recrystallized from ethanol, and dried over $CaCl_2$ in a desiccator. $T_{\text{m.p.}}$: 157 ± 2°C. Yield was 525 mg (85%). Calculated for $C_{10}H_{10}N_2O_3$: C 58.25; H 4.85; N 13.59%. Found: C 58.35; H 4.98; N 12.95%. ^{1}H NMR (300 MHz, CD_4O): δ 7.91–7.48 (4d, t, 5H at benzene ring); 2.10 (s, 3H CH_3).

Preparation of metal complexes with LH_2

To obtain metal complexes with LH_2, solutions of the corresponding metal salts in methanol and the ligand in ethanol were used. For this purpose, solutions of $Pr(NO_3)_3$, $Sm(NO_3)_3$, $Eu(NO_3)_3 \cdot 6H_2O$, and $Gd(ClO_4)_3 \cdot 6H_2O$ salts in molar ratio of 1 : 3 to the ligand were used. Solutions of metal salts and the ligand were stirred upon mild heating. Following filtration, the obtained light yellow and yellowish-orange precipitates were washed with distilled water, and then with alcohol. The obtained complexes were dried over $CaCl_2$ in a desiccator until constant weight was reached. The melting points of praseodymium, samarium, europium, and gadolinium complexes were 200°C, over 260°C, 230°C and over 250°C. Yields were 172, 179, 197, and 173 mg, for 75, 72, 79, and 69%, respectively. Calculated for $Me(C_{10}H_9N_2O_3)_3$: C 47.65; H 3.59; N 11.11%; C 47.06; H 3.56; N 10.98%; C 46.96; H 3.55; N 10.95%; C 46.64; H 3.52; N 10.88%. Found: C 47.59; H 3.65; N 11.35%; C 46.95; H 3.65; N 11.05%; C 46.91; H 3.68; N 11.02%; C 46.72; H 3.59; N 11.01%, respectively, for praseodymium, samarium, europium, and gadolinium complexes.

RESULTS AND DISCUSSION

(*Z*)-2-(2-acetylhydrazineylidene)-2-phenylacetic acid is a potential tridentate dianionic ligand. Such a two-charged ligand can be realized at the expense of carboxylic and enolized acetyl groups (compound **3**) as presented in Scheme 1. However, NMR and IR spectroscopy data point to the presence of the keto form in ligand (compound **2**).

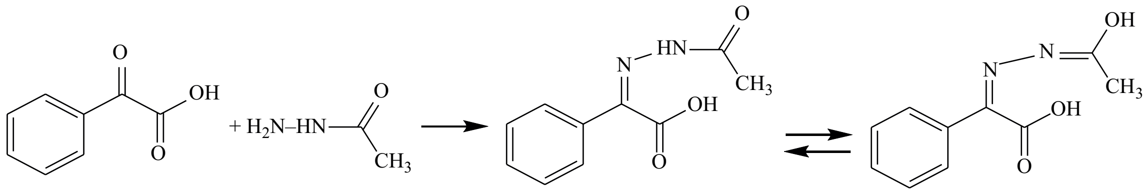

1 **2** **3**

Scheme 1. Synthesis of the ligand and its tautomeric forms. **1**. Phenylglyoxylic acid. **2**. Keto form. **3**. Enol form

Electronic spectra

Electronic absorption spectra of compounds were recorded in ethanol in the UV region at room temperature (Fig. 1). There are three absorption bands in the wavelength range of 205–306 nm in the spectrum of the ligand.

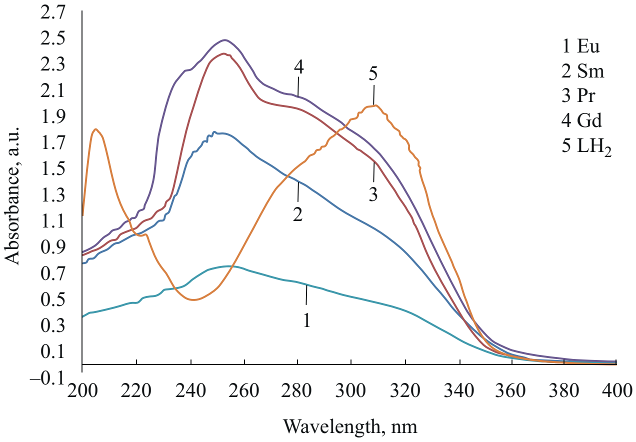

Fig. 1. UV-spectra of LH_2 and complexes

The band appearing at 306 nm and corresponding to low energy side is considered to be n–π* transition of conjugation between the lone pair of electrons of nitrogen atom in azomethine group and a conjugated π bond of benzene ring.

Other peaks appearing at higher energy sides of 205 and 223 nm are associated with π–π* and n–π* transitions of carbonyl moiety and aromatic ring [28, 31]. Complexation of ligand with metal ions results in a bathochromic shift in the spectra of all complexes. Thus, in the spectra of all complexes, a broad peak is observed in the wavelength range of 250–260 nm due to the coordination and the formation of chelate rings in the complexes [32].

IR spectroscopy

The IR spectra of ligand and its complexes are studied. It is known from the literature that the band of stretching vibrations of the non-ionized and non-coordinated COO^- group lies in the range of 1750–1700 cm^{-1}, while the ionized and coordinated COO^- group lies in the range of 1650–1590 cm^{-1} [33]. No ligand absorption band at 1745 cm^{-1} corresponding to the non-coordinated carboxyl group is observed in the spectra of complexes. On the contrary, peaks corresponding to the coordinated carboxyl group are observed in the spectra of all complexes at 1570, 1589, 1571 and 1507 cm^{-1}, for Pr, Sm, Eu, and Gd, respectively. These bands are observed because the hydroxyl group of the ligand is ionized to form a bond with the central ion.

As described in [33], bands of stretching vibrations of the C=N group appear at 1590–1604 cm^{-1}. Bands resulting from CN stretching vibration are observed in the spectra of complexes as shifted peaks (1603, 1608, 1604, 1575 cm^{-1}, respectively, for Pr, Sm, Eu, and Gd complexes) comparatively with the ligand (1605 cm^{-1}) due to involvement of the iminic nitrogen atom in coordination [34]. Bands corresponding to the peptide bond (1655–1630 cm^{-1}) [35] are slightly shifted (1676, 1669, 1629, and 1594 cm^{-1}, respectively, for Pr, Sm, Eu, and Gd) as compared with the bands in the spectrum of the ligand (1685 cm^{-1}) due to δ(NH)+ν(CN) coupled vibrations. This indicates that oxygen atom in the amide group is involved in coordination. The spectra of both the ligand and the complexes have some medium peaks that may be attributed to stretching vibration of ν(NH) 3000–3200 cm^{-1}. It shows that NH group was not coordinated with metal. This band also proves that the coordination form of the ligand is the keto form. All bands characterizing the ligand and complexes are given in the Table.

NMR spectroscopic studies

The NMR spectrum of the obtained ligand is consistent with literature data. The ^1H NMR spectrum of the ligand exhibits some peaks in the range of 7.91–2.10 ppm (Fig. 2). Peaks in the range of 7.91–7.48 ppm are accepted as benzene ring protons. One ***s*** upfield peak observed at 2.10 ppm is suitable for representing the hydrogen atoms in the methyl group.

Table. Absorption bands of the ligand and its complexes

Substance	Non-coordinated carboxyl group	Coordinated carboxyl group	C=N stretching vibration	δ(NH)+ν(CN)
Ligand	1745	–	1605	1685
Praseodymium	–	1570	1603	1676
Samarium	–	1589	1608	1669
Europium	–	1571	1604	1629
Gadolinium	–	1507	1575	1594

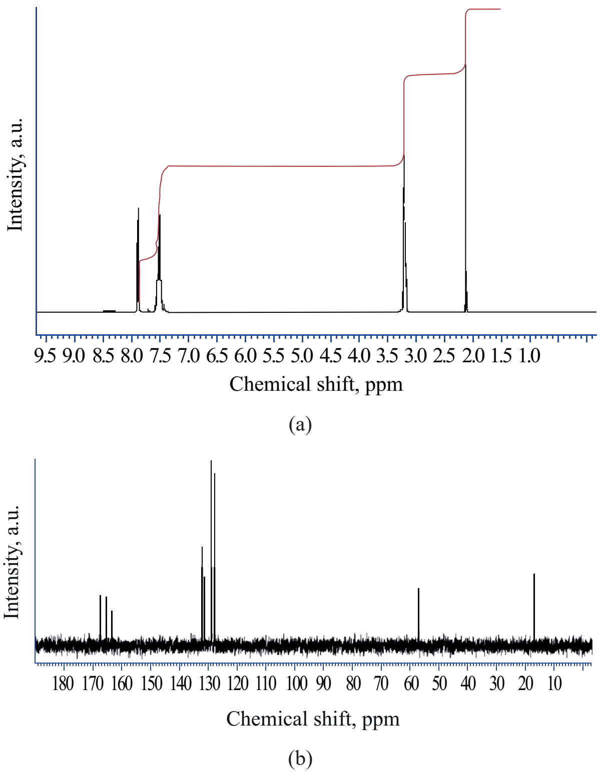

Fig. 2. (a) ^{1}H NMR spectrum of LH_2 in CD_4O; (b) ^{13}C NMR spectrum of LH_2 in CD_4O

Thermogravimetric analysis

The thermal decomposition of the obtained complexes was studied in the temperature range 25–995°C with a heating rate of 40.0°C/min, according to the data of thermogravimetric analysis. Figures 3 and 4 depict thermogravimetry and differential thermal analysis curves for the samarium and europium complexes, respectively.

Thermogravimetric analysis data show that the decomposition proceeds in four stages. For the europium complex at the first stage (25–198°C), a weight loss of 6.861–23.652% occurs due to the removal of crystallization water. The second stage, which is observed with the weight loss of 16.381% in the temperature range of 198–322°C, occurs due to the elimination of carbonyl group and coordination bond between nitrogen and metal. At the next stage, decomposition starts at the temperature of 322°C, and lasts until 448°C; the corresponding weight loss (16.321%) is accompanied by breaking the bond of the carboxyl group to the metal. The last stage observed in the temperature range of 447–980°C, which involves a weight loss of 14.322%, corresponds to the complete destruction of the organic part. The remaining mass (~22.5%) corresponded to the europium content (19.8% theoret.) in the sample.

In the case of samarium complex (Fig. 4), the first stage is accompanied by a weight loss of 6.467% at a temperature of 25–137°C. The second stage of decomposition occurs in a temperature range of 137–198°C with a weight loss of 28.656%, while the third stage is observed in the temperature range of 198–398°C. The significant weight loss observed during decomposition, which mainly occurs in stages 2 and 3, is due to the elimination of carbonyl group and coordination bond between nitrogen and metal. The last stage, which

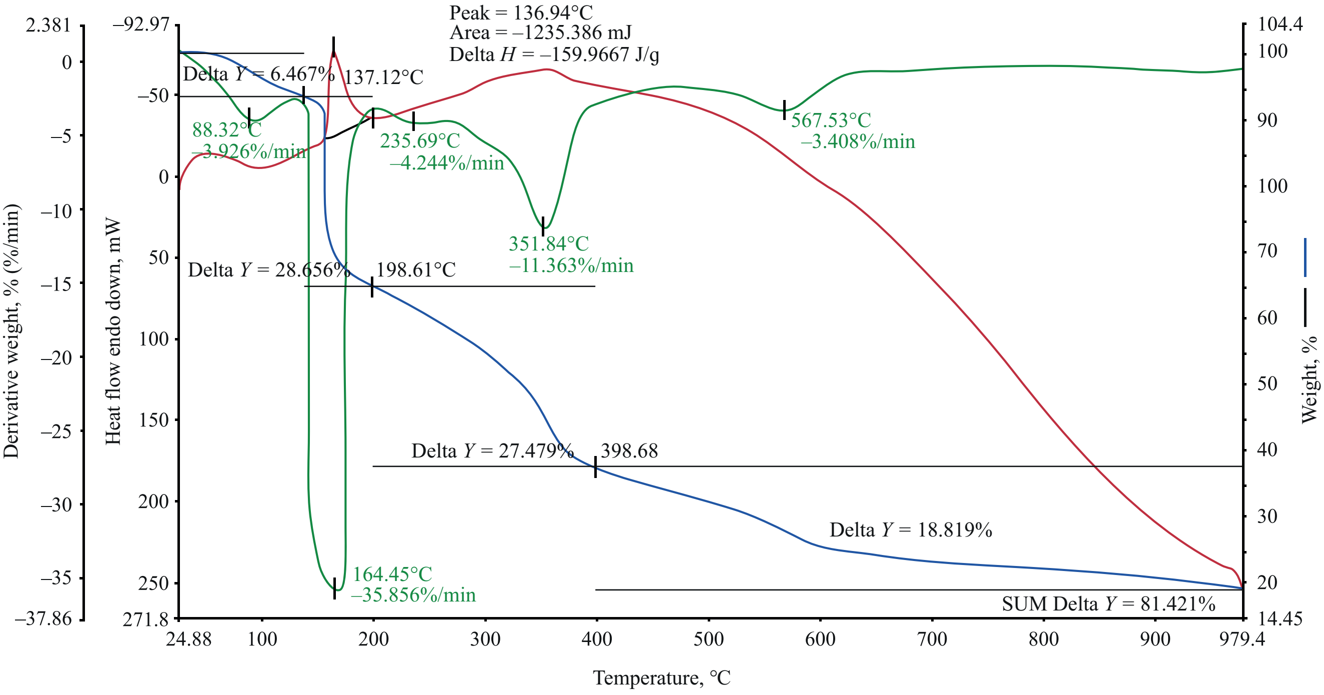

Fig. 3. Derivatogram of the complex of Sm with Schiff base

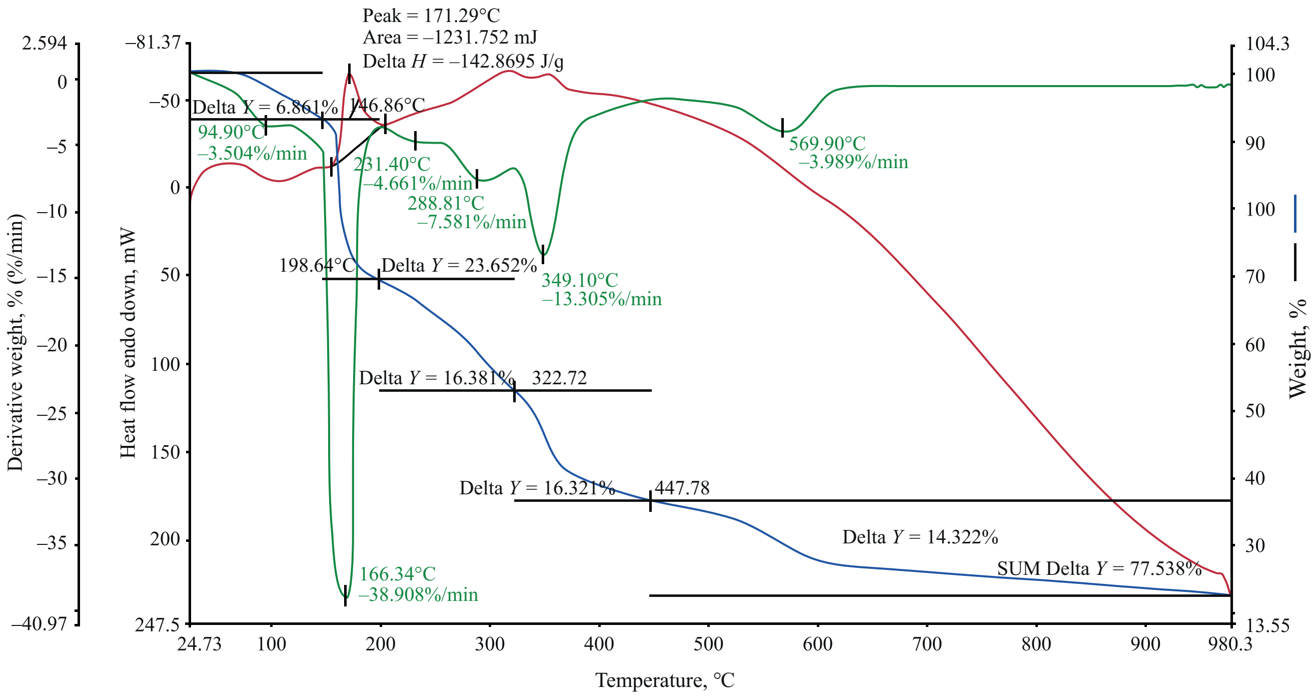

Fig. 4. Derivatogram of the complex of Eu with Schiff base

is observed in the temperature range of 398–980°C and involves a weight loss of 18.819%, corresponds to the fragmentation and complete destruction of the organic ligand. The remaining mass ~18.6% (19.6% theoret.) following heating up to 980°C is predicted to be Sm_2O_3. In all cases, metal percentages calculated from thermogravimetric curves are suitable for the results of elemental analyses.

Based on the results of physicochemical studies and the spectral data of the literature [28–35], the following proposed structure of the metal complexes is assumed (Scheme 2).

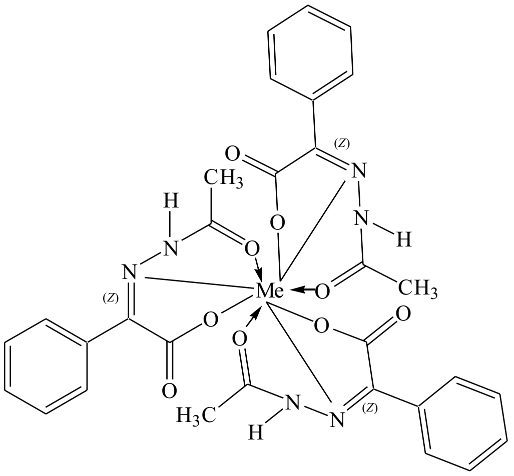

Scheme 2. Proposed structure of the metal complexes

CONCLUSIONS

A new Schiff base ligand was synthesized together with its complexes with rare earth elements. The ligand and complexes were characterized by various physicochemical methods. Metal to ligand stoichiometry in the composition of complexes was found as 1 : 3.

Authors' contribution

All authors equally contributed to the research work.

The authors declare no conflicts of interest. This research received no specific funding.

REFERENCES

1. Golcu A., Tumer M., Demirelli H., Wheatley R.A. Cd(II) and Cu(II) complexes of polydentate Schiff base ligands: synthesis, characterization, properties and biological activity. *Inorg. Chim. Acta.* 2005;358(6):1785–1797. https://doi.org/10.1016/j.ica.2004.11.026
2. Sinha D., Tiwari A.K., Singh S., Shukla G., Mishra P., Chandra H., Mishra A.K. Synthesis, characterization and biological activity of Schiff base analogues of indole-3-carboxaldehyde. *Eur. J. Med. Chem*. 2008;43(1):160–165. https://doi.org/10.1016/j.ejmech.2007.03.022
3. Abbasova G.D., Pashajanov A.M., Ganbarova M.I., Gasanova S.M., Mammadova Z.A., Nasibova A.M. Synthesis and characterization of new metal complexes with tridentate hydrazone ligand. *Azerbaijan Chemical Journal*. 2023;4:84–90. https://doi.org/10.32737/0005-2531-2023-4-84-90
4. Mohamed G.G. Synthesis, characterization and biological activity of bis(phenylimine) Schiff base ligands and their metal complexes. *Spectrochim. Acta A*. 2006;64(1):188–195. https://doi.org/10.1016/j.saa.2005.05.044
5. Tofazzal M., Tarafder H., Ali M.A., Saravanan N., Weng W.Y., Kumar S., Tsafe N.U., Crouse K.A. Coordination chemistry and biological activity of two tridentate ONS and NNS Schiff bases derived from S-benzyldithiocarbazate. *Trans. Met. Chem*. 2000;25:295–298. https://doi.org/10.1023/A:1007044910814
6. Chandra S., Jain D., Sharma A.K., Sharma P. Coordination Modes of a Schiff Base Pentadentate Derivative of 4-Aminoantipyrine with Cobalt(II), Nickel(II) and Copper(II) Metal Ions: Synthesis, Spectroscopic and Antimicrobial Studies. *Molecules*. 2009;14(1):174–190. https://doi.org/10.3390/molecules14010174
7. Karmakar M., Chattopadhyay S. A comprehensive overview of the orientation of tetradentate N_2O_2 donor Schiff base ligands in octahedral complexes of trivalent 3d metals. *J. Molec. Struct*. 2019;1186:155–186. https://doi.org/10.1016/j.molstruc.2019.02.091
8. Abu-Dief A.M., Mohamed I.M.A. A review on versatile applications of transition metal complexes incorporating Schiff bases. *Beni-Suef Univ. J. Basic Appl. Sci*. 2015;4(2):119–133. https://doi.org/10.1016/j.bjbas.2015.05.004
9. More M.S., Joshi P.G., Mishra Y.K., Khanna P.K. Metal complexes driven from Schiff bases and semicarbazones for biomedical and allied applications: a review. *Mater. Today. Chem*. 2019;14:100195. https://doi.org/10.1016/j.mtchem.2019.100195
10. Khalil M.M.H., Ismail E.H., Mohamed G.G., Zayed E.M., Badr A. Synthesis and characterization of a novel Schiff base metal complexes and their application in determination of iron in different types of natural water. *Open J. Inorg. Chem.* 2012;2(2):13–21. http://dx.doi.org/10.4236/ojic.2012.22003
11. Kajal A., Bala S., Kamboj S., Sharma N., Saini V. Schiff Bases: A Versatile Pharmacophore. *J. Catalysts*. 2013;2013:893512. https://doi.org/10.1155/2013/893512
12. Alsaygh A., Al-Humaidi J., Al-Najjar I. Synthesis of Some New Pyridine-2-yl-Benzylidene-Imines. *Int. J. Org. Chem.* 2014;4(2). http://doi.org/10.4236/ijoc.2014.42013
13. Utreja D., Vibha B.S.P., Singh S., Kaur M. Schiff Bases and their Metal Complexes as Anti-Cancer Agents: A Review. *Current Bioactive Compounds*. 2015;11(4):215–230. http://doi.org/10.2174/1573407212666151214221219
14. Chaudhary N.K. Synthesis and medicinal use of Metal complexes of Schiff Bases. *Bibechana*. 2013;9:75–80. https://doi.org/10.3126/bibechana.v9i0.7178
15. Sheikhshoaie I., Ebrahimipour S.Y., Sheikhshoaie M., Rudbari H.A., Khaleghi M., Bruno G. Combined experimental and theoretical studies on the X-ray crystal structure, FT-IR, ^{1}HNMR, ^{13}CNMR, UV–Vis spectra, NLO behavior andantimicrobial activity of 2-hydroxyacetophenone benzoylhydrazone. *Spectrochim. Acta A.* 2014;124:548–555. https://doi.org/10.1016/j.saa.2014.01.043
16. Krishnamoorthy P., Sathyadevi P., Butorac R.R.,.Cowley A.H, Bhuvanesh N.S., Dharmaraj N. Copper(I) and nickel(II) complexes with 1 : 1 *vs.* 1 : 2 coordination of ferrocenyl hydrazone ligands: Do the geometry and composition of complexes affect DNA binding/cleavage, protein binding, antioxidant and cytotoxic activities? *Dalton Trans*. 2012;41:4423–4436. https://doi.org/10.1039/C2DT11938B
17. Sharma M., Chauhan K., Srivastava R.K., Singh S.V., Srivastava K., Saxena J.K., Puri S.K., Chauhan P. Design and Synthesis of a New Class of 4-Aminoquinolinyl- and 9-Anilinoacridinyl Schiff Base Hydrazones as Potent Antimalarial Agents. *Chem. Biol. Drug Des*. 2014;84(2):175–181. https://doi.org/10.1111/cbdd.12289
18. Vyas K.M., Jadeja R., Patel D., Devkar R., Gupta V.K. A new pyrazolone based ternary Cu(II) complex: Synthesis, characterization, crystal structure, DNA binding, protein binding and anti-cancer activity towards A549 human lung carcinoma cells with a minimum cytotoxicity to non-cancerous cells. *Polyhedron*. 2013;65:262–274. https://doi.org/10.1016/j.poly.2013.08.051
19. Kratz F., Beyer U., Roth T., Tarasova N., Collery P., Lechenault F., Cazabat A., Schumcher P., Unger C., Falken U. Transferrin Conjugates of Doxorubicin: Synthesis, Characterization, Cellular Uptake, and *in Vitro* Efficacy. *J. Pharm. Sci.* 1998;87(3):338–346. https://doi.org/10.1021/js970246a
20. Jaividhya P., Dhivya R., Akbarsha M.A., Palaniandavar M. Efficient DNA cleavage mediated by mononuclear mixed ligand copper(II) phenolate complexes: The role of co-ligand planarity on DNA binding and cleavage and anticancer activity. *J. Inorg. Biochem*. 2012;114:94–105. https://doi.org/10.1016/j.jinorgbio.2012.04.018
21. Apelgot S., Coppey J., Fromentin A., Guille E., Poupon M., Roussel A. Altered distribution of copper (64Cu) in tumor-bearing mice and rats. *Anticancer Res*. 1986;6(2):159–164. https://europepmc.org/article/med/3707051#impact
22. Hasinoff B.B., Yadav A.A., Patel D., Wu X. The cytotoxicity of the anticancer drug elesclomol is due to oxidative stress indirectly mediated through its complex with Cu(II). *J. Inorg. Biochem*. 2014;137:22–30. https://doi.org/10.1016/j.jinorgbio.2014.04.004
23. Ebrahimipour S.Y., Sheikhshoaie I., Crochet A., Khaleghi M., Fromm K.M. A new mixed-ligand copper(II) complex of (*E*)-*N'*-(2-hydroxybenzylidene) acetohydrazide: Synthesis, characterization, NLO behavior, DFT calculation and biological activities. *J. Mol. Struct*. 2014;1072:267–276. https://doi.org/10.1016/j.molstruc.2014.05.024
24. Marzano C., Pellei M., Tisato F., Santini C. Copper complexes as anticancer agents. *Anticancer Agents Med. Chem.* 2009;9(2):185–211. https://doi.org/10.2174/187152009787313837
25. Garbutcheon-Singh K.B., Grant M.P., Harper B.W., Krause-Heuer A.M., Manohar M., Orkey N., Aldrich-Wright J.R. Transition Metal Based Anticancer Drugs. *Curr. Top. Med. Chem*. 2011;11(5):521–542. https://doi.org/10.2174/156802611794785226
26. Vogel H.G. (Ed.). *Drug Discovery and Evaluation: Pharmacological Assays*. Berlin: Springer; 2008. 2068 p. http://dx.doi.org/10.1007/978-3-540-70995-4

27. Ebrahimipour S.Y., Sheikhshoaie I., Castro J., Haase W., Mohamadi M., Foro S., Sheikhshoaie M., Mahani S.E. A novel cationic copper(II) Schiff base complex: Synthesis, characterization, crystal structure, electrochemical evaluation, anti-cancer activity, and preparation of its metal oxide nanoparticles. *Inorganica Chimica Acta*. 2015;430:245–252. https://doi.org/10.1016/j.ica.2015.03.016
28. Sheikhshoaie I., Ebrahimipour S.Y., Sheikhshoaie M., Mohamadi M., Abbasnejad M., Rudbari H.A., Bruno G. Synthesis, characterization, X-ray crystal structure, electrochemical evaluation and anti-cancer studies of a mixed ligand Cu(II) complex of (*E*)-*N*′-((2-hydroxynaphthalen-1-yl)methylene)acetohydrazide *J. Chem. Sci*. 2015;127(12): 2193–2200. https://doi.org/10.1007/s12039-015-0978-8
29. Guliyeva E.A., Fatullayeva P.A., Hagverdiyeva T.M. Synthesis and studies of Cu(II), Ni(II), Co(II) complexes with *bis*(saliciliden)-hydrazon. *Azerbaijan Chemical Journal*. 2023;2:116–122. https://doi.org/10.32737/0005-2531-2023-2-116-122
30. Abbasova G., Medjidov A. One-pot Synthesis of a New Hydroxamic Acid and its Complexes with Metals. *Letters in Organic Chemistry.* 2022;19(10):837–841. http://doi.org/10.2174/1570178619666220111121743
31. Sarwar A., Shamsuddin M.B., Lingtang H. Synthesis, Characterization and Luminescence Studies of Metal-Diimine Complexes. *Mod. Chem. Appl*. 2018;6(3):1000262. http://doi.org/10.4172/2329-6798.1000262
32. Naemi H., Moradian M. Synthesis and characterization of nitro-Schiff bases derived from 5-nitro-salicylaldehyde and various diamines and their complexes of Co(II). *J. Coord. Chem*. 2010;63(1):156–162. http://doi.org/10.1080/00958970903225866
33. Nakamoto K. *Infrared and Raman spectra of Inorganic and Coordination Compounds*. Wiley; 1991. 410 p.
34. Calinescu M., Manea L., Pavelescu G. Synthesys and spectroscopic properties of new complex compounds of europium(III) and terbium(III) with 2-hydroxy-1-naphthaldehyde acetylhydrazone and heterocyclic bases. *Rev. Roum.Chim*. 2011;56(3):231–237. http://web.icf.ro/rrch/
35. Tarasevich B.N. *IK spektry osnovnykh klassov organicheskikh soedinenii* (*IR Spectra of the Main Classes of Organic Compounds*). Moscow; MSU; 2012. 54 p. (in Russ.).

About the authors

Gulu G. Abbasova, PhD, Ministry of Science and Education of the Republic of Azerbaijan, Academician M. Nagiyev Institute of Catalysis and Inorganic Chemistry (113, H. Javid Avenue, Baku, AZ 1143, Azerbaijan). E-mail: veliyeva_g23@yahoo.com. Scopus Author ID 57836278800, https://orcid.org/0000-0003-0553-8873

Ajdar A. Medjidov, Academician at the Azerbaijan National Academy of Sciences, Dr. Sci. (Chem.), Ministry of Science and Education of the Republic of Azerbaijan, Academician M. Nagiyev Institute of Catalysis and Inorganic Chemistry (113, H. Javid Avenue, Baku, AZ 1143, Azerbaijan). E-mail: ajdarmedjidov@gmail.com. Scopus Author ID 57208439465, https://orcid.org/0000-0002-1766-5450

Rayyat H. Ismayilov, Dr. Sci., Ministry of Science and Education of the Republic of Azerbaijan, Academician M. Nagiyev Institute of Catalysis and Inorganic Chemistry (113, H. Javid Avenue, Baku, AZ 1143, Azerbaijan). E-mail: ismayilov.rayyat@gmail.com. Scopus Author ID 12799990200, https://orcid.org/0000-0003-0553-8873

Aydin M. Pashajanov, PhD, Ministry of Science and Education of the Republic of Azerbaijan, Academician M. Nagiyev Institute of Catalysis and Inorganic Chemistry (113, H. Javid Avenue, Baku, AZ 1143, Azerbaijan). E-mail: aydin.pashajanov@gmail.com. Scopus Author ID 57373936700, https://orcid.org/0000-0002-5923-0420

Perizad A. Fatullayeva, Dr. Sci., Ministry of Science and Education of the Republic of Azerbaijan, Academician M. Nagiyev Institute of Catalysis and Inorganic Chemistry (113, H. Javid Avenue, Baku, AZ 1143, Azerbaijan). E-mail: pfatullayeva@gmail.com. Scopus Author ID 17134702200, https://orcid.org/0000-0002-2702-7321

Об авторах

Аббасова Гюлю Ганимат, к.х.н., Министерство науки и образования Азербайджанской республики, Институт катализа и неорганической химии имени академика М. Нагиева (Азербайджан, AZ 1143, Баку, пр-т Гусейна Джавида, 113). E-mail: veliyeva_g23@yahoo.com. Scopus Author ID 57836278800, https://orcid.org/0000-0003-0553-8873

Меджидов Аждар Акпер, Академик Национальной академии наук Азербайджана, д.х.н., Министерство науки и образования Азербайджанской республики, Институт катализа и неорганической химии имени академика М. Нагиева (Азербайджан, AZ 1143, Баку, пр-т Гусейна Джавида, 113). E-mail: ajdarmedjidov@gmail.com. Scopus Author ID 57208439465, https://orcid.org/0000-0002-1766-5450

Исмаилов Раййат Гусейн, д.х.н., Министерство науки и образования Азербайджанской республики, Институт катализа и неорганической химии имени академика М. Нагиева (Азербайджан, AZ 1143, Баку, пр-т Гусейна Джавида, 113). E-mail: ismayilov.rayyat@gmail.com. Scopus Author ID 12799990200, https://orcid.org/0000-0003-0553-8873

Пашаджанов Айдын Магомед, к.х.н., Министерство науки и образования Азербайджанской республики, Институт катализа и неорганической химии имени академика М. Нагиева (Азербайджан, AZ 1143, Баку, пр-т Гусейна Джавида, 113). E-mail: aydin.pashajanov@gmail.com. Scopus Author ID 57373936700, https://orcid.org/0000-0002-5923-0420

Фатуллаева Перизат Амрулла, д.х.н., Министерство науки и образования Азербайджанской республики, Институт катализа и неорганической химии имени академика М. Нагиева (Азербайджан, AZ 1143, Баку, пр-т Гусейна Джавида, 113). E-mail: pfatullayeva@gmail.com. Scopus Author ID 17134702200, https://orcid.org/0000-0002-2702-7321

*The text was submitted by the authors in English
and edited for English language and spelling by Thomas A. Beavitt*

Tonkie Khimicheskie Tekhnologii = Fine Chemical Technologies.
2025;20(1):55–62

ISSN 2686-7575 (Online)

UDC 548.55
https://doi.org/10.32362/2410-6593-2025-20-1-55-62
EDN WCZOAO

RESEARCH ARTICLE

Optimization of KRS-5 single crystal growth process by calculation of temperature gradient using finite element method

Sergey V. Erohin✉**, Ksenia S. Zaramenskikh, Mikhail S. Kuznetsov, Stanislav M. Pilyushko**
Federal State Research and Design Institute of Rare Metal Industry (Giredmet), Moscow, 111524 Russia
✉ *Corresponding author, e-mail: fizteh1993@gmail.com*

Abstract

Objectives. Thallium halides, in particular KRS-5 (TlBr–TlI), represent one of the most promising classes of optical crystals for applications in the mid- and far-infrared ranges. Nevertheless, the high-quality standards applied to materials used for such applications present considerable challenges in the manufacture of single thallium halide crystals. In particular, when failing to adhere to exacting growth conditions, the samples exhibit polycrystalline characteristics, rendering them unsuitable for utilization. Given the high cost of experiments carried out to ascertain the optimal conditions for growth, computer modeling may present a viable alternative. When taking such an approach to satisfy the specific requirements, it becomes possible to analyze key effects as standalone entities, thus avoiding unnecessary complications resulting from the introduction of a high number of simultaneous unknown variables. Thus, the aim of the present work is to simulate the growth conditions of KRS-5 crystal to ascertain the causes of polycrystallinity in the samples and identify the optimal parameters for obtaining single crystals.

Methods. In order to solve the problem, the finite element method was used. This method is employed for the calculation of temperature distribution, mechanical stresses, convective effects, the rate of spreading of the crystallization front, deformations due to thermal expansion, and other phenomena that arise during the process of crystal formation. The MATLAB package, which includes a module for solving partial differential equations, was used to simulate the crystal growth ampoule. The problem of temperature gradient was solved in axisymmetric approximation.

Results. A computer simulation was employed to calculate the temperature distribution within the material during the growth process. This was used to determine the position and shape of the crystallization front. It is established that polycrystalline samples develop as a consequence of the crystallization front assuming a flat configuration. The optimum temperature in the furnace was determined. The work demonstrated the successful growth of a KRS-5 crystal under the calculated conditions.

Conclusions. The calculations used to identify the underlying cause of polycrystallinity in the samples enabled a determination of the optimal parameters for single crystal growth. On the basis of the calculations, a growth experiment was conducted on the KRS-5 sample. The obtained sample met the requisite criteria for commercial utilization.

Keywords

finite element method, temperature gradient calculation, optical crystals, thallium halide, KRS-5

Submitted: 20.09.2024
Revised: 30.10.2024
Accepted: 24.12.2024

For citation

Erohin S.V., Zaramenskikh K.S., Kuznetsov M.S., Pilyushko S.M. Optimization of KRS-5 single crystal growth process by calculation of temperature gradient using finite element method. *Tonk. Khim. Tekhnol. = Fine Chem. Technol.* 2025;20(1):55–62. https://doi.org/10.32362/2410-6593-2025-20-1-55-62

НАУЧНАЯ СТАТЬЯ

Оптимизация процесса роста монокристалла КРС-5 с помощью расчета градиента температуры методом конечных элементов

С.В. Ерохин✉, К.С. Зараменских, М.С. Кузнецов, С.М. Пилюшко

Государственный научно-исследовательский и проектный институт редкометаллической промышленности «Гиредмет» имени Н.П. Сажина, Москва, 111524 Россия

✉*Автор для переписки, e-mail: fizteh1993@gmail.com*

Аннотация

Цели. Галогениды таллия, в частности, КРС-5 (TlBr–TlI), являются одними из наиболее перспективных оптических кристаллов среднего и дальнего инфракрасного диапазона. Однако высокие требования к качеству материала приводят к существенным сложностям производства данных монокристаллов, т.к. при несоблюдении точных условий роста образцы получаются поликристаллическими, непригодными для коммерческого использования. Для определения оптимальных условий роста необходимо проведение десятков дорогостоящих экспериментов. В таком случае альтернативным решением является компьютерное моделирование. В зависимости от требований можно анализировать ключевые параметры по отдельности, не усложняя модель множеством неизвестных одновременно. Целью данной работы является определение условий роста кристалла КРС-5 вычислительными методами для установления причин поликристалличности образцов и нахождения оптимальных параметров получения монокристаллов.

Методы. Для решения поставленной задачи использовали метод конечных элементов, с помощью которого можно выполнить расчеты температурного распределения, механических напряжений, конвективных эффектов, скорости распространения фронта кристаллизации, деформаций из-за теплового расширения и других явлений, возникающих в процессе кристаллообразования. Для построения модели ампулы использовался пакет MATLAB с модулем для решения уравнений в частных производных. Задача о температурном градиенте решалась в осесимметричном приближении.

Результаты. С помощью компьютерного моделирования рассчитано распределение температур в материале в процессе роста, на основе чего определено положение и форма фронта кристаллизации. Сделан вывод, что поликристалличные образцы растут в результате прохождения фронта кристаллизации плоской формы. Определена оптимальная температура в печи, необходимая для формирования выпуклого фронта кристаллизации. Продемонстрирован выращенный монокристалл КРС-5.

Выводы. Расчеты позволили быстро определить причину поликристалличности образцов, получить оптимальные параметры роста монокристаллов и на основе их провести эксперимент роста КРС-5. В полученном образце не наблюдалась блочная структура, и кристалл успешно подвергался механической обработке.

Ключевые слова

метод конечных элементов, расчет градиента температур, оптические кристаллы, галогенид таллия, КРС-5

Поступила: 20.09.2024
Доработана: 30.10.2024
Принята в печать: 24.12.2024

Для цитирования

Ерохин С.В., Зараменских К.С., Кузнецов М.С., Пилюшко С.М. Оптимизация процесса роста монокристалла КРС-5 с помощью расчета градиента температуры методом конечных элементов. *Тонкие химические технологии*. 2025;20(1):55–62. https://doi.org/10.32362/2410-6593-2025-20-1-55-62

INTRODUCTION

Thallium halides exhibit uniform transparency across a broad wavelength range that encompasses the visible and mid-infrared regions from 0.35 to 50 μm. The transmission is up to 70% with a reflection coefficient of 30%. Absorption bands are not present within the transmission range. Depending on the composition, thallium halides are used in various fields. Among the thallium halides, KRS-5 crystals (Kristalle aus dem Schmelzfluss, German; 42.5% TlBr and 57.5% TlI) are the most promising for applications in space astrophysics, thermal imaging, and spectrophotometry. The crystals have mechanical, chemical, and vibrational strength and moisture resistance, which makes them suitable for use in atmospheric conditions without special protection. The combination of the characteristics of KRS-5 crystals has the potential to enhance the properties of equipment in the range of up to 10 μm, thereby providing a foundation for the development of novel devices operating in the range from 10 to 50 μm [1, 2].

Thallium bromide, a semiconductor with a band gap of 2.68 eV, is also promising. Due to its large atomic numbers (81 and 35) and high density (7.56 g/cm^3), it has excellent gamma radiation stopping ability [3, 4], which makes it ideal for detecting radiation at room temperature. Thallium bromide is also a promising material for positron emission tomography, as it provides very good energy resolution and the possibility of 3D segmentation, as well as detection efficiency superior to that of widely used scintillators [5, 6]. However, despite the good resolution of TlBr-based detectors, there is still instability in their operation. Attempts to solve this problem including adding iodine I or chlorine Cl atoms to the crystal [7], as well as doping with compensatory impurities [8, 9].

The growth of thallium halide crystals can be achieved using the Bridgman–Stockbarger method, which is particularly suited to the generation of single crystals of this composition [10]. Nevertheless, there are a number of problems in the production of these crystals, especially those having diameters over 50 mm. While key properties of these materials are their purity and structural perfection, methods for achieving material with an impurity content of no more than 10^{-5} wt % are not sufficiently worked out; consequently, the defect-free crystals often turn out to be far from perfect [11–13]. The technological process for obtaining single thallium halide crystals is additionally complicated by the toxicity of the material. The degree of polycrystallinity of the KRS-5 crystal significantly depends on the growth parameters in a multizone furnace. However, due to equipment wear, previously tested modes do not always provide the necessary quality of single crystals; the consequent search for new growth conditions through trial and error can entail unacceptable costs both in terms of expensive materials and time.

In this case, a computer simulation can serve as a solution [14]. Numerical methods have long proven themselves as an effective way to solve technological problems. When taking such an approach, it becomes possible to analyze key effects as standalone entities, thus avoiding unnecessary complications resulting from the introduction of a high number of simultaneous unknown variables. For example, calculations of temperature distribution, mechanical stresses, convection effects, propagation velocity of the crystallization front, deformations as a result of thermal expansion, as well as other phenomena occurring during crystal growth, are available within the framework of numerical methods. This work presents a solution to a simplified problem of searching for a temperature distribution to determine the growth parameters of high-quality crystal samples.

MATERIALS AND METHODS

All calculations were performed in the MATLAB package[1] using the Partial Differential Equation Toolbox (PDEs[2]) module for solving partial differential equations. The issue of temperature distribution was addressed by means of an axisymmetric approximation. The height of the ampoule model was 0.35 m, the radius was 0.04 m, and the angle at the tip of the cone was 45°C. The ampoule model was divided into a grid with triangular elements no larger than 0.005 m in size with a quadratic division of the grid nodes and a mesh growth rate of 1.5.

The following properties of the KRS-5 crystal were taken: heat capacity C = 151 W·s/(kg·°C), thermal conductivity k = 0.544 W/(m·°C), and density ρ = 7.37 g/cm^3 [15]. Crystal growth was carried out in *Giredmet* (Russia) from a charge comprising a compound of two salts of iodide and thallium bromide (*Giredmet*, Russia) in an EDG11-D4 Sunfire furnace (*MELLEN*, USA).

RESULTS AND DISCUSSION

The growth of single crystals of vertically directed crystallization can be achieved in a multizone furnace without the necessity for a membrane to separate the cold and hot zones. In this case, instead of moving the ampoule with the melt, it is possible to change the temperature of the heating elements and thereby shift the position of the crystallization isotherm (Fig. 1a).

A charge of the KRS-5 composition is placed in an ampoule made of heat-resistant glass, after which the ampoule is suspended inside the furnace (Fig. 1b). Subsequently, the temperature within the entire working area increases to a level above the melting point causing the material to enter a molten state. The temperature of the heating elements is then consistently reduced to values below the crystallization temperature of KRS-5, commencing with the elements situated beneath the ampoule containing the material. This subsequently results in the formation of a crystalline phase within the ampoule. However, the acquisition of high-quality samples relies on more comprehensive information pertaining to the growth parameters in question. For example, Fig. 1c shows a sample of polycrystalline KRS-5 obtained by maintaining a temperature gradient of up to 10°C/cm and a crystal

---

[1] MATLAB. version 9.14.0 (R2023a). Natick, Massachusetts: The MathWorks Inc.; 2023.

[2] Partial Differential Equation Toolbox. version 9.14 (R2023a). Natick, Massachusetts: The MathWorks Inc.; 2023.

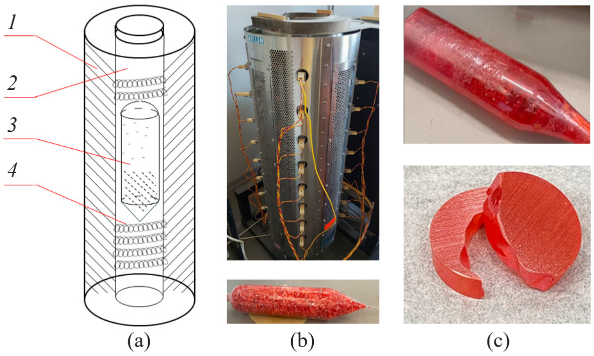

Fig. 1. (a) Schematic representation of a multizone furnace: (*1*) insulator; (*2*) working zone; (*3*) ampoule with KRS-5; (*4*) heating elements. The temperature of each heating element is regulated independently, allowing for the coexistence of the crystal phase and the melt within the ampoule (illustrated by dotted lines and waves). (b) Photo of a multizone furnace and an ampoule with powder that is suspended within the heating zone. (c) KRS-5 crystal grown in the furnace (photo above). If the temperature regime is not correct, the crystal falls apart during processing (photo below)

growth rate of no more than 1.5 mm/h. Since one of the key applications of KRS-5 is optics, the obtained samples are subsequently subjected to mechanical processing. Polycrystalline samples cannot withstand such processing and are therefore unsuitable. The growth of polycrystals may be attributed to a number of factors, including the shape of the crystallization front, stresses at the ampoule/material contact boundary, convection mechanisms, and the presence of multiple crystallization centers. Since the process of searching for a solution by selecting parameters is both costly and time-consuming, a decision was taken to employ numerical modeling.

In order to ascertain the shape of the crystallization front, it was considered to be sufficient to concentrate on the calculation of the isotherms within the ampoule, i.e., without considering convection or mechanical stresses at the interface between the material and the ampoule. Should the necessity arise, the latest effects may be incorporated into the complex model.

To carry out finite element modeling, an axisymmetric 2D model of an ampoule with a material was created in the MATLAB package, see Fig. 2a. As part of the task, the standard equation of thermal conductivity was solved:

$$\rho C_{\mathrm{p}} \frac{\partial T}{\partial t} = \nabla \left(k \nabla T \right),$$

where T is the temperature; t is the time. The elements were given the characteristics of heat capacity (C_{p}), thermal conductivity (k) and density (ρ) corresponding to the KRS-5 crystal. Given that a sufficiently slow rate of crystal growth allows the system to reach thermal equilibrium, the effect of the heat of crystallization was not considered in the problem. The temperature of the heating elements was fixed at the edges of the model. The dimensions of the temperature-controlled sites and the size of the model were in accordance with the specifications of the experimental setup. The position of the crystallization front was further assumed to correspond to the position of the crystallization isotherm ($T_{\mathrm{cr}} = 414$°C).

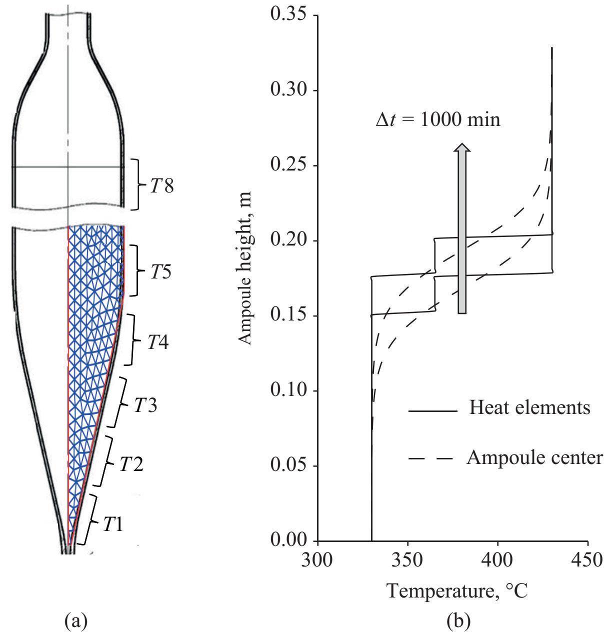

Fig. 2. (a) Model of the ampoule made of heat-resistant glass. The blue color shows the mesh. Each element has the properties of the KRS-5 material. The positions of the heating elements are indicated by T1–T8.
(b) The temperature of the heating elements (solid line) and the corresponding temperature at the center of the flask (dashed line) at two points in time are illustrated. The arrow indicates where the dependencies shift over time

The temperature of the heating elements changed over time according to the following algorithm: first, the temperature of all heaters was equal to the maximum temperature: $T1 = T2 = \ldots = T8 = T_{\max}$. Then the temperature of the first heater changed according to the ratio

$$T1 = T_{\max} - \left(\frac{t - t_1}{1000 \cdot \left(T_{\max} - T_{\min} \right)} \right),$$

where t_1 is the time of the start of cooling of the element $T1$ (min); t is the calculation time (min). After cooling the element $T1$ to $T_{\min}$, the temperature on the element $T2$ was changed similarly. The temperatures $T_{\min}$ and $T_{\max}$ varied in different calculations in the ranges 330–360°C and 430–460°C. The profile of temperatures and heaters depending on height is shown in Fig. 2b. At these specified parameters, the crystallization isotherm exhibits a shift of 2.5 cm over the course of

1000 min, which corresponds to a crystal growth rate of 1.5 mm per hour.

Figure 3 shows the 3D surfaces of a part of the model having a temperature below the crystallization temperature of 414°C; a change in the shape of the isotherms is seen when the temperature of the heaters is switched both in the cone region and in the cylindrical region of the ampoule. Figures 3a and 3b show a comparison of two temperature regimes in which, at the same difference in maximum and minimum temperatures, a fundamentally different form of the crystallization isotherm is observed. If the range is shifted so that the maximum temperature is close to the crystallization temperature T_{cr}, the shape of the isotherm is convex (Fig. 3a). In the converse case, if the minimum temperature is close to T_{cr}, the shape of the crystallization isotherm is concave.

In quasi-stationary mode, when the growth rate is markedly slower than the rate of establishment of temperature equilibrium, it is postulated that the position of the crystallization front correlates with the crystallization isotherm. The morphology of the crystallization front exerts a considerable influence on the quality of the developing crystal. For example, according to studies conducted in the 20th century [16], the convex boundary of the crystallization front prevents the appearance of new nucleation centers on the path of further growth of the main crystal; this is due to the part of the crystal that has advanced into the melt being furthest from the walls, where the formation of new nuclei is most likely. It is also crucial to highlight that the ampoule cone is the area with the highest likelihood of defect growth. The greater the angle at the tip of the cone, the greater the probability of polycrystallinity. Therefore, the shape of the ampoule is of great importance, as it affects the probability of polycrystalline formation.

Furthermore, the degree of polycrystallinity exhibited by the crystal may be contingent upon the morphology of the crystallization front. Since polycrystallinity is often formed as a result of accumulation of dislocations, which move mainly perpendicular to the growth boundary, dislocations can be "pushed out" of the crystal with a convex front without creating a high density of defects [17]. Thus, in order to obtain high-quality samples, it is necessary to use the mode shown in Fig. 3a. From calculations, it is also possible to determine the magnitude of the gradient in the crystallization front zone. According to the isotherms at Figs. 3a and 3b, the gradient in the center of the ampoule is 11°C/cm for the first mode and 14°C/cm for the second.

According to the calculated regime, a new KRS-5 crystal was grown in a multizone furnace. The sample is presented in Fig. 3c. The quality control of the crystals was conducted through visual examination in well-illuminated conditions without the utilization of a microscope or other optical instruments. The observation was carried out at sharp angles to the surface of the samples. Under such inspection conditions, blocks due to imperfection of the crystal structure are visible. However, no block structure was observed in the obtained sample and the crystal was successfully machined.

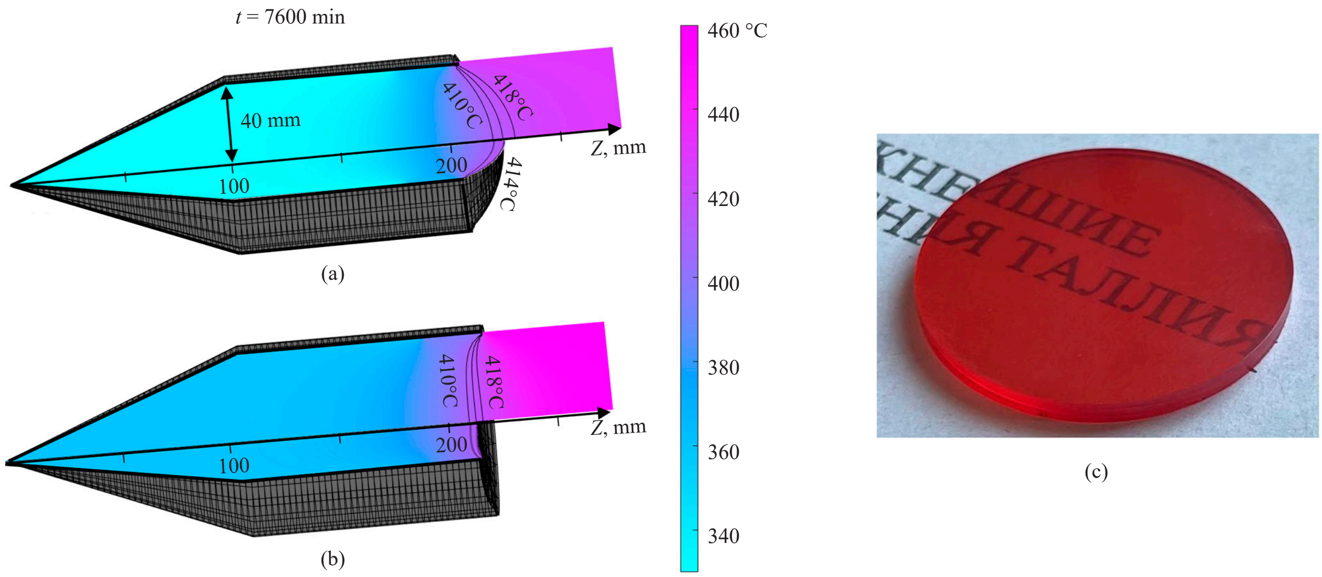

(a)

(b)

(c)

Fig. 3. (a), (b) 3D models of the crystallized part of the material inside the ampoule in the case of two temperature regimes: (a) 330–430°C; (b) 360–460°C. The color gradient shows the temperature distribution within the material. Three isotherms, for 410, 414, and 418°C, are marked with black lines. (c) Processed sample of KRS-5 crystal obtained using the temperature regime (a)

CONCLUSIONS

Using the finite element method implemented in the MATLAB package, the temperature distribution in a multizone furnace was obtained. Given that the crystallization front is located along the crystallization isotherm in the case of sufficiently slow crystal growth, it can be posited that the polycrystalline nature of previously grown crystals stems from the flat shape of the crystallization front, which, in turn, leads to the emergence of multiple crystallization centers, thus giving rise to a polycrystalline structure. Subsequently, new growth parameters were established to set the corresponding temperature values on the heating elements, thereby enabling the growth of a KRS-5 crystal with a low degree of polycrystallinity, which is suitable for commercial use.

Authors' contributions

S.V. Erohin—carrying out calculations, writing the text of the article.

K.S. Zaramenskikh—developing growth regimes, writing the text of the article.

M.S. Kuznetsov—growing crystals in a multizone furnace, planning the experiment.

S.M. Pilyushko—preparing samples and mechanical processing.

The authors declare no conflict of interest. The work was done without financial support.

REFERENCES

1. Kuznetsov M.S., Zaramenskikh K.S., Lisitskii I.S., Polyakova G.V., Morozov M.V., Pimkin N.A., Soskov O.V., Butvina L.N. Gradient materials based on thallium halide crystals for optical elements and optical fibers of the IR range. *Foton-Ekspress = Photon-Express*. 2021;6(174):76–77 (in Russ.). https://doi.org/10.24412/2308-6920-2021-6-76-77
2. Khorkin V.S., Voloshinov V.B., Kuznetsov M.S. Anisotropic acousto-optic interaction in a KRS-5 crystal. *Appl. Opt*. 2022;61(15):4397–4403. https://doi.org/10.1364/AO.453606
3. Kim H., Ogorodnik Y., Kargar A., Cirignano L., Thrall C.L., Koehler W., O'Neal S.P., He Z., Swanberg E., Payne S.A., Squillante M.R., Shah K. Thallium Bromide Gamma-Ray Spectrometers and Pixel Arrays. *Front Phys*. 2020;8:55. https://doi.org/10.3389/fphy.2020.00055
4. Hitomi K., Kim C., Nogami M., Shimazoe K., Takahashi H. Characterization of coincidence time resolutions of $TlBr_xCl_{1-x}$ crystals as Cherenkov radiators. *Jpn. J. Appl. Phys*. 2023;62:081001. https://doi.org/10.35848/1347-4065/ace5fa
5. Ariño-Estrada G., Du J., Kim H., Cirignano L.J., Shah K.S., Cherry S.R., Mitchell G.S. Development of TlBr detectors for PET imaging. *Phys. Med. Biol*. 2018;63(13):13NT04. https://doi.org/10.1088/1361-6560/aac27e
6. Ellin J., Rebolo L., Backfish M., Prebys E., Ariño-Estrada G. Prompt gamma timing for proton range verification with TlBr and TlCl as pure Cherenkov emitters. *Phys. Med. Biol*. 2024;69(11):115002. https://doi.org/10.1088/1361-6560/ad4304
7. Kim H., Churilov A., Ciampi G., Cirignano L., Higgins W., Kim S., O'Dougherty P., Olschner F., Shah K. Continued development of thallium bromide and related compounds for gamma-ray spectrometers. *Nucl. Instrum. Methods Phys. Res. Sect. A: Accelerators, Spectrometers, Detectors and Associated Equip*. 2011;629(1):192–196. https://doi.org/10.1016/j.nima.2010.10.097
8. Smirnov I.S., Govorkov A.V., Kozhukhova E.A., Lisitsky I.S., Kuznetsov M.S., Zaramenskikh K.S., Polyakov A.Ya. The influence of growth conditions and donor doping on conductivity mode and deep traps spectra in TlBr single crystals. *Izvestiya Vysshikh Uchebnykh Zavedenii. Materialy Elektronnoi Tekhniki = Materials of Electronics Engineering*. 2013;3:4–12 (in Russ.). https://doi.org/10.17073/1609-3577-2013-3-4-12

СПИСОК ЛИТЕРАТУРЫ

1. Кузнецов М.С., Зараменских К.С., Лисицкий И.С., Полякова Г.В., Морозов М.В., Пимкин Н.А., Сосков О.В., Бутвина Л.Н. Градиентные материалы на основе кристаллов галогенидов таллия для оптических элементов и оптоволокна ИК-диапазона. *Фотон-Экспресс*. 2021;6(174):76–77. https://doi.org/10.24412/2308-6920-2021-6-76-77
2. Khorkin V.S., Voloshinov V.B., Kuznetsov M.S. Anisotropic acousto-optic interaction in a KRS-5 crystal. *Appl. Opt*. 2022;61(15):4397–4403. https://doi.org/10.1364/AO.453606
3. Kim H., Ogorodnik Y., Kargar A., Cirignano L., Thrall C.L., Koehler W., O'Neal S.P., He Z., Swanberg E., Payne S.A., Squillante M.R., Shah K. Thallium Bromide Gamma-Ray Spectrometers and Pixel Arrays. *Front Phys*. 2020;8:55. https://doi.org/10.3389/fphy.2020.00055
4. Hitomi K., Kim C., Nogami M., Shimazoe K., Takahashi H. Characterization of coincidence time resolutions of $TlBr_xCl_{1-x}$ crystals as Cherenkov radiators. *Jpn. J. Appl. Phys*. 2023;62:081001. https://doi.org/10.35848/1347-4065/ace5fa
5. Ariño-Estrada G., Du J., Kim H., Cirignano L.J., Shah K.S., Cherry S.R., Mitchell G.S. Development of TlBr detectors for PET imaging. *Phys. Med. Biol*. 2018;63(13):13NT04. https://doi.org/10.1088/1361-6560/aac27e
6. Ellin J., Rebolo L., Backfish M., Prebys E., Ariño-Estrada G. Prompt gamma timing for proton range verification with TlBr and TlCl as pure Cherenkov emitters. *Phys. Med. Biol*. 2024;69(11):115002. https://doi.org/10.1088/1361-6560/ad4304
7. Kim H., Churilov A., Ciampi G., Cirignano L., Higgins W., Kim S., O'Dougherty P., Olschner F., Shah K. Continued development of thallium bromide and related compounds for gamma-ray spectrometers. *Nucl. Instrum. Methods Phys. Res. Sect. A: Accelerators, Spectrometers, Detectors and Associated Equip*. 2011;629(1):192–196. https://doi.org/10.1016/j.nima.2010.10.097
8. Смирнов И.С., Говорков А.В., Кожухова Е.А., Лисицкий И.С., Кузнецов М.С., Зараменских К.С., Поляков А.Я. Влияние условий выращивания и легирования донорными примесями на механизм проводимости и спектры глубоких уровней в кристаллах TlBr. *Известия высших учебных заведений. Материалы электронной техники*. 2013;3:4–12. https://doi.org/10.17073/1609-3577-2013-3-4-12

9. Bishop S.R., Higgins W., Ciampi G., Churilov A., Shah K.S., Tuller H.L. The Defect and Transport Properties of Donor Doped Single Crystal TlBr. *J. Electrochem. Soc.* 2011;158(2):J47. http://doi.org/10.1149/1.3525243
10. Salimgareev D., Lvov A., Yuzhakova A., Pestereva P., Shmygalev A., Korsakov A., Zhukova L. Optical materials for IR fiber optics based on solid solutions of $AgCl_{0.25}Br_{0.75}$ – $TlCl_{0.74}Br_{0.26}$, $AgCl_{0.25}Br_{0.75}$ – $TlBr_{0.46}I_{0.54}$ systems. *Opt. Mat.* 2023;143(3):114304. https://doi.org/10.1016/j.optmat.2023.114304
11. Lisitsky I.S., Golovanov V.F., Kuznetsov M.S., Polyakova G.V. Macroscopic defects of thallium halide single crystals grown from the melt by the Stockbarger method. *Tsvetnye Metally*. 2004;2:81–84 (in Russ.).
12. Kozlov V., Leskelä M., Sipilä H. Annealing and characterisation of TlBr crystals for detector applications. *Nucl. Instrum. Methods Phys. Res. Sect. A: Accelerators, Spectrometers, Detectors and Associated Equip.* 2005;546(1):200–204. https://doi.org/10.1016/j.nima.2005.03.025
13. Kozlov V., Leskelä M., Prohaska T., Schultheis G., Stingeder G., Sipilä H. TlBr crystal growth, purification and characterisation. *Nucl. Instrum. Methods Phys. Res. Sect. A: Accelerators, Spectrometers, Detectors and Associated Equip.* 2004;531(1):165–173. https://doi.org/10.1016/j.nima.2004.06.002
14. Aronov P.S., Gusev A.O., Rodin A.S. Modeling of the stress-strain state of the crystal grown by Bridgman method. *Preprinty IPM im. M.V. Keldysha = Keldysh Inst Prepr.* 2023;8:26 p. (in Russ.). https://doi.org/10.20948/prepr-2023-8
15. Avdienko K.I., Artyushenko V.G., Belousov A.S., *et al. Kristally galogenidov talliya. Poluchenie, svoistva i primenenie* (*Crystals of Thallium Halides. Synthesis, Properties and Applications*). Novosibirsk: Nauka; 1989. 151 p. (in Russ.).
16. Laudise R.A., Parker R.L. *Rost monokristallov* (*The Growth of Single Crystals*): transl. from Engl. Moscow: Mir; 1974. 540 p. (in Russ.).
   [Laudise R.A. *The Growth of Single Crystals*. N.Y.: Prentice-Hall Publ., 1970. 352 p.]
17. Aust K.T., Chalmers B. Control of lineage structure in aluminum crystals grown from the melt. *Can. J. Phys.* 1958;36(7):977–980. https://doi.org/10.1139/p58-103

9. Bishop S.R., Higgins W., Ciampi G., Churilov A., Shah K.S., Tuller H.L. The Defect and Transport Properties of Donor Doped Single Crystal TlBr. *J. Electrochem. Soc.* 2011;158(2):J47. http://doi.org/10.1149/1.3525243
10. Salimgareev D., Lvov A., Yuzhakova A., Pestereva P., Shmygalev A., Korsakov A., Zhukova L. Optical materials for IR fiber optics based on solid solutions of $AgCl_{0.25}Br_{0.75}$ – $TlCl_{0.74}Br_{0.26}$, $AgCl_{0.25}Br_{0.75}$ – $TlBr_{0.46}I_{0.54}$ systems. *Opt. Mat.* 2023;143(3):114304. https://doi.org/10.1016/j.optmat.2023.114304
11. Лисицкий И.С., Голованов В.Ф., Кузнецов М.С., Полякова Г.В. Макроскопические дефекты монокристаллов галогенидов таллия, выращенных из расплава методом Стокбаргера. *Цветные металлы*. 2004;2:81–84.
12. Kozlov V., Leskelä M., Sipilä H. Annealing and characterisation of TlBr crystals for detector applications. *Nucl. Instrum. Methods Phys. Res. Sect. A: Accelerators, Spectrometers, Detectors and Associated Equip.* 2005;546(1):200–204. https://doi.org/10.1016/j.nima.2005.03.025
13. Kozlov V., Leskelä M., Prohaska T., Schultheis G., Stingeder G., Sipilä H. TlBr crystal growth, purification and characterisation. *Nucl. Instrum. Methods Phys. Res. Sect. A: Accelerators, Spectrometers, Detectors and Associated Equip.* 2004;531(1):165–173. https://doi.org/10.1016/j.nima.2004.06.002
14. Аронов П.С., Гусев А.О., Родин А.С. Моделирование напряженно-деформированного состояния кристалла, выращенного методом Бриджмена. *Препринты ИПМ им. М.В. Келдыша.* 2023;8:26 с. https://doi.org/10.20948/prepr-2023-8
15. Авдиенко К.И., Артюшенко В.Г., Белоусов А.С. и др. *Кристаллы галогенидов таллия. Получение, свойства и применение*. Новосибирск: Наука; 1989. 151 с.
16. Лодиз Р.А., Паркер Р.Л. *Рост монокристаллов*: пер. с англ. М.: Мир; 1974. 540 с.
17. Aust K.T., Chalmers B. Control of lineage structure in aluminum crystals grown from the melt. *Can. J. Phys.* 1958;36(7):977–980. https://doi.org/10.1139/p58-103

About the authors

Sergey V. Erohin, Cand. Sci. (Phys.-Math.), Researcher, Laboratory of High-Purity Halogenide Materials for Optics, Giredmet (2-1, Electrodnaya ul., Moscow, 111524, Russia). E-mail: fizteh1993@gmail.com. Scopus Author ID 57003750600, ResearcherID AFR-7212-2022, RSCI SPIN-code 6549-5344, https://orcid.org/0000-0002-7464-8454

Ksenia S. Zaramenskikh, Cand. Sci. (Chem.), Leading Researcher, Laboratory of High-Purity Halogenide Materials for Optics, Giredmet (2-1, Electrodnaya ul., Moscow, 111524, Russia). E-mail: kszaramenskikh@rosatom.ru. Scopus Author ID 56743216200, RSCI SPIN-code 3904-6167, https://orcid.org/0000-0001-8573-3470

Mikhail S. Kuznetsov, Head of the Laboratory of High-Purity Halogenide Materials for Optics, Giredmet (2-1, Electrodnaya ul., Moscow, 111524, Russia). E-mail: gradan@mail.ru. Scopus Author ID 55421893200, https://orcid.org/0000-0002-8441-4424

Stanislav M. Pilyushko, Process Engineer, Laboratory of High-Purity Halogenide Materials for Optics, Giredmet (2-1, Electrodnaya ul., Moscow, 111524, Russia). E-mail: vorpat2402@bk.ru. Scopus Author ID 57854000900, RSCI SPIN-code 4397-6926, https://orcid.org/0009-0005-3650-4694

Об авторах

Ерохин Сергей Владимирович, к.ф.-м.н., научный сотрудник, лаборатория высокочистых галогенидных материалов для оптики, АО «Государственный научно-исследовательский и проектный институт редкометаллической промышленности «Гиредмет» имени Н.П. Сажина (111524, Россия, Москва, Электродная ул., д. 2, стр. 1). E-mail: fizteh1993@gmail.com. Scopus Author ID 57003750600, ResearcherID AFR-7212-2022, SPIN-код РИНЦ 6549-5344, https://orcid.org/0000-0002-7464-8454

Зараменских Ксения Сергеевна, к.х.н., лаборатория высокочистых галогенидных материалов для оптики, АО «Государственный научно-исследовательский и проектный институт редкометаллической промышленности «Гиредмет» имени Н.П. Сажина (111524, Россия, Москва, Электродная ул., д. 2, стр. 1). E-mail: kszaramenskikh@rosatom.ru. Scopus Author ID 56743216200, SPIN-код РИНЦ 3904-6167, https://orcid.org/0000-0001-8573-3470

Кузнецов Михаил Сергеевич, начальник лаборатории высокочистых галогенидных материалов для оптики, АО «Государственный научно-исследовательский и проектный институт редкометаллической промышленности «Гиредмет» имени Н.П. Сажина (111524, Россия, Москва, Электродная ул., д. 2, стр. 1). E-mail: gradan@mail.ru. Scopus Author ID 55421893200, https://orcid.org/0000-0002-8441-4424

Пилюшко Станислав Михайлович, инженер-технолог, лаборатория высокочистых галогенидных материалов для оптики, АО «Государственный научно-исследовательский и проектный институт редкометаллической промышленности «Гиредмет» имени Н.П. Сажина (111524, Россия, Москва, Электродная ул., д. 2, стр. 1). E-mail: vorpat2402@bk.ru. Scopus Author ID 57854000900, SPIN-код РИНЦ 4397-6926, https://orcid.org/0009-0005-3650-4694

Translated from Russian into English by N. Isaeva
Edited for English language and spelling by Thomas A. Beavitt

Tonkie Khimicheskie Tekhnologii = Fine Chemical Technologies.
2025;20(1):63–74
ISSN 2686-7575 (Online)

Chemistry and technology of inorganic materials

Химия и технология неорганических материалов

UDC 544.032
https://doi.org/10.32362/2410-6593-2025-20-1-63-74
EDN XZSYPF

RESEARCH ARTICLE

Structure and properties of Li ferrite synthesized from Fe_2O_3–Li_2CO_3–Sm_2O_3 powders

Elena N. Lysenko✉, **Vitaly A. Vlasov, Yuliya S. Elkina, Anatoly P. Surzhikov**
National Research Tomsk Polytechnic University, Tomsk, 634050 Russia
✉ *Corresponding author, e-mail: lysenkoen@tpu.ru*

Abstract

Objectives. To study the structure and properties of lithium ferrites obtained by preliminary solid-phase synthesis of samples based on Fe_2O_3–Li_2CO_3–Sm_2O_3 powder mixtures having various concentrations of samarium oxide (0, 4.7, and 14.7 wt %) at 900°C and their subsequent high-temperature sintering at 1150°C.

Methods. The structural and morphological characteristics of the synthesized and sintered samples were studied by X-ray powder diffraction analysis, scanning electron microscopy, thermogravimetric analysis, and differential scanning calorimetry.

Results. The preliminary synthesis gives a two-phase composite structure containing unsubstituted lithium ferrite $Li_{0.5}Fe_{2.5}O_4$ having a spinel structure and a perovskite-like $SmFeO_3$ phase. An increase in the Sm_2O_3 content from 4.7 to 14.7 wt % in the initial Fe_2O_3–Li_2CO_3–Sm_2O_3 mixture leads to an increase in the amount of the secondary $SmFeO_3$ phase in the synthesized samples from 4.9 to 18.2 wt %. The high Curie temperature values (631–632°C) and obtained values of the enthalpy of the $\alpha \rightarrow \beta$ phase transitions in lithium ferrite indicate that the main product in all synthesized samples is the ordered α-$Li_{0.5}Fe_{2.5}O_4$ phase. Subsequent sintering at elevated temperatures leads to a decrease in the $SmFeO_3$ phase content to 3.8 and 16.5 wt % and to an increase in the content of the lithium ferrite phase. The sample not modified with samarium contains a significant amount of the disordered β-$Li_{0.5}Fe_{2.5}O_4$ phase, as confirmed by the reduced values of the Curie temperature and phase transition enthalpy. The density of such a sample is 4.4 g/cm^3. The introduction of samarium ions leads to the preservation of the ordered α-$Li_{0.5}Fe_{2.5}O_4$ phase during sintering. The density of the sintered samples decreases to 4.3 and 4.1 g/cm^3 with an increase in the concentration of samarium oxide introduced at the synthesis stage to 4.7 and 14.7 wt %, respectively.

Conclusions. The introduction of samarium oxide to low concentrations (up to 4.7 wt %) during ferrite synthesis leads to the formation of a two-phase composite structure during sintering, which mainly consists of an unsubstituted lithium ferrite phase having more regular polyhedral grains and a low content of the secondary perovskite-like phase. The formation of the secondary phase, whose properties differ from those of ferrite, along with the characteristics obtained for such samples, which include a slight decrease in density while maintaining a high Curie temperature corresponding to the main magnetic phase, make ferrites modified with low concentrations of rare earth elements promising for further study of their electromagnetic properties in the microwave range.

Keywords
lithium ferrite, samarium oxide, perovskite, microstructure, solid-phase synthesis, sintering

Submitted: 10.09.2024
Revised: 09.11.2024
Accepted: 25.12.2024

For citation
Lysenko E.N., Vlasov V.A., Elkina Yu.S., Surzhikov A.P. Structure and properties of Li ferrite synthesized from Fe_2O_3–Li_2CO_3–Sm_2O_3 powders. *Tonk. Khim. Tekhnol. = Fine Chem. Technol.* 2025;20(1):63–74. https://doi.org/10.32362/2410-6593-2025-20-1-63-74

НАУЧНАЯ СТАТЬЯ

Структура и свойства Li феррита, синтезированного из порошков Fe_2O_3–Li_2CO_3–Sm_2O_3

Е.Н. Лысенко✉, В.А. Власов, Ю.С. Елькина, А.П. Суржиков

Национальный исследовательский Томский политехнический университет, Томск, 634050 Россия

✉*Автор для переписки, e-mail: lysenkoen@tpu.ru*

Аннотация

Цели. Исследование структуры и свойств литиевых ферритов, полученных путем предварительного твердофазного синтеза образцов на основе порошковых смесей Fe_2O_3–Li_2CO_3–Sm_2O_3 с различной концентрацией оксида самария (0, 4.7, 14.7 мас. %) при 900°C и последующего их высокотемпературного спекания при 1150°C.

Методы. Структурные и морфологические характеристики синтезированных и спеченных образцов исследованы методами рентгенофазового и термогравиметрического анализов, дифференциально-сканирующей калориметрии и сканирующей электронной микроскопии.

Результаты. В результате предварительного синтеза происходит образование двухфазной композиционной структуры, содержащей незамещенный литиевый феррит $Li_{0.5}Fe_{2.5}O_4$ со структурой шпинели и перовскитоподобную фазу $SmFeO_3$. Увеличение содержания Sm_2O_3 с 4.7 до 14.7 мас. % в исходной смеси Fe_2O_3–Li_2CO_3–Sm_2O_3 приводит к увеличению во время синтеза количества вторичной фазы $SmFeO_3$ с 4.9 до 18.2 мас. % в образцах. Высокие значения температуры Кюри, равные 631–632°C, а также полученные значения энтальпии фазовых переходов $\alpha \rightarrow \beta$ в литиевом феррите свидетельствуют об основном образовании упорядоченной α-фазы $Li_{0.5}Fe_{2.5}O_4$ во всех синтезированных образцах. Последующее спекание при повышенной температуре приводит к уменьшению содержания фазы $SmFeO_3$ и увеличению фазы литиевого феррита. При этом образец, не модифицированный самарием, содержит значительное количество разупорядоченной β-фазы $Li_{0.5}Fe_{2.5}O_4$, что было подтверждено заниженными значениями температуры Кюри и энтальпии фазового перехода. Плотность такого образца 4.4 г/см^3. Введение ионов самария приводит к сохранению во время спекания упорядоченной α-фазы $Li_{0.5}Fe_{2.5}O_4$. При этом плотность спеченных образцов уменьшилась до 4.3 и 4.1 г/см^3 с увеличением концентрации вводимого на этапе синтеза оксида самария соответственно до 4.7 и 14.7 мас. %.

Выводы. Введение малых концентраций оксида самария (до 4.7 мас. %) при синтезе феррита приводит к формированию во время спекания двухфазной композиционной структуры, характеризующейся основным содержанием незамещенной литиевой ферритовой фазы с более правильными многогранными зернами и небольшим содержанием вторичной перовскитоподобной фазы. Формирование вторичной фазы, которая имеет отличные от феррита свойства, а также полученные характеристики для таких образцов, включающие незначительное уменьшение их плотности с сохранением высокого значения температуры Кюри, соответствующей основной магнитной фазе, делают ферриты, модифицированные низкими концентрациями редкоземельных элементов, перспективными для дальнейшего изучения их электромагнитных свойств в сверхвысокочастотном диапазоне.

Ключевые слова

литиевый феррит, оксид самария, перовскит, микроструктура, твердофазный синтез, спекание

Поступила: 10.09.2024
Доработана: 09.11.2024
Принята в печать: 25.12.2024

Для цитирования

Лысенко Е.Н., Власов В.А., Елькина Ю.С., Суржиков А.П. Структура и свойства Li феррита, синтезированного из порошков Fe_2O_3–Li_2CO_3–Sm_2O_3. *Тонкие химические технологии*. 2025;20(1):63–74. https://doi.org/10.32362/2410-6593-2025-20-1-63-74

INTRODUCTION

Ferrites having a spinel structure are widely used in microwave devices, such as isolators, circulators, phase shifters, and absorbers [1–5], as well as in magnetically controlled photocatalysts [6]. The tightening of operating conditions for devices based on such ferrites determines the importance of research into the creation of new ferrite materials offering a required set of properties, as well as the development and improvement of their production technology.

Unsubstituted lithium ferrite $Li_{0.5}Fe_{2.5}O_4$ (or $LiFe_5O_8$), which has a high Curie temperature and a high saturation magnetization, is successfully used in practice, e.g., as ferrite cores in memory devices, for power conversion in electronics, in antennas and high-speed digital tapes [7, 8]. However, the use of lithium ferrites in microwave technology is limited by their excessive magnetic and dielectric losses. Therefore, lithium-containing ferrites often have more complex compositions [9–12] associated lower values of losses, anisotropy, and coercivity, as well as higher density, etc.

Recently, the properties of ferrites with rare-earth elements (REEs) have been actively studied. Many scientists explored the effect of various REEs on the properties of ferrites of Li [13], Ni [14–16], Co [17, 18], Li–Ni [19–21], Ni–Zn [22], Ni–Mn [23], Co–Mn [24], and Cu–Co [25]. At the same time, it has been shown [14, 16, 20, 22, 24, 25] that the properties of ferrites can be modified by substituting REE ions in the ferrite structure. For this purpose, various chemical synthesis methods are used, such as the sol–gel method [14, 22, 25], citrate method [16], coprecipitation [18], microemulsion method [20], hydrothermal method [24], etc. In other works [13, 15, 17, 21, 23], when producing ferrites by various methods that include the widespread solid-phase synthesis method, it has been shown that the addition of REEs simultaneously with substituted ferrite phases leads to the formation of a small amount of secondary perovskite-like phases based on REEs. Such phases can have a significant effect on the properties of the synthesized ferrites. However, there is insufficient data on the production of lithium ferrites with REEs using preliminary synthesis of ferrites by the solid-phase method and subsequent high-temperature sintering.

Our previous studies showed [26] that the solid-phase synthesis of lithium ferrites from Fe_2O_3–Li_2CO_3–Sm_2O_3 mixtures, regardless of the conditions of mechanical activation of the initial powders, gives a two-phase product consisting of unsubstituted lithium ferrite $Li_{0.5}Fe_{2.5}O_4$ and $SmFeO_3$. This work is aimed at studying the structure and properties of lithium ferrite produced using a two-stage technology based on preliminary solid-phase synthesis of ferrite with the addition of REE (Sm_2O_3) at various concentrations and subsequent high-temperature sintering to obtain ferrite ceramics. The process conditions for the synthesis and sintering of this group of ferrites are also considered in detail.

EXPERIMENTAL

The production of the ferrites under study (Fig. 1) is based on the mechanical mixing of oxide powders and carbonate powders. Let us consider in more detail the process stages of synthesis and sintering of the ferrite under study.

Figure 1a presents the stage of the preliminary synthesis (ferritization) of lithium ferrite. Prior to their synthesis, powders of the initial reagents Li_2CO_3 (special purity grade 20-2, *Vekton*, Russia), Fe_2O_3 (analytical purity grade, *Vekton*, Russia), and Sm_2O_3 (99.99%, *MOS International Co*., China) were dried in a laboratory oven at a temperature of 200°C for 180 min and then weighed on an AUW-D scale (*Shimadzu*, Japan) to obtain weight proportions in accordance with the proposed formulas:

$$\begin{aligned}&Li_2CO_3 + 5Fe_2O_3 \rightarrow\\&\rightarrow 4Li_{0.5}Fe_{2.5}O_4 + CO_2 \text{ (sample N0)},\end{aligned} \tag{1}$$

$$\begin{aligned}&Li_2CO_3 + 4.88Fe_2O_3 + 0.12Sm_2O_3 \rightarrow\\&\rightarrow 4Li_{0.5}Sm_{0.06}Fe_{2.44}O_4 + CO_2 \text{ (sample N1)},\end{aligned} \tag{2}$$

$$\begin{aligned}&Li_2CO_3 + 4.6Fe_2O_3 + 0.4Sm_2O_3 \rightarrow\\&\rightarrow 4Li_{0.5}Sm_{0.2}Fe_{2.3}O_4 + CO_2 \text{ (sample N2)}.\end{aligned} \tag{3}$$

Next, the initial reagents were mixed to obtain a Fe_2O_3–Li_2CO_3–Sm_2O_3 powder mixture in weight ratios of 91.5 : 8.5 : 0 (sample N0), 87.1 : 8.2 : 4.7 (sample N1), and 77.5 : 7.8 : 14.7 (sample N2) in two steps.

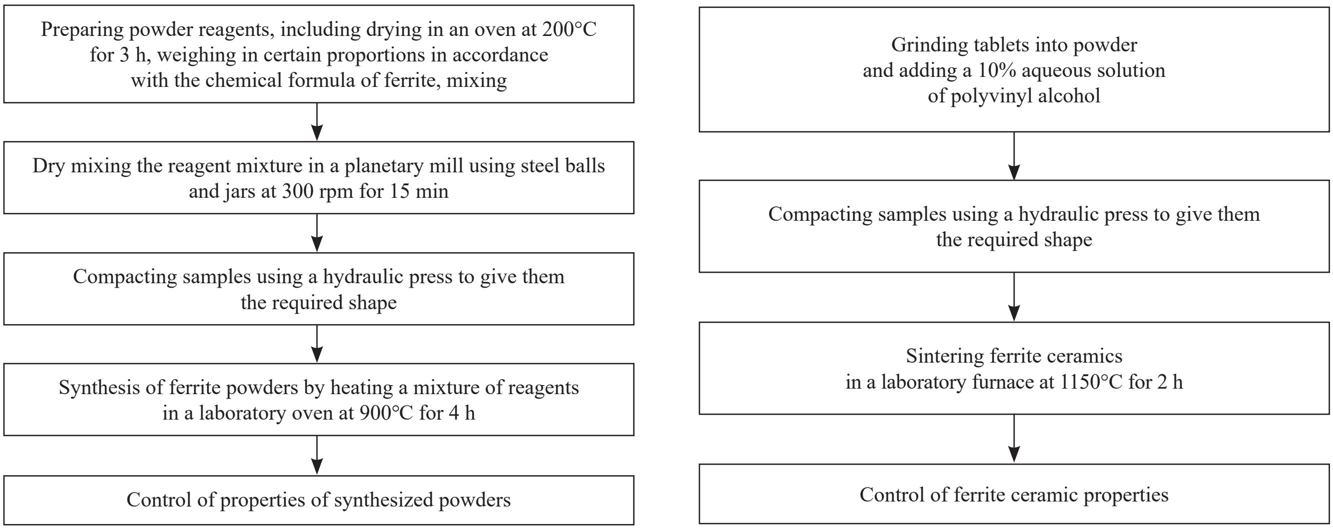

(a) (b)

Fig. 1. Process flow diagrams for the (a) synthesis and (b) sintering of ferrites

At the first step, the powders were gradually mixed by rubbing through fine steel sieves with a cell size of 100 µm. At the second step, for the mixing to be more thorough and for the obtained mixture to be more uniform in volume, the powders were mechanically ground in a planetary ball mill with steel grinding jars and balls at 300 rpm for 15 min.

Next, the samples were compacted into 2-mm-thick pellets 15 mm in diameter to create closer contacts between particles and thus encourage the synthesis reaction to occur better and more completely. The samples were synthesized in a laboratory furnace in air at a temperature of 900°C for a holding time of 240 min. Following synthesis, the phase composition and Curie temperature of the obtained samples were determined.

Figure 1b presents the stage of the high-temperature sintering of lithium ferrite. First, the synthesized samples were ground again and stirred. Then, the samples were recompacted into pellets of the described shape.

The compactibility of powders is typically improved by adding various binders (plasticizers) to promote mutual adhesion of individual particles, followed grinding the mass in a mortar. The main requirement for all binders is that they should be completely removed from the compacted parts when heating to 600°C. In this work, a 10% aqueous solution of polyvinyl alcohol was used as a binder.

The samples were compacted in a hydraulic press using steel molds. It is known that the pressing pressure depends on the pellet size and the design of the mold. In the work, the compaction parameters of the samples were selected experimentally: pressing pressure—200 MPa; pressing time—3 min. The set pressure was 20% lower than the maximum pressure at which the sample has not yet delaminated.

The molded samples were sintered at a temperature of 1150°C for 120 min. High-temperature sintering in the furnace consisted of three steps: heating at a certain rate to the sintering temperature, isothermal holding at this temperature, and cooling. The heating and cooling rate was 5 deg/min.

The purpose of the sintering stage is to obtain ferrite products with a certain set of properties. Sintering is known to be accompanied by recrystallization processes consisting in the formation and migration of intergranular boundaries. This forms a microstructure that largely determines the properties of the resulting ferrites. Thus, the purpose of the high-temperature sintering in this work is to ensure the formation of lithium ferrite of cubic structure having a certain grain size and porosity, as well as minimum internal stresses in crystallites at a given chemical composition.

The sintered samples were sent for analysis of their phase composition, microstructure, and Curie temperature. X-ray powder diffraction analysis (XRD) of the samples was carried out with an ARL X'TRA X-ray diffractometer (*Thermo Fisher Scientific*, Switzerland). Phases were identified using the PDF-4+ powder database of the International Center for Diffraction Data (ICDD[1]). The microstructure of the samples was studied with a TM-3000 scanning electron microscope (*Hitachi*, Japan). The average grain size was calculated from scanning electron microscopy (SEM) results. The density of the samples was determined by hydrostatic weighing. The Curie temperature of lithium ferrites and phase transitions in them were studied, respectively, by thermogravimetry (TG) with the application of an external magnetic field (thermomagnetometry), as well as differential scanning calorimetry (DSC) using an STA 449C Jupiter thermal analyzer (*Netzsch*, Germany).

RESULTS AND DISCUSSION

The results of X-ray powder diffraction analysis (Fig. 2) showed that the preliminary synthesis and high-temperature sintering of REE-free samples (sample N0) produce a spinel magnetic phase. The X-ray powder diffraction patterns of sample N0 correspond to the ordered phase α-$Li_{0.5}Fe_{2.5}O_4$ (PDF No. 04-015-5965) and the disordered phase β-$Li_{0.5}Fe_{2.5}O_4$ (PDF No. 00-017-0114) with cubic space groups ($Fd3m$).

In samples N1 and N2, a secondary crystalline phase identified as $SmFeO_3$ (PDF No. 00-039-1490) is formed along with the spinel phase. $SmFeO_3$ is an orthoferrite with a perovskite-like crystal structure and orthorhombic space group ($Pnma$).

Thus, initial reactions (2) and (3) in samples N1 and N2 have different forms. In the case of the formation of the $Li_{0.5}Fe_{2.5}O_4$ and $SmFeO_3$ phases, the excess lithium, which is initially loaded at the stage of mixing the initial reagents, is released in the reaction products. Previously [27], it was detected that part of the lithium oxide formed by the decomposition of lithium carbonate during the synthesis of lithium ferrites sublimates at a temperature above 900°C and volatilizes together with oxygen. Therefore, the interaction reactions in the Fe_2O_3–Li_2CO_3–Sm_2O_3 system can proceed in samples N1 and N2 according to the following equations, respectively:

$$Li_2CO_3 + 4.88Fe_2O_3 + 0.12Sm_2O_3 \rightarrow \\ \rightarrow 3.808Li_{0.5}Fe_{2.5}O_4 + 0.24SmFeO_3 + 0.048Li_2O + CO_2, \tag{4}$$

$$Li_2CO_3 + 4.6Fe_2O_3 + 0.4Sm_2O_3 \rightarrow \\ \rightarrow 3.36Li_{0.5}Fe_{2.5}O_4 + 0.4SmFeO_3 + 0.16Li_2O + CO_2. \tag{5}$$

---

[1] URL: http://www.icdd.com. Accessed October 3, 2023.

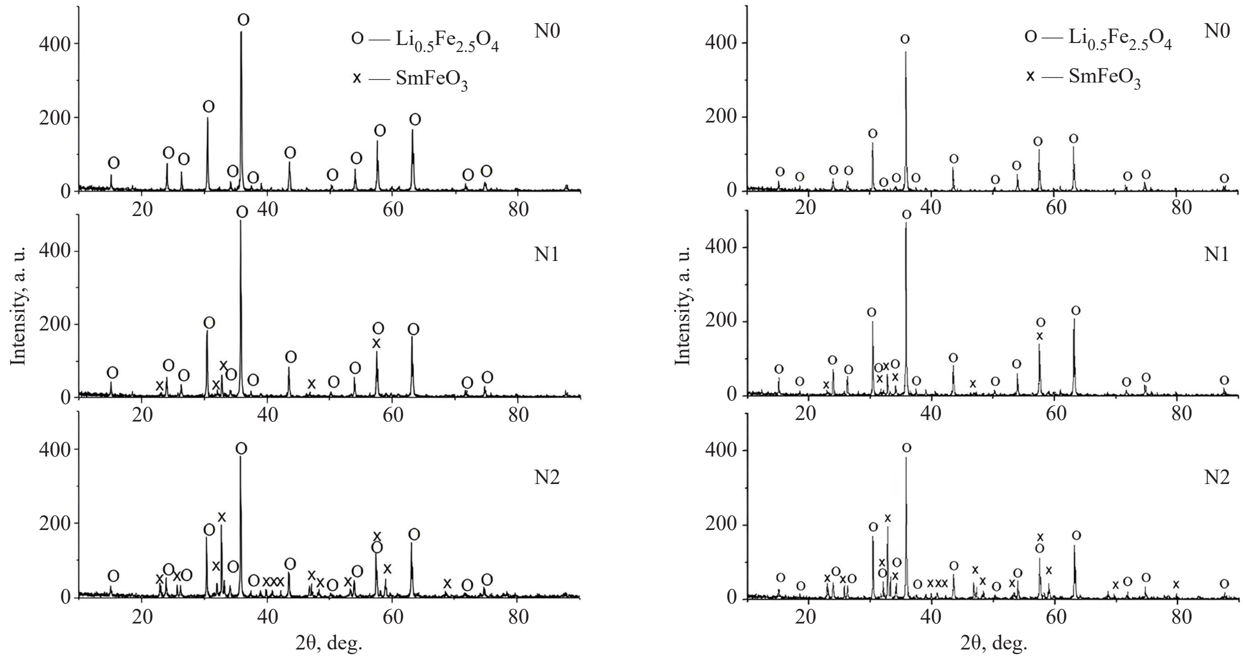

(a)

(b)

Fig. 2. X-ray powder diffraction analysis of (a) synthesized and (b) sintered ferrites N0, N1, and N2

Figure 3 shows the crystal lattices of the identified phases as generated by the PowderCell 2.4 powder pattern calculation program[2]. The quantitative contents of the synthesized phases presented in Table 1 depend on the concentration of the introduced Sm_2O_3. An increase in the Sm_2O_3 content from 4.7 (sample N1) to 14.7 wt % (sample N2) in the Fe_2O_3–Li_2CO_3–Sm_2O_3 mixture leads to an increase in the concentration *C* of the secondary phase $SmFeO_3$ in the synthesized samples from 4.9 to 18.2 wt %. Accordingly, the content of lithium ferrite decreases (Table 1).

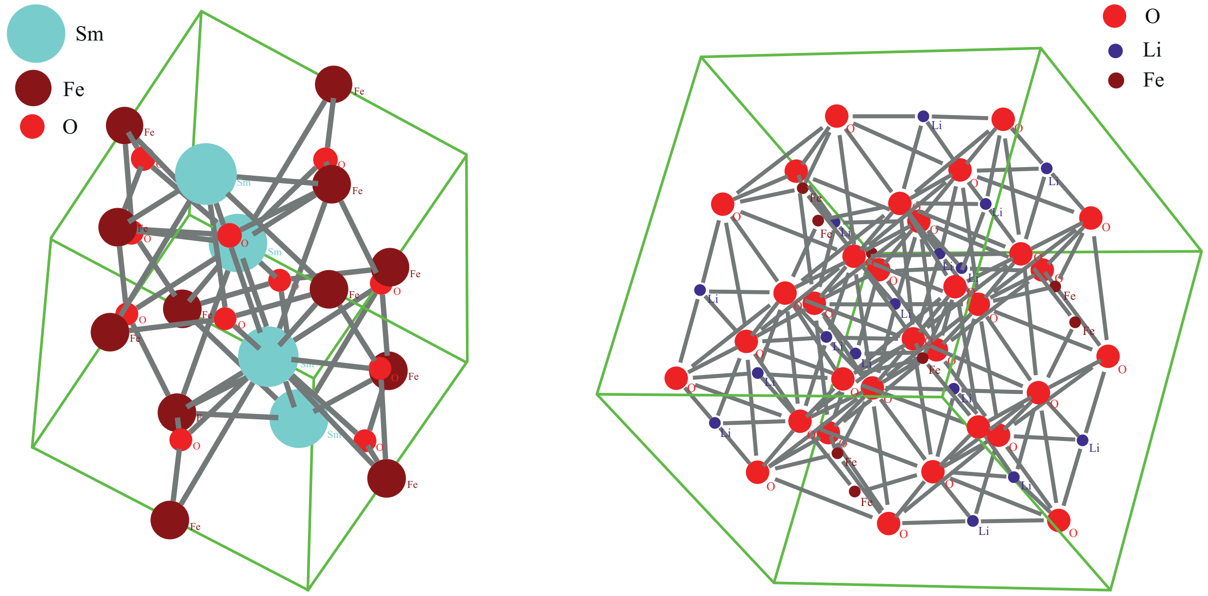

(a)

(b)

Fig. 3. Crystal lattices of (a) $SmFeO_3$ and (b) $Li_{0.5}Fe_{2.5}O_4$

---

[2] Kraus W., Nolze G. POWDERCELL – a program for representation and manipulation of crystal structures and calculations of the resulting X-ray powder patterns. *J. Appl. Cryst.* 1996:29;301–303.

Table 1. Phase composition and properties of synthesized ferrites

Sample	Phase composition	Lattice parameter, Å	*C*, wt %	T_C, °C
N0	$Li_{0.5}Fe_{2.5}O_4$	$a = b = c = 8.329$ (±0.002)	100.0	632.4
N1	$Li_{0.5}Fe_{2.5}O_4$	$a = b = c = 8.330$ (±0.002)	95.1	632.5
	$SmFeO_3$	$a = 5.592$ (±0.002); $b = 7.706$ (±0.003); $c = 5.400$ (±0.003)	4.9	
N2	$Li_{0.5}Fe_{2.5}O_4$	$a = b = c = 8.331$ (±0.002)	81.8	631.9
	$SmFeO_3$	$a = 5.594$ (±0.002); $b = 7.705$ (±0.003); $c = 5.400$ (±0.003)	18.2	

Note: *C* is the concentration; T_C is the Curie temperature.

In the sintered samples (Fig. 2b; Table 2), the concentration of the $Li_{0.5}Fe_{2.5}O_4$ phase slightly increases, while the amount of the secondary phase $SmFeO_3$ decreases in comparison with the synthesized samples. The lattice parameters obtained in this work are in satisfactory agreement with the literature data [27].

The quantitative analysis of the phase content of two polymorphs of $Li_{0.5}Fe_{2.5}O_4$ (α and β) using the X-ray powder diffraction patterns recorded in this study is complicated by the angular coincidences of these reflections (close lattice parameters). Unlike β-$Li_{0.5}Fe_{2.5}O_4$, the α polymorph has superstructural reflections at $2\theta \approx 15°$ (110), 23.9° (210), and 26.2° (211). The presence of high-intensity superstructural reflections in the diffraction patterns indicates ordering of the lithium spinel structure. Therefore, we assessed and explained the obtained results by analyzing the changes in the intensities of the superstructural reflections (110), (210), and (211) (Table 3). According to these data, the intensities of superstructure reflections for samples N0 and N1 are high following preliminary synthesis, their sum being greater than that for sample N2. This shows a large amount of α-$Li_{0.5}Fe_{2.5}O_4$ in these samples, whereas the low intensities for N2 samples are likely to be due to an increase in the amount of the perovskite phase.

The intensities of superstructure reflections for sintered sample N0 are low, their sum being smaller than that for samples N1 and N2. This indicates the presence of a large amount of the β-$Li_{0.5}Fe_{2.5}O_4$ phase, which could have formed during high-temperature sintering due to a violation of the stoichiometric composition in oxygen within the single-phase composition [28].

Table 2. Phase composition and properties of sintered ferrites

Sample	Phase composition	Lattice parameter, Å	*C*, wt %	*D*, µm	ρ, g/cm^3	T_C, °C
N0	$Li_{0.5}Fe_{2.5}O_4$	$a = b = c = 8.332$ (±0.002)	100.0	7.9	4.4	622.6
N1	$Li_{0.5}Fe_{2.5}O_4$	$a = b = c = 8.327$ (±0.002)	96.2	2.9	4.3	628.5
	$SmFeO_3$	$a = 5.594$ (±0.002); $b = 7.706$ (±0.003); $c = 5.401$ (±0.003)	3.8			
N2	$Li_{0.5}Fe_{2.5}O_4$	$a = b = c = 8.329$ (±0.002)	83.5	1.7	4.1	630.0
	$SmFeO_3$	$a = 5.592$ (±0.002); $b = 7.707$ (±0.003); $c = 5.400$ (±0.003)	16.5			

Note: *C* is the concentration, *D* is the average grain size, ρ is the density, and T_C is the Curie temperature.

Table 3. Intensities of the maxima of superstructural reflections (110), (210), and (211) for α-$Li_{0.5}Fe_{2.5}O_4$

Sample	Synthesis				Sintering			
	(110)	(210)	(211)	∑	(110)	(210)	(211)	∑
N0	51	79	66	196	30	35	29	94
N1	54	83	58	195	50	73	53	176
N2	27	36	30	93	29	45	37	111

The SEM results (Fig. 4) demonstrate different particle morphology in the studied samples. A structure having high density (ρ = 4.4 g/cm^3, Table 2), low porosity, and large irregular shaped grains (average grain size *D* = 7.9 µm, Table 2) is characteristic of lithium ferrite without the addition of REE.

The results of scanning electron microscopy of samples N1 and N2 confirm the previous conclusions about the formation of a two-phase product during the production of ferrite from the Fe_2O_3–Li_2CO_3–Sm_2O_3 powder mixture. In the SEM images, two shades can be clearly distinguished, one being the main spinel ferrite phase (gray), while the other represents the secondary phase $SmFeO_3$ (white). The presence of the secondary phase leads to a decrease in the density of the samples during sintering (Table 2), especially at high concentrations of introduced Sm_2O_3, as well as to a decrease in the average grain size. At the same time, sample N1 with a small addition of REE has ferrite grains having a more regular polyhedral shape characteristic of lithium ferrite.

The peaks in the DSC curves (Fig. 5) due to the α→β phase transition in $Li_{0.5}Fe_{2.5}O_4$ confirm the formation of a certain amount of ordered α-phase of lithium ferrite during synthesis and sintering. The areas of these peaks depend on the amount of lithium ferrite. The enthalpy of the α→β transition at a high content of α-$Li_{0.5}Fe_{2.5}O_4$ is known to be 12–13 J/g [29]. In the preliminary synthesis of ferrites, the DSC peak areas are approximately within this range of enthalpies for all samples (Fig. 5a). The Curie temperature range of ~630–632°C obtained from derivative TG curves was reported [30–32] to correspond to unsubstituted lithium ferrite with the chemical formula α-$Li_{0.5}Fe_{2.5}O_4$.

The high-temperature sintering of samples without the addition of REE in a dilatometer leads to an increase in the weight step in the TG measurements, which is related to the high magnetization of the obtained samples (Fig. 5b). At the same time, the Curie temperature is reduced (622°C), which may be a consequence of a violation of the stoichiometric composition of the samples due to the release of lithium and oxygen to form a disordered β-$Li_{0.5}Fe_{2.5}O_4$ phase. The excessively low Curie temperature for β-$Li_{0.5}Fe_{2.5}O_4$ is confirmed by literature data [33]. The small area (2 J/g) of the DSC peak for samples N0 also indicates a high content of the disordered β phase.

The area of the DSC peaks for samples N1 and N2 (Fig. 5) is 12.2 and 11.6 J/g, which values are close to the enthalpy of the α→β transformation in lithium ferrite. For sintered sample N2, which contains a large amount of REE, the weight step in the TG measurements decreases due to a decrease in the concentration of the magnetic phase of lithium ferrite. In the studied samples,

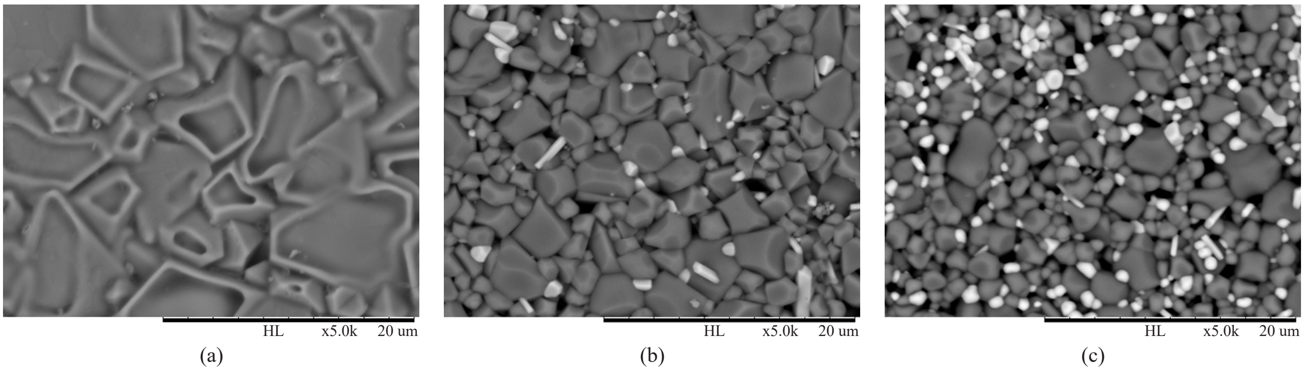

Fig. 4. SEM images of sintered samples: (a) N0, (b) N1, and (c) N2

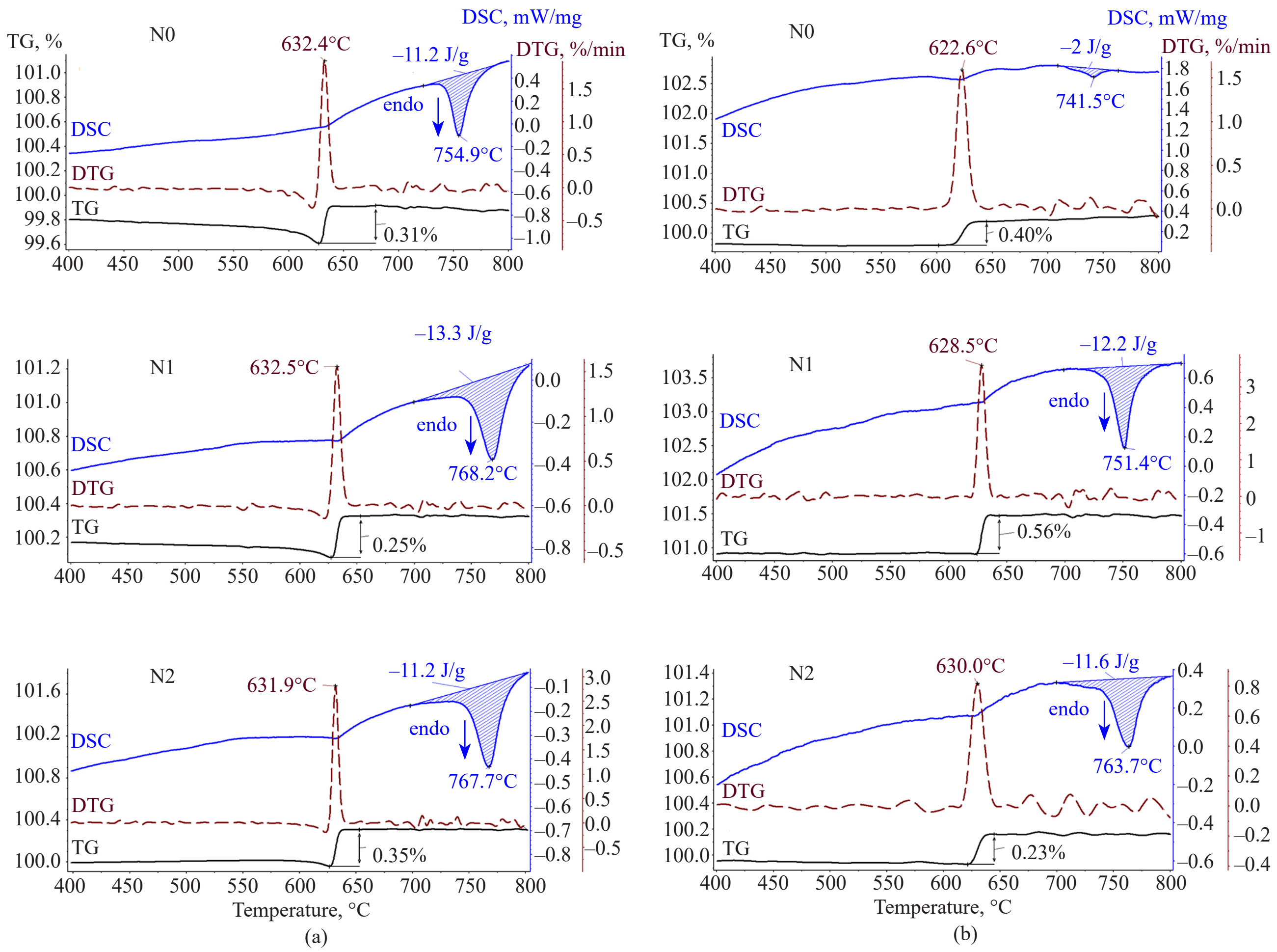

(a)

(b)

Fig. 5. Thermomagnetometric and differential scanning calorimetric analyzes of samples N0, N1, and N2 obtained by (a) preliminary synthesis and (b) sintering

neither X-ray powder diffraction nor thermal analyses revealed the formation of substituted lithium ferrite phases during preliminary synthesis or during high-temperature sintering.

CONCLUSIONS

In this work, the structure and properties of lithium ferrite obtained by preliminary solid-phase synthesis and subsequent high-temperature sintering from the initial reagents Fe_2O_3–Li_2CO_3–Sm_2O_3 were studied by XRD, TG, DSC and SEM analyses. The interaction between the initial reagents was shown to lead to the formation of a product consisting mainly of lithium ferrite $Li_{0.5}Fe_{2.5}O_4$ (α and β polymorphs) having a spinel structure, while the $SmFeO_3$ phase had a perovskite-like structure. The quantity of the latter increased with an increase in the Sm_2O_3 content in the initial mixture. Along with the obtained values of the enthalpy of α→β phase transitions in lithium ferrite, the high Curie temperatures indicate that the main product in all synthesized samples was the ordered α-$Li_{0.5}Fe_{2.5}O_4$ phase. Sintering at elevated temperature resulted in a slight decrease in the content of the $SmFeO_3$ phase and an increase in the lithium ferrite phase. As confirmed by the reduced values of the Curie temperature and the phase transition enthalpy, the sample not modified with samarium contained a significant amount of the disordered β-$Li_{0.5}Fe_{2.5}O_4$ phase. The introduction of samarium ions at the synthesis stage led to the preservation of the ordered α-$Li_{0.5}Fe_{2.5}O_4$ phase during sintering, whose morphology depends on the concentration of the secondary phase $SmFeO_3$. In the case of the introduction of a low concentration of Sm_2O_3 (up to 4.7 wt %), the structure of the samples was characterized by the presence of more regular polyhedral grains. In this case, the density of the samples insignificantly decreased while maintaining a high Curie temperature corresponding to unsubstituted lithium ferrite. The obtained results can support future more detailed studies of the electromagnetic properties of lithium ferrites modified with low concentrations of REEs in the microwave range.

Acknowledgments

The work was supported by the Ministry of Science and Higher Education of the Russian Federation within the framework of the State Assignment in the Field of Scientific Activity (project FSWW-2023-0011).

Authors' contributions

E.N. Lysenko—research idea, analyzing and discussing the results, and editing the text of the article.

V.A. Vlasov—development of a methodology for conducting the experiment, participation in experimental work, discussion of the results, and writing and formatting the text of the article.

Yu.S. Elkina—participation in experiments, processing the obtained data, search for scientific publications on the topic of the article, formation of the list of references, and participation in editing the text of the article.

A.P. Surzhikov—setting up and planning experiments, and discussion of the results.

The authors declare no conflicts of interest.

REFERENCES

1. Trukhanov A.V., Tishkevich D.I., Timofeev A.V., *et al.* Structural and electrodynamic characteristics of the spinel-based composite system. *Ceram. Int.* 2024;50(12):21311–21317. https://doi.org/10.1016/j.ceramint.2024.03.241
2. Kostishin V.G., Vergazov R.M., Menshova S.B., Isaev I.M. Prospects for the use of ferrites with high magnetic permeability and permittivity as radio-absorbing materials. *Russ. Technol. J.* 2020;8(6):87–108 (in Russ.). https://doi.org/10.32362/2500-316X-2020-8-6-87-108
3. Kostishin V.G., Isaev I.M., Salogub D.V. Radio-Absorbing Magnetic Polymer Composites Based on Spinel Ferrites: A Review. *Polymers*. 2024;16(7):1003. https://doi.org/10.3390/polym16071003
4. Sherstyuk D.P., Starikov A.Yu., Zhivulin V.E., Zherebtsov D.A., Mikhailov G.G., Vinnik D.A. Study of the effect of cobalt substitution on the structure of nickel-zinc ferrite. *Vestnik Yuzhno-Ural'skogo gosudarstvennogo universiteta. Seriya: Metallurgiya = Bulletin of the South Ural State University. Ser. Metallurgy*. 2020;20(2):51–56 (in Russ.). https://doi.org/10.14529/met200205
5. Nikishina E.E. Heterophase synthesis of cobalt ferrite. *Tonk. Khim. Tekhnol. = Fine Chem. Technol.* 2021;16(6):502–511. https://doi.org/10.32362/2410-6593-2021-16-6-502-511
6. Gavrilova M.A., Gavrilova D.A., Kondrashkova I.S., Krasilin A.A. Formation of $Zn_{0.5}Ni_{0.5}Fe_2O_4$ Nanocrystals in Conditions of Solution Combustion: Effect of the Type of Fuel on the Structure and Morphology. *Fizika i khimiya stekla*. 2023;49(4):459–470 (in Russ.). https://doi.org/10.31857/S013266512260090X
7. Ahmad M., Shahid M., Alanazi Y.M., ur Rehman A., Asif M., Dunnill C.W. Lithium ferrite ($Li_{0.5}Fe_{2.5}O_4$): synthesis, structural, morphological and magnetic evaluation for storage devices. *J. Mater. Res. Technol.* 2022;18:3386–3395. https://doi.org/10.1016/j.jmrt.2022.03.113
8. Askarzadeh N., Shokrollahi H. A review on synthesis, characterization and properties of lithium ferrites. *Results in Chemistry.* 2024;10:101679. https://doi.org/10.1016/j.rechem.2024.101679
9. Nikolaeva S.A., Lysenko E.N., Nikolaev E.V., Vlasov V.A., Surzhikov A.P. Microstructure and electromagnetic properties of $Li_{0.65}Fe_{1.6}Ti_{0.5}Zn_{0.2}Mn_{0.05}O_4$–$Bi_2O_3$–$ZrO_2$ composite ceramics. *J. Alloy. Compd.* 2023;941:169025. https://doi.org/10.1016/j.jallcom.2023.169025
10. Lysenko E., Nikolaev E., Vlasov V., Surzhikov A. Microstructure and reactivity of Fe_2O_3-Li_2CO_3-ZnO ferrite system ball-milled in a planetary mill. *Thermochim. Acta*. 2018; 664:100–107. https://doi.org/10.1016/j.tca.2018.04.015

СПИСОК ЛИТЕРАТУРЫ

1. Trukhanov A.V., Tishkevich D.I., Timofeev A.V., *et al.* Structural and electrodynamic characteristics of the spinel-based composite system. *Ceram. Int.* 2024;50(12):21311–21317. https://doi.org/10.1016/j.ceramint.2024.03.241
2. Костишин В.Г., Вергазов Р.М., Меньшова С.Б., Исаев И.М. Перспективы применения ферритов с высокими значениями магнитной и диэлектрической проницаемостей в качестве радиопоглощающих материалов. *Russ. Technol. J.* 2020;8(6):87–108. https://doi.org/10.32362/2500-316X-2020-8-6-87-108
3. Kostishin V.G., Isaev I.M., Salogub D.V. Radio-Absorbing Magnetic Polymer Composites Based on Spinel Ferrites: A Review. *Polymers*. 2024;16(7):1003. https://doi.org/10.3390/polym16071003
4. Шерстюк Д.П., Стариков А.Ю., Живулин В.Е., Жеребцов Д.А., Михайлов Г.Г., Винник Д.А**.** Изучение влияния замещения кобальтом на структуру никель-цинкового феррита. *Вестник Южно-Уральского государственного университета. Серия: Металлургия*. 2020;20(2):51–56. https://doi.org/10.14529/met200205
5. Никишина Е.Е. Гетерофазный синтез феррита кобальта. *Тонкие химические технологии*. 2021;16(6):502–511. https://doi.org/10.32362/2410-6593-2021-16-6-502-511
6. Гаврилова М.А., Гаврилова Д.А., Кондрашкова И.С., Красилин А.А. Формирование нанокристаллов $Zn_{0.5}Ni_{0.5}Fe_2O_4$ в условиях растворного горения: влияние типа "топлива" на структуру и морфологию. *Физика и химия стекла*. 2023;49(4):459–470. https://doi.org/10.31857/S013266512260090X
7. Ahmad M., Shahid M., Alanazi Y.M., ur Rehman A., Asif M., Dunnill C.W. Lithium ferrite ($Li_{0.5}Fe_{2.5}O_4$): synthesis, structural, morphological and magnetic evaluation for storage devices. *J. Mater. Res. Technol.* 2022;18:3386–3395. https://doi.org/10.1016/j.jmrt.2022.03.113
8. Askarzadeh N., Shokrollahi H. A review on synthesis, characterization and properties of lithium ferrites. *Results in Chemistry.* 2024;10:101679. https://doi.org/10.1016/j.rechem.2024.101679
9. Nikolaeva S.A., Lysenko E.N., Nikolaev E.V., Vlasov V.A., Surzhikov A.P. Microstructure and electromagnetic properties of $Li_{0.65}Fe_{1.6}Ti_{0.5}Zn_{0.2}Mn_{0.05}O_4$–$Bi_2O_3$–$ZrO_2$ composite ceramics. *J. Alloy. Compd.* 2023;941:169025. https://doi.org/10.1016/j.jallcom.2023.169025
10. Lysenko E., Nikolaev E., Vlasov V., Surzhikov A. Microstructure and reactivity of Fe_2O_3-Li_2CO_3-ZnO ferrite system ball-milled in a planetary mill. *Thermochim. Acta*. 2018; 664:100–107. https://doi.org/10.1016/j.tca.2018.04.015

11. Martinson K.D., Ivanov A.A., Panteleev I.B., *et al.* Pre-Ceramic Nanostructured Liznmn-Ferrite Powders: Synthesis, Structure, and Electromagnetic Properties. *Glass and Ceramics*. 2020;77(5–6):215–220. https://doi.org/10.1007/s10717-020-00274-9
    [Original Russian Text: Martinson K.D., Ivanov A.A., Panteleev I.B., Popkov V.I. Pre-Ceramic Nanostructured LiZnMn-Ferrite Powders: Synthesis, Structure, and Electromagnetic Properties. *Steklo i keramika*. 2020;6:16–23 (in Russ.).]
12. Isaev I.M., Kostishin V.G., Korovushkin V.V., *et al.* Crystal chemistry and magnetic properties of polycrystalline spinel ferrites $Li_{0.33}Fe_{2.29}Zn_{0.21}Mn_{0.17}O_4$. *Russ. J. Inorg. Chem.* 2021;66(12):1917–1924. https://doi.org/10.1134/S0036023621120056
    [Original Russian Text: Isaev I.M., Kostishin V.G., Korovushkin V.V., Shipko M.N., Timofeev A.V., Mironovich A.Yu., Salogub D.V., Shakirzyanov R.I. Crystal chemistry and magnetic properties of polycrystalline spinel ferrites $Li_{0.33}Fe_{2.29}Zn_{0.21}Mn_{0.17}O_4$. *Zhurnal neorganicheskoi khimii*. 2021;66(12):1792–1800 (in Russ.). https://doi.org/10.31857/S0044457X21120059]
13. Mahmoudi M., Kavanlouei M., Maleki-Ghaleh H. Effect of composition on structural and magnetic properties of nanocrystalline ferrite $Li_{0.5}Sm_xFe_{2.5-x}O_4$. *Powd. Metal. Metal. Ceram.* 2015;54:31–39. https://doi.org/10.1007/s11106-015-9676-9
14. Slimani Y., Almessiere M.A., Güner S., Kurtan U., Shirsath S.E., Bayka A., Ercan I. Magnetic and microstructural features of Dy^{3+} substituted $NiFe_2O_4$ nanoparticles derived by sol–gel approach. *J. Sol-Gel Sci. Techn*. 2020;95:202–210. https://doi.org/10.1007/s10971-020-05292-1
15. Jacob B.P., Thankachan S., Xavier S., Mohammed E.M. Effect of Tb^{3+} substitution on structural, electrical and magnetic properties of sol–gel synthesized nanocrystalline nickel ferrite. *J. Alloys Compd.* 2013;578:314–319. https://doi.org/10.1016/j.jallcom.2013.04.147
16. Heiba Z.K., Mohamed M.B., Arda L., Dogan N. Cation distribution correlated with magnetic properties of nanocrystalline gadolinium substituted nickel ferrite. *Magn. Magn. Mater.* 2015;391:195–202. https://doi.org/10.1016/j.jmmm.2015.05.003
17. Ahmad S.I., Ansari S.A., Kumar D.R. Structural, morphological, magnetic properties and cation distribution of Ce and Sm co-substituted nano crystalline cobalt ferrite. *Mater. Chem. Phys.* 2018;208:248–257. https://doi.org/10.1016/j.matchemphys.2018.01.050
18. Nikumbh A.K., Pawar R.A., Nighot D.V., Gugale G.S., Sangale M.D., Khanvilkar M.B., Nagawade A.V. Structural, electrical, magnetic and dielectric properties of rare-earth substituted cobalt ferrites nanoparticles synthesized by the co-precipitation method. *Magn. Magn. Mater.* 2014;355:201–209. https://doi.org/10.1016/j.jmmm.2013.11.052
19. Ahmad I., Abbas T., Ziya A.B., Maqsood A. Structural and magnetic properties of erbium doped nanocrystalline Li–Ni ferrites. *Ceram. Int.* 2014;40(6):7941–7945. https://doi.org/10.1016/j.ceramint.2013.12.142
20. Junaid M., Khan M.A., Iqbal F., Murtaza G., Akhtar M.N., Ahmad M., Shakir I., Warsi M.F. Structural, spectral, dielectric and magnetic properties of Tb–Dy doped Li-Ni nano-ferrites synthesized via microemulsion route. *Magn. Magn. Mater.* 2016;419:338–344. https://doi.org/10.1016/j.jmmm.2016.06.043

11. Мартинсон К.Д., Иванов А.А., Пантелеев И.Б., Попков В.И. Предкерамические наноструктурированные порошки LiZnMn-феррита: получение, структура и электромагнитные свойства. *Стекло и керамика*. 2020;6:16–23.
12. Исаев И.М., Костишин В.Г., Коровушкин В.В., Шипко М.Н., Тимофеев А.В., Миронович А.Ю., Салогуб Д.В., Шакирзянов Р.И. Кристаллохимия и магнитные свойства поликристаллических ферритов-шпинелей $Li_{0.33}Fe_{2.29}Zn_{0.21}Mn_{0.17}O_4$. *Журн. неорган. химии.* 2021;66(12):1792–1800. https://doi.org/10.31857/S0044457X21120059
13. Mahmoudi M., Kavanlouei M., Maleki-Ghaleh H. Effect of composition on structural and magnetic properties of nanocrystalline ferrite $Li_{0.5}Sm_xFe_{2.5-x}O_4$. *Powd. Metal. Metal. Ceram.* 2015;54:31–39. https://doi.org/10.1007/s11106-015-9676-9
14. Slimani Y., Almessiere M.A., Güner S., Kurtan U., Shirsath S.E., Bayka A., Ercan I. Magnetic and microstructural features of Dy^{3+} substituted $NiFe_2O_4$ nanoparticles derived by sol–gel approach. *J. Sol-Gel Sci. Techn*. 2020;95:202–210. https://doi.org/10.1007/s10971-020-05292-1
15. Jacob B.P., Thankachan S., Xavier S., Mohammed E.M. Effect of Tb^{3+} substitution on structural, electrical and magnetic properties of sol–gel synthesized nanocrystalline nickel ferrite. *J. Alloys Compd.* 2013;578:314–319. https://doi.org/10.1016/j.jallcom.2013.04.147
16. Heiba Z.K., Mohamed M.B., Arda L., Dogan N. Cation distribution correlated with magnetic properties of nanocrystalline gadolinium substituted nickel ferrite. *Magn. Magn. Mater.* 2015;391:195–202. https://doi.org/10.1016/j.jmmm.2015.05.003
17. Ahmad S.I., Ansari S.A., Kumar D.R. Structural, morphological, magnetic properties and cation distribution of Ce and Sm co-substituted nano crystalline cobalt ferrite. *Mater. Chem. Phys.* 2018;208:248–257. https://doi.org/10.1016/j.matchemphys.2018.01.050
18. Nikumbh A.K., Pawar R.A., Nighot D.V., Gugale G.S., Sangale M.D., Khanvilkar M.B., Nagawade A.V. Structural, electrical, magnetic and dielectric properties of rare-earth substituted cobalt ferrites nanoparticles synthesized by the co-precipitation method. *Magn. Magn. Mater.* 2014;355:201–209. https://doi.org/10.1016/j.jmmm.2013.11.052
19. Ahmad I., Abbas T., Ziya A.B., Maqsood A. Structural and magnetic properties of erbium doped nanocrystalline Li–Ni ferrites. *Ceram. Int.* 2014;40(6):7941–7945. https://doi.org/10.1016/j.ceramint.2013.12.142
20. Junaid M., Khan M.A., Iqbal F., Murtaza G., Akhtar M.N., Ahmad M., Shakir I., Warsi M.F. Structural, spectral, dielectric and magnetic properties of Tb–Dy doped Li-Ni nano-ferrites synthesized via microemulsion route. *Magn. Magn. Mater.* 2016;419:338–344. https://doi.org/10.1016/j.jmmm.2016.06.043
21. Al-Hilli M.F., Li S., Kassim K.S. Structural analysis, magnetic and electrical properties of samarium substituted lithium–nickel mixed ferrites. *Magn. Magn. Mater*. 2012;324(5):873–879. https://doi.org/10.1016/j.jmmm.2011.10.005
22. Li D.-Y., Sun Y.-K., Xu Y., Ge H.-L., Wu Q., Yan C. Effects of Dy^{3+} substitution on the structural and magnetic properties of $Ni_{0.5}Zn_{0.5}Fe_2O_4$ nanoparticles prepared by a sol-gel self-combustion method. *Ceram. Int.* 2015;41(3B):4581–4589. https://doi.org/10.1016/j.ceramint.2014.11.156

21. Al-Hilli M.F., Li S., Kassim K.S. Structural analysis, magnetic and electrical properties of samarium substituted lithium–nickel mixed ferrites. *Magn. Magn. Mater*. 2012;324(5):873–879. https://doi.org/10.1016/j.jmmm.2011.10.005
22. Li D.-Y., Sun Y.-K., Xu Y., Ge H.-L., Wu Q., Yan C. Effects of Dy^{3+} substitution on the structural and magnetic properties of $Ni_{0.5}Zn_{0.5}Fe_2O_4$ nanoparticles prepared by a sol-gel self-combustion method. *Ceram. Int.* 2015;41(3B):4581–4589. https://doi.org/10.1016/j.ceramint.2014.11.156
23. Zhao L., Yang H., Yu L., Cui Y., Feng S. Effects of Gd_2O_3 on structure and magnetic properties of Ni–Mn ferrite. *J. Mater. Sci*. 2006;41:3083–3087. https://doi.org/10.1007/s10853-005-1545-3
24. Almessiere M.A., Slimani Y., Guner S., Nawaz M., Baykal A., Aldakheel F., Sadaqat A., Ercan I. Effect of Nb substitution on magneto-optical properties of $Co_{0.5}Mn_{0.5}Fe_2O_4$ nanoparticles. *J. Mol. Struct.* 2019;1195:269–279. https://doi.org/10.1016/j.molstruc.2019.05.075
25. Lin Q., Yuan G., He Y., Wang L., Dong J., Yu Y. The Influence of La-substituted $Cu_{0.5}Co_{0.5}Fe_2O_4$ nanoparticles on its structural and magnetic properties. *Mater. Des.* 2015;78:80–84. https://doi.org/10.1016/j.matdes.2015.04.029
26. Lysenko E.N., Vlasov V.A., Nikolaeva S.A., Nikolaev E.V. TG, DSC, XRD, and SEM studies of the substituted lithium ferrite formation from milled $Sm_2O_3/Fe_2O_3/Li_2CO_3$ precursors. *J. Therm. Anal. Calorim.* 2023;148:1445–1453. https://doi.org/10.1007/s10973-022-11665-1
27. Ridley D.H., Lessoff H., Childress J.D. Effect of lithium and oxygen losses on magnetic and crystallographic properties of spinel lithium ferrite. *J. Am. Ceram. Soc.* 1970;53(6):304–311. https://doi.org/10.1111/j.1151-2916.1970.tb12113.x
28. Surzhikov A.P., Frangulyan T.S., Ghyngazov S.A., Lysenko E.N. Investigation of structural states and oxidation processes in $Li_{0.5}Fe_{2.5}O_{4-\delta}$ using TG analysis. *J. Therm. Anal. Calorim.* 2012;108:1207–1212. https://doi.org/10.1007/s10973-011-1734-z
29. Lysenko E.N., Malyshev A.V., Vlasov V.A., Nikolaev E.V., Surzhikov A.P. Microstructure and thermal analysis of lithium ferrite pre-milled in a high-energy ball mill. *J. Therm. Anal. Calorim.* 2018;134:127–133. https://doi.org/10.1007/s10973-018-7549-4.
30. Berbenni V., Marini A., Capsoni D. Solid state reaction study of the system Li_2CO_3/Fe_2O_3. *Z. Naturforschung – Sect. J. Phys. Sci.* 1998;53:997–1003. https://doi.org/10.1515/zna-1998-1212
31. An S.Y., Shim I.B., Kim C.S. Synthesis and magnetic properties of $LiFe_5O_8$ powders by a sol–gel process. *Magn. Magn Mater.* 2005;290–291:1551–1554. https://doi:10.1016/j.jmmm.2004.11.244
32. Mazen S.A., Abu-Elsaad N.I. Characterization and magnetic investigations of germanium-doped lithium ferrite. *Ceram. Int.* 2014;40:11229–11237. https://doi.org/10.1016/j.ceramint.2014.03.167
33. Ahniyaz A., Fujiwara T., Song S.-W., Yoshimura M. Low temperature preparation of β-$LiFe_5O_8$ fine particles by hydrothermal ball milling. *J. Solid State Ion.* 2002;151:419–423. https://doi.org/10.1016/S0167-2738(02)00548-9

23. Zhao L., Yang H., Yu L., Cui Y., Feng S. Effects of Gd_2O_3 on structure and magnetic properties of Ni–Mn ferrite. *J. Mater. Sci*. 2006;41:3083–3087. https://doi.org/10.1007/s10853-005-1545-3
24. Almessiere M.A., Slimani Y., Guner S., Nawaz M., Baykal A., Aldakheel F., Sadaqat A., Ercan I. Effect of Nb substitution on magneto-optical properties of $Co_{0.5}Mn_{0.5}Fe_2O_4$ nanoparticles. *J. Mol. Struct.* 2019;1195:269–279. https://doi.org/10.1016/j.molstruc.2019.05.075
25. Lin Q., Yuan G., He Y., Wang L., Dong J., Yu Y. The Influence of La-substituted $Cu_{0.5}Co_{0.5}Fe_2O_4$ nanoparticles on its structural and magnetic properties. *Mater. Des.* 2015;78:80–84. https://doi.org/10.1016/j.matdes.2015.04.029
26. Lysenko E.N., Vlasov V.A., Nikolaeva S.A., Nikolaev E.V. TG, DSC, XRD, and SEM studies of the substituted lithium ferrite formation from milled $Sm_2O_3/Fe_2O_3/Li_2CO_3$ precursors. *J. Therm. Anal. Calorim.* 2023;148:1445–1453. https://doi.org/10.1007/s10973-022-11665-1
27. Ridley D.H., Lessoff H., Childress J.D. Effect of lithium and oxygen losses on magnetic and crystallographic properties of spinel lithium ferrite. *J. Am. Ceram. Soc.* 1970;53(6):304–311. https://doi.org/10.1111/j.1151-2916.1970.tb12113.x
28. Surzhikov A.P., Frangulyan T.S., Ghyngazov S.A., Lysenko E.N. Investigation of structural states and oxidation processes in $Li_{0.5}Fe_{2.5}O_{4-\delta}$ using TG analysis. *J. Therm. Anal. Calorim.* 2012;108:1207–1212. https://doi.org/10.1007/s10973-011-1734-z
29. Lysenko E.N., Malyshev A.V., Vlasov V.A., Nikolaev E.V., Surzhikov A.P. Microstructure and thermal analysis of lithium ferrite pre-milled in a high-energy ball mill. *J. Therm. Anal. Calorim.* 2018;134:127–133. https://doi.org/10.1007/s10973-018-7549-4.
30. Berbenni V., Marini A., Capsoni D. Solid state reaction study of the system Li_2CO_3/Fe_2O_3. *Z. Naturforschung – Sect. J. Phys. Sci.* 1998;53:997–1003. https://doi.org/10.1515/zna-1998-1212
31. An S.Y., Shim I.B., Kim C.S. Synthesis and magnetic properties of $LiFe_5O_8$ powders by a sol–gel process. *Magn. Magn Mater.* 2005;290–291:1551–1554. https://doi:10.1016/j.jmmm.2004.11.244
32. Mazen S.A., Abu-Elsaad N.I. Characterization and magnetic investigations of germanium-doped lithium ferrite. *Ceram. Int.* 2014;40:11229–11237. https://doi.org/10.1016/j.ceramint.2014.03.167
33. Ahniyaz A., Fujiwara T., Song S.-W., Yoshimura M. Low temperature preparation of β-$LiFe_5O_8$ fine particles by hydrothermal ball milling. *J. Solid State Ion.* 2002;151:419–423. https://doi.org/10.1016/S0167-2738(02)00548-9

About the authors

Elena N. Lysenko, Dr. Sci. (Eng.), Professor, Head of the Laboratory, Research Laboratory for Electronics, Semiconductors and Dielectrics, Research School of High-Energy Physics, Tomsk Polytechnic University (30, Lenina pr., Tomsk, 634034, Russia). E-mail: lysenkoen@tpu.ru. Scopus Author ID 25027787100, ResearcherID K-1582-2013, RSCI SPIN-code 6536-9390, https://orcid.org/0000-0002-5093-2207

Vitaly A. Vlasov, Cand. Sci. (Phys.-Math.), Senior Researcher, Research Laboratory for Electronics, Semiconductors and Dielectrics, Research School of High-Energy Physics, Tomsk Polytechnic University (30, Lenina pr., Tomsk, 634034, Russia). E-mail: vlvitan@tpu.ru. Scopus Author ID 7202194125, ResearcherID K-1257-2013, RSCI SPIN-code 2003-8431, https://orcid.org/0000-0002-5946-2117

Yuliya S. Elkina, Postgraduate Student, Engineer, Research Laboratory for Electronics, Semiconductors and Dielectrics, Research School of High-Energy Physics, Tomsk Polytechnic University (30, Lenina pr., Tomsk, 634034, Russia). E-mail: ysm7@tpu.ru. Scopus Author ID 58892380200, ResearcherID HHS-0003-2022, RSCI SPIN-code 6717-1540, https://orcid.org/0000-0002-2708-9872

Anatoly P. Surzhikov, Dr. Sci. (Phys.-Math.), Professor, Head of the Department, Division for Testing and Diagnostics, School of Non-Destructive Testing, Tomsk Polytechnic University (30, Lenina pr., Tomsk, 634034, Russia). E-mail: surzhikov@tpu.ru. Scopus Author ID 6603494148, ResearcherID K-1224-2013, RSCI SPIN-code 1875-0293, https://orcid.org/0000-0003-2795-398X

Об авторах

Лысенко Елена Николаевна, д.т.н., профессор, заведующая лабораторией, Проблемная научно-исследовательская лаборатория электроники диэлектриков и полупроводников, Исследовательская школа физики высокоэнергетических процессов, ФГАОУ ВО «Национальный исследовательский Томский политехнический университет» (634050, Россия, г. Томск, пр-т Ленина, д. 30). E-mail: lysenkoen@tpu.ru. Scopus Author ID 25027787100, ResearcherID K-1582-2013, SPIN-код РИНЦ 6536-9390, https://orcid.org/0000-0002-5093-2207

Власов Виталий Анатольевич, к.ф.-м.н., старший научный сотрудник, Проблемная научно-исследовательская лаборатория электроники диэлектриков и полупроводников, Исследовательская школа физики высокоэнергетических процессов, ФГАОУ ВО «Национальный исследовательский Томский политехнический университет» (634050, Россия, г. Томск, пр-т Ленина, д. 30). E-mail: vlvitan@tpu.ru. Scopus Author ID 7202194125, ResearcherID K-1257-2013, SPIN-код РИНЦ 2003-8431, https://orcid.org/0000-0002-5946-2117

Елькина Юлия Сергеевна, аспирант, инженер, Проблемная научно-исследовательская лаборатория электроники диэлектриков и полупроводников, Исследовательская школа физики высокоэнергетических процессов, ФГАОУ ВО «Национальный исследовательский Томский политехнический университет» (634050, Россия, г. Томск, пр-т Ленина, д. 30). E-mail: ysm7@tpu.ru. Scopus Author ID 58892380200, ResearcherID HHS-0003-2022, SPIN-код РИНЦ 6717-1540, https://orcid.org/0000-0002-2708-9872

Суржиков Анатолий Петрович, д.ф.-м.н., профессор, заведующий кафедрой – руководитель отделения на правах кафедры, Отделение контроля и диагностики, Инженерная школа неразрушающего контроля и безопасности, ФГАОУ ВО «Национальный исследовательский Томский политехнический университет» (634050, Россия, г. Томск, пр-т Ленина, д. 30). E-mail: surzhikov@tpu.ru. Scopus Author ID 6603494148, ResearcherID K-1224-2013, SPIN-код РИНЦ 1875-0293, https://orcid.org/0000-0003-2795-398X

Translated from Russian into English by V. Glyanchenko
Edited for English language and spelling by Thomas A. Beavitt

Tonkie Khimicheskie Tekhnologii = Fine Chemical Technologies.
2025;20(1):75–88 ISSN 2686-7575 (Online)

Mathematical methods and information systems
in chemical technology

Математические методы и информационные системы
в химической технологии

UDC 66.081.6:66.011
https://doi.org/10.32362/2410-6593-2025-20-1-75-88
EDN WUFZOJ

RESEARCH ARTICLE

Modeling of membrane separation of liquid mixture in Aspen HYSYS

Alexander V. Malygin✉**, Ilya I. Emel'yanov, Roman V. Semin, Azat R. Fazlyev, Nadir N. Ziyatdinov, Alexander V. Klinov**

Kazan National Research Technological University, Kazan, 420015 Russia

✉ *Corresponding author, e-mail: MalyginAV@corp.knrtu.ru*

Abstract

Objectives. To develop and subsequently verify the calculation block of the mass transfer process in the pervaporation membrane module based on a HybSi® ceramic membrane using experimental data as a basis for the verification process.

Methods. The task was implemented using a mathematical simulation within the Aspen HYSYS application package, which is designed for modeling chemical engineering processes. The differential equations of the mathematical model were represented as a system of difference equations, which were then solved numerically with an adaptive area step. The membrane pervaporation module of area S during its modeling is divided into n intervals, based on ensuring within the ith interval the condition that the temperature change ΔT is less than 1°C. A model was constructed to simulate the performance of the membrane module under isothermal and adiabatic operating conditions.

Results. The mathematical model of the pervaporation process employed in the developed computational membrane pervaporation module considers variations in the concentration and temperature of the feedstock flux along the surface of the HybSi® membrane. The performance of the software module was evaluated by comparing the calculated results with the available experimental data for the dehydration of ethanol and isopropanol. The results demonstrated a high degree of agreement for three isotherms (60, 70, and 80°C) and two variations of pressure on the permeate side (5 and 20 mm Hg). Modeling of the operation of the membrane module with the area of 1 m^2 in adiabatic mode showed that the processes of alcohol dehydration on HybSi® membranes are accompanied by significant thermal effects associated with heat consumption to provide evaporation through the membrane due to large transmembrane fluxes.

Conclusions. The comparative analysis of the results of modeling the HybSi® membrane module in isothermal and adiabatic modes of operation demonstrated that the calculation of the membrane module without consideration of thermal effects results in significant errors. These include an overestimation of the permeate flow rate by up to 50% and an underestimation of the water concentration in the retentate by up to 1.3–1.8 times. It can be reasonably deduced that the omission of thermal effects in design calculations will result in a considerable underestimation of the requisite membrane module surface area.

Keywords

modeling, pervaporation, HybSi® membrane, Aspen HYSYS, alcohol dehydration

Submitted: 26.08.2024
Revised: 06.11.2024
Accepted: 25.12.2024

For citation

Malygin A.V., Emel'yanov I.I., Semin R.V., Fazlyev A.R., Ziyatdinov N.N., Klinov A.V. Modeling of membrane separation of liquid mixture in Aspen HYSYS. *Tonk. Khim. Tekhnol. = Fine Chem. Technol.* 2025;20(1):75–88. https://doi.org/10.32362/2410-6593-2025-20-1-75-88

НАУЧНАЯ СТАТЬЯ

Моделирование процесса мембранного разделения жидкой смеси в среде Aspen HYSYS

А.В. Малыгин✉, И.И. Емельянов, Р.В. Семин, А.Р. Фазлыев, Н.Н. Зиятдинов, А.В. Клинов

Казанский национальный исследовательский технологический университет, Казань, 420015 Россия

✉ *Автор для переписки, e-mail: MalyginAV@corp.knrtu.ru*

Аннотация

Цели. Разработка и последующая верификация на основе экспериментальных данных расчетного блока процесса массопереноса в первапорационном мембранном модуле на основе керамической мембраны HybSi®.

Методы. Задача решалась при помощи математического моделирования в прикладном пакете Aspen HYSYS, предназначеном для моделирования химико-технологических процессов. Дифференциальные уравнения математической модели были представлены в виде системы разностных уравнений, которая решалась численным способом с адаптивным шагом по площади. Мембранный первапорационный модуль площадью S в ходе его моделирования разбивается на n интервалов, исходя из обеспечения внутри i-го интервала условия, чтобы изменение температуры ΔT было меньше 1°C. Работоспособность программного модуля проверялась на основе сравнения результатов расчета с имеющимися экспериментальными данными по обезвоживанию этанола и изопропанола. Моделирование работы разработанного мембранного модуля проводилось в изотермических и адиабатических режимах.

Результаты. Используемая в разработанном расчетном первапорационном мембранном модуле математическая модель процесса первапорации учитывает изменение концентрации и температуры потока сырья вдоль поверхности мембраны HybSi®. Показано хорошее согласование для трех изотерм (60, 70 и 80°C) и двух вариантов давления со стороны пермеата (5 и 20 мм рт. ст.). Моделирование мембранного модуля площадью 1 м^2 в адиабатическом режиме работы показало, что процессы обезвоживания спиртов на мембранах HybSi® сопровождаются значительными тепловыми эффектами, связанными с расходом тепла на испарение через мембрану ввиду больших трансмембранных потоков для данной мембраны.

Выводы. Сравнительный анализ результатов моделирования мембранного модуля HybSi® в изотермическом и адиабатическом режимах работы показал, что расчет мембранного модуля без учета тепловых эффектов приводит к существенным ошибкам: в определении расхода пермеата — до 50%, в определении концентрации воды в ретанте до 1.3–1.8 раз. Поэтому выполнение проектных расчетов без учета тепловых эффектов будет приводить к существенному занижению требуемой поверхности мембранного модуля.

Ключевые слова

моделирование, первапорация, мембрана HybSi®, Aspen HYSYS, обезвоживание спирта

Поступила: 26.08.2024
Доработана: 06.11.2024
Принята в печать: 25.12.2024

Для цитирования

Малыгин А.В., Емельянов И.И., Семин Р.В., Фазлыев А.Р., Зиятдинов Н.Н., Клинов А.В. Моделирование процесса мембранного разделения жидкой смеси в среде Aspen HYSYS. *Тонкие химические технологии.* 2025;20(1):75–88. https://doi.org/10.32362/2410-6593-2025-20-1-75-88

INTRODUCTION

The separation processes of multicomponent liquid mixtures represent a fundamental aspect of chemical technology. The most energy-intensive processes are those involved in the separation of azeotropic mixtures, including extractive and azeotropic distillation, extraction, etc. [1]. In order to enhance the efficiency of liquid mixture separation processes, a range of measures are currently being explored. These encompass the thermal integration of technological process flows and the modification of the agents employed in the separation process itself [2, 3]. In this instance, an alternative to the aforementioned processes may be the separation of liquid mixtures by the pervaporation method, which represents a promising avenue of development within the field of membrane technologies. Initially, pervaporation was regarded as a potential technology for the dewatering of alcohols. The world's first industrial scale pervaporation plant was constructed for the purpose of ethanol dehydration at a pulp and paper mill in Germany [4]. Depending on the membrane used, pervaporation can be a successful approach for solving complex separation processes, including dehydration of organic solvents [5–7], extraction of organic compounds from aqueous solutions [8], separation of organic mixtures [9, 10], removal of sulfur components [11], and water desalination [12]. Currently, membranes made of organic (polymer), inorganic (ceramic, zeolite) and hybrid (combined organic and inorganic) materials are used in the processes of pervaporation [13].

The topic of membrane technology in production, encompassing its development, design, and implementation, has recently been the subject of growing interest. Mathematical modeling of chemical technology processes constitutes a principal instrument for the investigation, conceptualization, and optimization of industrial procedures. In practice, universal modeling programs (UMP) for mathematical modeling of chemical technological processes and systems are used to solve these problems. The products of *Aspen Technologies*, *Chemstations*, and *Invensys Systems* are most widely used for modeling membrane separation processes [14]. Unfortunately, the libraries of the UMP calculation modules, including Aspen HYSYS (*Aspen Technologies*, USA), which was used in this work, do not have a built-in module for modeling pervaporation processes. However, the open architecture of Aspen HYSYS offers the advantage of enabling the creation of bespoke thermodynamic and kinetic models, as well as models of equipment units, through the utilization of the integrated programming language. This presents the opportunity to develop a calculation module for the pervaporation process in Aspen HYSYS. The inclusion of the calculation module of the pervaporation in the UMP allows users to design both individual membrane installations themselves and technological systems that include these installations.

When modeling the separation of liquid mixtures according to the pervaporation method using UMP, issues of solvent dehydration are mainly considered: ethanol when feeding the initial mixture in liquid form [15–17] (on an industrial PERVAP 2210 membrane and a silicon dioxide-based membrane) and when feeding the initial mixture in a vapor phase state [18] (membrane with a selective layer of polyvinyltrimethylsilane); isopropanol (on an industrial PERVAP 2210 membrane) [19]; isobutanol (on industrial membranes PERVAP 4060 and 1510) [17, 20]; acetic acid (on a membrane based on silicon dioxide) [16].

Due to their being among the first polymer composite membranes made available for commercial use, PERVAP membranes are the most represented in research. When describing the process of pervaporation on polymer membranes, the dissolution–diffusion model, originally proposed by R. Reitenbach [21], is used. Later, due to problems in describing the process of pervaporation of water–alcohol mixtures with a high-water content in the initial mixture, it was improved [22]. This model has proven itself well in the calculation of organophilic and hydrophilic pervaporation processes on polymer composite membranes [20, 23]. The separation properties of polymer membranes strongly depend on their structural materials and manufacturing methods used, as well as membrane thickness and operating conditions, such as temperature and partial pressure differences above the membrane. This leads to the need to determine the parameters of the transmembrane flow model from experimental data for each membrane [24].

In the present work, the HybSi® ceramic pervaporation membrane [25–27], another commercially available membrane designed to solve the problems of alcohol dehydration, was considered. A HybSi® membrane represents a three-layer composite membrane in which a selective layer of an organo-inorganic hybrid material with an inorganic silicon dioxide base is applied to a supporting layer of amorphous silicon dioxide, which is located in turn on the inner surface of ceramic porous tubes made of $\alpha\text{-}Al_2O_3$.

Mathematical model of the membrane pervaporation module

As a basis for the model of the membrane module, a three-parameter mathematical model of the stationary process of pervaporation separation of a water–alcohol binary mixture on a HybSi® membrane was used [27]:

$$\beta\left(x_A^F - x_A^B\right) + jx_A^B = P_A^m \frac{\left(p_A^B - p_A^P\right)}{\delta_m}\varepsilon_a, \tag{1}$$

$$\beta\left(x_A^B - x_A^F\right) + j\left(1 - x_A^B\right) = P_B^m \frac{\left(p_B^B - p_B^P\right)}{\delta_m}\varepsilon_a, \tag{2}$$

$$x_A^P = \frac{\beta\left(x_A^F - x_A^B\right) + jx_A^B}{j}, \tag{3}$$

where j is the total molar flux of the two components through the membrane, mol/(m^2·s); x_A and x_B are the molar fractions of component A (water) and B (alcohol), respectively; the upper indices F, B, P correspond to the concentrations of the components in the initial mixture, at the boundary with the membrane and in the permeate, respectively; δ_m is the thickness of the selective layer of the HybSi® material, $\delta_m = 200$ nm; β is the mass transfer coefficient, mol/(m^2·s); p_A^B and p_A^P are the partial pressures of component A at the boundary with the membrane in solution and in permeate, respectively, Pa; P_A^m and P_B^m are the permeability coefficients for component A and B, respectively, mol/(m·s·Pa); ε_a is the share of active pores of the selective membrane layer:

$$\varepsilon_a = \frac{1}{1 + Cx_B k_B}, \tag{4}$$

where C is the molar density of the mixture, mol/m^3; k is the dimensionless coefficient:

$$k_B = 8.078 \cdot 10^{-9} \exp\left(-\frac{5446.374}{T}\right).$$

The permeability coefficients P_A^m and P_B^m for the components were determined by the following expression:

$$P^m = \frac{(C_1 T + C_2)\delta_m}{M(p^V - p)}, \tag{5}$$

where T is the temperature, °C, M is the molecular weight of the component; p^V is the saturated vapor pressure of the component, Pa; p is the pressure from the permeate, Pa; C_1 and C_2 are the coefficients of linear approximation of the flow of the pure component through the membrane (see Table).

Table. Linear approximation coefficients for the flow of matter [27]

Substance	C_1	C_2
Water	0.2775	−10.2183
Ethanol	0.004	−0.16
Isopropanol	0.000915	−0.05315

The partial pressure of the component from the initial mixture was determined by the formula $p_A^B = p_A^V \gamma_A^B x_A^B$, where p_A^V is the saturated vapor pressure of component A; γ_A^B is the activity coefficient of component A in the liquid phase. The Non-Random Two Liquid model was used in the calculations. The partial pressure in the permeate was determined by the formula $p_A^P = p \cdot x_A^P$.

A feature of the pervaporation process is the presence of a phase transition of components from a liquid state to a vaporous one, for which energy, i.e., the heat of vaporization, is required. In [27], an isothermal pervaporation regime was provided during experiments to determine the characteristics of the membrane at a constant driving force of the process. In practice, the process occurs under adiabatic conditions within the membrane module, the energy required for permeate formation being derived from the feed stream. Consequently, the temperature of the retentate will decline throughout this process. In accordance with the dissolution–diffusion model [28], a decline in temperature can influence the rate of permeate sorption on the membrane and diffusion capacity of permeate within the membrane, as well as the driving force of pervaporation. Consequently, the overall selectivity and permeate flow will change significantly with a drop in temperature, which may not be observed in other membrane processes occurring without a phase transition. Therefore, the applied membrane area in the module should be limited to a size that provides an acceptable temperature drop. If the temperature drops below 50°C, the pervaporation process is usually stopped [17].

In most cases, during the pervaporation process, the evaporation heat is supplied only from the initial mixture, so the temperature gradient develops mainly in the direction of the flow of the initial mixture. In this case, the thermal balance for the membrane module will be written as follows [29]:

$$FC_p^F \Delta T = -P\Delta H, \tag{6}$$

where F and P are the molar flow rates of the initial mixture and permeate; C_p^F is the heat capacity of the initial mixture; ΔH is the heat of permeate vaporization; ΔT is the temperature drop between the input and output streams of the module. From the Eq. (6) The temperature drop in the membrane module can be determined:

$$\Delta T = -\frac{P\Delta H}{FC_p^F}. \tag{7}$$

To describe the flow structure inside the HybSi® membrane module, consisting of cylindrical tubes inside which the raw material flow must move at a linear velocity of at least 2 m/s [26, 27], an ideal displacement model was used:

$$\frac{dF}{dz} = -\frac{j(T)dS}{dz}, \tag{8}$$

$$\frac{dT}{dz} = -\frac{j(T)\Delta H}{FC_p^F}\frac{dS}{dz}. \tag{9}$$

The system of Eqs. (8) and (9) can be used calculate the process of pervaporation in a membrane module with an area of S taking into account the model of substance transfer through the membrane (1)–(3).

Since there are no built-in mathematical functions in HYSYS, the system of differential Eqs. (8) and (9) was presented as a system of difference equations

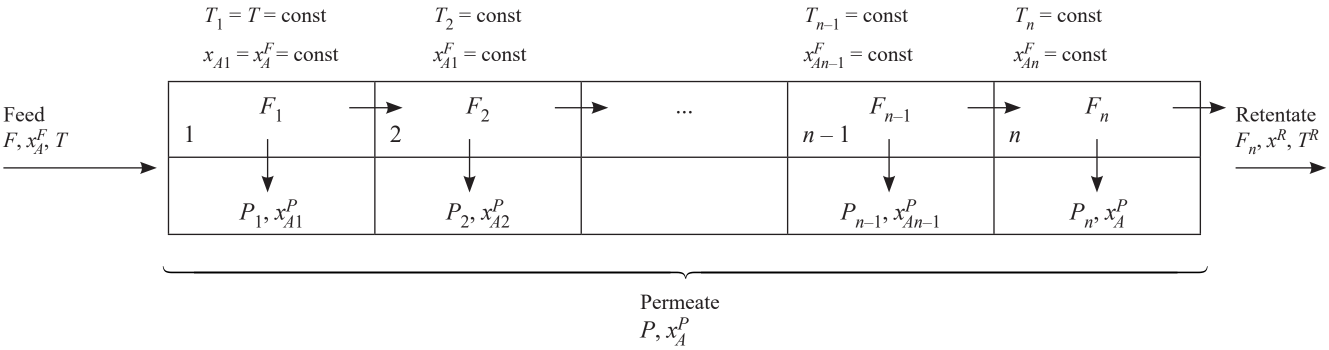

Fig. 1. Schematic of membrane module modeling

to be solved numerically with an adaptive area step. The process conditions should be close to isothermal $\Delta T \leq 1°C$; therefore, the magnitude of the temperature change was checked at each step. If this condition was not met, the area step was reduced until the process became isothermal. In the task, an assumption was made about the constancy of the composition and temperature of the raw materials at each step. Thus, the membrane pervaporation module with an area of S was divided into n intervals. Figure 1 shows a schematic of the membrane module modeling.

The amount of permeate passed through the membrane at the ith step was determined as follows:

$$P_i = \left(\sum_{l=1}^{k} J_l\right)\Delta S_i, \tag{10}$$

where ΔS_i is the area step; J_l is the flow of the lth component; k is the number of components passing through the membrane. The feed stream F_n determined at the last step will be retentate R coming out of the membrane module.

Creating a custom membrane pervaporation module in Aspen HYSYS

The equations of the mathematical model (8), (9) and their corresponding solution methods for the pervaporation process were refined for direct use in HYSYS without the need for external special programming.

The program code of the membrane module is implemented using the built-in editor MacroLanguageEditor and includes three main routines:

1) Initialize(), which defines the view of the window of the technological object;
2) Execute(), which includes the equations of the mathematical model and calling methods for calculating the properties of a mixture of components;
3) StatusQuery(), which generates messages about the status of program code execution.

The developed pervaporation process module is universal to the input mixture of components. The selection of the key components of permeate and retentate is carried out by the user based on their ID in the list of components of the mixture. The calculation of vapor–liquid equilibrium, physicochemical and thermodynamic properties of mixtures of substances is performed in real time based on the user-selected package of properties in HYSYS. The pervaporation module has a unique identifier in HYSYS that allows it to be accessed from third-party applications. An enlarged algorithm for calculating the pervaporation module, objects and their main properties are shown in Fig. 2.

Container.Feeds1 defines the module's input stream object (.Item(1)), its properties, and access methods. Container.Products1 contains a set of permeate and retentate output streams (.Item(0), .Item(1)). The initial data of the process is defined in the form of user variables through a graphical interface, the current values of internal variables are displayed as a spreadsheet.SpreadsheetOp using an .Operations object.

The parameters of the components that make up the mixture are accessed by the component name "CompName" in the form:

ActiveCase.Flowsheet.FluidPackage.Components.
Item("CompName").

The parameters of the selected thermodynamic package are accessed through the property. PropertyPackage of the FluidPackage object:

ActiveCase.Flowsheet.FluidPackage.PropertyPackage.

After the membrane module added by the user in the project is adjusted to the conditions of the pervaporation process, the calculation is carried out. As a result of the solution, permeate and retentate streams are transferred from the developed module to the HYSYS environment in the required HYSYS package format, which can be sent further along the separation process scheme.

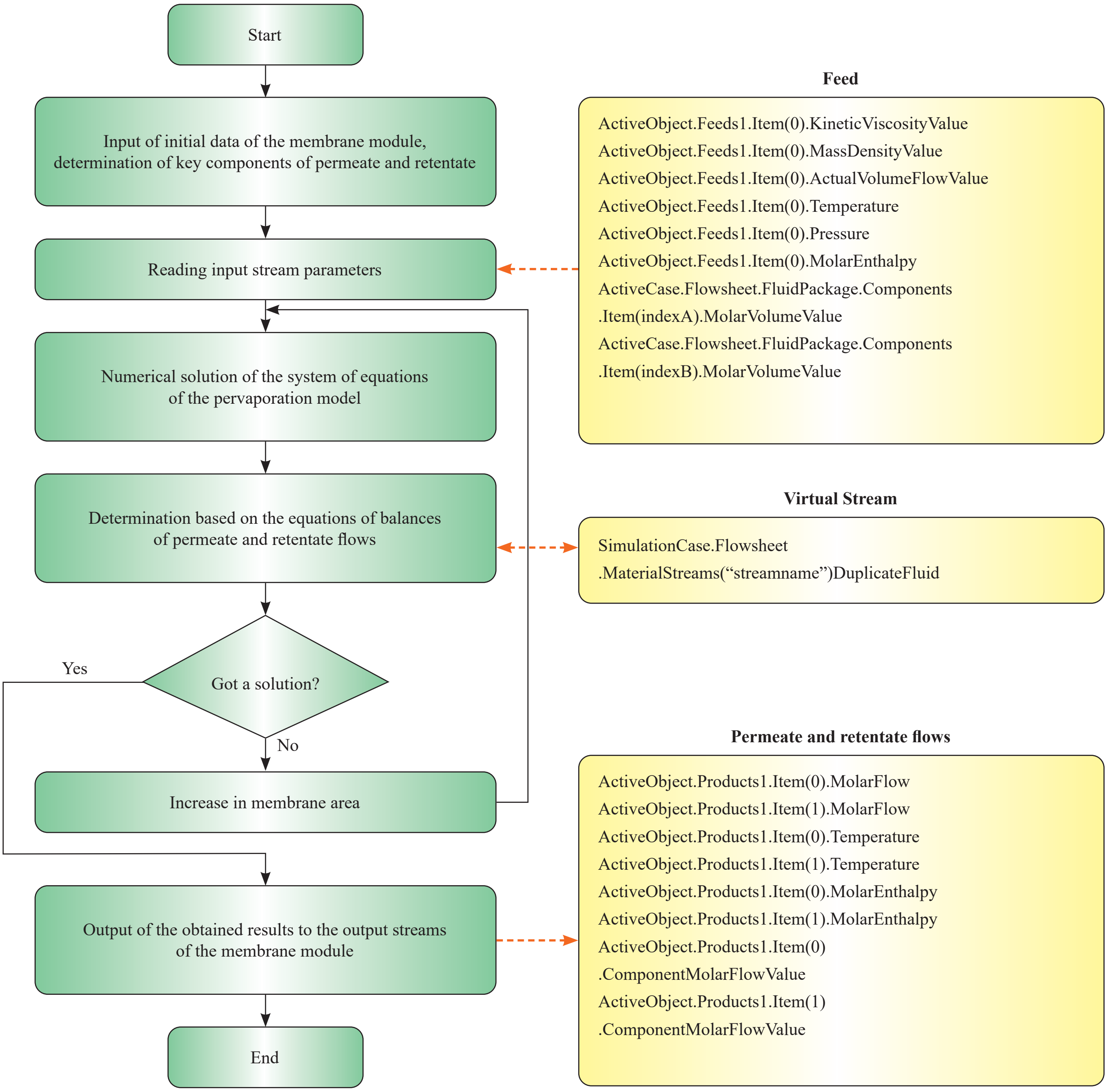

Feed

```
ActiveObject.Feeds1.Item(0).KineticViscosityValue
ActiveObject.Feeds1.Item(0).MassDensityValue
ActiveObject.Feeds1.Item(0).ActualVolumeFlowValue
ActiveObject.Feeds1.Item(0).Temperature
ActiveObject.Feeds1.Item(0).Pressure
ActiveObject.Feeds1.Item(0).MolarEnthalpy
ActiveCase.Flowsheet.FluidPackage.Components
.Item(indexA).MolarVolumeValue
ActiveCase.Flowsheet.FluidPackage.Components
.Item(indexB).MolarVolumeValue
```

Virtual Stream

```
SimulationCase.Flowsheet
.MaterialStreams("streamname")DuplicateFluid
```

Permeate and retentate flows

```
ActiveObject.Products1.Item(0).MolarFlow
ActiveObject.Products1.Item(1).MolarFlow
ActiveObject.Products1.Item(0).Temperature
ActiveObject.Products1.Item(1).Temperature
ActiveObject.Products1.Item(0).MolarEnthalpy
ActiveObject.Products1.Item(1).MolarEnthalpy
ActiveObject.Products1.Item(0)
.ComponentMolarFlowValue
ActiveObject.Products1.Item(1)
.ComponentMolarFlowValue
```

Fig. 2. Enlarged algorithm for calculating the membrane module

Comparison of calculation results in Aspen HYSYS with experimental data

The adequacy of the developed module was tested for binary water–alcohol mixtures. Figures 3 and 4 show a comparison of the calculation results of the pervaporation process for a mixture of ethanol–water and isopropanol–water at a permeate pressure of 5 and 20 mm Hg with experimental data presented in [27].

As can be seen from the results presented of modeling the operation of the membrane module in isothermal mode, the data obtained are in good agreement with the experimental data for 3 isotherms at different permeate pressures, representing a test of the operability of the module and the correct use of the HYSYS data structure in it.

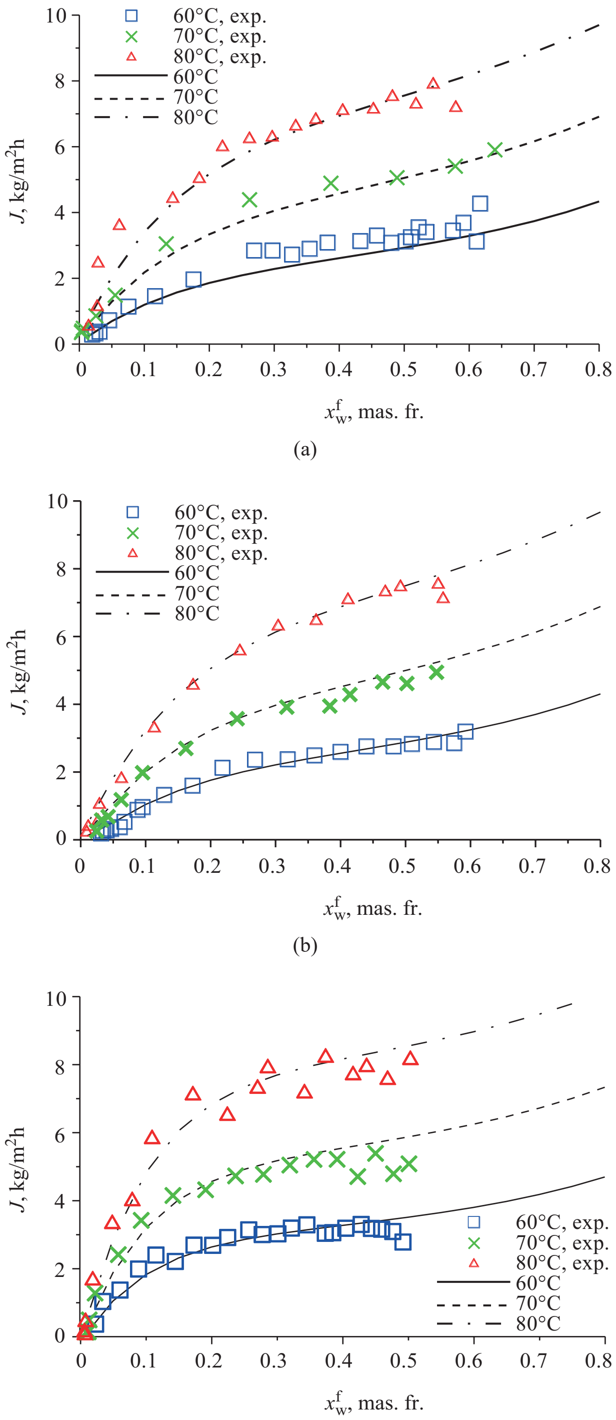

(a)

(b)

(c)

Fig. 3. Total permeate flow *J* through the HybSi® membrane depending on the concentration of water in the feed x_w^f:
(a) ethanol–water, 5 mm Hg;
(b) ethanol–water, 20 mm Hg;
(c) isopropanol–water, 20 mm Hg.
Geometric shapes are experimental data [27]

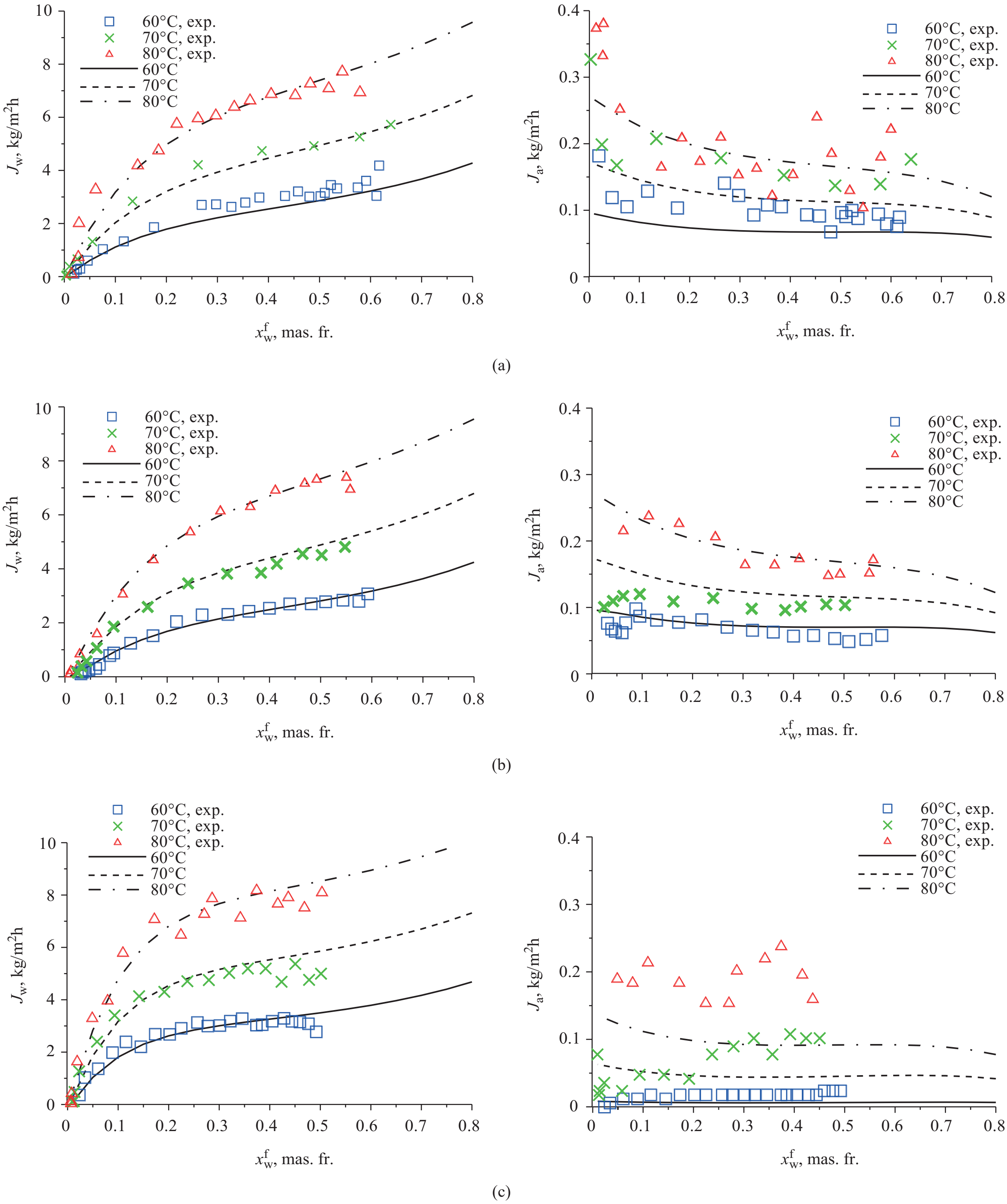

Fig. 4. Flow of individual components through the HybSi® membrane depending on the concentration of water in the feed x_w^f. The left graphs show the flow of water J_w, the right graphs show the flow of alcohol J_a:
(a) ethanol–water, 5 mm Hg;
(b) ethanol–water, 20 mm Hg;
(c) isopropanol–water, 20 mm Hg.
Geometric shapes are experimental data [27]

SIMULATION RESULTS AND DISCUSSION

The next stage of the research was to calculate the membrane module in adiabatic mode. Figure 5 depicts a comparative analysis of the dehydration process of ethanol and isopropanol. In the first case (Fig. 5a), the simulation results are presented depending on the water content in the initial mixture on a membrane module with an area of 1 m^2. In the second case (Fig. 5b), the results of modeling the separation of a mixture of alcohols with an initial water content of 15 wt % as a function of the membrane module area are obtained. In both cases the simulation was carried out with a permeate side pressure of 20 mm Hg and a capacity of 100 kg/h for the initial mix.

If taking the value of the temperature difference between the inlet and outlet of the membrane module to be equal to 5°C, an isothermal operating mode can be assumed to be approximately maintained. Then, as can be seen from Fig. 5a, when isopropanol is dehydrated on a module of equal area, the area of isothermal operation for the concentration of water in the initial mixture will be smaller. At an inlet temperature of 60°C, these are mixtures of isopropanol and ethanol having an initial water content of no more than 4.75 and 10.4 wt %, respectively. Similarly, the water content in these mixtures at 70°C will be 2.95 and 5.23 wt %; at 80°C, 2.1 and 3.3 wt %, respectively. In addition, the temperature change at the outlet of the module for isopropanol is characterized by a greater drop than for ethanol. This behavior is fully correlated with the values of the total fluxes for these alcohols (see Fig. 3): for an isopropanol mixture, the total flux is greater than for an ethanol mixture all other things being equal.

As can be seen from Fig. 5b, when dehydrating isopropanol with a water content of 15 wt % in the feedstock, the size of the module in which conditions are maintained close to the isothermal regime is smaller compared to ethanol. Ethanol at 80°C requires ~1.6 times the membrane area than isopropanol. When the temperature drops to 60°C, the area difference increases to ~1.8 times. From this point of view, when modeling the operation of the pervaporation module on a HybSi® membrane, it is advisable not to be guided by the same size of membrane modules, but rather by the constant temperature of the retentate at the outlet of the module, which, as shown by the example of commercial polymer membranes, is more advantageous [30]. In this case, an additional amount of heat must be added to the retentate flow after each module to increase the driving force of the process.

Figure 6 shows the results of modeling the process of first stage dehydration of ethanol and isopropanol with an initial water content of 15 wt % in the initial mixture on membrane modules with different surface areas. The simulation of the membrane module operation

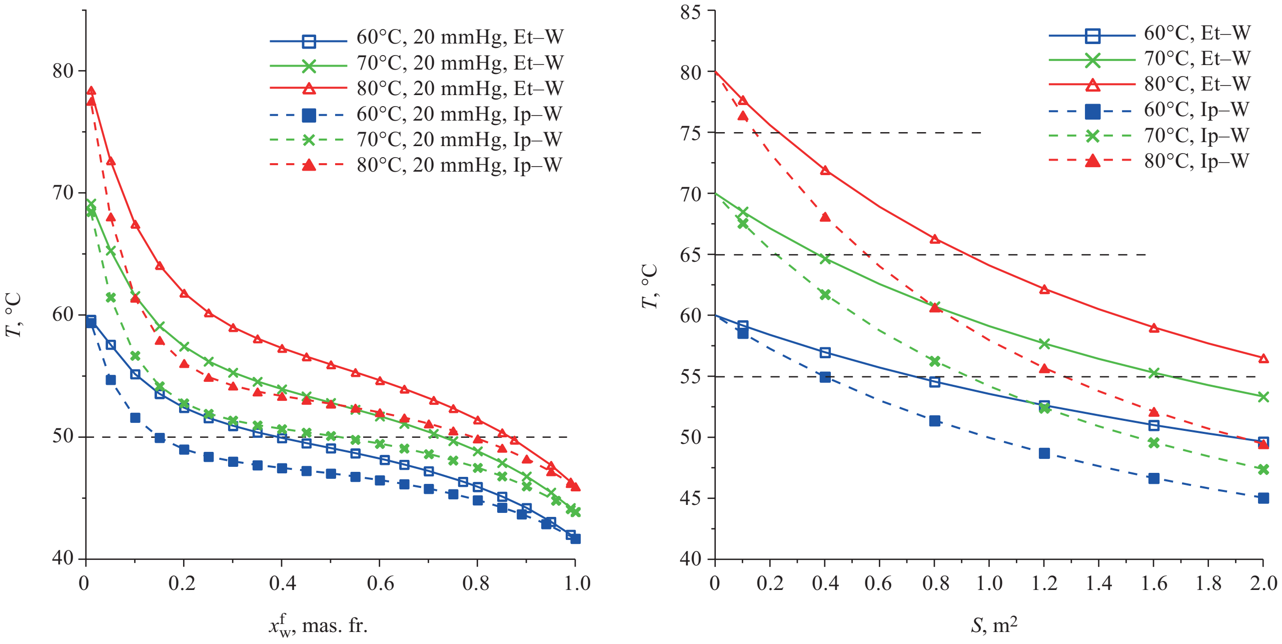

(a) (b)

Fig. 5. Retentate temperature T at the outlet of the HybSi® membrane module for a mixture of ethanol–water (Et–W) and isopropanol–water (Ip–W) depending on the composition x_w^f and area S:
(a) $S = 1$ m^2;
(b) mixture with a water content of 15 wt %

was carried out in adiabatic mode and without taking into account thermal effects (in isothermal mode), at a pressure on the permeate side of 20 mm Hg. Figure 6 shows the values of the total permeate flow and the concentration of water in the retentate at the outlet of a single membrane module as a function of its surface area.

As can be seen from Fig. 6, the discrepancy between the total permeate flow for ethanol in isothermal and adiabatic modes of operation will be 20.9% at 60°C and 30.1% at 80°C for a module with an area of 1 m^2. For modules with a larger area (2 m^2), the discrepancy will already be at 34.7 and 44.3% for 60 and 80°C, respectively. For isopropanol, with a module area of 1 m^2, the total flow discrepancy will be 30.6% at 60°C and 38.0% at 80°C, and with a module area of 2 m^2, the discrepancy will already be 46.8 and 51.8% at 60 and 80°C, respectively. A similar pattern is observed for the water concentration in the retentate: in the isothermal mode, where it decreases significantly, the discrepancy between concentrations can reach 1.3–1.8 times compared to the adiabatic mode.

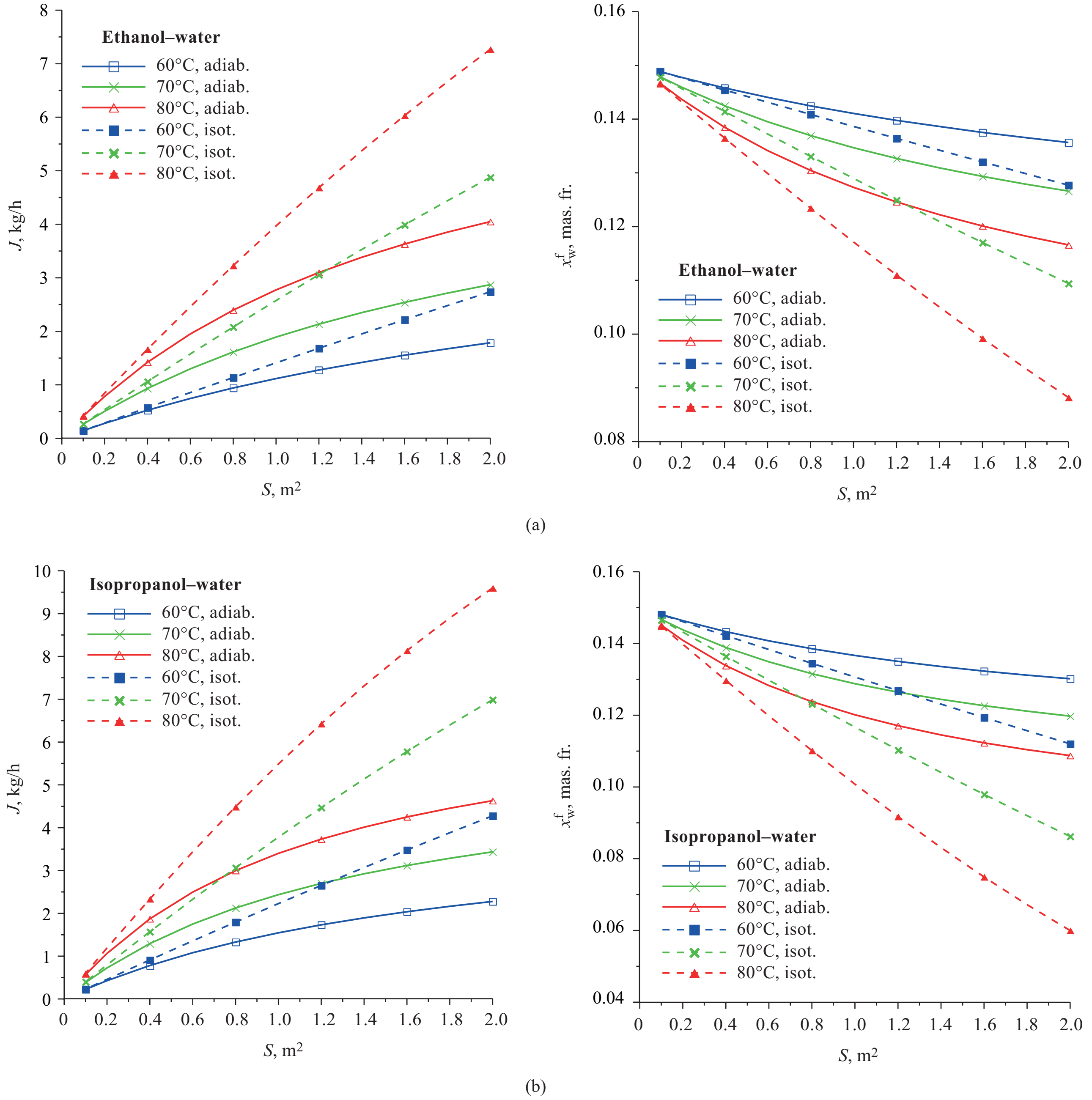

(a)

(b)

Fig. 6. Total permeate flow *J* and water concentration in the retentate x_w^r in isothermal and adiabatic modes of operation:
(a) ethanol–water, the water content is 15 wt %;
(b) isopropanol–water, the water content is 15 wt %

As can be seen from the results presented (Figs. 5 and 6), the processes of alcohol dehydration on HybSi® membranes are accompanied by significant thermal effects. In order to avoid errors in determining the required surface area of membrane modules, these effects must be taken into account in the development and design of membrane modules. In addition, the error in determining the required surface area of the membrane module is not constant, but increases with the temperature of the raw materials supplied.

If we compare the flow rates through HybSi® membranes with commercial PERVAP 2210 polymer membranes [31], the permeate flow at a water content of 5 wt % is several times higher for ceramic membranes under the same process conditions. This suggests that a smaller total surface area of HybSi® membrane modules is required to perform the alcohol dehydration process.

CONCLUSIONS

In order to calculate the process of pervaporation on a HybSi® ceramic membrane, an algorithm was developed along with a software module in the Aspen HYSYS UMP. A three-parameter mathematical model of initial separation (1)–(3) was used as the basis for the development of the module. This model was supplemented with the heat balance Eq. (6) to determine the temperature change of the raw material stream (7) passing through the module. Comparison of the simulation results with experimental data for dehydration of ethanol and isopropanol at different feed temperatures and permeate pressures confirmed the reliability of the developed membrane pervaporation module (Figs. 3 and 4).

The research results showed that the processes of alcohol dehydration on HybSi® membranes are accompanied by significant thermal effects (Fig. 5) due to large transmembrane currents (Fig. 3). Calculating the module in isothermal mode without taking thermal effects into account can lead to significant errors. When determining the permeate consumption, these errors, which increase with increasing feed temperature, can be up to 50%; when determining the water concentration in the retentate, they can be 1.3–1.8 times (Fig. 6). When performing design calculations, this will result in a significant underestimation of the required surface area of the membrane module.

The calculation module of the pervaporation process developed in the work can be considered as a tool for use in Aspen HYSYS UMP for modeling the processes of alcohol dehydration both as a separate module and for modeling various schemes of dehydration processes.

Acknowledgments

The work was financially supported by the Ministry of Science and Higher Education of the Russian Federation, grant No. 075-01261-22-00 “Energy-saving processes of separation of liquid mixtures for the separation of industrial solvents.”

Authors’ contributions

A.V. Malygin—development of the idea and algorithm for creating a calculation module of the pervaporation process, analysis and interpretation of the results obtained, and writing the text of the article.

I.I. Emel’yanov—development of algorithms of numerical methods for the calculation module of the pervaporation process at Aspen HYSYS, analysis and interpretation of the results obtained.

R.V. Semin—writing the program code of the membrane module, debugging and testing it.

A.R. Fazlyev—graphical preparation of experimental data, consulting.

N.N. Ziyatdinov—management and scientific consulting, analysis of research materials.

A.V. Klinov—management and scientific consulting, analysis of research materials.

The authors declare no conflicts of interest.

REFERENCES

1. Timoshenko A.V., Anokhina E.A., Rudakov D.G., Tatsievskaya G.I., Matyushenkova Yu.V. Power saving in distillation using complexes with coupled flows. *Vestnik MITHT* (*Fine Chem. Technol*.). 2011;6(4):28–39 (in Russ.).
2. Anokhina E.A., Shleynikova E.L., Timoshenko A.V. Energy efficiency of complexes with partially coupled thermal and material flows for extractive distillation of methyl acetate – chloroform mixture. *Vestnik MITHT* (*Fine Chem. Technol*.). 2013;8(2):18–25 (in Russ.).
3. Raeva V.M., Sebyakin A.Y., Sazonova A.Y., Frolkova A.K. The choice of possible entrainers for the extractive distillation of binary mixture benzene – cyclohexane. *Vestnik MITHT* (*Fine Chem. Technol*.). 2011;6(1):43–53 (in Russ.).

СПИСОК ЛИТЕРАТУРЫ

1. Тимошенко А.В., Анохина Е.А., Рудаков Д.Г., Тимофеев В.С., Тациевская Г.И., Матюшенкова Ю.В. Энергосбережение в ректификации с использованием комплексов со связанными потоками. *Вестник МИТХТ им. М.В. Ломоносова* (*Тонкие химические технологии*). 2011;6(4):28–39.
2. Анохина Е.А., Шлейникова Е.Л., Тимошенко А.В. Энергоэффективность комплексов с частично связанными тепловыми и материальными потоками в экстрактивной ректификации смеси метилацетат – хлороформ. *Вестник МИТХТ им. М.В. Ломоносова* (*Тонкие химические технологии*). 2013;8(2):18–25.

4. Sander U., Soukup P. Design and operation of a pervaporation plant for ethanol dehydration. *J. Membr. Sci*. 1988;36:463–475. https://doi.org/10.1016/0376-7388(88)80036-X
5. Jyothi M.S., Reddy K.R., Soontarapa K., *et al.* Membranes for dehydration of alcohols via pervaporation. *J. Environ. Manage*. 2019;242:415–429. https://doi.org/10.1016/j.jenvman.2019.04.043
6. Raza W., Wang J., Yang J., Tsuru T. Progress in pervaporation membranes for dehydration of acetic acid. *Sep. Purif. Technol.* 2021;262:11833. https://doi.org/10.1016/j.seppur.2021.118338
7. Akberov R.R., Farakhov M.I., Klinov A.V., *et al.* Dehydration of diethylene glycol by pervaporation using HybSi ceramic membranes. *Theor. Found. Chem. Eng.* 2014;48(5):650–655. https://doi.org/10.1134/S0040579514030014

   [Original Russian Text: Akberov R.R., Farakhov M.I., Maryakhina V.A., Kirichenko S.M., Fazlyev A.R., Klinov A.V., Malygin A.V. Dehydration of diethylene glycol by pervaporation using HybSi ceramic membranes. *Teoreticheskie Osnovy Khimicheskoi Tekhnologii.* 2014;48(5):594–600 (in Russ.). https://doi.org/10.7868/S0040357114030014]
8. Zheng P., Li C., Wang N., Li J., An Q. The potential of pervaporation for biofuel recovery from fermentation: An energy consumption point of view. *Chinese J. Chem. Eng.* 2019;27(6):1296–1306. https://doi.org/10.1016/j.cjche.2018.09.025
9. Liu H.-X., Wang N., Zhao C., Ji S., Li J.-R. Membrane materials in the pervaporation separation of aromatic/aliphatic hydrocarbon mixtures. *Chinese J. Chem. Eng.* 2018;26(1):1–16. https://doi.org/10.1016/j.cjche.2017.03.006
10. Yushkin A.A., Golubev G.S., Podtynnikov I.A., *et al.* Separation of mixtures of polar and nonpolar organic liquids by pervaporation and nanofiltration (review). *Pet. Chem.* 2020;60(11):1317–1327. https://doi.org/10.1134/S0965544120110201

    [Original Russian Text: Yushkin A.A., Golubev G.S., Podtynnikov I.A., Borisov I.L., Volkov V.V., Volkov A.V. Separation of mixtures of polar and nonpolar organic liquids by pervaporation and nanofiltration (review). *Neftekhimiya.* 2020;60(6):863–874 (in Russ.). https://doi.org/10.31857/S0028242120060209]
11. Mortaheb H., Ghaemmaghami F., Mokhtarani B. A review on removal of sulfur components from gasoline by pervaporation. *Chem. Eng. Res. Des*. 2012;90(3):409–432. https://doi.org/10.1016/j.cherd.2011.07.019
12. Mukherjee M., Roy S., Bhowmick K., *et al.* Development of high performance pervaporation desalination membranes. *Process Safety and Environmental Protection*. 2022;159:1092–1104. https://doi.org/10.1016/j.psep.2022.01.076
13. Vane L. Review of pervaporation and vapor permeation process factors affecting the removal of water from industrial solvents. *J. Chem. Technol. Biotechnol*. 2020;95(3):495–512. https://doi.org/10.1002/jctb.6264
14. Kancherla R., Nazia S., Kalyani S., Sridhar S. Modeling and simulation for design and analysis of membrane-based separation processes. *Computer. & Chem. Eng.* 2021;148:107258. https://doi.org/10.1016/j.compchemeng.2021.107258
15. Koczka K., Mizsey P., Fonyo Z. Rigorous modelling and optimization of hybrid separation processes based on pervaporation. *Central European Journal of Chemistry*. 2007;5(4):1124–1147. https://doi.org/10.2478/s11532-007-0050-8
16. Verhoef A., Degreve J., Huybrechs B., *et al.* Simulation of a hybrid pervaporation–distillation process. *Computer. & Chem. Eng*. 2008;32(6):1135–1146. https://doi.org/10.1016/j.compchemeng.2007.04.014
17. Valentínyi N., Mizsey P. Comparison of pervaporation models with simulation of hybrid separation processes. *Periodica Polytechnica: Chemical Engineering*. 2014;58(1):7–14. https://doi.org/10.3311/PPch.7120

3. Раева В.М., Себякин А.Ю., Сазонова А.Ю., Фролкова А.К. Выбор потенциальных разделяющих агентов для экстрактивной ректификации смеси циклогексан – бензол. *Вестник МИТХТ им. М.В. Ломоносова* (*Тонкие химические технологии*). 2011;6(1):43–53.
4. Sander U., Soukup P. Design and operation of a pervaporation plant for ethanol dehydration. *J. Membr. Sci*. 1988;36:463–475. https://doi.org/10.1016/0376-7388(88)80036-X
5. Jyothi M.S., Reddy K.R., Soontarapa K., *et al.* Membranes for dehydration of alcohols via pervaporation. *J. Environ. Manage*. 2019;242:415–429. https://doi.org/10.1016/j.jenvman.2019.04.043
6. Raza W., Wang J., Yang J., Tsuru T. Progress in pervaporation membranes for dehydration of acetic acid. *Sep. Purif. Technol.* 2021;262:11833. https://doi.org/10.1016/j.seppur.2021.118338
7. Акберов Р.Р., Фазлыев А.Р., Клинов А.В., Малыгин А.В., Фарахов М.И., Маряхина В.А., Кириченко С.М. Обезвоживание диэтиленгликоля методом первапорации с помощью керамических мембран Hybsi. *Теоретические основы химической технологии*. 2014;48(5):594–600. https://doi.org/10.7868/S0040357114030014
8. Zheng P., Li C., Wang N., Li J., An Q. The potential of pervaporation for biofuel recovery from fermentation: An energy consumption point of view. *Chinese J. Chem. Eng.* 2019;27(6):1296–1306. https://doi.org/10.1016/j.cjche.2018.09.025
9. Liu H.-X., Wang N., Zhao C., Ji S., Li J.-R. Membrane materials in the pervaporation separation of aromatic/aliphatic hydrocarbon mixtures. *Chinese J. Chem. Eng.* 2018;26(1):1–16. https://doi.org/10.1016/j.cjche.2017.03.006
10. Юшкин А.А., Голубев Г.С., Подтынников И.А., Борисов И.Л., Волков В.В., Волков А.В. Разделение смесей полярных и неполярных органических жидкостей методами первапорации и нанофильтрации. *Нефтехимия*. 2020;60(6):863–874. https://doi.org/10.31857/S0028242120060209
11. Mortaheb H., Ghaemmaghami F., Mokhtarani B. A review on removal of sulfur components from gasoline by pervaporation. *Chem. Eng. Res. Des*. 2012;90(3):409–432. https://doi.org/10.1016/j.cherd.2011.07.019
12. Mukherjee M., Roy S., Bhowmick K., *et al.* Development of high performance pervaporation desalination membranes. *Process Safety and Environmental Protection*. 2022;159:1092–1104. https://doi.org/10.1016/j.psep.2022.01.076
13. Vane L. Review of pervaporation and vapor permeation process factors affecting the removal of water from industrial solvents. *J. Chem. Technol. Biotechnol*. 2020;95(3):495–512. https://doi.org/10.1002/jctb.6264
14. Kancherla R., Nazia S., Kalyani S., Sridhar S. Modeling and simulation for design and analysis of membrane-based separation processes. *Computer. & Chem. Eng.* 2021;148:107258. https://doi.org/10.1016/j.compchemeng.2021.107258
15. Koczka K., Mizsey P., Fonyo Z. Rigorous modelling and optimization of hybrid separation processes based on pervaporation. *Central European Journal of Chemistry*. 2007;5(4):1124–1147. https://doi.org/10.2478/s11532-007-0050-8
16. Verhoef A., Degreve J., Huybrechs B., *et al.* Simulation of a hybrid pervaporation–distillation process. *Computer. & Chem. Eng*. 2008;32(6):1135–1146. https://doi.org/10.1016/j.compchemeng.2007.04.014
17. Valentínyi N., Mizsey P. Comparison of pervaporation models with simulation of hybrid separation processes. *Periodica Polytechnica: Chemical Engineering*. 2014;58(1):7–14. https://doi.org/10.3311/PPch.7120

18. Kozlova A.A., Trubyanov M.M., Atlaskin A.A., *et al.* Modeling membrane gas and vapor separation in the aspen plus environment. *Membranes and Membrane Technologies.* 2019;1(1):1–5. https://doi.org/10.1134/S2517751619010049
[Original Russian Text: Kozlova A.A., Trubyanov M.M., Atlaskin A.A., Yanbikov N.R., Shalygin M.G. Modeling membrane gas and vapor separation in the aspen plus environment. *Membrany i membrannye tekhnologii.* 2019;9(1):3–8 (in Russ.). https://doi.org/10.1134/S2218117219010048]
19. Csefalvay E., Szitkai Z., Mizsey P., Fonyo Z. Experimental data based modelling and simulation of isopropanol dehydration by pervaporation. *Desalination*. 2008;29(1–3):4–108. https://doi.org/10.1016/j.desal.2007.07.029
20. Toth A.J., Andre A., Haaz E., Mizsey P. New horizon for the membrane separation: Combination of organophilic and hydrophilic pervaporations. *Sep. Purif. Technol.* 2015;156(2):432–443. https://doi.org/10.1016/j.seppur.2015.10.032
21. Rautenbach R., Herion C., Meyer-Blumenroth U. Engineering aspects of pervaporation: Calculation of transport resistances, module optimization and plant design. In: Huang R.Y.M. (Ed.). *Pervaporation Membrane Separation Processes*. Amsterdam: Elsevier; 1991. Chap. 3. P. 181–191.
22. Valentínyi N., Cséfalvay E., Mizsey P. Modelling of pervaporation: Parameter estimation and model development. *Chem. Eng. Res. Des*. 2013;91(1):174–183. https://doi.org/10.1016/j.cherd.2012.07.001
23. Tóth A.J., Mizsey P. Methanol removal from aqueous mixture with organophilic pervaporation: Experiments and modeling. *Chem. Eng. Res. Des*. 2015;98:123–135. https://doi.org/10.1016/j.cherd.2015.04.031
24. Koch K., Gorak A. Pervaporation of binary and ternary mixtures of acetone, isopropyl alcohol and water using polymeric membranes: Experimental characterisation and modeling. *Chem. Eng. Sci*. 2014;115:95–114. https://doi.org/10.1016/j.ces.2014.02.009
25. Castricum H.L., Kreiter R., van Veen H.M., *et al.* High-performance hybrid pervaporation membranes with superior hydrothermal and acid stability. *J. Membrane Sci*. 2008;324(1–2):111–118. https://doi.org/10.1016/j.memsci.2008.07.014
26. Van Veen H.M., Rietkerk M.D.A., Shanahan D.P., *et al.* Pushing membrane stability boundaries with HybSi® pervaporation membranes. *J. Membrane Sci*. 2011;380(1–2):124–131. https://doi.org/10.1016/j.memsci.2011.06.040
27. Klinov A.V., Akberov R.R., Fazlyev A.R., Farakhov M.I. Experimental investigation and modeling through using the solution-diffusion concept of pervaporation dehydration of ethanol and isopropanol by ceramic membranes HybSi. *J. Membrane Sci*. 2017;524:321–333. https://doi.org/10.1016/j.memsci.2016.11.057
28. Wijmans J.G., Baker R.W. The solution-diffusion model: a review. *J. Membrane Sci.* 1995;107(1–2):1–21. https://doi.org/10.1016/0376-7388(95)00102-I
29. Song K.M., Hong Y.K., Yu J., *et al*. Influence of Temperature Drop by Phase Transition on Pervaporation Processes in Vapor Phase Feed. *Korean J. Chem. Eng.* 2002;19(2):290–295. http://doi.org/10.1007/BF02698416
30. Vatankhah F., Moheb A., Mehrabani-Zeinabad A. A study on the effects of feed temperature and concentration on design of a multi-stage pervaporation system for isopropanol-water separation using commercial available modules with inter-stage heating. *J. Membrane Sci*. 2021;618:118717. https://doi.org/10.1016/j.memsci.2020.118717
31. Kubaczka A., Kamiński W., Marszałek J. Predicting mass fluxes in the pervaporation process using Maxwell-Stefan diffusion coefficients. *J. Membrane Sci*. 2018;546:111–119. https://doi.org/10.1016/j.memsci.2017.08.074

18. Козлова А.А., Трубянов М.М., Атласкин А.А., Янбиков Н.Р., Шалыгин М.Г. Моделирование процесса мембранного разделения газов и паров в среде Aspen Plus. *Мембраны и мембранные технологии*. 2019;9(1):3–8. https://doi.org/10.1134/S2218117219010048

19. Csefalvay E., Szitkai Z., Mizsey P., Fonyo Z. Experimental data based modelling and simulation of isopropanol dehydration by pervaporation. *Desalination*. 2008;29(1–3):4–108. https://doi.org/10.1016/j.desal.2007.07.029
20. Toth A.J., Andre A., Haaz E., Mizsey P. New horizon for the membrane separation: Combination of organophilic and hydrophilic pervaporations. *Sep. Purif. Technol.* 2015;156(2):432–443. https://doi.org/10.1016/j.seppur.2015.10.032
21. Rautenbach R., Herion C., Meyer-Blumenroth U. Engineering aspects of pervaporation: Calculation of transport resistances, module optimization and plant design. In: Huang R.Y.M. (Ed.). *Pervaporation Membrane Separation Processes*. Amsterdam: Elsevier; 1991. Chap. 3. P. 181–191.
22. Valentínyi N., Cséfalvay E., Mizsey P. Modelling of pervaporation: Parameter estimation and model development. *Chem. Eng. Res. Des*. 2013;91(1):174–183. https://doi.org/10.1016/j.cherd.2012.07.001
23. Tóth A.J., Mizsey P. Methanol removal from aqueous mixture with organophilic pervaporation: Experiments and modeling. *Chem. Eng. Res. Des*. 2015;98:123–135. https://doi.org/10.1016/j.cherd.2015.04.031
24. Koch K., Gorak A. Pervaporation of binary and ternary mixtures of acetone, isopropyl alcohol and water using polymeric membranes: Experimental characterisation and modeling. *Chem. Eng. Sci*. 2014;115:95–114. https://doi.org/10.1016/j.ces.2014.02.009
25. Castricum H.L., Kreiter R., van Veen H.M., *et al.* High-performance hybrid pervaporation membranes with superior hydrothermal and acid stability. *J. Membrane Sci.* 2008;324(1–2):111–118. https://doi.org/10.1016/j.memsci.2008.07.014
26. Van Veen H.M., Rietkerk M.D.A., Shanahan D.P., *et al.* Pushing membrane stability boundaries with HybSi® pervaporation membranes. *J. Membrane Sci*. 2011;380(1–2):124–131. https://doi.org/10.1016/j.memsci.2011.06.040
27. Klinov A.V., Akberov R.R., Fazlyev A.R., Farakhov M.I. Experimental investigation and modeling through using the solution-diffusion concept of pervaporation dehydration of ethanol and isopropanol by ceramic membranes HybSi. *J. Membrane Sci*. 2017;524:321–333. https://doi.org/10.1016/j.memsci.2016.11.057
28. Wijmans J.G., Baker R.W. The solution-diffusion model: a review. *J. Membrane Sci.* 1995;107(1–2):1–21. https://doi.org/10.1016/0376-7388(95)00102-I
29. Song K.M., Hong Y.K., Yu J., *et al*. Influence of Temperature Drop by Phase Transition on Pervaporation Processes in Vapor Phase Feed. *Korean J. Chem. Eng.* 2002;19(2):290–295. http://doi.org/10.1007/BF02698416
30. Vatankhah F., Moheb A., Mehrabani-Zeinabad A. A study on the effects of feed temperature and concentration on design of a multi-stage pervaporation system for isopropanol-water separation using commercial available modules with inter-stage heating. *J. Membrane Sci*. 2021;618:118717. https://doi.org/10.1016/j.memsci.2020.118717
31. Kubaczka A., Kamiński W., Marszałek J. Predicting mass fluxes in the pervaporation process using Maxwell-Stefan diffusion coefficients. *J. Membrane Sci*. 2018;546:111–119. https://doi.org/10.1016/j.memsci.2017.08.074

About the authors

Alexander V. Malygin, Cand. Sci. (Eng.), Acting Head of the Department of Systems Engineering, Kazan National Research Technological University (68, Karl Marx ul., Kazan, 420015, Russia). E-mail: mav@kstu.ru. Scopus Author ID 57189716825, ResearcherID J-8948-2017, RSCI SPIN-code 7953-7259, https://orcid.org/0000-0002-0674-6773

Ilya I. Emel’yanov, Cand. Sci. (Eng.), Associate Professor, Department of Systems Engineering, Kazan National Research Technological University (68, Karl Marx ul., Kazan, 420015, Russia). E-mail: EmelyanovII@corp.knrtu.ru. Scopus Author ID 56609966600, ResearcherID AAH-7924-2019, RSCI SPIN-code 1838-4010, https://orcid.org/0000-0003-0257-0739

Roman V. Semin, Master Student, Kazan National Research Technological University (68, Karl Marx ul., Kazan, 420015, Russia). E-mail: prodigy19913@mail.ru. https://orcid.org/0009-0004-0439-6185

Azat R. Fazlyev, Cand. Sci. (Eng.), Associate Professor, Department of Processes and Apparatuses of Chemical Technology, Kazan National Research Technological University (68, Karl Marx ul., Kazan, 420015, Russia). E-mail: FazlyevAR@corp.knrtu.ru. Scopus Author ID 56413092300, ResearcherID F-5385-2016, RSCI SPIN-code 5951-6042, https://orcid.org/0000-0002-2956-3558

Nadir N. Ziyatdinov, Dr. Sci. (Eng.), Professor, Department of Systems Engineering, Kazan National Research Technological University (68, Karl Marx ul., Kazan, 420015, Russia). E-mail: nnziat@yandex.ru. Scopus Author ID 8157424700, ResearcherID AAH-7789-2019, RSCI SPIN-code 9966-4183, https://orcid.org/0000-0002-2314-8935

Alexander V. Klinov, Dr. Sci. (Eng.), Professor, Head of the Department of Processes and Apparatuses of Chemical Technology, Kazan National Research Technological University (68, Karl Marx ul., Kazan, 420015, Russia). E-mail: alklin@kstu.ru. Scopus Author ID 36907475500, ResearcherID K-8270-2017, RSCI SPIN-code 2116-4141, https://orcid.org/0000-0002-7833-8330

Об авторах

Малыгин Александр Владимирович, к.т.н., и.о. заведующего кафедрой «Системотехника», ФГБОУ ВО «Казанский национальный исследовательский технологический университет» (420015, Россия, Казань, ул. Карла Маркса, д. 68). E-mail: mav@kstu.ru. Scopus Author ID 57189716825, ResearcherID J-8948-2017, SPIN-код РИНЦ 7953-7259, https://orcid.org/0000-0002-0674-6773

Емельянов Илья Игоревич, к.т.н., доцент, кафедра «Системотехника», ФГБОУ ВО «Казанский национальный исследовательский технологический университет» (420015, Россия, Казань, ул. Карла Маркса, д. 68). E-mail: EmelyanovII@corp.knrtu.ru. Scopus Author ID 56609966600, ResearcherID AAH-7924-2019, SPIN-код РИНЦ 1838-4010, https://orcid.org/0000-0003-0257-0739

Семин Роман Вадимович, магистрант, ФГБОУ ВО «Казанский национальный исследовательский технологический университет» (420015, Россия, Казань, ул. Карла Маркса, д. 68). E-mail: prodigy19913@mail.ru. https://orcid.org/0009-0004-0439-6185

Фазлыев Азат Равилевич, к.т.н., доцент, кафедра «Процессы и аппараты химической технологии», ФГБОУ ВО «Казанский национальный исследовательский технологический университет» (420015, Россия, Казань, ул. Карла Маркса, д. 68). E-mail: FazlyevAR@corp.knrtu.ru. Scopus Author ID 56413092300, ResearcherID F-5385-2016, SPIN-код РИНЦ 5951-6042, https://orcid.org/0000-0002-2956-3558

Зиятдинов Надир Низамович, д.т.н., профессор, кафедра «Системотехника», ФГБОУ ВО «Казанский национальный исследовательский технологический университет» (420015, Россия, Казань, ул. Карла Маркса, д. 68). E-mail: nnziat@yandex.ru. Scopus Author ID 8157424700, ResearcherID AAH-7789-2019, SPIN-код РИНЦ 9966-4183, https://orcid.org/0000-0002-2314-8935

Клинов Александр Вячеславович, д.т.н., заведующий кафедрой «Процессы и аппараты химической технологии», ФГБОУ ВО «Казанский национальный исследовательский технологический университет» (420015, Россия, Казань, ул. Карла Маркса, д. 68). E-mail: alklin@kstu.ru. Scopus Author ID 36907475500, ResearcherID K-8270-2017, SPIN-код РИНЦ 2116-4141, https://orcid.org/0000-0002-7833-8330

Translated from Russian into English by N. Isaeva
Edited for English language and spelling by Thomas A. Beavitt

MIREA – Russian Technological University
78, Vernadskogo pr., Moscow, 119454, Russian Federation.
Publication date *February 27, 2025.*
Not for sale

МИРЭА – Российский технологический университет
119454, РФ, Москва, пр-т Вернадского, д. 78.
Дата опубликования *27.02.2025.*
Не для продажи

www.finechem-mirea.ru